MORPHOLOGY AND GEOCHEMISTRY OF GLAUCONITE FROM THE TE KUITI GROUP, SOUTH AUCKLAND REGION, NEW ZEALAND

A thesis
submitted in partial fulfillment of the
requirements for the degree of
Master of Science in **Earth Sciences**
at the
University of Waikato

---

by

Martyn Stephen Compton

1989

Abstract

The late Eocene - Oligocene Te Kuiti Group comprises calcareous mudstone, calcareous sandstone and skeletal or sandy limestone formed in marginal marine to fully marine shelf settings. Glauconite is ubiquitous in all sedimentary units in low concentration (5-10%), but at unconformities or near formation boundaries can attain concentrations >75%.

Binocular microscope studies show the following morphological form abundances: ovoidal(40-55%) > fragmentary(20-40%) > lobate(5-15%) > casts (0-5%) with trace quantities of tabular, capsule, and vermicular grains. The abundance of ovoidal and fragmentary glauconite suggests the glauconite is dominantly allogenic. Only the highly fragile cast and lobate grains are considered reliable indicators of authigenic glauconite.

Because distinction of morphological types using the binocular microscope is subjective, an alternative classification based on measured variables using image analysis was attempted. Seven measurements (area, formfactor, convexicity, length, fractal, aspect, and fibre) were made for each grain image. Seven glauconite morphological types were investigated: capsule, cauliflower, fragmentary, lobate, ovoidal, tabular, and vermicular. Measurement data were analysed using canonical variate analysis. The calculated discriminating vectors were then used to distinguish the seven morpological forms. Using two canonical variates 81.5% of the variability within the database was accounted for.

X-ray diffraction studies shows a predominance of poorly crystalline glauconite. Many difficulties were encountered when applying previous literature techniques for calculating the expandable content of glauconite. An alternative technique based on the relationship between $\%K_2O$ and %expandables is favoured for the calculation of %expandables. A relationship between host sediment lithology and glauconite expandable content was found; siltstone = 20-32% expandables in the glauconite, sandstone = 8-15% expandables in the glauconite.

Major element data were obtained with the electron microprobe for 327 individual glauconite grain centres of 70 samples from 45 sites and 7 formations in the Te Kuiti Group. The chemical data were analysed using canonical variate analysis and the seven formations were clearly distinguished. Because only a small glauconite sample size is required (4-5 grains) the technique has potential for determining the stratigraphic correlation of drill core samples and small hand specimens of Te Kuiti Group material containing glauconite.

The range composition of Te Kuiti Group glauconite calculated from EMP major element data using the "Clayform" program is:

$(Si_{3.40\text{-}3.68}\ Al_{0.32\text{-}0.60})\ (Al_{0.08\text{-}0.41}\ Fe^{3+}_{1.00\text{-}1.36}\ Fe^{2+}_{0.19\text{-}0.26}\ Mg_{0.40\text{-}0.60})$
$(Ca_{0.02\text{-}0.16}\ Na_{0.00\text{-}0.04}\ K_{0.49\text{-}0.67})\ O_{10}(OH_2)$

The Te Kuiti Group passes stratigraphically upward from terrigenous and mixed terrigenous-skeletal carbonate deposits to very pure limestones. Early post-depositional diagenetic processes probably released Mg from the carbonate lattice of accumulating skeletal grains. Some of the released Mg was incorporated into the glauconite lattice as evidenced by the increase in Mg content of glauconite stratigraphically upward, parallel with the increased carbonate content of the rocks.

Major and trace element data were obtained using X-ray fluorescence for 29 bulk glauconite concentrates from 21 sites and 5 formations. Notably there were anomalous Mg, Pb and Ni concentrations in glauconite from the Otorohanga - Waitomo - Te Kuiti area. This suggests the area existed as a small semi-enclosed embayment, with a significantly higher terrigenous input compared with adjacent depocentres.

A strong correlation between the La/Ce ratio of glauconite and paleontological and oxygen isotope-derived sea-water temperatures suggests glauconite La/Ce ratio may be a useful paleotemperature indicator.

The data collected in this study show no single previously suggested process adequately decribes the development of glauconite. Rather, glauconite should be considered polygenetic.

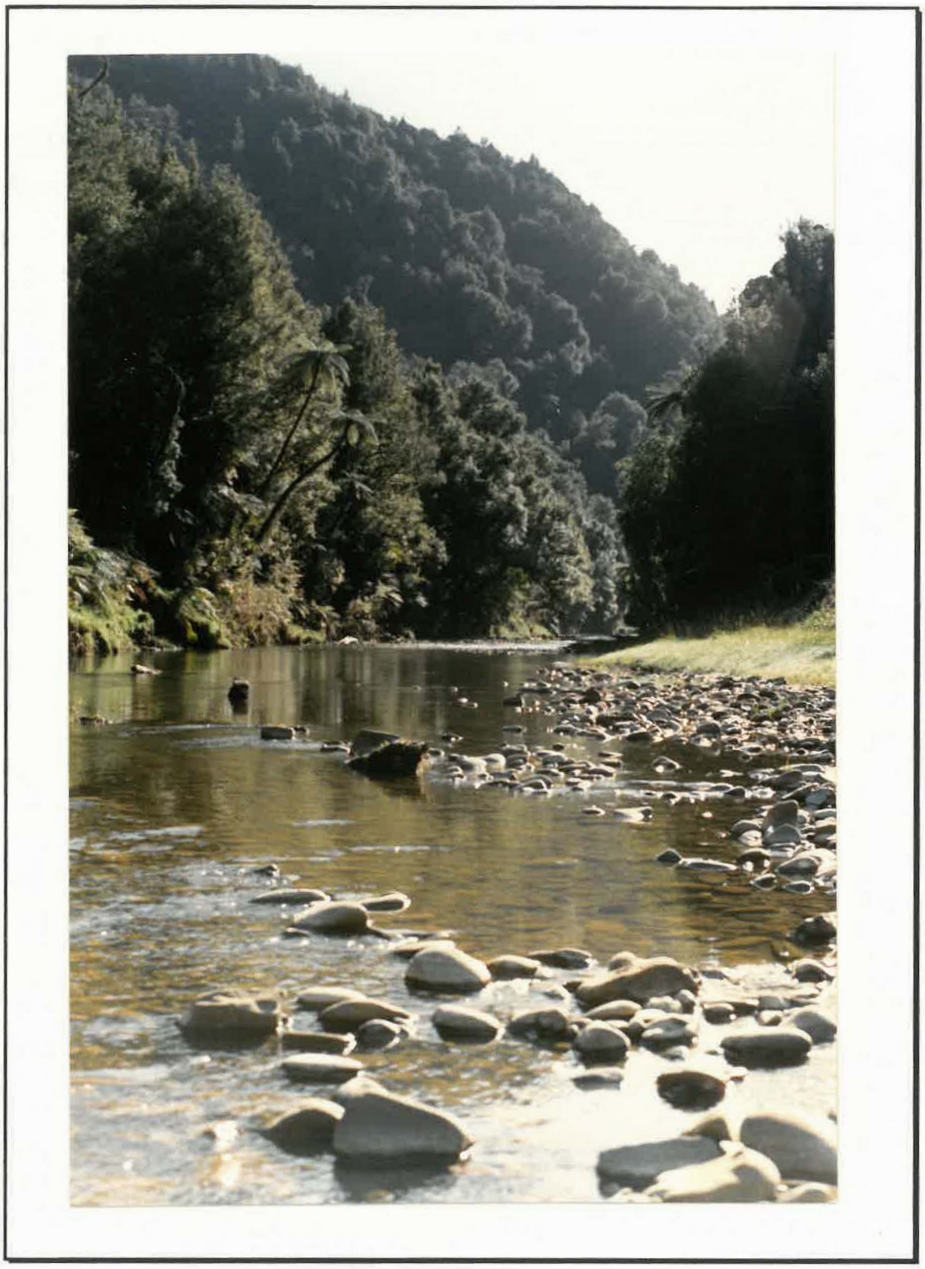

Melius recens quam nunquam

Acknowledgements

Without the assistance of numerous people the completion of a project of this nature would never have been possible. Obviously, I am unable to thank everyone who has been connected with this thesis but I would especially like to thank the following people.

Firstly, I thank my supervisors Cam Nelson and Peter Hodder (Earth Sciences, University of Waikato) for their interest, critical comment, and useful discussion throughout the course of this study.

I thank the kind farmers throughout the South Auckland region who unreservedly permitted me access to their properties for the purpose of collecting glauconite samples, even if those near Huntly took some convincing I was not from Coal-Corp! I also thank Steve Edbrooke and Phillip Kirk (N.Z. Geological Survey, D.S.I.R.) for supplying the drill-hole glauconite samples and for their enthusiasm and interest in the project.

Special thanks to Les Arnold (Chemistry, University of Waikato) for assistance with my eternal and infernal computing problems (and the hours of work on my golf swing!); John Wells (Geography, University of Waikato) for writing the software enabling the interfacing of the image analyzer with the University of Waikato VAX system; Brian Nicholson (Chemistry, University of Waikato) for assistance with the "Lazy Pulverex" and the "Shellx" programs; Books and Open-file Reports Section U.S. Geological Survey for the "Clayform" program; Ray Littler (Statistics, University of Waikato) for assistance with the multivariate statistical analysis portion of this study; Ken Palmer (Geology Department, Victoria University) for use of the x-ray fluorescence and electron microprobe facilities in Wellington; and the staff and my colleagues in the Earth Sciences Department University of Waikato for their humour and often useful discussions on glauconite.

Last, but by no means least, many thanks to my family (the "Compton tribe") whose encouragement and financial assistance made this thesis a reality.

Table Of Contents

Figures

Tables

CHAPTER (1)

INTRODUCTION

(1) INTRODUCTION

(1-1) GENERAL AIMS OF THIS STUDY

Glauconite is commonly found in the late Eocene - Oligocene sediments of the Te Kuiti Group in the South Auckland region of the North Island, New Zealand. The Te Kuiti Group is aerially exposed through much of the western portion of the South Auckland land district (Map 1). Generally the concentration of the glauconite within the Te Kuiti Group sediments is less than 10% but in some localized areas the glauconite concentration may increase up to 75%. Several investigations on the lithology, distribution and formations of the Te Kuiti Group have been made (e.g., Henderson & Grange 1926; Marwick 1946; Player 1958; Kear & Schofield 1959; Hopkins 1966,1970; Hay 1967; Vella 1967; Nelson 1978a; Kear & Schofield 1978; Fergusson 1986). Most authors, however, have made only brief mention of the glauconitic component of the sedimentary units.

The widespread exposure of the Te Kuiti Group, the glauconitic nature of the sedimentary units, and the lack of intensive research on the glauconitic component of the sediment was a major factor in the decision to base an M.Sc. research topic on Te Kuiti Group glauconite.

The decision to investigate the chemical and morphological characteristics of the Te Kuiti Group was prompted by a similarly based study in the South Island of New Zealand by McConchie (1978). The variables obtained from such an investigation can be numerically collated and as such are amenable to computer manipulation and presentation. This was an important consideration with the large data base acquired during this study.

Glauconite has been used in overseas literature studies as a stratigraphic correlation tool (e.g., Burst 1958a; Triplehorn 1966; Xingzhen 1983). These studies used unique properties of the glauconite in the constituent horizons as a discriminator between the horizons. Because numerical data were obtained for chemical and morphological characteristics of Te Kuiti Group horizons it was hoped statistical discrimination techniques (e.g., Stoffers et al. 1984) could distinguish different lithological units within the Te Kuiti Group.

This study relies on a central hypothesis proposed by Burst (1958a, p.324) "reconstruction of sedimentary environments can be aided by glauconite mineral data" or restated within the framework of this thesis:

> *Glauconite of similar lithological origin and/or age in a particular group of deposits should exhibit similar morphological and chemical characteristics.*

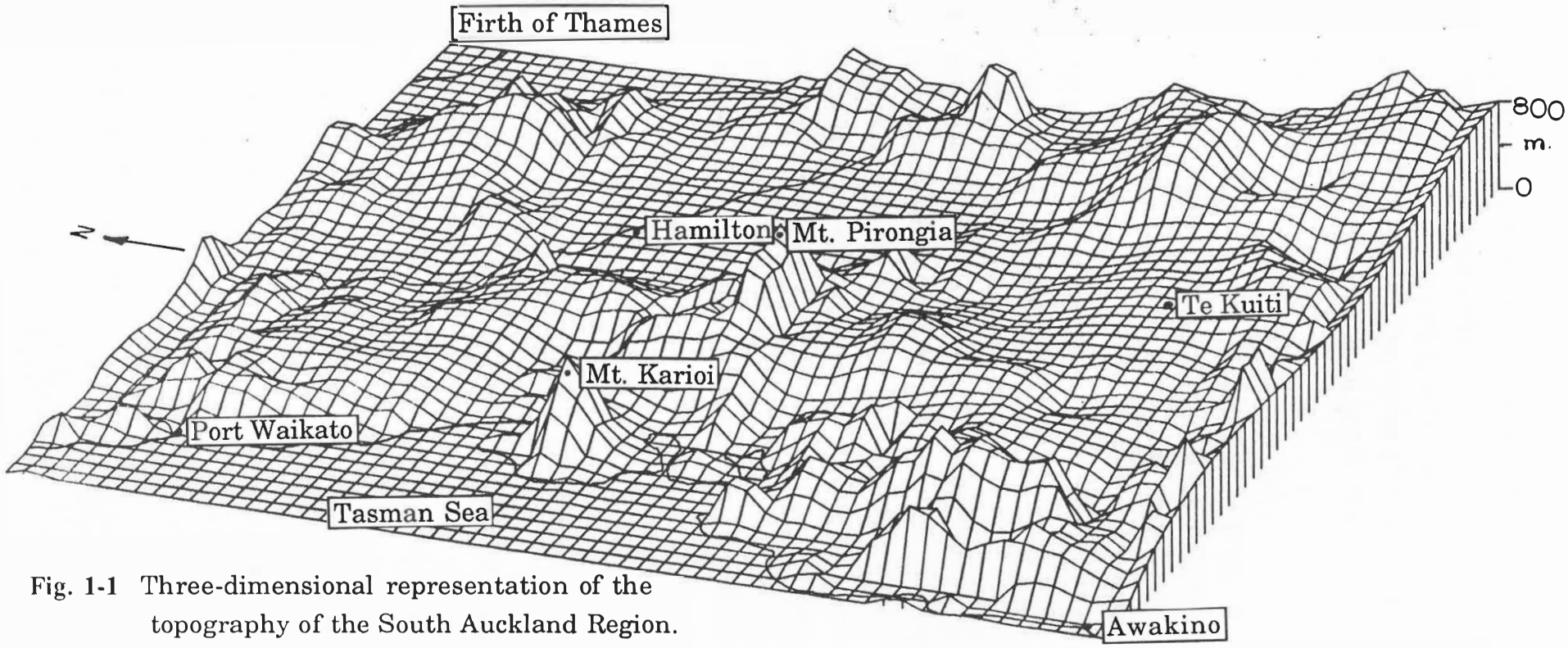

Fig. 1-1 Three-dimensional representation of the topography of the South Auckland Region.

The principal aims of this study are:

(1) Use morphological and chemical characteristics of the constituent glauconite to distinguish between stratigraphic horizons of the Te Kuiti Group.

(2) Increase the understanding of the sedimentological regime present during the deposition of the Te Kuiti Group.

(3) Increase the available knowledge on glauconite *per sē*.

(1-2) LOCATION OF FIELD AREA

The boundaries of the field area for this study were based on:

(1) The field exposure of the Te Kuiti Group in the South Auckland land district (Map 1).

(2) Known glauconitic field exposures and glauconitic core samples.

(3) The logistics of time and accessibility of the investigation area.

The defined field area is shown as a dashed line on Map 1. To show topographical expression in and adjacent to the field area a three dimensional topographical map was developed on the SAS VAX/VMS version 4.7 graphical package (Fig. 1-1). There appears to be a correlation between two major Te Kuiti Group emergent regions in Map 1 (northern and southern areas) and hill country in Fig. 1-1. The distribution of the Te Kuiti Group and the correlation of present topography with the original depositional areas of the group is discussed more fully in Section 3-1.

(1-3) DEFINITION OF MINERAL GLAUCONITE

1-3-1 What is mineral glauconite?

The origin of the term "glauconite" is debated. Cloud (1955, p.484) suggests the name originated "from the mythical fisherman, Glaucus, who was turned into a sea-god, with green hair, a fish's tail, and was unable ever again to leave the sea". Brown (1954), Burst (1958a,b), and McRae (1972) suggest the Greek γλαυκοσ (glaucos), meaning bluish or pale green, is the origin of the term.

The literature use of the term glauconite has become confused since the introduction of the synonym terminology into scientific literature by Brongiart (1823) ("la glauconite"), Von Humboldt (1823) ("grun erde") (in Schneider 1927) and later Keferstein (1828) ("glaukonit") (in McRae 1972). Whether the intended use of glauconite by these early researchers was to describe the earthy green marine pellets found on the sea-floor by

oceanographic research vessels (as described by Von Gumbel 1886 and Murray & Renard 1891, in Bell & Goodell 1967), or whether glauconite was intended to describe a particular mineral, is not clear. Inconsistent terminological has led to the reclassification of many glauconite-like materials, depending on the mineralogical or morphological bias of the author (e.g., the classifications of Dana 1882; Schneider 1927; Gruner 1935; and Correns 1937, in Burst 1958a).

To help clarify the problem McRae (1972) proposed that "glauconite" be restricted to morphological interpretations and "mineralogical glauconite" be restricted to a distinct mineral species. This interpretation was originally suggested by Hendricks & Ross (1941) based on Von Humboldt's (1823) and Keferstein's (1828) use of glauconite in a descriptive sense. French literature has avoided the linguistic problem by adoption of la glaucony (pl. glauconie) for morphological glauconite and restricting the name glauconite to a distinct mineral species (Millot 1964; Odin & Matter 1981; Berg-Madsen 1983). There is no current movement towards the French convention and McRae's (1972) recommendation seems adequate.

1-3-2 Definition of Mineral Glauconite

"The derivation of a formula for glauconite has occasioned considerable discussion" (Hutton & Seelye 1941, p.603). Glauconitic minerals are a hydrous, iron-alumino silicate compositional series, ranging from a low iron, low potassium (~3 wt.% K) smectite to a 10Å dioctahedral mica (Burst 1958a,b; Hower 1961; Bentor & Kastner 1965; McRae 1972; Van Houten & Purucker 1984; Amouric & Parron 1985). The 1978 AIPEA Nomenclature Committee has arbitrarily defined mineral glauconite as "an Fe-rich dioctahedral mica with tetrahedral Al(or Fe^{3+}) usually greater than 0.2 atoms per formula unit and octahedrally coordinated R^{3+} correspondingly greater than 1.2 atoms" (Bailey 1980a,p.75).

1-3-3 Polytypism in mineral glauconite

X-ray diffraction (XRD) precession photographs of monomineralic glauconite have revealed 3 basic structural polytypes (Table 1-1).

Table 1-1 Structural polytypes of mineral glauconite (adapted from Warshaw 1957; Burst 1958a, 1958b; Hower 1961; Bentor & Kastner 1965; McRae 1972; McConchie & Lewis 1980; Amouric & Parron 1985).

(1) Well ordered **1M structure**. Characterized by a basal lattice spacing of 10 Å (001), sharp symmetrical peaks at 4.53Å (020), 3.33Å (003), and 2.50Å (130), reflections 112 and 112 always present. Smectitic (expandable) component <10%. Moderately abundant.

(2) Disordered **1Md structure**. Asymmetric basal broadened XRD peaks, reflections 112 and 112 are absent. Smectitic (expandable) component 10-50%. Most abundant glauconite mineralogical form.

(3) Unstable **$2M_1$ structure**. Recently revealed by high resolution transmission electron microscopy. The relationship of this group to the above groups has not been clearly demonstrated. Possibly this structure represents an unstable intermediary, formed locally due to octahedral layer charge anomalies.

1-3-4 Structural formulae for mineral glauconite

Development of a structural formula for glauconite has paralleled the advancement of chemical analytical techniques and the availability of XRD facilities. Using total chemical analyses early workers could only conclude that glauconite was a hydrated potassium aluminium silicate (e.g., Hoskins 1895; Clarke 1903 in McConchie 1978; Clarke 1908 (Table 1-2); Hallimond 1922). The advent of XRD technology led to the realization that glauconite has a mica-type structure. Structural formulae were modified to account for this factor (e.g., Ross 1926; Schneider 1927; Gruner 1935; Takahashi 1939) (Table 1-2). The heterogeneity of mineral glauconite involving interstratification within the morphologically classified glauconite pellets, was not established until publication of the researches of Warshaw (1957) and (Burst 1958a,b). Further significant studies on the interlayered nature of glauconite included Hower (1961), Manghani & Hower (1964), and Bentor & Kastner (1965). Work by Buckley et al. (1978) and Bailey (1980b) led to refinement of earlier proposed

Table 1-2 Mineral formulae proposed for glauconite (only a small portion of **all** proposed glauconite formulae are presented). An orderly progression with time from a hydrated iron-silicate composition, to a variable composition micaceous-type silicate is evident from the table.

Author	Proposed mineral formula for glauconite
Clarke 1908	$Fe^{3+}KSi_2O_6$ + aq.
Ross 1926	From K_2O-2(Mg,Fe)O-2$(Fe,Al)_2O_3$-10SiO_2 + 5H_2O to K_2O(Mg,Fe)O-3$(Fe,Al)_2O_3$ -10SiO_2 + 5H_2O
Schneider 1927	(K,Na)(Fe,Mg)$(Fe,Al)_3.Si_6O_{18}.3H_2O$
Gruner 1935	$K_{2-3}(Mg,Fe^{2+},Ca)_{1-3}(Fe^{3+},Al,Si)_{3-6}(Si_{13-14}, Al_{2-3})O_{38-40}(OH)_{6-10}$
Takahashi 1939	$(K,Na)_{2.7-3.3}(Mg,Fe^{2+})_{2.1-2.6}(Fe^{3+},Al,Si)_{4.9-6.1}(Si_{14}Al_2)O_{37-41}(OH)_{11-14}$
Hendricks & Ross 1941	$(K,Ca_{0.5},Na)_{0.84}(Al_{0.47}Fe^{3+}_{0.97}Fe^{2+}_{0.19}Mg_{0.40})(Si_{3.65}Al_{0.35})O_{10}(OH)_2$
Burst 1958a	$K_{0.79}Ca_{0.05}(Al_{0.35}Fe^{3+}_{1.06}Fe^{2+}_{0.25}Mg_{0.41})(Si_{3.61}Al_{0.39})O_{10}(OH)_2$ or $K_{0.76}(Na,Ca)_{0.13}(Al_{0.40}Fe^{3+}_{0.87}Fe^{2+}_{0.49}Mg_{0.40})(Si_{3.42}Al_{0.58})O_{10}(OH)_2$
Buckley et.al. 1978	$R^{1+}_{0.91}(R^{3+}_{1.34}R^{2+}_{0.69})(Si_{3.73}Al_{0.27})O_{10}(OH)_2$
Bailey 1980b	$K(R^{3+}_{1.33}R^{2+}_{0.67})(Si_{3.67}Al_{0.33})O_{10}(OH)_2$
Odin & Matter 1981	$K_{(x+y)}(Fe^{3+},Al,Fe^{2+},Mg)_{\sim 2}(Si_{(4-x)}Al_x)_{\sim 4}O_{10}(OH)_2$, x varies from 0.2 - 0.6, and y varies from 0.4 - 0.6
Koster 1982	$K^+_{0.8}(Al_{0.5}Fe^{3+}_{1.0}Fe^{2+}_{0.1}Mg_{0.4})(Si_{3.7}Al_{0.3})O_{10}(OH)_2$

mineral formulae for glauconite. Two recent pieces of literature by Odin & Matter (1981) and Koster (1982) show opposite approaches to the problem of defining mineral glauconite (Table 1-2). Odin & Matter give a generalized compositional range formula, while Koster uses a group mean approach. The latter approach is probably the more fruitful in the long term search for a **type-mineral** glauconite, the former may offer suitable boundaries for the field of glauconite-like minerals.

Problems inherent in defining a mineralogical formula for glauconite include:

(1) The known interlayering within the glauconite structure. Interlayering variation will cause changes between calculated structural formulae (see McRae 1972, p.410).

(2) Formulae are rarely corrected for the presence of impurities, e.g. exchangeable cations (Foster 1951), mineral inclusions (Hendricks & Ross 1941; Alexiades & Jackson 1966), and non-structural metal hydroxides (Bentor & Kastner 1965,Murray & Mackintosh 1968; Thompson & Hower 1975). If octahedral occupancy is within 0.05 of the ideal (i.e., two per three octahedral sites) then significant interlayer metal-hydroxy complexes are probably absent (Thompson & Hower 1975; Rolf et al. 1977).

CHAPTER (2)

PREVIOUS STUDIES OF GLAUCONITE

(2) PREVIOUS STUDIES OF GLAUCONITE

(2-1) MORPHOLOGICAL CHARACTERISTICS OF GLAUCONITE

2-1-1 External morphology of glauconite

External morphological classifications of glauconite can broadly be divided into those concerning features observed under macro- and micro-magnification. Macro-morphological classifications are based on binocular microscope observations. Micro-morphological classifications have been developed to describe the morphological features observed under the scanning electron microscope (SEM).

2-1-1A Macro-morphological divisions

Glauconitic grains are generally of fine to medium sand-sized divisions of the Wentworth scale (100 - 500 μm (in McRae 1972)). Differences in the morphology of glauconite have been attributed to mineralogical variability (Ehlmann et al. 1963) and environmental conditions acting upon the grains (Triplehorn 1966; Berg-Madsen 1983).

Most authors have adopted Triplehorn's (1966) classification scheme, with 9 morphological classes and the amendments suggested by Konta (1967) (Table 2-1). McConchie & Lewis (1980) have suggested the addition of two new classes to this scheme: (a) fragmentary, and (b) spongy, cauliflower, or serrulate grains. Berg-Madsen (1983) has proposed the term "moldic" replace the "fossil casts and internal moulds" division of Triplehorn (1966). The moldic term is not adopted in this study because internal mould does not imply a solely organic origin, as suggested by Berg-Madsen (1983). A more general objection to Berg-Madsen's assertion is that genetic considerations should not be included in a descriptive morphological classification.

The characteristics of the macro-morphological divisions adopted for this study are shown in Table 2-1.

Table 2-1 External macro-morphological classification scheme (adapted from Triplehorn 1966; Konta 1967; McRae 1972; McConchie & Lewis 1980; Van Houten & Purucker 1984).

MORPHOLOGICAL SUBCLASS TYPE	COLOUR	SHAPE	SURFACE	ORIGIN	GENERAL	PICTORIAL
Ovoidal or Spheroidal	Generally med-dark green	Simple, rounded, equidimensional	Generally smooth	Chem/colloid ppt., abrasion product, not diagnostic	Surface polish indicates transport	Fig. 2-1A
Tabular or Discoidal	Pale to medium green	Flattened, plate-like, disk-shaped	Smooth, may be pock-marked	Cleaved from vermicular grains, inherited shell fragment shape, clay shale chips	May be mammillated or single grains	Fig. 2-1B
Lobate	Pale with dark green zones	Irregular	Triangular radial cracks, resembles popcorn	Fragility suggests in situ		Fig. 2-1C
Vermicular		Elongate, concertina, often curved	Lateral cracks well developed, micaceous	Long stacks suggest in situ, biotite progenitor (Galliher 1939)		Fig. 2-1D

(continued next page)

MORPHOLOGICAL TYPE	SUBCLASS	COLOUR	SHAPE	SURFACE	ORIGIN	GENERAL	PICTORIAL
Capsule-Shaped Pellets		Earthy to dark green	Compact, oblong, ellipsoidal	Generally smooth, some porous less developed pellets	Fecal pellets (Takahashi & Yagi 1929)		
Fossil casts and internal moulds			Mirrors cavity infilled	Generally fine grained, highly variable surface	Alteration or direct ppt. within test cavities or inorganic moulds	Easily destroyed by transport, very fragile	Fig. 2-1E to Fig. 2-1H
Fragmentary	Subclass A Roundness <0.5		Physically broken grains indeterminate origin	Variable determined by transport, source, etc.	Perigenic abrasion of original particle	Roundness indicates distance of transport	
	Subclass B Roundness >0.5 (Powers 1953 scale)		Physically broken grains indeterminate origin	Variable determined by transport, source, etc.	Allogenic, abrasion product of Subclass A	Roundness indicates distance of transport	
Spongy, Cauliflower, Serrulate			Variable, dominantly ovoid, generally grain origin determines	Porous, rounded and distinct angular edged pores	Surface texture from diagenetic chemical attack (McConchie & Lewis 1978)		Fig. 2-1I

(continued next page)

MORPHOLOGICAL SUBCLASS TYPE	COLOUR	SHAPE	SURFACE	ORIGIN	GENERAL	PICTORIAL
Composite	2 or more optically distinct mineral species	Variable generally ovoid or fragmentary	Variable, often porous	Multiple glauconitisation episodes, inclusions of unaltered minerals		Fig. 2-1J and Fig. 2-1K

MORPHOLOGICAL PHOTOGRAPHS TO ACCOMPANY TABLE 2-1

NOTE - Morphological slide, 3D slide, and thin section terms refer to the manner in which the slide was prepared, as described in Fig. 4-1.

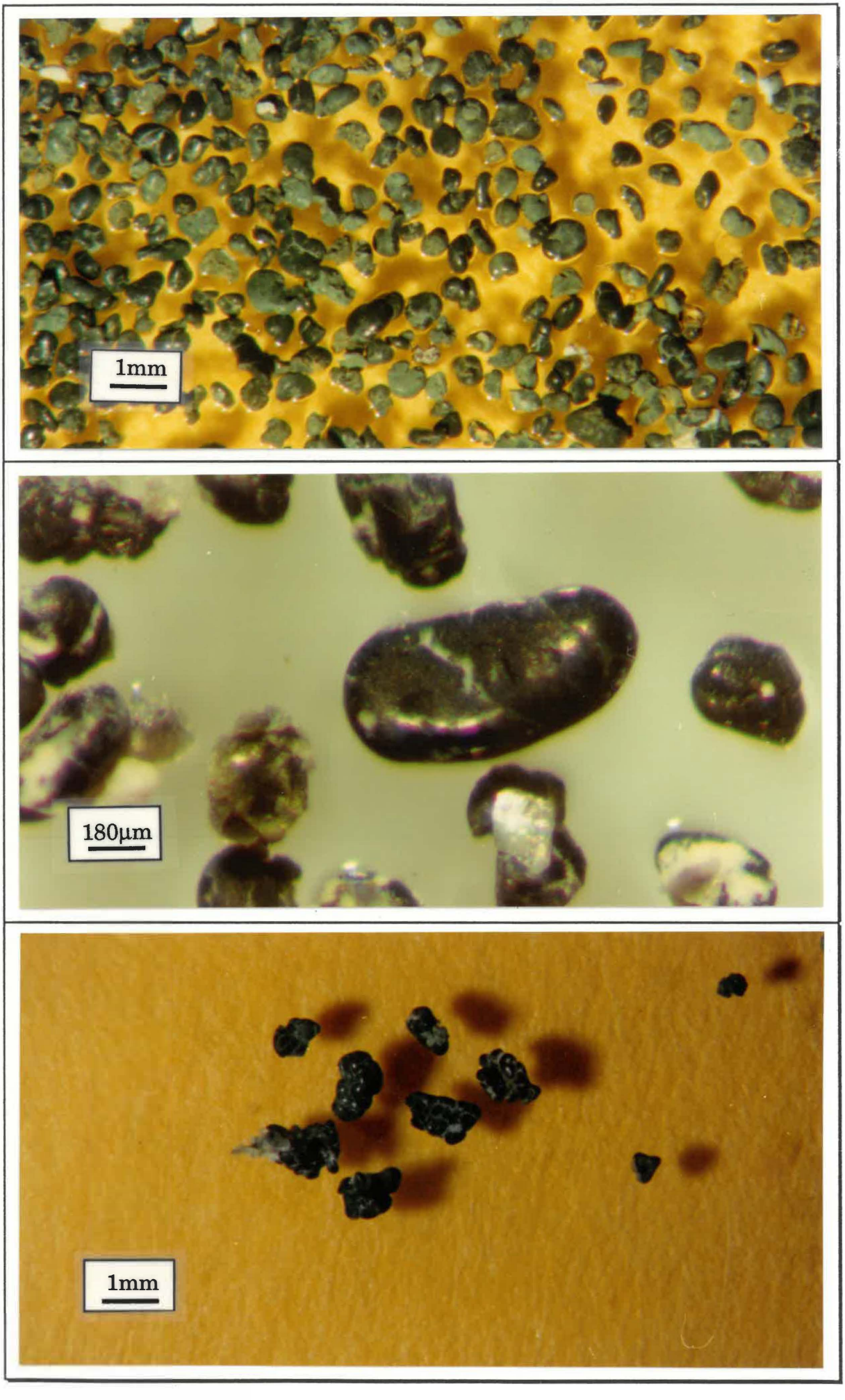
1mm
180µm
1mm

Fig. 2-1A Dominantly ovoidal shaped grains, with occasional fragmentary shaped grains. Dark-green grains are highly evolved glauconite, lighter-green grains are moderately evolved glauconite. Sample MC11b (Elgood Limestone). 10X magnification. Reflected light inclined at 30°. Morphological slide.

Fig. 2-1B Single tabular or discoidal grain (centre of photograph). Highly evolved glauconite. Sample MC18 (Aotea Sandstone Ao5). 55X magnification. Reflected light inclined at 60°. Morphological slide.

Fig. 2-1C Lobate morphological form glauconite grains. Highly evolved glauconite. Angular crystalline adherance on lower left grain is quartz. Sample MC19a (Orahiri Limestone OrB5). 10X magnification. Reflected light inclined at 30°. Morphological slide.


31µm
1mm
167µm

Fig. 2-1D Dominantly vermicular form grains. Moderately evolved glauconite. Sample MC19b (Aotea Sandstone Ao4). Reflected light inclined at 60°. Morphological slide.

Fig. 2-1E Fossil cast with three evolutionary stages evident. The lower right form has dark flecks which are glauconitic. Morphological form is referred to by Nelson (1973) as steinkern. Sample courtesy of C.S.Nelson. 10X magnification.

Fig. 2-1F Central porous sponge like grain is a partially glauconitised echinoderm spine. Cast formed glauconite. The glauconite is only in the nascent stage of Odin & Matter (1981). Sample MC22 (Orahiri Limestone OrB1). 60X magnification. Reflected light inclined at 60°. Morphological slide.

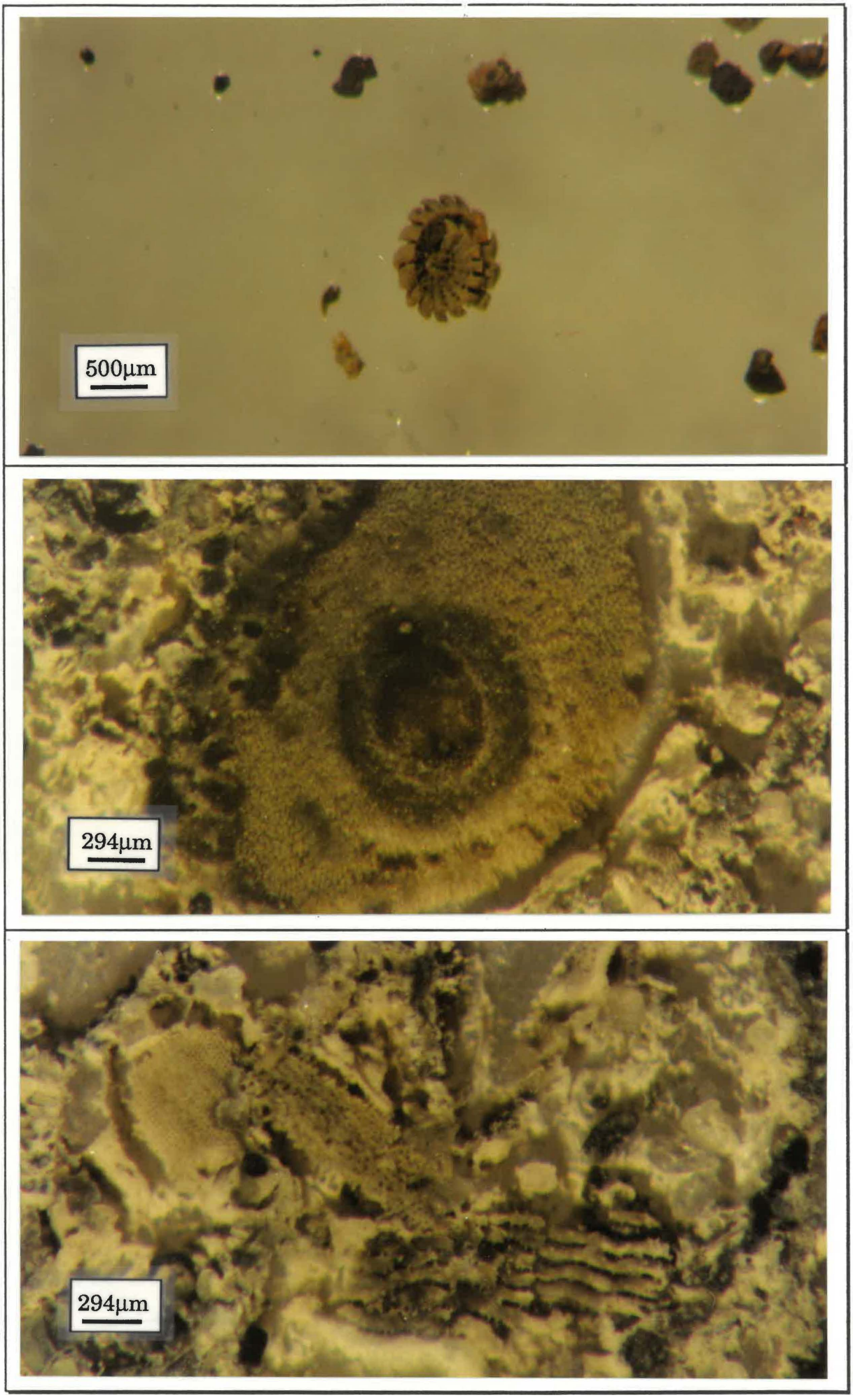
500µm
294µm
294µm

Fig. 2-1G Benthic foraminifera cast-infill. Moderately glauconitic. Highly fragile nature suggests transportation of this glauconite grain has been minimal. Sample MC22 (Orahiri Limestone OrB1). 20X magnification. Reflected light inclined at 60°. Binocular morphology slide.

Fig. 2-1H Section through an echinoderm plate or spine showing concentrically orientated zones of variable glauconitisation. The central portion of the plate or spine has more evolved glauconite compared with the outer portions of the grain. Sample MC29 (Orahiri Limestone OrB2). 34X magnification. Reflected light inclined at 30°. 3D slide.

Fig. 2-1I Poorly evolved glauconite as a cast infill features. Wavy feature at the bottom centre of the photograph is a bryozoan cast. Sponge or mat like feature at the middle left of the photograph is an echinoderm plate cast. Sample MC29 (Orahiri Limestone OrB2). 34X magnification. Reflected light inclined at 30°. 3D slide.

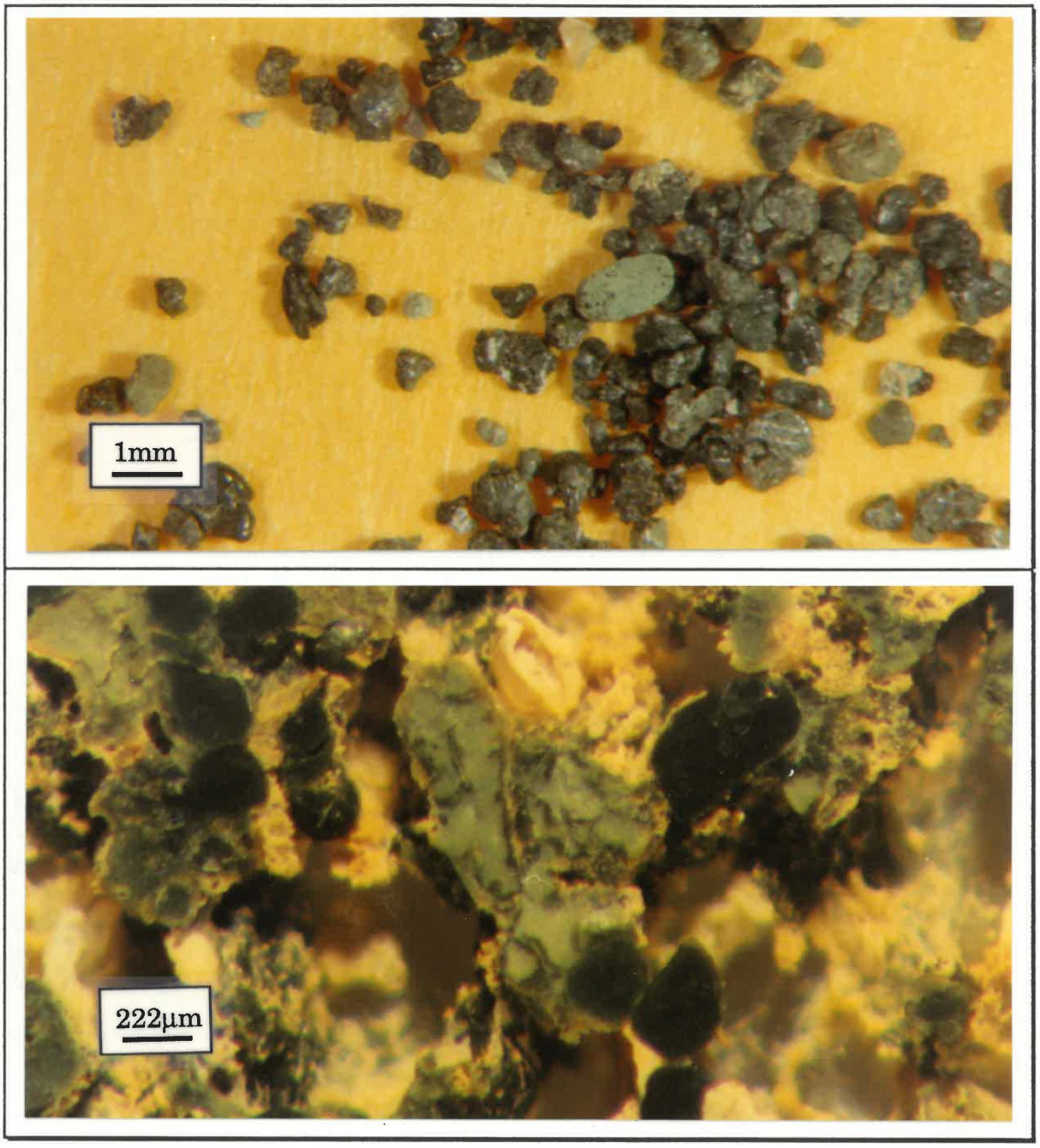
1mm
222µm

Fig. 2-1J Single large composite grain (light green) within a more glauconitised (dark green) predominantly fragmentary form glauconite. Dark specks on composite grain are thought to represent a secondary phase of glauconitisation. Sample MC36b (Aotea Sandstone Ao3). 10X magnification. Reflected light inclined at 30°. Morphological slide.

Fig. 2-1K Section through a fragmented lobate grain. There are two stages of glauconitisation evident: an outer peripheral-crack zone of highly evolved glauconite; and a central grain portion of less evolved glauconite. This appears to be a complete reversal of the glauconitisation pattern seen in Fig. 2-1H. Possibly the different substrates upon which the glauconitisation process are acting influences the pattern of glauconitisation. Sample MC11b (Elgood Limestone). 45X magnification. Reflected light inclined at 30°. 3D slide.

2-1-1B Micro-morphological divisions

The SEM has revealed several micro-morphological features of glauconite grains. The large number of terms proposed to describe the micro-morphological structures of glauconite include:

(1) lath-shaped booklets (Burst 1958b);
(2) lath-shaped plates, equilateral plates (McRae 1972);
(3) globules, caterpillar, box-work, rosette, lamellae (Van Wie 1971; Hein et al.1974; Odom 1976; Odin & Matter 1981; Valeton et al. 1982);
(4) lamellar (Amouric & Parron 1985); and
(5) laminated, wheatsheaf, automorphic rosette (Hughes & Whitehead 1987).

Many of the descriptive terms within the above classes are synonyms and as such are redundant.

The association of grain type with evolutionary stage proposed by Odin & Matter (1981) is adopted for this study. The divisions are:

(a) nascent glauconite - dominated by globular or caterpillar structures;
(b) evolved glauconite - dominated by box-work or rosette structures (equivalent to wheatsheaf or automorphic rosette); and
(c) highly-evolved glauconite - dominated by lamellae structures (equivalent to lath-shaped booklets and plates, equilateral plates, and laminated structures).

The above evolutionary divisions imply that the degree of development of the glauconite within a deposit may be determined by the predominance of a micro-morphological form.

2-1-2 Internal morphology of glauconite

Internal morphology of glauconite grains can aid in the deduction of processes acting upon the glauconite during formation. The nomenclature divisions of Carozzi (1958,1960), Wermund (1961), Triplehorn (1966), McRae (1972) and McConchie & Lewis (1980) can be combined to give the following classification of internal structure for glauconite grains:

(1) Random microcrystalline - "homogeneous aggregates of overlapping micaceous flakes without any preferred orientation....by far the most common internal structure [for glauconite grains]" (Triplehorn 1966, p.258).
(2) Oriented microcrystalline - probably lamellar aggregates of micaceous sheets with a high degree of parallel orientation (Warshaw 1957).
(3) Micaceous or vermicular - similar to the orientated microcrystalline division but with incipient micaceous cleavage.
(4) Concentrically orientated coatings on detrital grains.
(5) Fibroradiated rims - peripheral zone of small elongated crystals with radial orientation if precipitated in situ (Zumpe 1971; Odom 1976;

McConchie & Lewis 1980), or a tangential corona if accreted by rolling (Triplehorn 1966; Van Houten & Purucker 1984).

(6) Patch-oriented microcrystalline - grains with a generally random microcrystalline fabric but significant regions of oriented crystallites within the matrix.

(2-2) X-RAY DIFFRACTION (XRD) STUDIES ON GLAUCONITE

XRD studies on glauconite have been an important factor in the determination of the interlayered nature of glauconite and the structural polymorphs of the mica-type sheet silicate present.

2-2-1 XRD classification schemes for glauconite

As a consequence of the extensive XRD investigations of glauconite (e.g., Schneider 1927; Gruner 1935; Galliher 1939; Grim et al.1951; Warshaw 1957; Burst 1958a,b; Hower 1961; Manghnani & Hower 1964; Bentor & Kastner 1965; Tapper & Fanning 1968; McConchie 1978; McConchie & Lewis 1980; Odin & Matter 1981), various classification schemes have been proposed for glauconite. However, most authors have tended toward a classification model based on the polytype divisions described in Section 1-3-3 (see Table 2-2).

Glauconite can be considered to be a "more or less continuous sequence of minerals with increasing amounts of expandable layers" (McRae 1972, p.405). The expandable component of the lattice is essentially smectite-like in form (Brindley 1980). Estimation of the percent expandable component has been made in two ways:

(1) The d(001) spacing has been correlated to computer-generated XRD trace patterns with varying proportions of expandable layers (e.g., Reynolds & Hower 1970; Thompson & Hower 1975; Reynolds 1980).

(2) Changes in the d(001) spacing have been observed after glycolation and subsequent heating (e.g., Bell & Goodell 1967; McConchie 1978).

Table 2-2 X-ray classification schemes proposed for glauconitic materials.

Burst (1958a,b)	Hower (1961)	Bentor & Kastner (1965)	McConchie & Lewis (1980)
Well-ordered - non-swelling high potassium content lattice showing sharp symmetrical peaks characteristic of a micaceous 10Å lattice at 10, 5, and 3.3Å. This constitutes type mineral glauconite.	≤ 10% expandable layers[1] (montmorillonite)	**Class 1:** mineral glauconite **(a)** well-ordered 1M polymorph with symmetric and sharp diffraction peaks at 10.1, 4.53, 3.3Å.Reflections (112) and (11$\bar{2}$) are always present.	**Class 1:** Well Ordered glauconite (mineral glauconite): Disorder coefficient (D.C.[2]) is ≤0.25. (Sharp symmetrical XRD peaks will be apparent. Most glauconites with <10% expandables [3] will be included).
Disordered - non-swelling, low potassium lattice, micaceous and monomineralic but with subdued peaks, displays broad bases and asymmetric peak sides.	10 - 20% expandable layers (montmorillonite)	**(b)**disordered 1Md polymorph with asymmetric basal diffractions broadened at the base. Reflections (112) and (112) are absent.	**Class 2:** Disordered glauconite **(a)**Moderately disordered glauconite: 0.25<D.C.≤0.5 and percent expandables ≤40%. (The XRD pattern may show some peak asymmetry).**(b)**Extremely disordered glauconite: D.C.>0.5 and percent expandables ≤40%. (The XRD pattern will show pronounced peak asymmetry).

(continued next page)

Interlayered clay mineral - extremely disordered, expandable, low potassium montmorillonite type lattice.	>20%expandable layers (montmorillonite)	**Class 2**: interlayered glauconite d(001) >10.15Å.	**Class 3:** Interlayered glauconite: Contains more than 40% expandable layers but only 1 distinct mineral type is apparent.
Mixed mineral - mixtures of two or more clay minerals as normal constituents - the most frequent combinations are illite with montmorillonite and illite with chlorite.		**Class 3:** Mixed mineral (a)two or more clay minerals (b)mixtures of clay with non-clay minerals.	**Class 4:** Shows the presence of 2 or more distinct mineral varieties, only 1 of which is glauconite. This class can be divided into the two subclasses (a)two or more clay minerals, (b)mixtures of clay with non-clay minerals.

[1] - % Expandables read from the curves of Brown & MacEwan (1951) and Weaver (1956), relates d-spacing of the d(001) reflection to the amount and type of interlayering.

[2] - Disorder coefficient (D.C.) as defined by McConchie et al.(1979) is:

$$D.C. = \frac{t*b}{(h-b)}$$

t = half-height line width of the 10Å peak for the 400°C heated oriented mount measured in 2θ degrees.

b = background intensity of the 10Å peak.

h = intensity of the 10Å peak.

[3] - % Expandables (in McConchie 1978)

$$\% \text{ Expandables} = \frac{(10ÅF)-(10ÅEG)*100}{10ÅF}$$

10ÅF = height of 10Å peak after firing to 400°C for 1 hour.

10ÅEG = height of 10Å peak after exposure to an ethylene glycol atmosphere for 48 hours.

2-2-2 Problems associated with XRD classification of glauconite

The method of glycolation and subsequent heating has been extensively used in the literature for the calculation of percent expandables, but problems with the method that require attention include:

(a) Various authors have advocated different temperatures of dehydration for the smectitic component (e.g., 180°C (Griffin 1971), 375°C (Austin & Leininger 1976), 400°C (McConchie 1978), 300°C (MacEwan & Wilson 1980)). The time for which the sample has been heated and whether the sample is cooled before scanning have also been shown to have significant effects on the 10Å peak height (i.e., the measured parameter of the expandable component calculation) (Austin & Leininger 1976).

(b) Associated with (a) has been the non-allowance of dehydration effects on interlayer metal-hydroxy complexes and the consequential change in XRD traces (Section 2-4-2 shows the temperature to metal-hydroxy dehydration relationship). In hydrated layer silicates, progressive contraction of the basal lattice spacing occurs with progressive heating. This can be accounted for by assuming dehydration causes the rotation of the surface oxygen triads of the silicate sheet (MacEwan & Wilson 1980). Eirish & Tret'yakova (1970), however, have shown that the b cell dimension of montmorillonite saturated with a variety of cations can **increase** on heating to 260°C. Therefore, to determine the percent expandables present the temperature at which the glauconite sample is heated should be above the temperature of smectitic layer expansion yet below the metal-hydroxy dehydration temperature.

For the calculation of a disorder coefficient (see McConchie & Lewis 1980 p.416) the heating temperature can be raised above the complete dehydroxylation temperature because the disorder coefficient measures lattice defects (which are enhanced by the elevated temperature).

The variation in optimum heating temperature required for calculation of percent expandables versus that required for the calculation of the disorder coefficient suggests there is little relationship between disorder coefficients and percent expandables.

(c) Jonas & Thomas (1960) have shown that the proportion of K^+ ions and other interlayer cations strongly influences the uptake of organic molecules such as ethylene glycol (in MacEwan & Wilson 1980). As glauconite has a variable K^+ content (3-8%), ethylene glycol will be variably uptaken by the lattice, depending on: (a) the percent expandables; and (b) the cationic distribution and content of the lattice. The assumption generally made is that 48 hours of exposure to an ethylene glycol atmosphere is sufficient time for complete expansion of the lattice to have

occurred. However, the lattice cationic distribution (which is a function of the initial substrate cation distribution and diagenetic modifications) combined with the proportion of expandable layers present controls the ability of the lattice to expand. Therefore, it is doubtful that the technique of ethylene glycol saturation is valid for a mineral of such variable composition.

(2-3) CHEMICAL STUDIES OF GLAUCONITE

2-3-1 Wet chemical techniques

Use of wet chemical techniques in the investigation of glauconite composition has become less common with the advent of machine-based electron excitation techniques (i.e., XRF, EMP). In general, wet chemical techniques involve the acid digestion of a given rock sample and subsequent analysis of the solute by atomic absorption spectrometry (e.g., Burst 1958b; Nelson 1973; Harder 1980; Bornhold & Giresse 1985), flame emission spectrometry (e.g., Nelson 1973), and titanometric techniques (e.g., Burst 1958b; Bentor & Kastner 1965; Nelson 1973; Harder 1980). Nelson (1973, p.872) gives a summary of some wet chemical techniques for the calculation of SiO_2, CaO, MgO, FeO, Fe_2O_3, Cr_2O_3, Na_2O, K_2O, TiO_2, MnO, P_2O_5, H_2O^+, H_2O^- (i.e., the oxides required for the calculation of a silicate mineral formula).

A major problem with wet chemical techniques is the quantity and purity of glauconite required to obtain a reliable and representative chemical analysis.

2-3-2 X-ray fluorescence technique (XRF)

"Previous attempts to use bulk chemistry as a basis for examining clay mixtures (e.g., Imbrie & Poldervaart 1959; Nicholls 1962; Miesch 1962; Pearson 1978) have met with limited success due to the variability of clay compositions" (Gold et al. 1983, p.193). However, rapid analysis of a wide range of elements with a high degree of analytical precision is possible using XRF. The XRF technique requires around 5 grams of pure glauconite extract. Since XRF provides a bulk average chemical analysis for the sample it cannot take into account any surface contaminants on the glauconite grains. This analysis may be misleading for a sample of multiple origin, as the average may in fact not represent the mean of either of the component populations.

2-3-3 Electron microprobe technique (EMP)

Recent investigations on glauconitic material (e.g., Velde & Odin 1975; Odom 1976; Velde 1976; Berg-Madsen 1983; Gold et al. 1983; Ireland et al. 1983; Hughes & Whitehead 1987) have adopted EMP as the most suitable technique for the investigation of the chemistry of glauconite. The advantage of EMP is that the micrometer size of the focused electron beam allows chemical analysis at specific sites on the glauconite grain. This allows the investigation of within-grain variation.

EMP analyses suffer from the fact that the inherent porosity of glauconite grains increases with decreased glauconitisation of the grain (Bornhold & Giresse 1985). This leads to increased random scatter of the beam and lower percentage total returns for the analysis of nascent glauconite grains. Berg-Madsen (1983) advocated that because analyses with less than 77% total return show low amounts of SiO_2 they should be discarded and this procedure is adopted here.

Since the ratio of percentage returns for a given element is constant irrespective of the total percentage return (i.e., 60% Fe_2O_3 [95% total probe return] is equivalent to 53% Fe_2O_3 [84% total probe return]), normalization is feasible. In this study 310 EMP analyses with more than 77% return were sampled, the group median was then calculated and used as a type mineral glauconite EMP analysis. Other EMP analyses were normalized to the type glauconite analysis. The percentage total return value will always be less than 100% in hydrated phyllosilicates (e.g., glauconite) because water is not accounted for in the analysis (it is volatilized during probing). Moreover, K, Ca, and Na are slightly volatile, although use of a defocused beam minimizes this problem.

(2-4) MINERALOGICAL STUDIES OF GLAUCONITE

2-4-1 Infrared (IR) studies of glauconite

The IR technique is useful in determining the proportion of substitution of iron by aluminium in the octahedral layer (Manghani & Hower 1964). Shifts in the 9-11μm peak have also been correlated to the percent expandables for glauconite by Manghani & Hower (1964) and McConchie & Lewis (1978). The relationship was previously shown by Ehlmann et al. (1963, fig.7) but the cause of the peak shift was not considered. This technique offers an alternative to the calculation of percent expandables by the XRD technique. IR traces were collected for several samples in this study and correlated to

the % expandable curves of Manghani & Hower (1964) and McConchie (1978) (see Section 5-4).

2-4-2 Thermogravimetric (TGA) and differential thermal analysis (DTA) of glauconite

Various TGA studies have been undertaken on glauconite (Ross 1926; Takahashi 1939; Nutting 1943; Sabatier 1949 in McRae 1972; Schultz 1971; Thompson & Hower 1975). The studies show weight losses occur in the 20°C to 150°C range and the 400°C to 600°C range (i.e., the endothermic peaks on DTA traces). A generalized TGA curve for glauconite minerals is shown in Fig. 2-2.

DTA studies of glauconite have also been undertaken by numerous authors (Table 2-3). The data from Table 2-3 were compiled to produce a generalized DTA graph for glauconite (Fig. 2-2). The principal peaks (1 to 5) on Fig. 2-2 have been assigned to:

(1) Loss of adsorbed water. McRae & Lambert (1968) note that the height of this peak is proportional to the percentage of expandable layers (McRae 1972).

(2) Oxidation of structural Fe^{2+} (Hoebeke & Dekeyser 1954a,b) associated with a loss of OH^- ions.

(3) Complete dehydroxylation of the lattice. Peak height and position are controlled by the heating rate (McRae 1972).

(4)&(5) Recrystallization to spinel-form minerals (Hoebeke & Dekeyser 1954a,b). Peak position relates to the percentage Fe^{3+} in the glauconite lattice (McConchie & Lewis 1978).

As previously mentioned, the position of peak (2) is important in XRD studies. If an expandable component is calculated based on the difference in peak height of the 10Å basal spacing after glycolation and heating it is important **not** to attain this temperature. At and above peak (2) dehydration of interlayer hydroxy complexes will alter basal lattice spacings; this is caused by rearrangement of the silicon-oxygen tetrahedra charge balance due to cation polarizing effects (Brindley 1980).

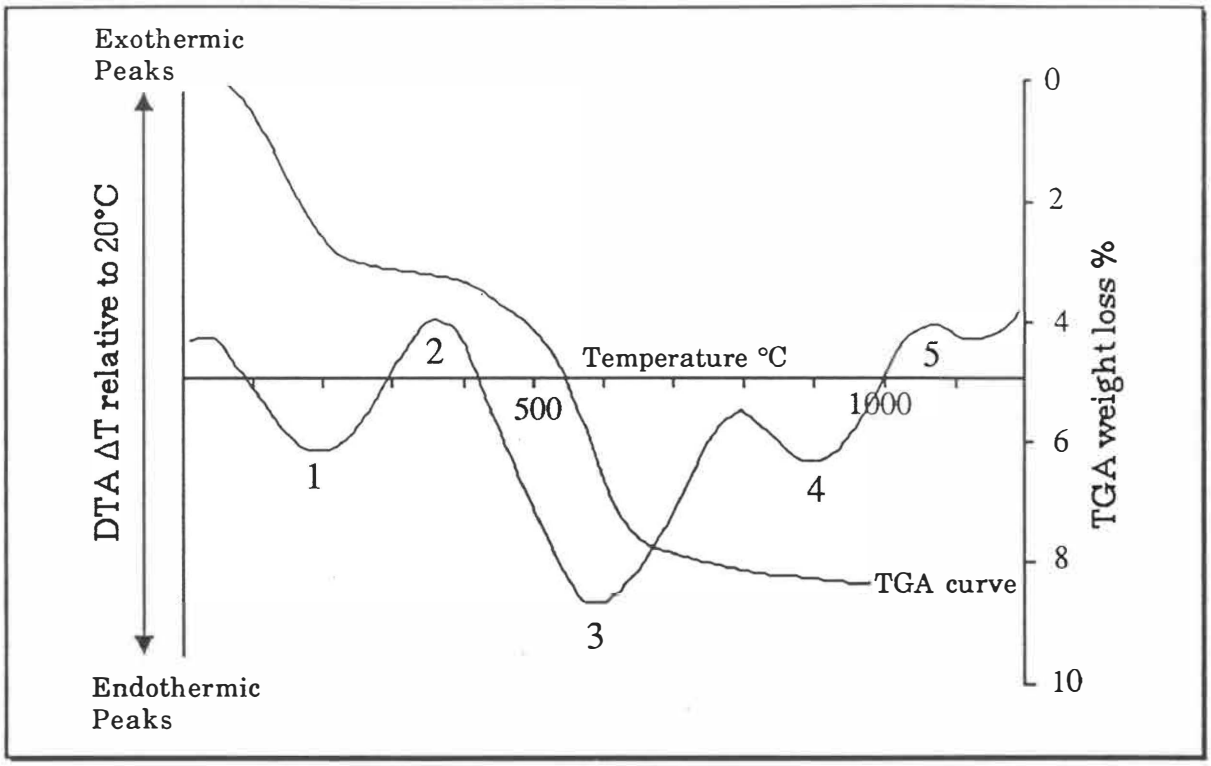

Fig. 2-2 Generalized TGA curve over the 20°C-1000°C temperature range and the corresponding DTA curve for an ideal glauconite-mica mineral. TGA data from Schultz (1971), Thompson & Hower (1975) and Logvinenko et al. (1985). DTA peak temperatures and literature sources in Table 2-3.

Table 2-3 DTA peak temperatures reported in the literature for glauconite (adapted from McRae 1972; McConchie & Lewis 1978; Xingzhen 1983; Logvinenko et al. 1985).

	Peak				
	1	2	3	4	5
	adsorbed water	oxidation of Fe^{2+}	dehydroxylation of lattice	recrystallization to spinel form minerals	
Author	**Temperature °C**				
Grim & Rowland (1942)	110		550		950
Grim et al. (1951)	145	340	600	865	915
de Bruyn & van der Marel (1954)	100	300	570		900-940
Hoebeke & Dekeyser (1954a)		350	570		925
Cloos et al. (1961)	170-245	355-390	600-620	860-930	
McConchie & Lewis (1978)	150-200	350-400	550-600	950-1000	
Xingzhen (1983)	85-150		450-665	900-985	
Logvinenko et al. (1985)	110		475		

2-4-3 Three-dimensional structural representation of glauconite

Mineral glauconite has a monoclinic C2/m symmetry group lattice structure. To show the spatial relationship between the interacting atoms of the lattice, three dimensional diagrams were created using Chem3d™ (Figs. 2-3 to 2-5). X-ray precession co-ordinates for celadonite which is also a C2/m mineral were used as co-ordinates for initial positioning of the glauconite atoms. The celadonite co-ordinates were from Zviagin (1957). A correction routine within Chem3d™ re-positions the calculated structural positions of the constituent atoms if unit cell dimensions and α, β, γ angles for the glauconite lattice are included in the input data. It should be emphasized that structural diagrams of this nature assign full occupancy to all sites. For a real mineral partial occupancy is the norm. The presented figures are only an approximation of "true" mineral glauconite.

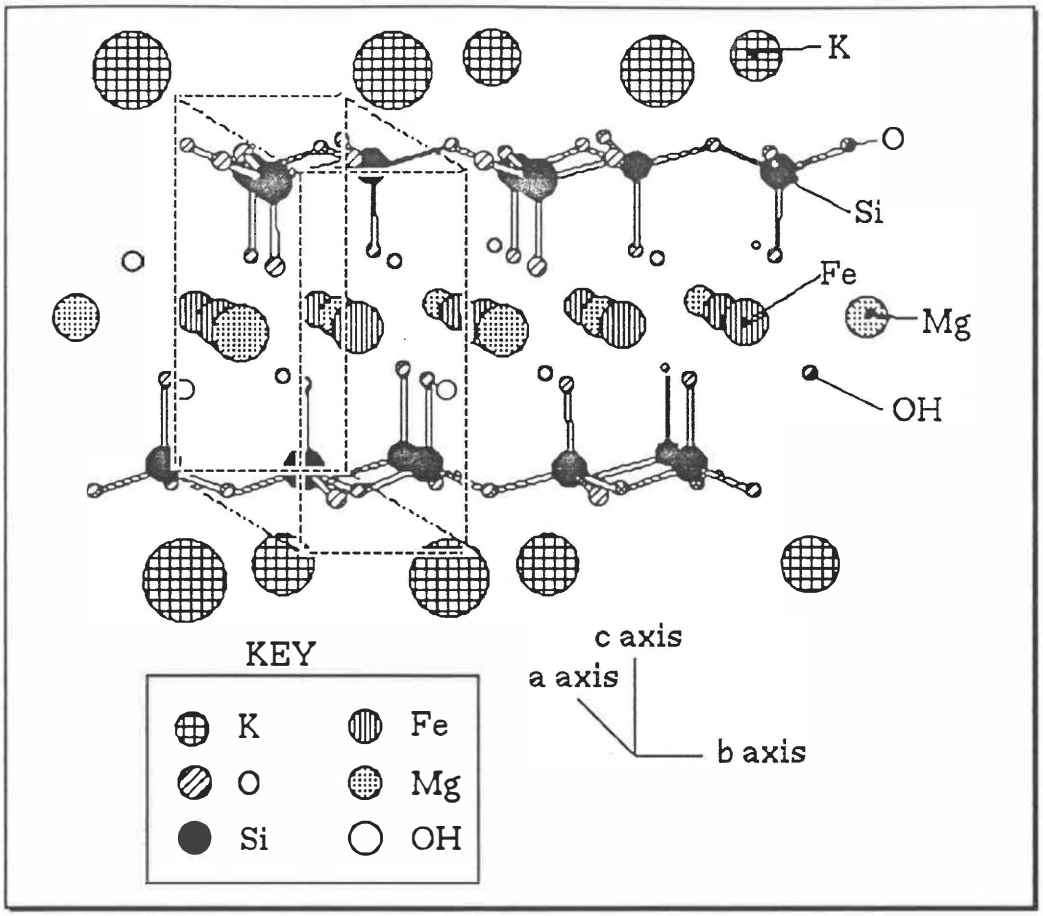

Fig. 2-3 Unit cell structural diagram of the glauconite lattice. Only the Si-O bonds are shown for clarity.

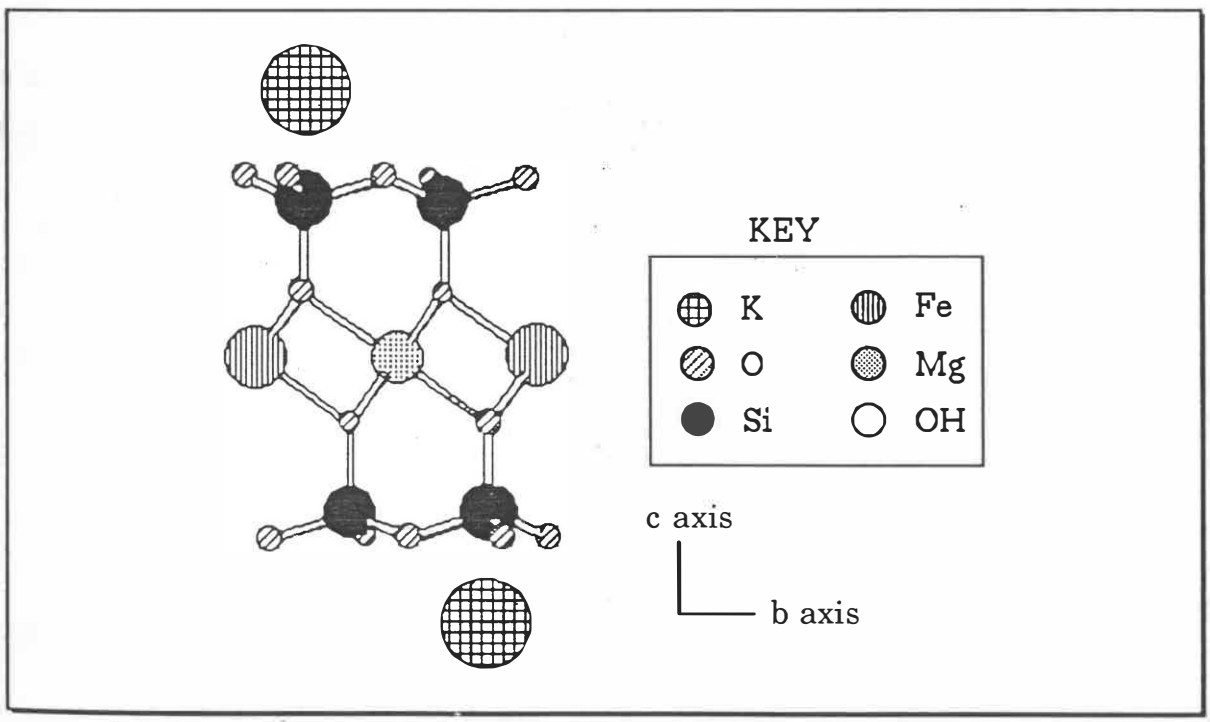

(caption next page)

Fig. 2-4 Transverse section through the glauconite lattice. The diagram represents an enlargement of the dashed enclosure of Fig. 2-3. Hydroxyl groups have been removed for clarity. The 1M polymorph structure is shown by the K interlayer ions which are shifted 0.5 of the unit b cell axis due to electrostatic repulsion.

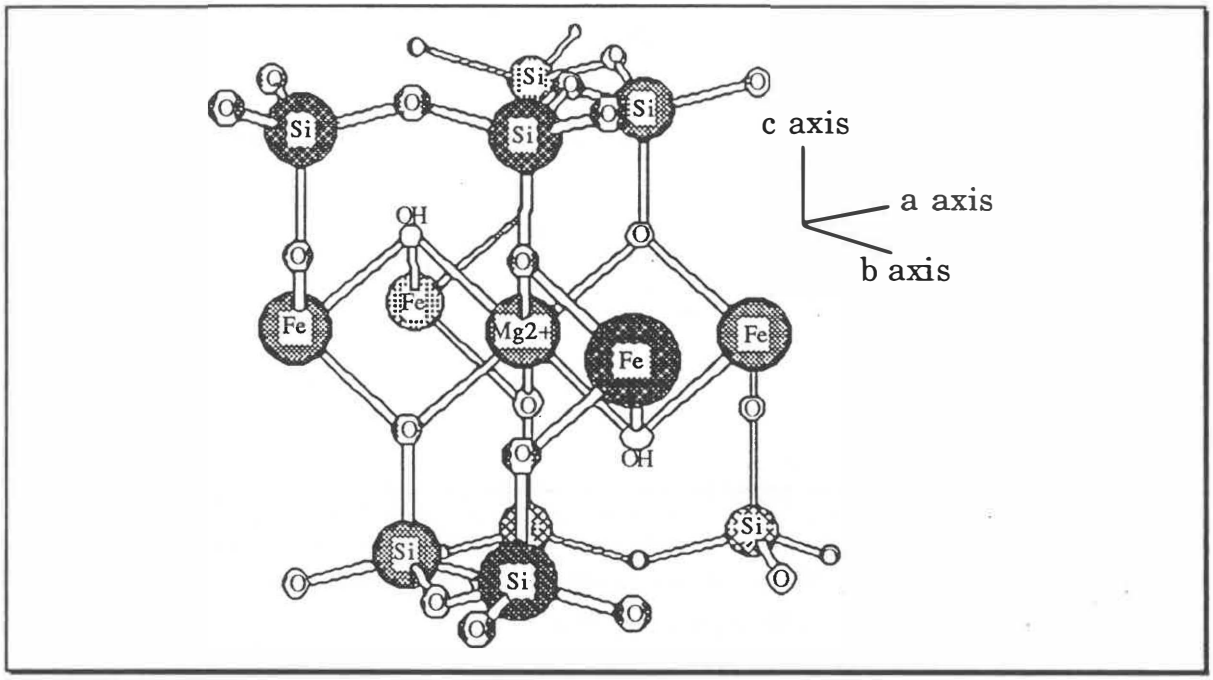

Fig. 2-5 30° a axis rotation and 5° b axis rotation of Fig. 2-4. The location of hydroxyl groups within the "holes" of the silicate tetrahedron causes rotation of the hydroxyl bond toward octahedral vacancies (Basset 1960; Giese 1971,1973; Thompson & Hower 1975). K ions in the glauconite-mica lattice occupy slightly elevated central positions in the hexagonal ring on the base of the linked silica tetrahedra (Barshad 1950).

(2-5) HYPOTHESIS ON THE GENESIS OF GLAUCONITIC MATERIAL

Early theories on the formation of mineral glauconite reflect the sparsity of mineral compositional data available to the early glauconite researchers.

Murray & Renard (1891) and Collet (1908) suggested co-precipitation of Mg-, Al-, and Si-gels occurred at sites of suitable depth, temperature, and chemical composition. The "gels" subsequently adsorbed K and formed glauconite (McRae 1972; Odin & Matter 1981). Takahashi & Yagi (1929) and Takahashi (1939) suggest a similar mechanism, however, rather than direct precipitation of the gels, they hypothesized that hydration of various sea-floor silicates occured followed by gelatinisation of the amorphous silicate. This theory was supported by Smulikowski (1954) who proposed that mixed ferri-alumino-siliceous gels which adsorbed potassium were the process pathway for glauconitisation.

2-5-2 Transformation of biotite

A significant set of papers by Galliher (1935a,b, 1936, 1939) proposed that glauconite was formed exclusively from the transformation of biotite in the marine environment. This theory received support in regions near micaceous source rocks (e.g., Hough 1940; Ballance 1964), and remains an advocated theory for the formation of vermicular pellets in the marine environment. However, Galliher's claim that all glauconites have a biotitic progenitor is not justifiable. Indeed, in Galliher's own field area (Monterey Bay, California), recent work by Hein et al. (1974) has shown only a limited number of glauconitic samples have a biotitic progenitor.

2-5-3 Layer lattice theory

Burst (1958a,b) proposed the layer lattice theory for the development of glauconite. The precise mechanisms by which the diagenetic change from a degraded silicate lattice to glauconite occurs have been documented by Hower (1961). The layer lattice theory requires:

(1) A degraded layer silicate lattice.

(2) A plentiful supply of iron and potassium.

(3) Suitable redox potential conditions.

Initial phyllosilicate degradation results in the loss of octahedral cations, the process of degradation occurs by:

(a) inorganic processes;

(b) organic bacterial metabolism (Prather 1905 in McConchie et al. 1979); and/or

(c) passage of sediments through the intestinal tract of organisms (Pryor 1975; McConchie et al. 1979; Bornhold & Giresse 1985).

The degraded lattice then adsorbs iron prior to its diffusion into the octahedral layer to replace aluminium (Hower 1961). Aluminium replacement causes an increase in the octahedral layer charge which is balanced by the adsorption of potassium from sea-water into interlayer positions. Because Fe^{2+}, Fe^{3+} and K^{+} occupy different structural positions in the glauconite lattice they are probably taken up independently, not simultaneously as suggested by Hower (1961) (Bentor & Kastner 1965; Foster 1969; Birch et al.1976). McConchie et al. (1979) note that James (1966) has established Fe^{3+} is geochemically immobile in solution (i.e., Fe^{3+} is not directly taken into the Al^{3+} bonding position). Therefore, McConchie et al. (1979) propose Fe is uptaken as Fe^{2+}, which once in the octahedral layer loses an electron during bond formation to form Fe^{3+}.

The layer lattice theory fails to explain:

(1) Authigenic crystal growth of glauconite in the open pore space between mica sheets (Odin 1972; Odin & Matter 1981).

(2) The abundant evidence of a calcitic progenitor for glauconite (e.g., foraminiferal test replacement, echinoderm substrate replacement).

(3) In some restricted spaces, such as within the chambers of empty foraminiferal tests, the ability to introduce silicate clays must be minimal. This suggests authigenic glauconite precipitation is the active process.

2-5-4 Epigenetic substitution

The epigenetic substitution theory proposed by Ehlmann et al. (1963) was forwarded to account for some of the problems encountered with the layer lattice theory. According to this model "the partially expanded mica layers of the detrital clay....act as templates upon which glauconite layers form through solution of the solid mixture using ions present in sea-water" (Ehlmann et al. 1963, p.96). As mentioned above, Odin (1972) has shown this to occur in micas, while Hughes & Whitehead (1987) have evidence of epigenetic substitution growth on detrital silica substrates.

2-5-5 Precipitation - dissolution - recrystallization

The process of precipitation - dissolution - recrystallization proposed by Odin & Matter (1981) begins with the precipitation of a void-filling iron-, potassium-rich glauconitic smectite phase in the fractures and pore spaces of the substrate grain. This initial substrate partially dissolves and is replaced by proto-glauconite. Following proto-glauconite formation, recrystallization

occurs and more evolved (micaceous) glauconite forms. Obviously, the two dissolution - recrystallization stages can be coincident with further replacement of the substrate. This suggests that all phases of glauconite should be evident in some grains.

Work by Amouric & Parron (1985) has shown destabilization of an "x-phase" and transformation of this phase into a non-crystalline product from which glauconite mica grows. This would appear to be analogous to the dissolution - recrystallization stages of Odin & Matter (1981). Odin & Letolle (1980) stress the importance of semi-confinement in their hypothesis for the formation of glauconite. Ireland et al. (1983) concur with the model of Odin & Matter (1981) and describe the geochemical conditions required for the formation of the glauconitic smectite. Importantly, Ireland et al. (1983) hypothesize a higher pH and oxidation environment than most authors (e.g., Hower 1961). Ireland et al. (1983) propose Fe^{2+} saturation and hence precipitation of ferric silicates occurs above the Fe mobilization zone in the sediment pile. If supersaturation levels are high, nontronite is formed; when saturation levels are lower, glauconitic smectite is precipitated (Bornhold & Giresse 1985).

2-5-6 Multiple process model

This theory was proposed by Bornhold & Giresse (1985, p.662) who noted: "Our studies .... lead us to support the model put forward by Odin & Matter (1981) and, basically, the refinements of Ireland et al. (1983) .... we do note minor differences from the model proposed by Odin & Matter (1981)". Bornhold & Giresse (1985) support the nascent development of glauconite proposed by Odin & Matter (1981), but a correlation between Fe and K in the latter stages of glauconite development is also noted. This leads Bornhold and Giresse (1985,p.662) to the conclusion that "the later stages of evolution (of glauconite) appear to conform to the layer lattice theory for glauconitisation".

2-5-7 The glauconite/bertherine (chamosite)/illite subspecies debate

Glauconite-like materials show considerable mineralogical variability. Whether the term mineral glauconite is realistic in terms of a distinct mineral species, or whether mineral glauconite should be considered the ferriferous or potassic end member of another defined mineral group is debatable. It has also been suggested that the glauconite family can be subdivided into smaller mineralogical units (e.g., soda glauconites of Hallimond (1922) and skolite of Smulikowski (1954) in McConchie 1978).

Mineralogical variability in glauconites is caused by isomorphous substitutions within the glauconite lattice:

(1) Al^{3+} and Fe^{3+} for tetrahedral Si^{4+} (Warshaw 1957; Burst 1958a,b; Rolf et al. 1977).

(2) Mg^{2+} ,Fe^{3+} ,Fe^{2+} and other transition metals for octahedral Al^{3+} and Fe^{3+} (Warshaw 1957; Burst 1958a,b; Ireland et al. 1983).

(3) Monovalent and divalent cations for interlayer K^{+} (McRae 1972; Odin 1975; McConchie 1978; McConchie & Lewis 1980).

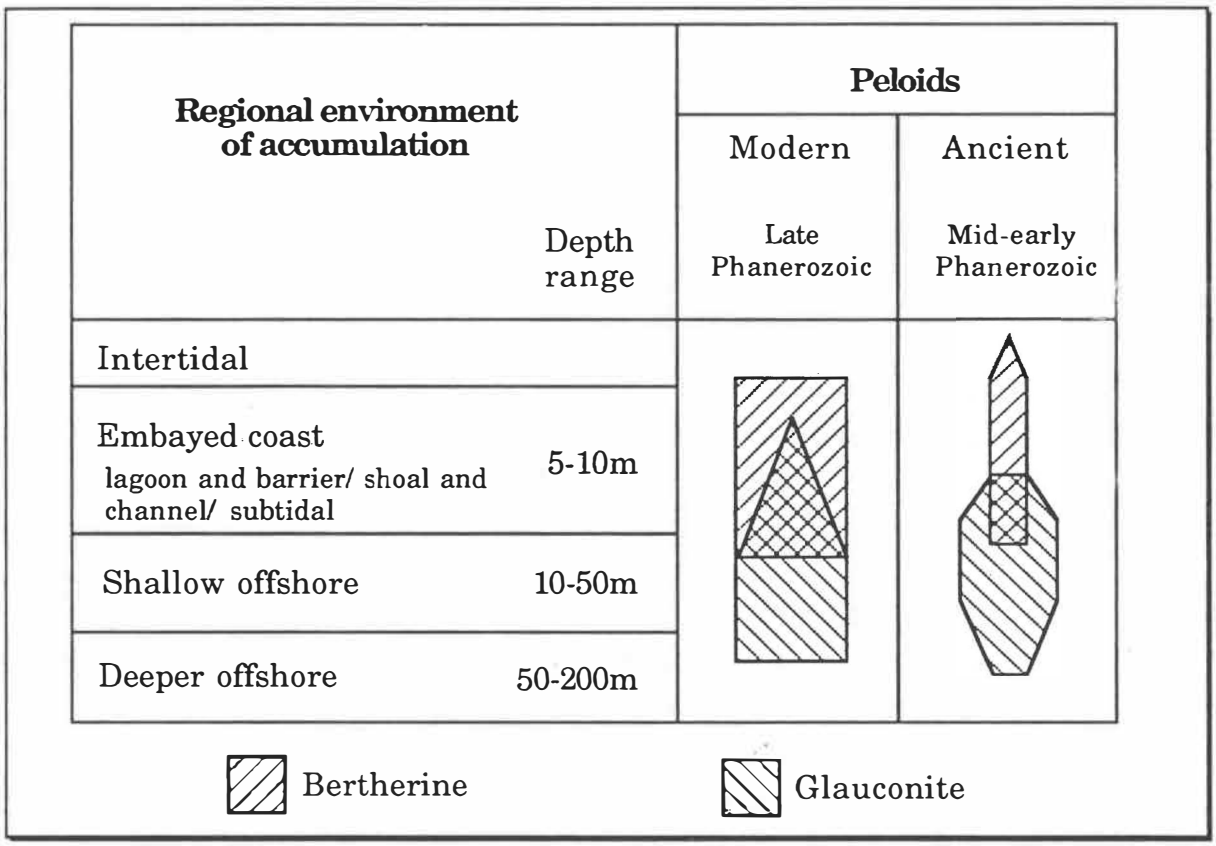

Fig. 2-6 Regional environment of accumulation of glauconite and bertherine. Bar width indicates relative abundances of modern and ancient peloids (adapted from Van Houten & Purucker 1984, fig. 3).

2-5-7A Bertherine or glauconite?

"Bertherine, formerly chamosite" (Bhattacharyya 1983, p.173) forms "ochrous to green granules ...visually often indistinguishable from glaucony" (Odin & Matter 1981, p.623). Both minerals are heptaphyllitic micas and have similar chemical compositions:

Bertherine (Weaver & Pollard 1973 in Bailey 1980)

$$R^{1+}_{0.83}(Fe^{3+}_{0.72}Al_{0.49}Mg_{0.63}Fe^{2+}_{0.21})_{2.05}(Si_{3.81}Al_{0.19})O_{10}(OH)_2$$

Glauconite (Weaver & Pollard 1973 in Bailey 1980)

$$R^{1+}_{0.78}(Fe^{3+}_{1.01}Al_{0.45}Mg_{0.39}Fe^{2+}_{0.20})_{2.05}(Si_{3.65}Al_{0.35})O_{10}(OH)_2$$

Hendricks & Ross (1941) noted that it is justifiable only on the grounds of paragenesis and occurrence to retain both glauconite and bertherine (chamosite) terms. Occurrence of bertherine in ancient sediments supports a division based on the position of formation on the shelf (Fig. 2-6) (Porrenga 1967). This division has been questioned for recent glauconite/bertherine deposits where there appears to be considerable overlap both in environment of deposition and mineralogy (Bailey 1980b,Van Houten & Purucker 1984). Recent evidence suggests that the production of glauconite or bertherine is controlled by the Si content of the pore waters of the substrate and hence is influenced by fresh-water incursions (Van Houten & Purucker 1984).

2-5-7B Ferric illite or glauconite?

It has also been suggested that glauconite is very similar to ferric illite (Odin & Matter 1981; Koster 1982; Berg-Madsen 1983). Again, this raises the question of retention of both names. There is chemical evidence however, to suggest glauconite and illite are separate mineral species: glauconite and illite are distinguishable on a plot of total iron content versus interlayer cation content (see Odin & Matter 1981 fig.8).

(2-6) COMMERCIAL USES OF GLAUCONITE

2-6-1 Industrial uses of glauconite

Various uses for glauconite in an industrial capacity have been suggested, or are in current use:

(a) Potassium source for industrial uses (Buck 1919; Charlton 1918; Holmes 1919; Shreve 1921; Mansfield 1922, in McRae 1972).

(b) Water softener (Simpson 1934; Cornes 1940; Smulikowski 1954).

(c) "Scavenger" for radioactive wastes (Schnepfe et al. 1964).

(d) Colouring agent in glass and paint (Oakley 1943).

(e) Decolouration of crude petroleum and sorbent for oils (Simpson 1934; Simulikowski 1954).

2-6-2 Agricultural uses of glauconite

The high K content of glauconite has lead to considerable commercial interest in the possibility of using crushed glauconite as a source of slow release potassium for fertilizers. McRae (1972) gives extensive literature citation of regions which have been investigated for this purpose, or where application has occurred. McConchie (1978) notes that previous work by Ahmad et al. (1968) and Twenhofel (1936) has shown soils derived from

glauconitic sandstones produce yields of up to 1.5 times that of soils derived from non-glauconitic sandstones.

(2-7) GLAUCONITE: LIMITS ON FORMATION, AND USE AS A STRATIGRAPHIC MARKER

2-7-1 Limits of glauconite formation

Factors thought to limit the location of glauconitic sediments include sediment input into the system, availability of organic matter at the sediment-water interface, temperature, depth and availability of a suitable progenitor lattice upon which the glauconitisation process can operate (Cloud 1955; Burst 1958a,b; McRae 1972; Odin & Letolle 1980)

2-7-1A Oxygenation and organic matter

Various conditions of oxygenation concurrent with active glauconite formation have been reported in the literature, ranging from moderately anaerobic to strongly oxidizing (Van Andel & Postma 1954; Cloud 1955; McRae 1972). Most authors (e.g., Krumbein & Garrels 1952; Cloud 1955; Burst 1958a,b; McRae 1972; Odin & Letolle 1980; Odin & Matter 1981; Logvinenko 1982; Berg-Madsen 1983; and others) support a slightly negative Eh system. The semi-confined micro-environment within tests, fecal pellets, and granules proposed by Odin & Letolle (1980) and Odin & Matter (1981) provides a negative Eh setting within an overall positive Eh system.

Decaying organic matter produces organic acids and a negative Eh at the sediment-water interface. The same organic acids may cause degradation of the phyllosilicate progenitor which is envisaged by Burst (1958a,b) as precursory to glauconite formation (McConchie et al. 1979). The common development of glauconite within fecal pellets (coprolite morphological form) further supports the association of glauconite and organic matter.

2-7-1B Temperature and depth

Several limits for the temperature of formation of glauconite have been quoted in the literature (e.g., Takahashi 1939; Cloud 1955; Porrenga 1967; Bjerkli & Ostomo-Saeter 1973; Odin & Letolle 1980). The large range, from 6°C to 20°C, suggests temperature may not be a significant factor in determining formation of glauconite.

The depth of formation of glauconite is highly variable, from 0-800m (Cloud 1955; Porrenga 1967; Odin & Letolle; Odin & Matter 1981; Owens & Sohl 1973, in Berg-Madsen 1983). Shallow high-alumina glauconite deposits at assumed depths of 0-50m, described by Owens & Sohl (1973), would seem incompatible

with current theories on glauconite formation. It is unlikely that active glauconite formation can occur in exposed marine settings at depths less than 30m owing to wave-induced turbulence (Cloud 1955; McRae 1972; Odin & Letolle 1980). In protected, low energy, shallow, marine settings glauconitisation may still proceed because the influence of turbulence (see Section 2-7-1D) is removed.

2-7-1C Source materials

Glauconitisation can occur on a variety of materials. The substrate upon which the glauconitisation process operates influences the composition of the initial mineral glauconite formed (McRae 1972; Odin & Letolle 1981). This causes glauconites formed in argillaceous sandstones and marls to have a higher proportion of expandable layers compared with glauconites formed in "clean" sandstones, limestones and dolomites (McRae 1972). However, with continued glauconitisation the initial mineral glauconite evolves toward a common micaceous-form end-member (Hower 1961; McRae 1972; Odin & Letolle 1981). Some hypothesized substrates upon which glauconitisation can occur are:

(1) mud coprolites (50 to 500μm).
(2) micro-organism test cavities.
(3) organic carbonate debris (50 to 5000μm).
(4) siliceous mineral debris of highly variable size range.

2-7-1D Turbulence and sedimentary input into the regional environment

Turbulence is a significant factor in limiting the availability of suitable environments for the formation of authigenic glauconite. Statements from Odin & Letolle (1980, p.230) epitomize current opinion on turbulence effects; "pellets...are often rounded and glazed....because they are eroded in an environment which *ipso facto* stops crystal growth ....Glauconitisation does not occur in an agitated....environment".

Glauconite-mica is claimed to require 10^5-10^6 years to form; nascent glauconite requires minimal deposition in an open marine environment for 10^3 years before it will develop (McRae 1972; Odin & Letolle 1980; Van Houten & Purucker 1984). Owing to the extended periods required to form glauconite, sediment input into the system must be minimal. High sediment rates would cause a change in the oxygenation and Eh conditions because of burial. This would affect the mobility of the iron component and thereby directly affect the glauconitisation process.

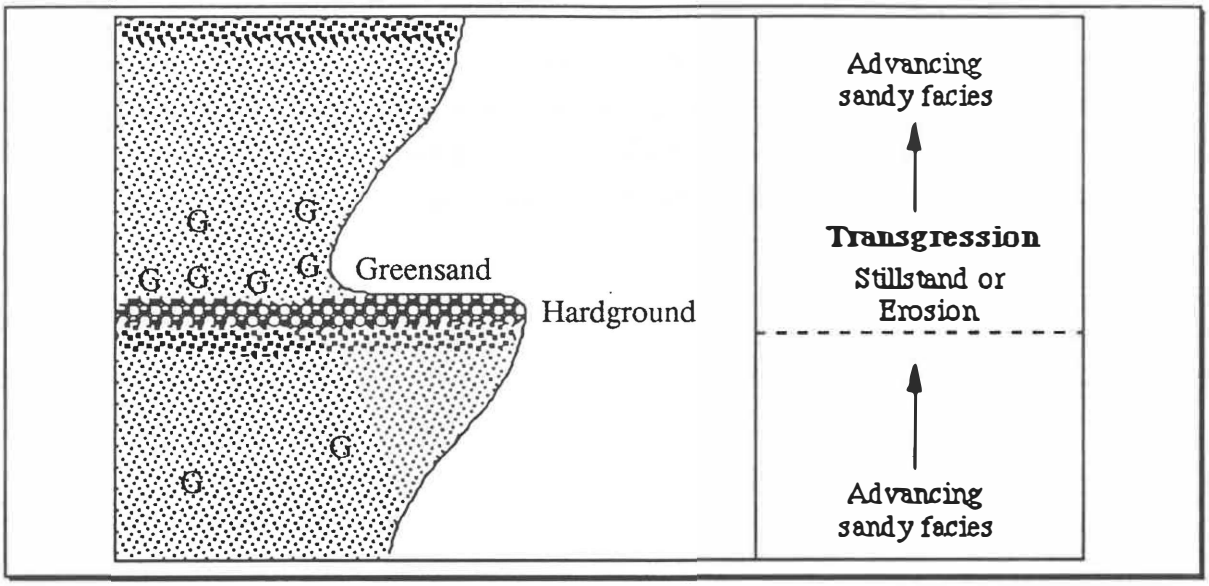

Fig. 2-7 Facies model for the development of glauconitic deposits. Shoaling- and coarsening-upward sequence is produced by regression (adapted Van Houten & Purucker 1984, fig.2).

2-7-2 Use of glauconite as a stratigraphic marker

The facies model developed by Van Houten & Purucker (1984) (Fig. 2-7) for glauconite formation indicates that transgressive sea levels or highly stable cratonic margins are the most favourable setting for glauconite formation (i.e., authigenic glauconite). Often glauconite is concentrated later in the deposit's history by erosion (i.e., allogenic glauconite). This leads to glauconite being concentrated in specific litho-stratigraphic deposits. Therefore glauconite may be useful as a stratigraphic correlation tool.

Although Wermund (1961) doubted the usefulness of glauconite as an environmental indicator and stratigraphic discriminator, recent attempts to apply glauconite to such problems have met with some success. These include:

(a) Burst (1958a) who used the d(001) XRD peak to distinguish between two glauconitic horizons in Texas.

(b) Triplehorn (1966) who noted that the occurrence and distribution of various morphologies and internal structures could be used to discriminate stratigraphic horizons. Hein et al. (1974) applied this theory to show a physiographic setting association with specific pellet morphologies in Monterey Bay, California.

(c) McConchie & Lewis (1980) who used chemical, XRD, DTA, and morphological data to characterize two protobasins in the east of the South Island of New Zealand.

(d) Xingzhen (1983) who showed a correlation between XRD, morphology, specific foraminiferal-test glauconite replacements, and different sedimentary environments across the South China Sea.

The above examples suggest that combinations of glauconite characteristics and application of a statistical multivariate technique makes glauconite a powerful stratigraphic and environmental discrimination tool.

CHAPTER (3)

GLAUCONITE IN THE TE KUITI GROUP

(3) GLAUCONITE IN THE TE KUITI GROUP

(3-1) CONTROLS ON THE DISTRIBUTION OF TE KUITI GROUP SEDIMENTS

The Te Kuiti Group, of late Eocene (Bortonian) to Oligocene (Waitakian) age (Kear & Schofield 1978; Nelson 1978a) represents a primarily transgressive marginal-marine to full-marine depositional sequence. The basal Waikato Coal Measures of the group are non-marine and are not investigated in this study.

The Te Kuiti Group is emergent through much of the western portion of the South Auckland and Taranaki land districts (Map 1). The distribution of the Group was far more extensive during it's active sedimentation phases (as shown by estimated isopachs of the late Whaingaroan sediment pile in Fig. 3-1). Post-depositional structural features that limit surface exposure of the Te Kuiti Group are:

(1) Infilling of structural depressions by recent sediment (e.g., north Waikato Basin). Drill core logs and drill core samples used in this study show the Te Kuiti Group is present beneath much of these overlying sediments.

(2) Volcanic structures (e.g., Pirongia complex) have locally buried or destroyed Te Kuiti Group sediments.

(3) Eversion of structural features (e.g., Hakarimata Anticline) has led to uplift and erosion of the Te Kuiti Group from many areas.

Nevertheless, extensive lateral and vertical sequences of the Te Kuiti Group are still evident in the South Auckland area.

The transgressive episode leading to deposition of the Te Kuiti Group can be related to the progressive southerly propagation of a rift system through western New Zealand from the mid-Eocene to early-Miocene (the Challenger Rift System of Kamp (1986)). The southerly direction of propagation of the Challenger Rift is evidenced by the pattern of late-Whaingaroan sedimentation (Fig. 3-1). The change in sediment composition south to north in Fig. 3-1 can be linked to a change in energy regime across a shelf depositional setting (Draper 1967; Swift 1970). Sites to the north which were further from near-shore high energy environments were dominated by finer grained sediments.

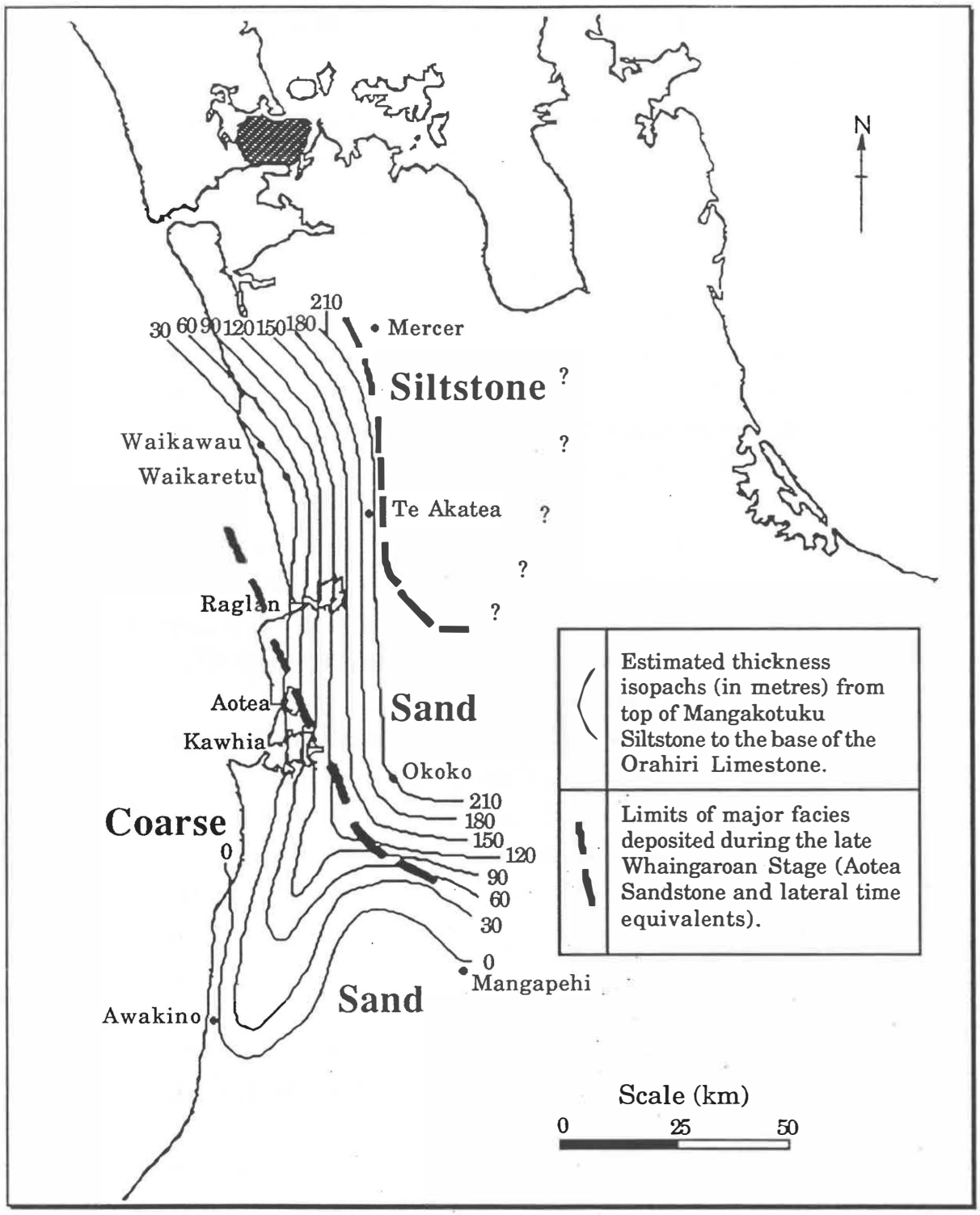

Fig. 3-1 Facies map and estimated isopach thickness of the late Whaingaroan Te Kuiti Group sediment pile (redrawn from Kear & Schofield 1959).

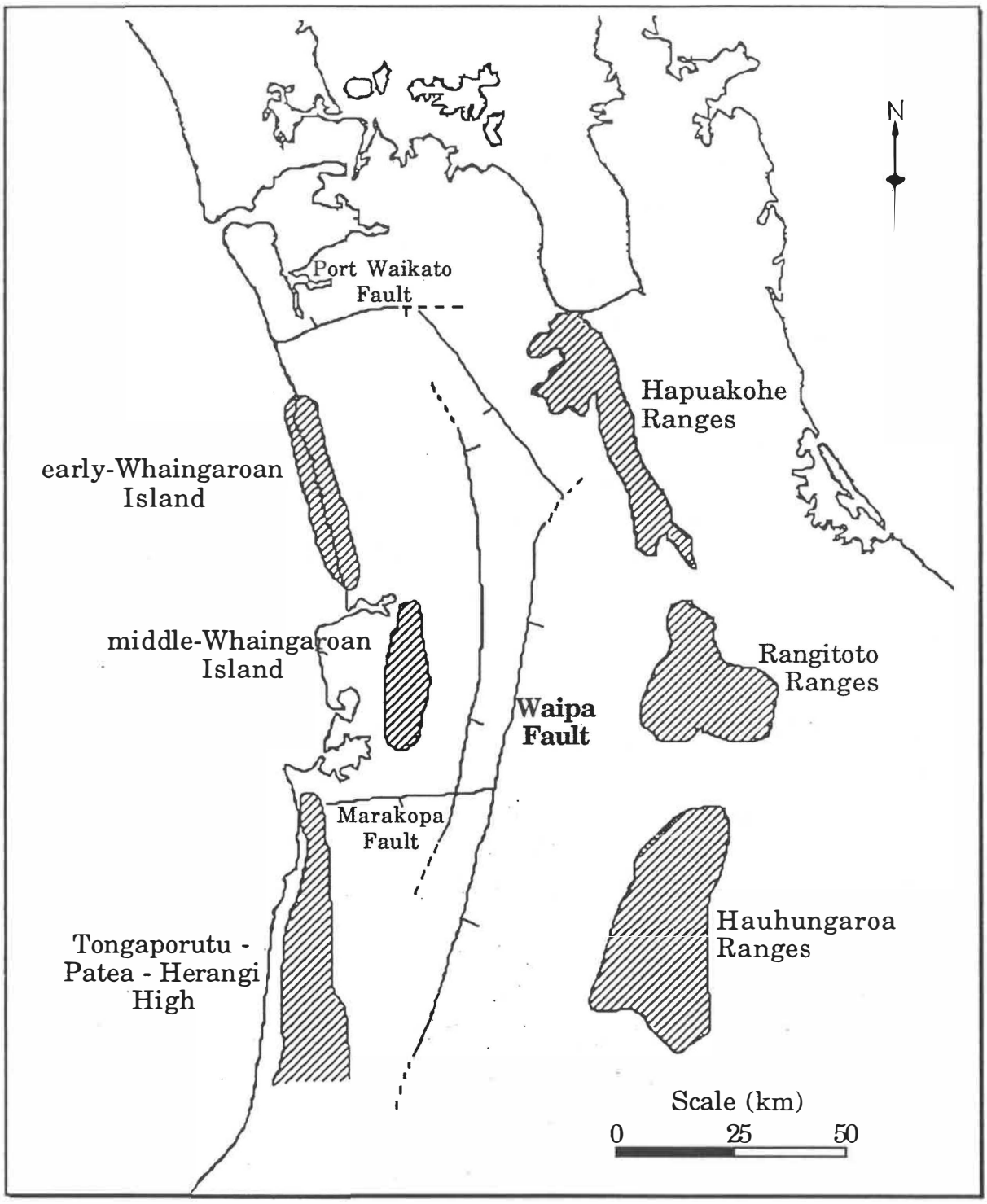

Fig. 3-2 Major structural features of the South Auckland and northern Taranaki land districts.

The western and eastern limits of the Te Kuiti Group are linked to the Challenger Rift, but rather than being a manifestation of the rift they are related to structural highs preserved during deposition of the Group. The major structural highs, namely:

(1) Hapuakohe Ranges in the northeast;
(2) Rangitoto Ranges in the east;
(3) Hauhungaroa Ranges in the southeast;
(4) Tongaporutu - Patea - Herangi High in the southwest;
(5) Middle Whaingaroan Island in the west;
(6) Early Whaingaroan Island in the northwest;

(Fig. 3-2) formed land barriers to the west and east. The Te Kuiti Group was deposited in the relatively sheltered seaway enclosed by these barriers.

Local variation in sedimentation patterns in the South Auckland depocentres was caused by reactivation of faults formed during the Kaikoura Orogeny and possibly rotational failure parallel to the Challenger Rift axis. Isolated fault block movement has led to abrupt lateral changes in lithofacies and bed thickness within the study area (Nelson & Hume 1977; Nelson et al. 1983).

(3-2) STRATIGRAPHY OF THE TE KUITI GROUP

3-2-1 Base of the Te Kuiti Group

The lower boundary of the Te Kuiti Group is represented by a major regional unconformity on Mesozoic basement rocks. The contact has a highly variable relief and, coupled with differential block movements during deposition of the Te Kuiti Group, means any formation within the Group may lie directly upon basement.

The basement stratigraphy can be separated into two major lithostratigraphic units divided by the Waipa Fault. West of the fault (Fig. 3-2) Oparau Facies rocks (volcanic greywackes, conglomerates, and tuffaceous siltstones) are present, while to the east of the fault Morrinsville Terrain (volcanic greywackes, chipwackes, and conglomerates of the Mania Hill Group) are present (Kear 1971; Kear & Schofield 1978; King 1978).

3-2-2 Generalized stratigraphy of the Te Kuiti Group

The stratigraphy of the Te Kuiti Group has been extensively investigated and descriptions of the lithological characteristics of the individual units are given in Nelson (1973,1978a), Kear & Schofield (1978), and Fergusson (1986). Some of the more significant contributions to the development of the

stratigraphic nomenclature adopted for the Te Kuiti Group are shown in Fig. 3-3. The column representation of Fig. 3-3 is an oversimplification of the complex biostratigraphy encountered in the field area of this study. The more complex nature of the sediment column over the field area is apparent from Fig. 3-4.

3-2-3 Upper limit of the Te Kuiti Group

Overlying the Te Kuiti Group in the study area are the Mahoenui Group to the south and the Waitemata Group to the north. In the northern part of the field area the upper Te Kuiti Group contact is represented by an unconformity. In the southern area the Otorohanga Limestone - Mahoenui Group contact is represented by a gradual increase in the terrigenous mud interflag lithologies of the Otorohanga Limestone facies (Nelson 1978a).

(3-3) PREVIOUS INVESTIGATIONS OF GLAUCONITE IN THE TE KUITI GROUP

Nelson (1973) undertook a limited investigation on Te Kuiti Group glauconite samples from the Waitomo region. The major results of Nelson's (1973) study of glauconite were:

(1) X-ray diffraction data indicated Te Kuiti Group glauconites fell in the disordered to mixed mineral assemblage divisions of Burst (1958a,b). Low crystallinity as evidenced by the small, broad, asymmetric d(001) peak in most of the samples investigated showed the 1Md polymorph dominates the Te Kuiti Group glauconite assemblage.

(2) A correlation between glauconite-rich lithologies and unconformities was observed.

(3) Most of the morphology groups defined by Triplehorn (1966) were present in the Te Kuiti Group glauconite samples (i.e., ovoidal, vermicular, composite, fossil-cast, and mammillated pellets).

(4) A mixed-layer illite-montmorillonite or chlorite-montmorillonite progenitor was proposed for Te Kuiti Group glauconites.

Most literature data from the northern portion of the study area has not been collated specifically about glauconite. Most information about glauconite from the north exists solely on drill logs or stratigraphic sections (e.g., Kear & Schofield 1978, p.48-73).

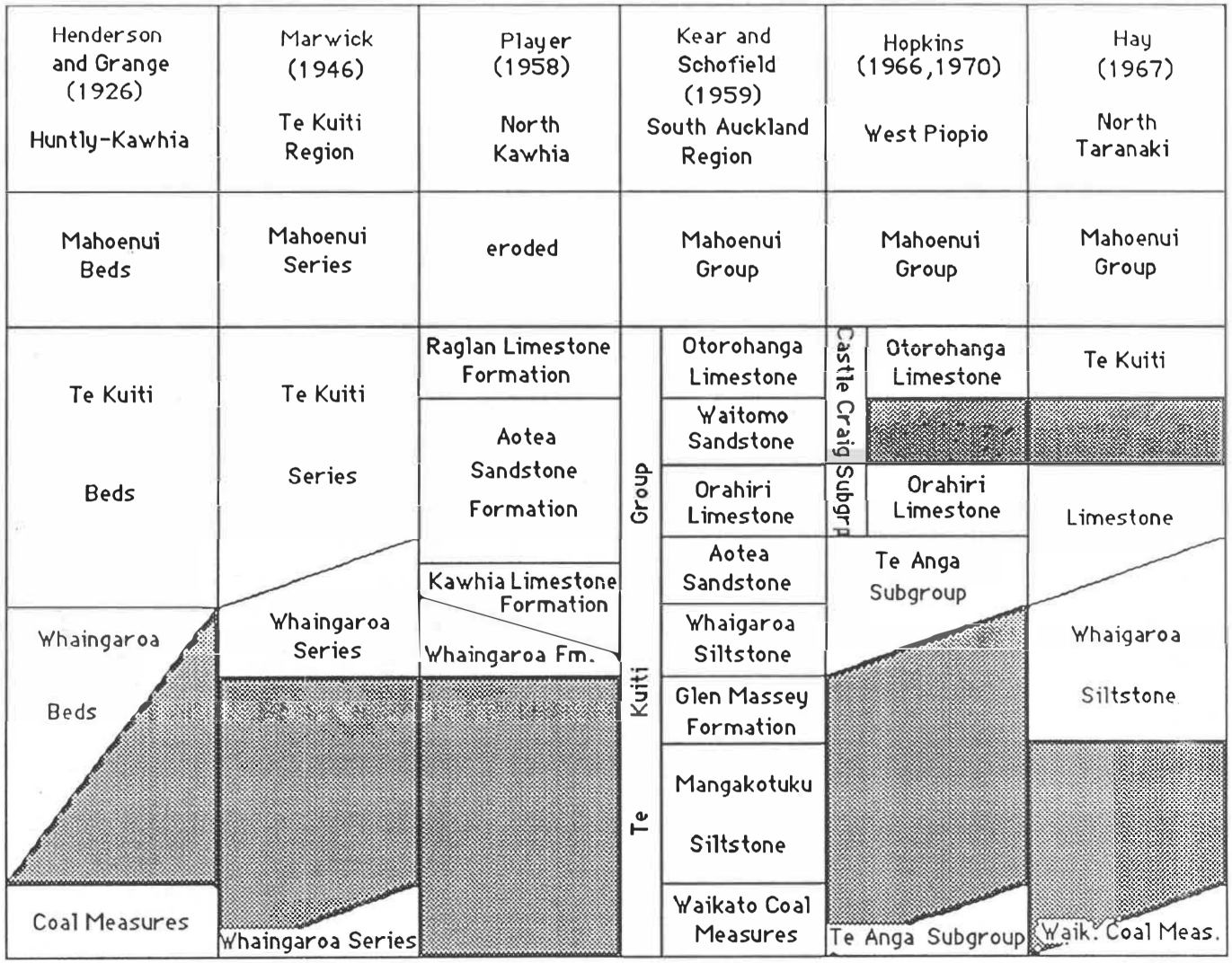
Henderson and Grange (1926)
Huntly-Kawhia
Marwick (1946)
Te Kuiti Region
Player (1958)
North Kawhia
Kear and Schofield (1959)
South Auckland Region
Hopkins (1966,1970)
West Piopio
Hay (1967)
North Taranaki
Mahoenui Beds
Mahoenui Series
eroded
Mahoenui Group
Mahoenui Group
Mahoenui Group
Te Kuiti Beds
Te Kuiti Series
Raglan Limestone Formation
Aotea Sandstone Formation
Kawhia Limestone Formation
Whaingaroa Fm.
Te Kuiti Group
Otorohanga Limestone
Waitomo Sandstone
Orahiri Limestone
Aotea Sandstone
Whaigaroa Siltstone
Glen Massey Formation
Mangakotuku Siltstone
Waikato Coal Measures
Castle Craig Subgrp
Otorohanga Limestone
Orahiri Limestone
Te Anga Subgroup
Te Kuiti
Limestone
Whaingaroa Beds
Whaingaroa Series
Whaigaroa Siltstone
Coal Measures
Whaingaroa Series
Te Anga Subgroup
Waik. Coal Meas.

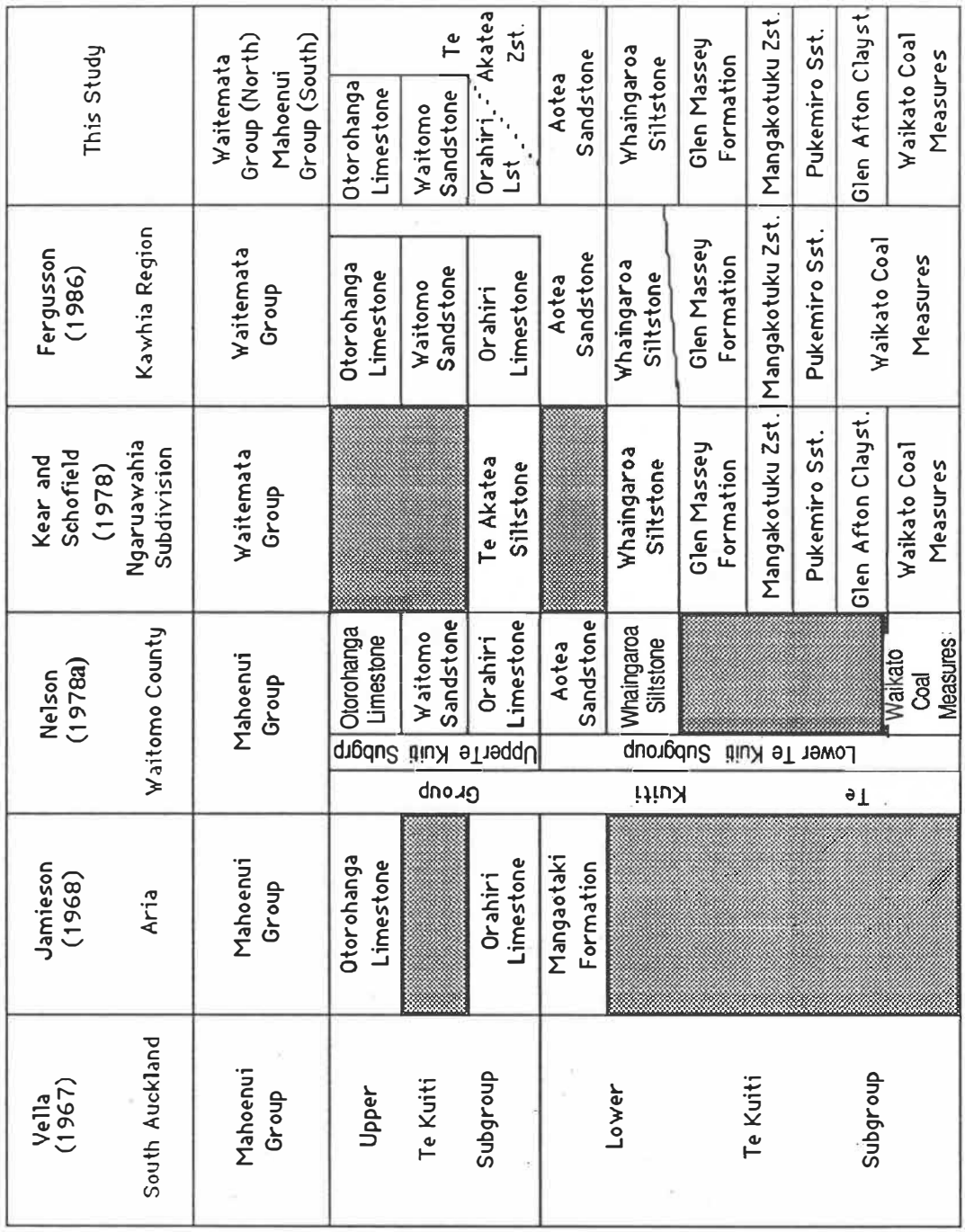

Fig. 3-3 Lithostratigraphic divisions proposed for the Te Kuiti Group (modified from Kear & Schofield 1978; Nelson 1978; Fergusson 1986).Shaded regions indicate formations proposed by Kear & Schofield (1959) are not applicable to the areas concerned.

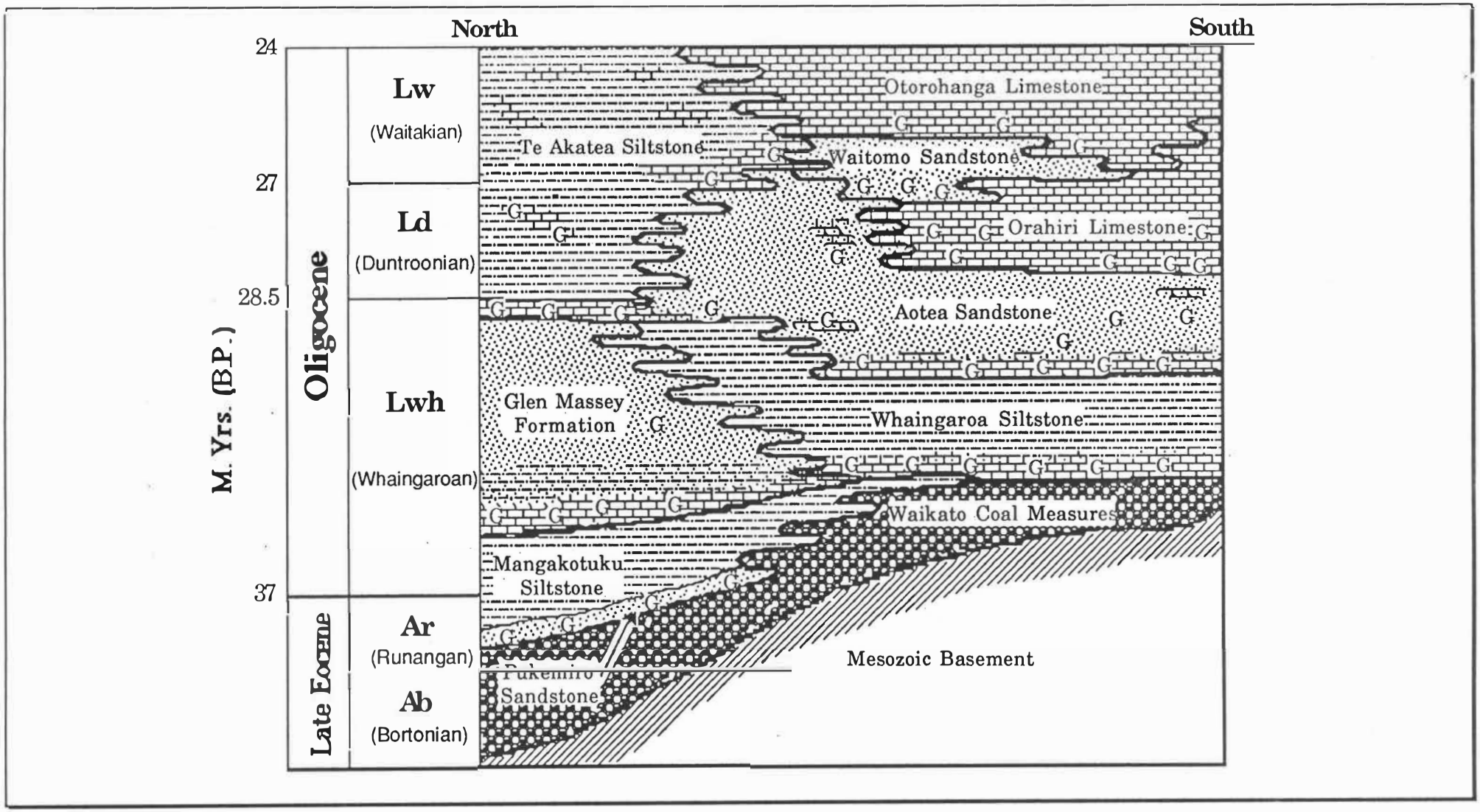

(caption next page)

Fig. 3-4 North-South section (Maramarua-Awakino) of the Te Kuiti Group. The generalised relationship between major formations within the group and glauconite rich lithologies (G) are shown (modified from Kear & Schofield 1978; Nelson & Hume 1987).

(3-4) LOCATION OF GLAUCONITE STUDY SAMPLES

The initial hypothesis of this study was that glauconite from similar lithologies should exhibit similar chemical and morphological characteristics. To test this, numerous samples were collected from various stratigraphic units within the Te Kuiti Group. The distribution of samples within a stratigraphic unit was problematic in that a single unit can comprise several lithofacies (e.g., Aotea Sandstone has muddy and clean stratigraphic lithologies). To minimize this problem, wherever possible, sampling was restricted to one lithofacies within a stratigraphic unit. The distribution of sample locations with respect to the local stratigraphy is shown by a series of panel diagrams in the map pocket (asterisks showing sample location represent best approximations of locality of the sample within the stratigraphic unit). The panel diagrams were created by extrapolating type sections and sample locations perpendicularly onto a north-south trending line. The geographic location of the sample points and the location of the panel diagram extrapolation line are shown on Map 2. Descriptions of the field exposure from which the sample was obtained (or relevant literature describing the sample locality) is presented in Appendix 2.

CHAPTER (4)

METHODOLOGY

(4) Methodology

Several analytical techniques were applied to the glauconite samples in this study. Many of the techniques (IR, DTA, XRF, XRD, EMP, and visual morphological) have been undertaken in previous studies on glauconite. Most have standard preparation and interpretation procedures and these were applied to the samples in this study. Image analysis of glauconite morphology has not been previously made. Hence techniques appropriate for this method of investigation had to be established, before data collection was initiated.

Methodology variations, establishment of new techniques, and literature sources of methods are more fully described in Appendix 1. The experimental pathways used in this study are shown as the logic flow chart (Fig. 4-1).

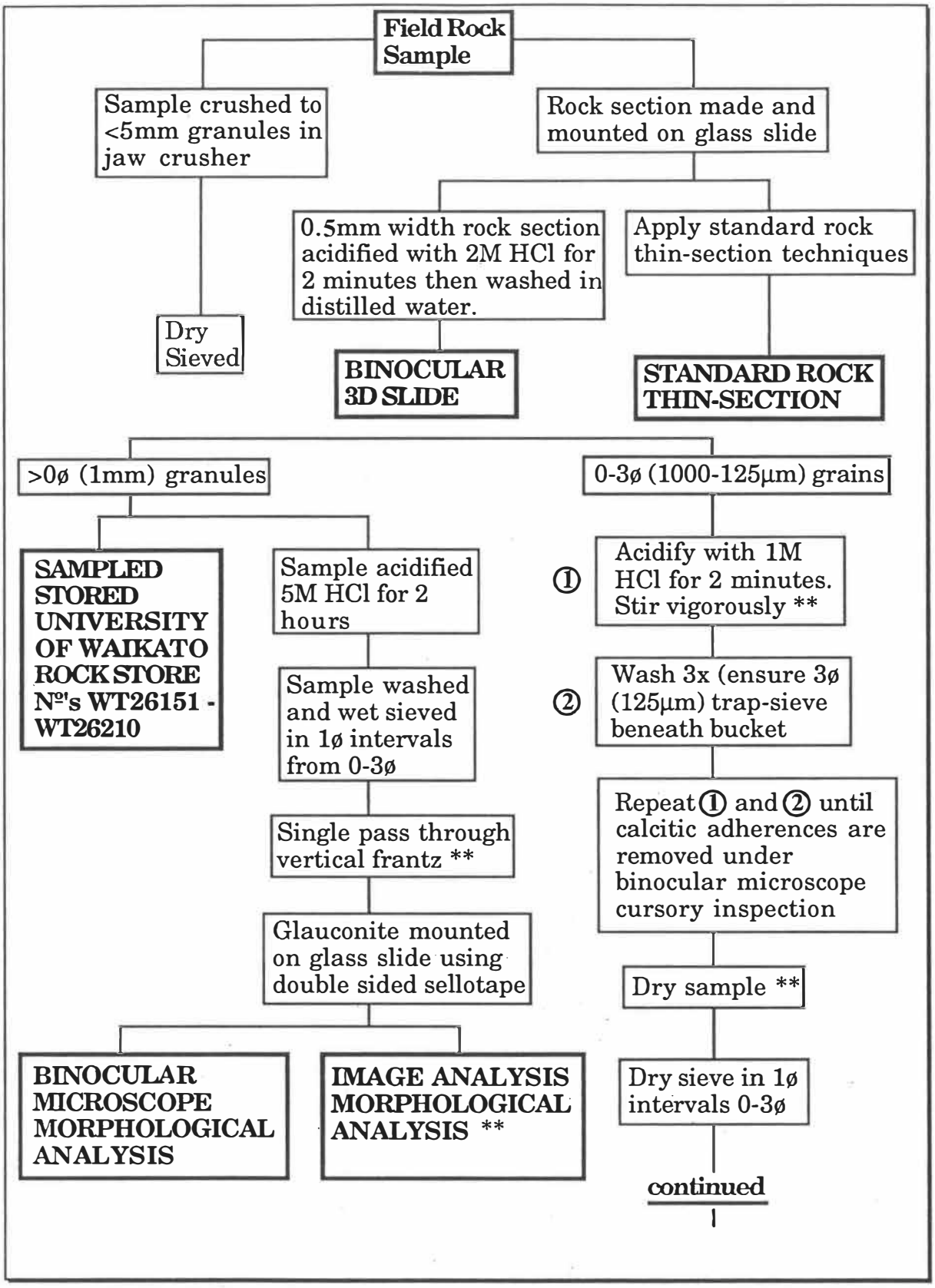
Field Rock Sample
Sample crushed to <5mm granules in jaw crusher
Rock section made and mounted on glass slide
0.5mm width rock section acidified with 2M HCl for 2 minutes then washed in distilled water.
Apply standard rock thin-section techniques
Dry Sieved
BINOCULAR 3D SLIDE
STANDARD ROCK THIN-SECTION
>0ø (1mm) granules
0-3ø (1000-125µm) grains
SAMPLED STORED UNIVERSITY OF WAIKATO ROCK STORE Nº's WT26151 - WT26210
Sample acidified 5M HCl for 2 hours
Sample washed and wet sieved in 1ø intervals from 0-3ø
Single pass through vertical frantz **
Glauconite mounted on glass slide using double sided sellotape
BINOCULAR MICROSCOPE MORPHOLOGICAL ANALYSIS
IMAGE ANALYSIS MORPHOLOGICAL ANALYSIS **
① Acidify with 1M HCl for 2 minutes. Stir vigorously **
② Wash 3x (ensure 3ø (125µm) trap-sieve beneath bucket
Repeat ① and ② until calcitic adherences are removed under binocular microscope cursory inspection
Dry sample **
Dry sieve in 1ø intervals 0-3ø
continued

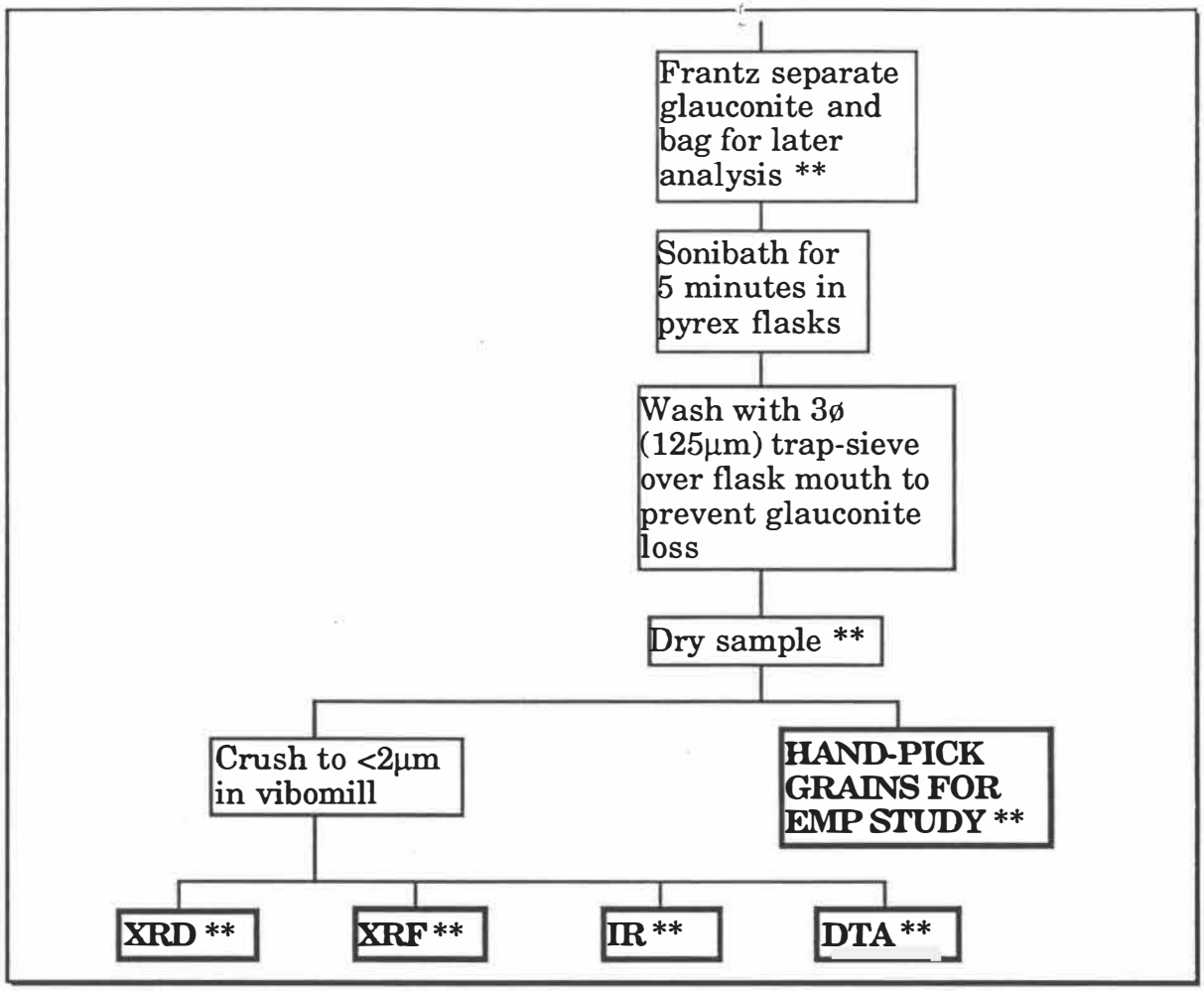

** - Specific conditions relating to these parameters or techniques are discussed more fully in Appendix 1.

Fig. 4-1 Experimental-design flow-chart used in the investigation of Te Kuiti Group glauconite samples.

CHAPTER (5)

RESULTS AND DISCUSSION

(5) RESULTS AND DISCUSSION

(5-1) MORPHOLOGY

5-1-1 Internal Fabric

Thin sections were made of several samples to determine the predominant internal fabric of Te Kuiti Group glauconites. Only two of the fabrics described in Section 2-1-2 were evident in thin section. Most samples showed a predominance of random microcrystalline fabric (Fig. 5-1 to 5-3). Samples with a high proportion of vermicular form glauconite also exhibited oriented microcrystalline to micaceous internal fabric glauconite (Fig. 5-4).

5-1-2 External morphology

Triplehorn (1966) suggested that exterior morphological characteristics of glauconite grains might be a useful provenance indicator; the hypothesis was based on studies of uncemented disaggregated glauconitic sediment. Difficulties arises when applying this hypothesis to highly-fossiliferous, glauconite-rich, cemented, limestones. If a 3D slide of a bryozoan-dominated limestone is made the high proportion of bryozoan and other fragile morphological casts is evident (Fig. 5-5). Infilling cavities within the casts in MC35 is extremely fragile glauconite. However, when a bulk sample of MC35 is disaggregated the glauconitic cavity infills are broken into fragmented material. For MC35 the binocular morphological study calculated a 3% cast and 35% fragmentary component; this is incongruous with visual appraisal of Fig. 5-5. To test if this problem was widespread for Te Kuiti Group samples the linear correlation of casts versus fragmentary component for all morphological data was calculated (R=-0.18). The low correlation suggests the problem is not significant throughout Te Kuiti Group glauconites.

Attributing fragmentary glauconite component to allogenic sedimentation should only be considered supporting evidence for other transport indicators such as rounding of quartz grains within the sample.

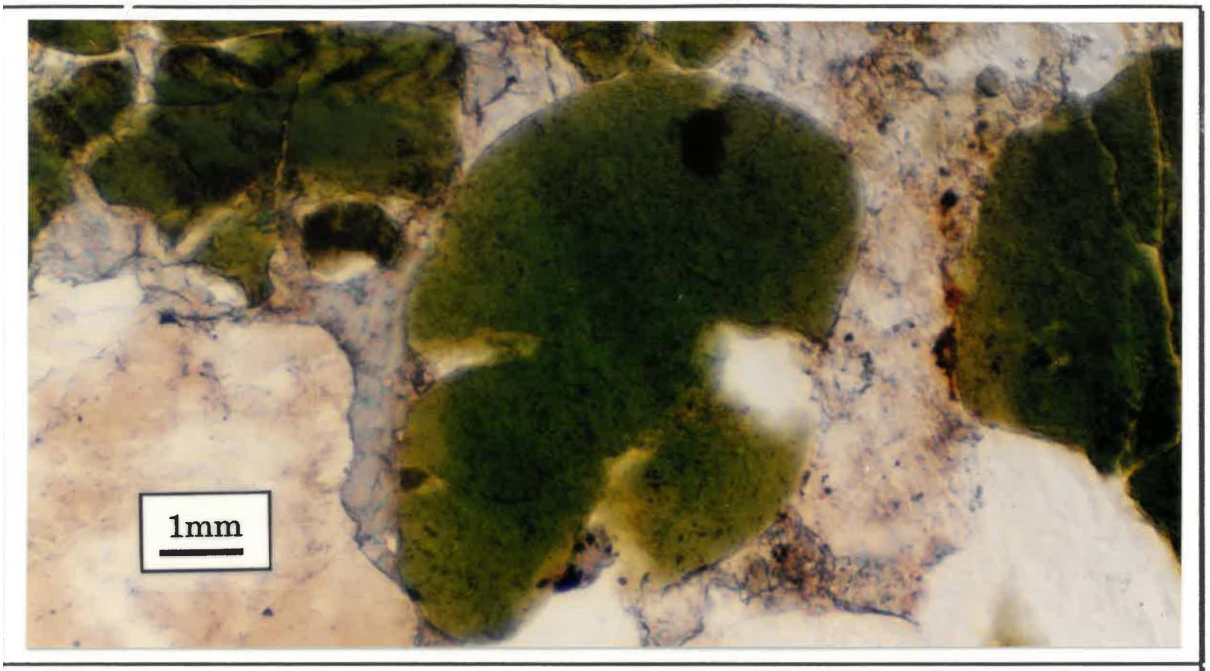
1mm

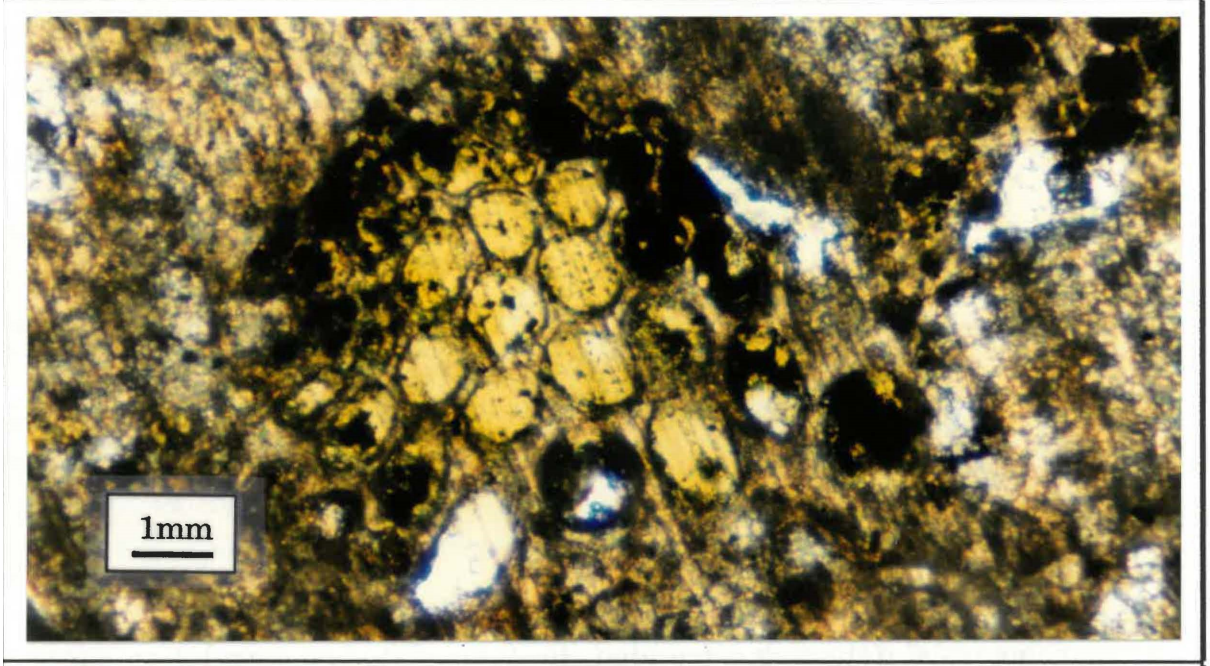
1mm

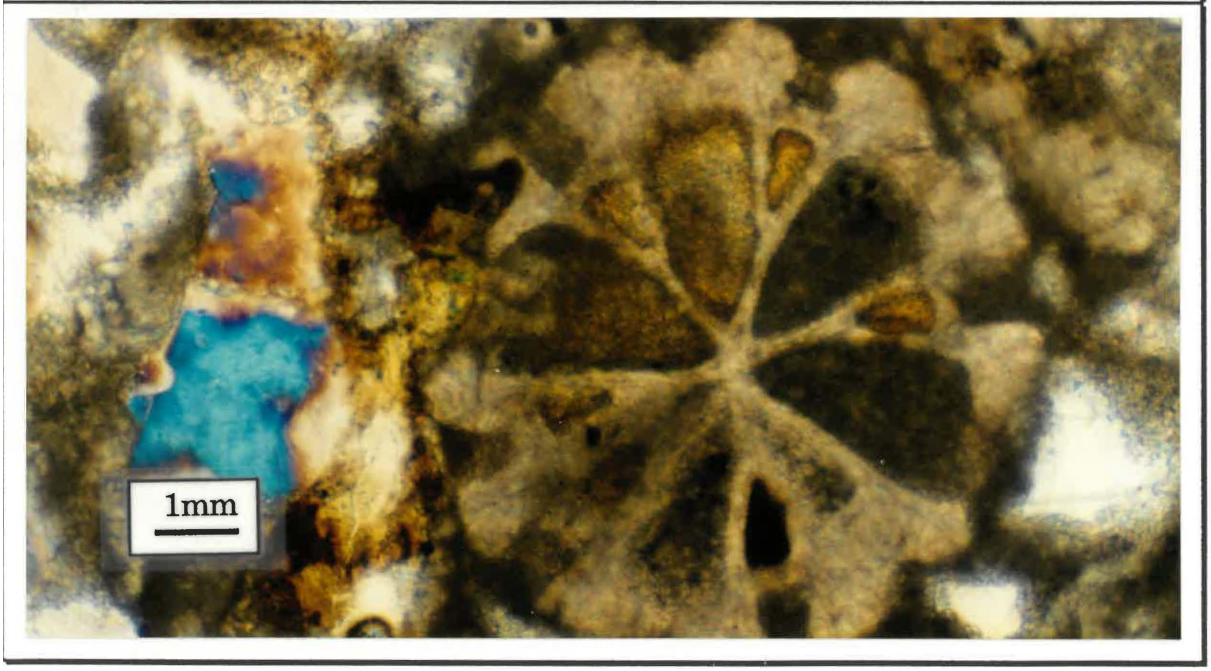
1mm

Fig. 5-1 Thin section of a large ovoidal glauconite grain showing an internal random microcrystalline fabric. Sample MC26 (Aotea Sandstone Ao4). 10X magnification. Transmitted plane polarised light.

Fig. 5-2 Thin section of authigenic glauconite infilling voids in a bryozoan test. The glauconite shows random microcrystalline internal fabric. Sample MC27E (Waitomo Sandstone). 10X magnification. Transmitted plane polarised light.

Fig. 5-3 Thin section (0.5mm thick) of nascent glauconite within the chambers of a bryozoan test. The glauconite shows random microcrystalline internal fabric. Sample MC29 (Orahiri Limestone OrB2). 10X magnification. Transmitted plane polarised light.

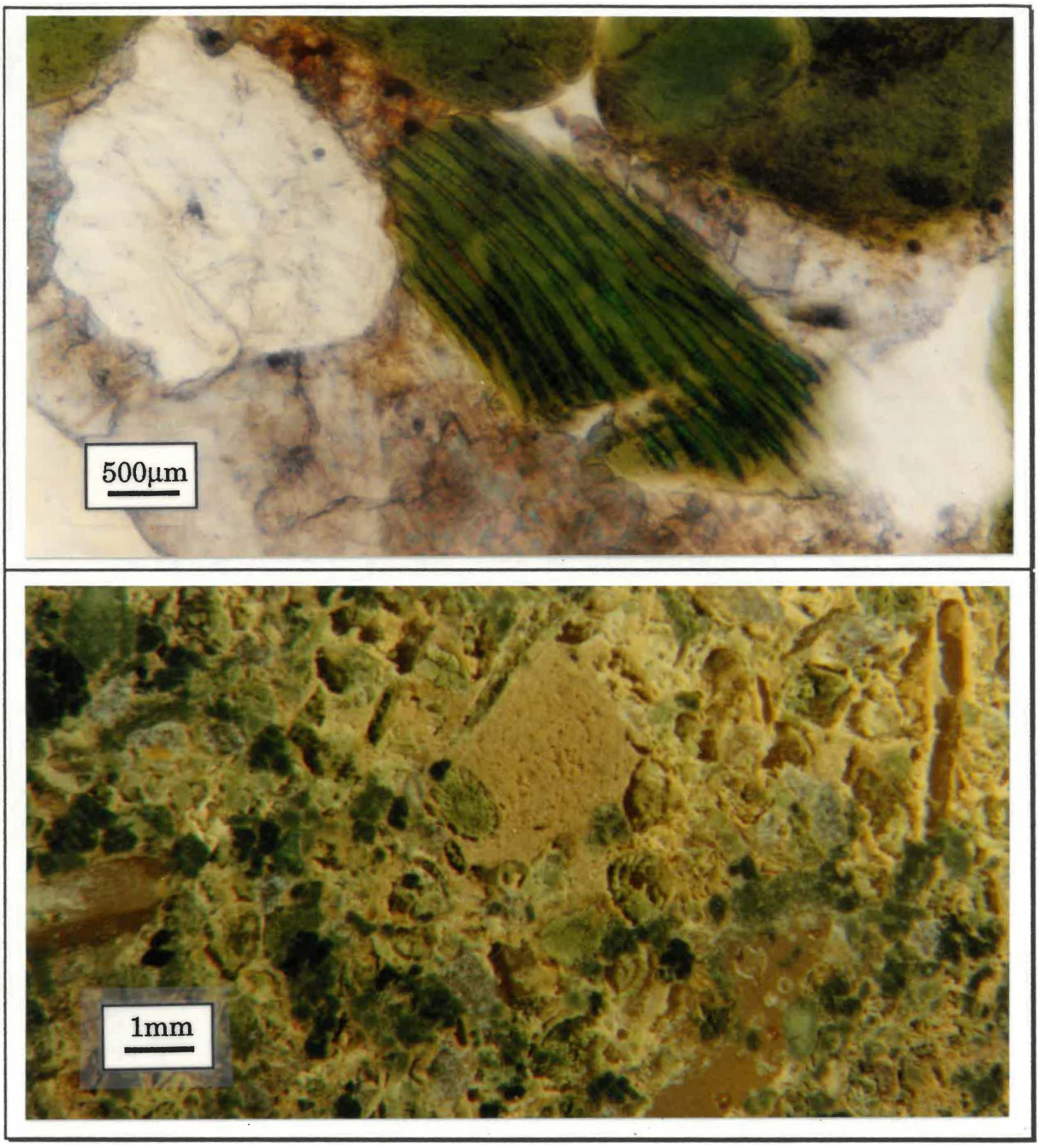
500μm
1mm

Fig. 5-4 Thin section of a fragment from a vermicular grain showing an internal oriented microcrystalline fabric. Sample MC26 (Aotea Sandstone Ao4). 20X magnification. Transmitted plane polarised light.

Fig. 5-5 Skeletal limestone 3D slide. Numerous skeletal types, especially bryozoan and bivalve. Acidification has removed the calcitic component leaving the highly fragile glauconite cast component. Sample MC35 (Aotea Sandstone AoA). 10X magnification. Reflected light inclined at 60°.

5-1-2A Binocular microscope investigation

Two hundred point grain analyses per sample were classified using the morphological grain divisions in Table 2-1; then the percentage of each morphological form in the sample was calculated. Results are presented in Section D2 of the data booklet. Fig. 5-6 shows a **decrease** in the average ovoidal grain content stratigraphically upward for the Elgood Limestone to Orahiri Limestone sequence. There is a corresponding **increase** in average lobate grain content stratigraphically upward for the Elgood Limestone to Orahiri Limestone sequence. Initially this suggested there was a decrease in depositional energy during glauconite formation, however, the full sedimentological characteristics of beds such as the Orahiri Limestone does not support this conclusion. Another possibility is that the deposits in the higher formations of the Te Kuiti Group were not subject to as much reworking as the lower formations of the Te Kuiti Group.

Casts and molds are significant only in Whaingaroa Siltstone and Orahiri Limestone formations. Whether the cast and mold content is real or an artefact of sample treatment was not ascertained.

Vermicular grains are only of significant content in some Orahiri Limestone samples (e.g., MC19, MC29). Further investigation of the Orahiri Limestone data revealed only Orahiri samples from the Honikiwi-Waitomo-Marakopa area had significant vermicular grain contents.

The average fragmentary component of all Te Kuiti Group formations is over 25%. The Aotea Sandstone beds have the highest percentage of fragmented materials (e.g., MC28 61%, MC44 75%). The high fragmentary component, lack of significant lobate grain content, and relative abundance of ovoidal glauconite suggests some reworking of sediments has occurred in all depositional settings within the Te Kuiti Group. Whether reworking was localized cannot be proven or disproved based on the available data.

To draw conclusions from Waitomo Sandstone morphological trends would seem inappropriate given the low number of samples investigated.

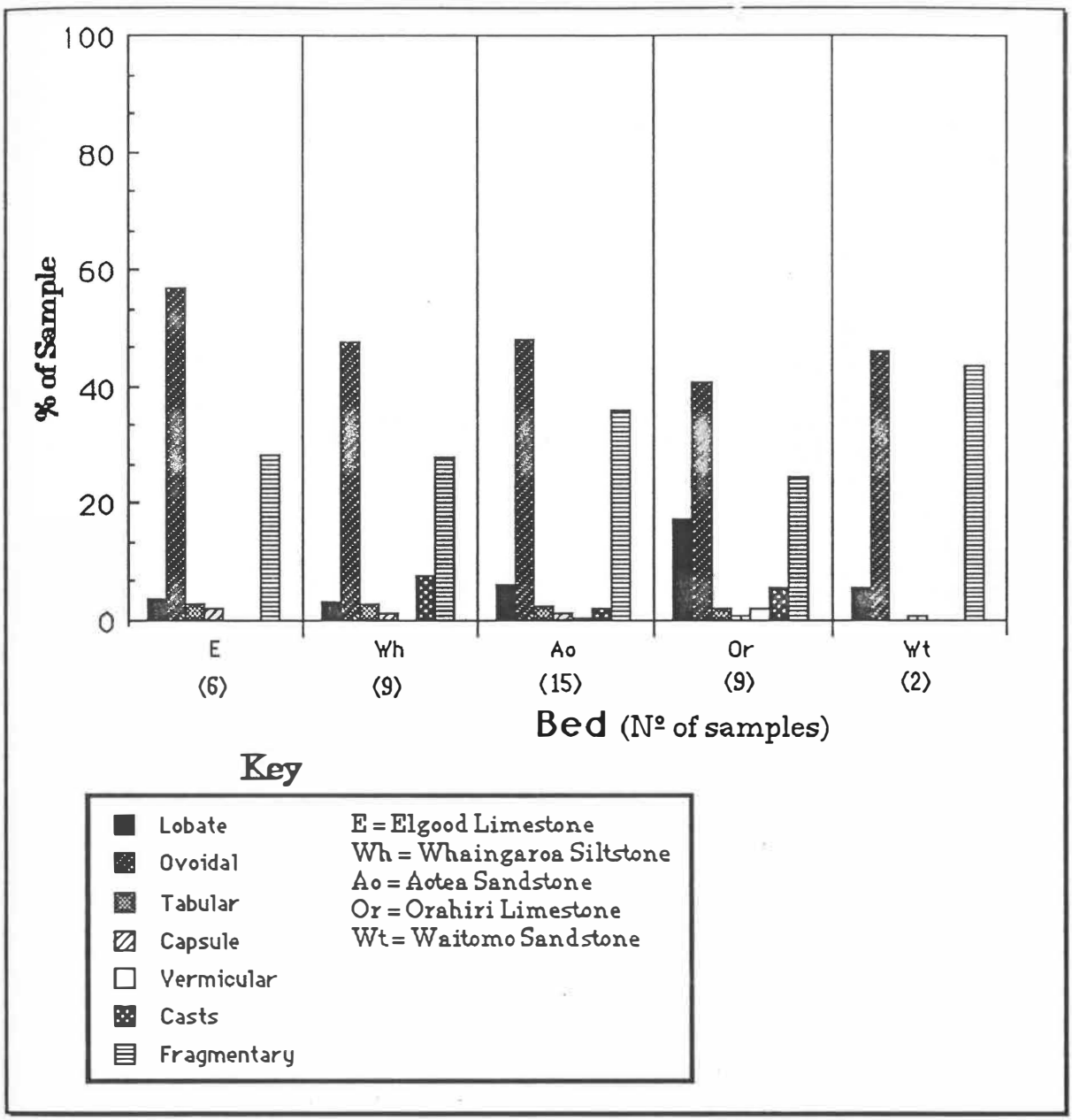

Fig. 5-6 Morphological forms present in selected beds of the Te Kuiti Group. Only major morphological forms are shown. Plotted data represent averages of each morphological form in a specified formation . The order of the the bars for each formation is the same as the listing of the morphological types in the key.

Table 5-1 Derived correlation matrix for binocular shape classification variables. Data from which correlations were calculated is contained in Section D2 of the data booklet . Samples MC29, MC30, and MC35 were omitted as their data appeared erroneous.

	lobate (l)	ovoid (o)	tabular (t)	capsule (c)	vermicular	casts	fragmentary	composite	cauliflower	l+o
ovoid (o)	0.11									
tabular (t)	0.54	0.18								
capsule (c)	0.34	0.42	0.35							
vermicular	0.08	-0.03	0.06	-0.19						
casts	-0.07	-0.33	-0.08	-0.13	-0.16					
fragmentary	-0.37	-0.71	-0.42	-0.44	-0.00	-0.24				
composite	0.09	-0.06	0.24	0.10	0.07	0.09	-0.22			
cauliflower	-0.31	-0.43	-0.21	-0.27	-0.16	0.48	-0.03	0.22		
l+o	#	#	0.34	0.49	-0.00	-0.33	-0.77	-0.03	-0.49	
o+c	0.14	#	0.20	#	-0.04	-0.33	-0.72	-0.05	-0.44	#
l+o+t	#	#	#	0.51	0.01	-0.32	-0.78	0.00	-0.49	#
l+t+c	#	0.22	#	#	0.04	-0.1	-0.48	0.16	-0.33	#
l+o+t+c	#	#	#	#	-0.01	-0.32	-0.79	0.01	-0.49	#
t+c	0.56	0.32	#	#	-0.03	-0.11	-0.51	0.22	-0.28	0.46

- These correlations have not been calculated as the derived variable contains the factor that is being correlated against.

Table 5-1 shows that for the Te Kuiti Group the strongest single variable correlation is between fragmentary and ovoid grain content (R=-0.71, Fig. 5-7). The lobate component of the studied samples is in general below 10% and the correlation between this morphological form and fragmentary glauconite is not high (R=0.37). The conclusion of McConchie & Lewis (1980, p.417) that "there is a strong inverse relationship between the abundance of lobate grains and the abundance of broken or fragmentary grains" does not appear to be valid for the Te Kuiti Group sediments. Probably the relatively small proportion of lobate grains within the samples and the fact that some fragmented material may be derived from destruction of cast glauconite may mask any relationship. The derived morphological variables show good correlation with the fragmentary component of the sediment. The influence of the ovoidal component on the correlations is high because of the large proportion of ovoidal grains relative to other grain types in the Te Kuiti Group sediments.

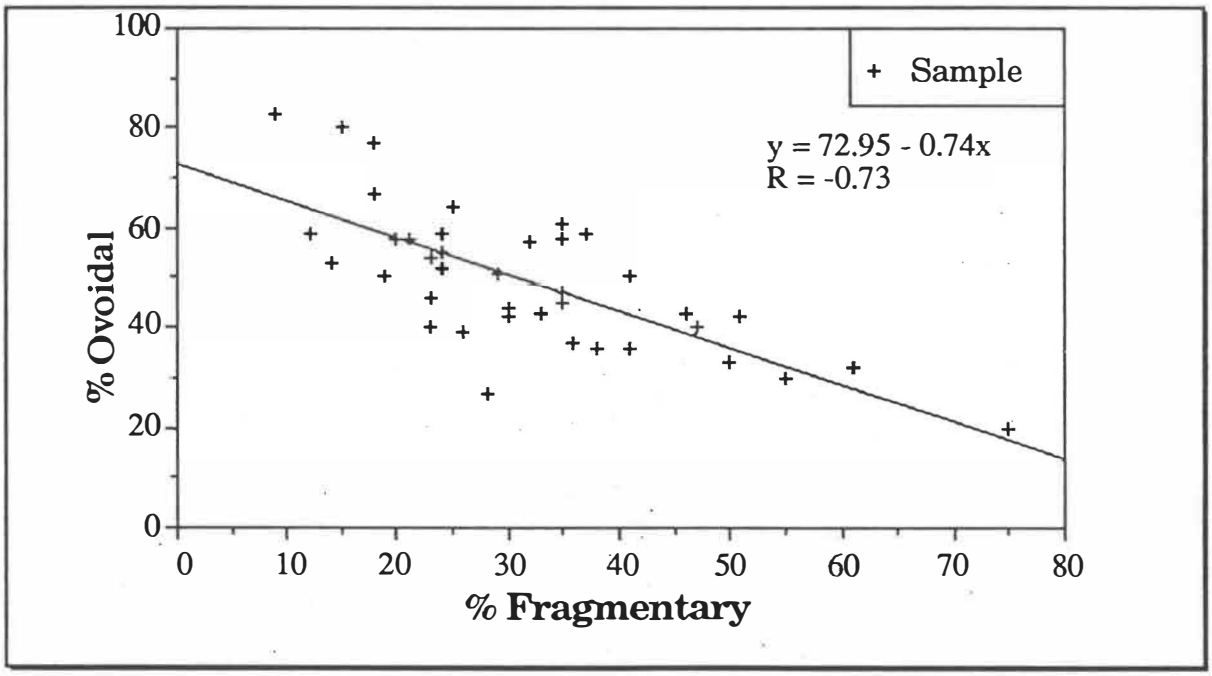

Fig. 5-7 Correlation between fragmentary and ovoid morphological form for Te Kuiti Group glauconites. Data in section D2 of the data booklet.

Subgrouping of Aotea Sandstone morphological data showed a very strong correlation between the derived variable l+o+t+c (lobate + ovoidal + tabular + capsule content) and the fragmentary component (R=-0.98, Fig. 5-8). The correlation between lobate and fragmentary grains is significantly improved over that for the collective data (R=-0.51 versus R=-0.37, Table 5-2). The strong correlations and lack of cast-form glauconite suggests the degree of fragmentation can be used as an indication of transportation in most Aotea Sandstone beds.

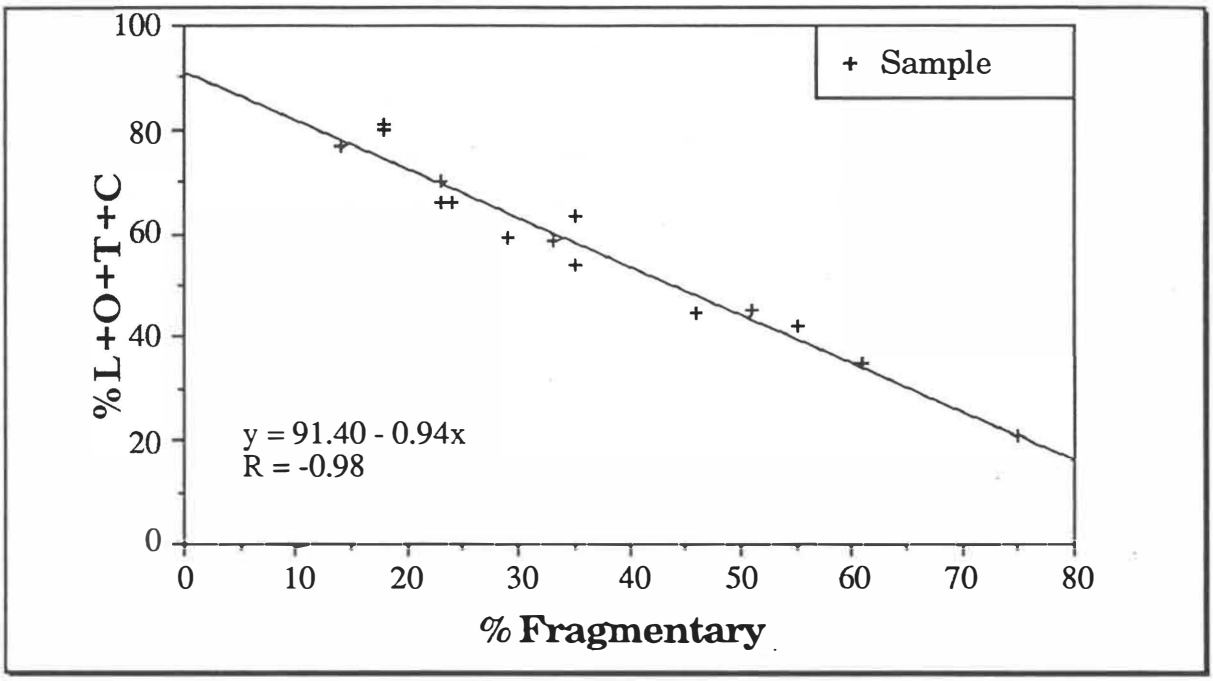

Fig. 5-8 Correlation between fragmentary and L+O+T+C morphological form for Te Kuiti Group glauconites. Data for Aotea sandstone samples in section D2 of the data booklet. (L = lobate, O = ovoidal, T = tabular, C = capsule).

Table 5-2 Derived correlation matrix for morphological data for Aotea Sandstone samples in Section D2 of the data booklet.

	lobate (l)	ovoid (o)	tabular (t)	capsule (c)	vermicular	casts	fragmentary	composite	cauliflower	l+o
ovoid (o)	0.06									
tabular (t)	0.75	0.08								
capsule (c)	0.28	0.45	0.18							
vermicular	0.30	-0.56	0.19	-0.27						
casts	0.43	0.14	0.36	0.36	-0.33					
fragmentary	-0.51	-0.85	-0.49	-0.59	0.42	-0.46				
composite	0.40	0.03	0.54	0.14	0.01	0.25	-0.37			
cauliflower	-0.06	-0.06	-0.07	0.22	-0.39	0.17	-0.09	0.60		
l+o	#	#	0.32	0.51	-0.42	0.27	-0.95	0.16	-0.08	
o+c	0.08	#	0.09	#	-0.56	0.16	-0.87	0.04	-0.04	#
l+o+t	#	#	#	0.50	-0.37	0.31	-0.97	0.23	-0.09	#
l+t+c	#	0.14	#	#	0.22	0.47	-0.60	0.47	-0.03	#
l+o+t+c	#	#	#	#	-0.38	0.32	-0.98	0.23	-0.07	#
t+c	0.74	0.26	#	#	0.04	0.45	-0.67	0.51	0.04	0.49

- These correlations have not been calculated as the derived variable contains the factor that is being correlated against.

5-1-2B Image analysis model

The data used in the construction of the discriminant model is presented in Section D3 of the data booklet. Principal component analysis (PCA) and canonical variate analysis (CVA) tests were made on the collected data to determine if the image analyser was capable of distinguishing morphological types of glauconite.

PCA calculates vector loadings to maximize the between group variation without consideration of within group variability (in essence the method assigns all values to the group centroid and maximizes centroid distances). CVA seeks linear combinations of the variates which have the greatest between-group variation relative to the within-group variability (Digby & Kempton 1987). Therefore, it was determined that CVA was the best method for the distinction of morphological types of glauconite.

CVA results for: (a) group variable means, (b) latent vector loadings of the first four latent vectors, and (c) percent variability accounted for by the appropriate latent vector, are shown in Table 5-3. The results show that using two latent vectors (CV1 and CV2) more than 80% of the variation between morphological groups using the seven listed variables can be accounted for. The canonical latent vector CV1 shows high loadings on the formfactor and convexicity variables; CV2 shows high loadings on the formfactor and fractal variables. It is possible to define all grains by multiplying the seven measured features of a grain by the canonical variates CV1 and CV2 then visually estimating field boundaries. However, Digby & Kempton (1987, p.77) note "it is more usual to construct only the smaller matrix of group means and project these". The morphological group mean data were used to calculate group centroids for the seven morphological forms in this study.

From the constraint that within-group variation is equally represented in all dimensions (i.e., the population is normally distributed) spheres can be drawn to represent probability fields of correct classification for a given morphological group. The chisquare test is used to determine the radius of the sphere encompassing a specified probability field of correct classification. The examples below show the sphere radius for the 95% and 80% confidence interval.

$$\sqrt{\chi^2_{2\ (P=0.95)}} = 2.45$$

$$\sqrt{\chi^2_{2\ (P=0.80)}} = 1.79$$

The 80% confidence interval was arbitrarily chosen and used to construct 80% probability ellipsoids of correct classification for the morphological types (Fig. 5-9).

Table 5-3 Morphological group image analysis results: **(1)** mean variable data, **(2)** latent vector loadings, **(3)** percentage variation explained by each latent vector.

Morphological	**Variable-Mean Data**						
Group	area	form.	conv.	leng.	fract.	aspect	fibre
capsule	0.1763	0.7172	0.8899	0.6045	1.038	2.006	0.7043
cauliflower	0.3774	0.6729	0.8609	0.8256	1.050	1.652	1.0910
fragmentary	0.0695	0.6715	0.8669	0.3443	1.069	1.762	0.4530
lobate	0.2283	0.6481	0.8492	0.6458	1.048	1.755	0.8590
ovoidal	0.2240	0.7293	0.8702	0.6091	1.067	1.600	0.7711
tabular	0.2299	0.7553	0.8897	0.6495	1.029	1.618	0.7874
vermicular	0.1505	0.6558	0.8853	0.5833	1.046	2.246	0.6973

form.=formfactor
conv.=convexicity
leng.=length
fract.=fractal

First four latent vectors (LV)

Variables	**LV1**	**LV2**	**LV3**	**LV4**
area	9.13	4.83	4.81	3.55
form.	-21.36	-17.34	-12.64	-3.13
conv.	26.16	0.59	20.27	50.85
leng.	-7.87	4.28	-7.84	-13.86
fract.	3.61	11.81	-21.30	24.99
aspect	0.22	-3.60	0.01	0.64
fibre	-2.08	-5.02	4.77	10.84

Percent Variation explained by LV(#)

	LV1	LV2	LV3	LV4
% variation	51.47	30.04	10.95	4.87

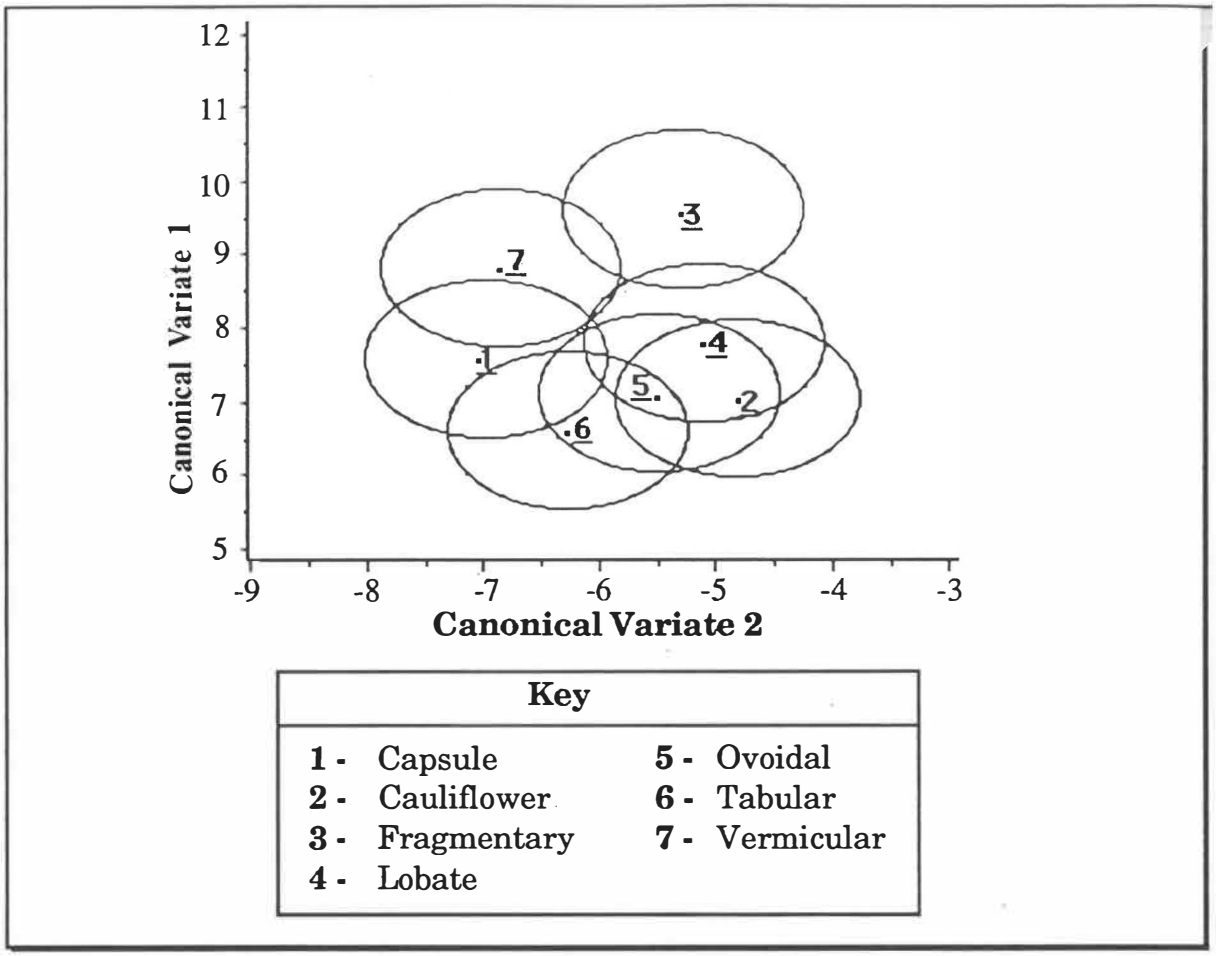

Fig. 5-9 Field boundaries and group centroids of the seven morphological forms (1-7) investigated using the image analyser. Centroids calculated from group and variable mean data, ellipsoids enclose 80% probability classification regions.

The classification ellipsoids show considerable overlap but clearly distinguish several important morphological groupings. Vermicular and fragmentary groups are well separated. Capsule and lobate groups are well separated. Unfortunately, the technique does not resolve similar morphological forms clearly (e.g., ovoidal, lobate, cauliflower). Possible causes for this are:

(1) Magnification changes. In some cases (e.g., assimilation of photographic images) the magnification used in collection of the grain image varied. This created a resolution problem. The problem can be exemplified using the Richardson principle. If a map of coastline is measured using dividers the length can be termed d_1, if the dividers are now set at half the previous width and the coastline re-measured the length of coastline (d_2) appears to increase

by a factor $d_2 = k * \log(d_1)$. Obviously, the true length of coastline does not increase, but with increased resolution (i.e., smaller divider widths) more irregularities in the coastline are accounted for. This problem manifests itself in image analysis work in that changes in magnification will cause changes in formfactor, convexicity, and fractal dimensions for the same grain. If extreme values are present in the data set because of this factor the location of the morphological group centroid will be incorrectly calculated. Therefore, the probability classification ellipsoid will be incorrectly located. The use of a large data base may partly negate the problem but it would seem more efficient to use only a set magnification for image assimilation and remove the problem altogether.

(2) Morphological genetic association. It has been suggested that lobate grains evolve from grains of different shapes rather than forming by direct chemical precipitation (Triplehorn 1966; Odin & Letolle 1980; Odin & Matter 1981). There is an abundance of ovoidal form glauconite in the Te Kuiti Group. Cracks in the ovoidal form are probable locations of secondary glauconite formation. Secondary glauconite growth would cause expansive dislocation of individual lobes on ovoidal grains. It would seem logical to suggest that there is a genetic association between lobate and ovoidal forms in Te Kuiti Group glauconites.

Cauliflower glauconite is probably formed by diagenetic chemical attack on glauconite (McConchie & Lewis 1980). As ovoidal glauconite dominates the Te Kuiti Group assemblage it is highly likely that this morphological form will have a high representation as the cauliflower precursory phase.

This suggests the three morphological types (ovoidal, lobate and cauliflower) are genetically related. Genetically related materials will show considerable overlap in Fig. 5-9 because the classification is based on probability fields not absolute divisions.

5-1-2C Image analysis: model test

Three sample slides used in the binocular microscope morphology investigation were used as the media from which 600 random grain images (200 per sample) were assimilated to test the canonical variate image analysis model developed above. As established by binocular microscope investigation the samples MC10a, MC29, and MC44 have specific morphological group bias (see Section D2 of the data booklet). For each individual grain image the image analysis variables were transformed using the model latent vector loadings and plotted on a CV1 versus CV2 graph; subsequent to this the 80% confidence interval ellipsoids were overlaid on the plots.

The resulting graphs (Figs. 5-10a to 5-10c) show several features. The data on Fig. 5-10a correlate reasonably well with the binocular classification of MC10a; numerous data points (approximately 40%) plot in the ovoidal field. The data distribution on Fig. 5-10a suggests that lobate (~33%), vermicular (~10%), and fragmentary (~26%) grains are statistically more significant than assigned using the binocular microscope classification technique.

A special cautionary note about the percentage of each morphological type listed above must be noted. Owing to the fact that the probability classification fields overlap a grain often exists in more than one morphology field for the calculation of percentages of each morphological type. To overcome this it would be necessary to write a computer program which calculated how many fields overlapped at a specific position on the graph then apportion a percentage of 1% to that morphological field. For example, if the calculated position of a grain of unknown morphology was near the centroid of tabular grains (point 6, Fig. 5-9), theoretically, it could also be classified as an ovoidal grain. Therefore, only 0.5% should be added to the total percentage of tabular and ovoidal grains. If three fields overlapped only 0.33% could be apportioned to any one of the three morphological type. I have not attempted to add this factor into my calculations of percentage for each morphological type as the complicated vectorial calculations and programming required is well beyond the scope of this study.

Fig. 5-10b is problematic in that most of the data points plot near probability field boundaries. This exemplifies a major problem with binocular microscope classification, that is, the requirement of fitting of grains into predefined divisions. The data in Fig. 5-10b suggest many grains in sample MC29 fall between the ovoid, capsule and lobate fields and cannot in many instances be assigned with certainty to one morphological group. Binocular studies suggest MC29 is dominated by lobate grains (57% in Section D2 of data booklet). A high proportion of lobate grains would be extremely difficult to prove based on Fig. 5-10b.

Data in Fig. 5-10c shows a strong correlation with the binocular microscope classification for the sample; MC44 is dominated by a high fragmentary component. Fig. 5-10c shows approximately 43% of the sampled grains plot in the fragmentary field, lower than the 75% calculated from the binocular investigation of grain morphology. However, numerous data points in Fig. 5-10c plot outside all probability field boundaries. This is probably a manifestation of the resolution problem described previously. Most of the data in Fig. 5-10c tend toward the fragmentary apex of the plot.

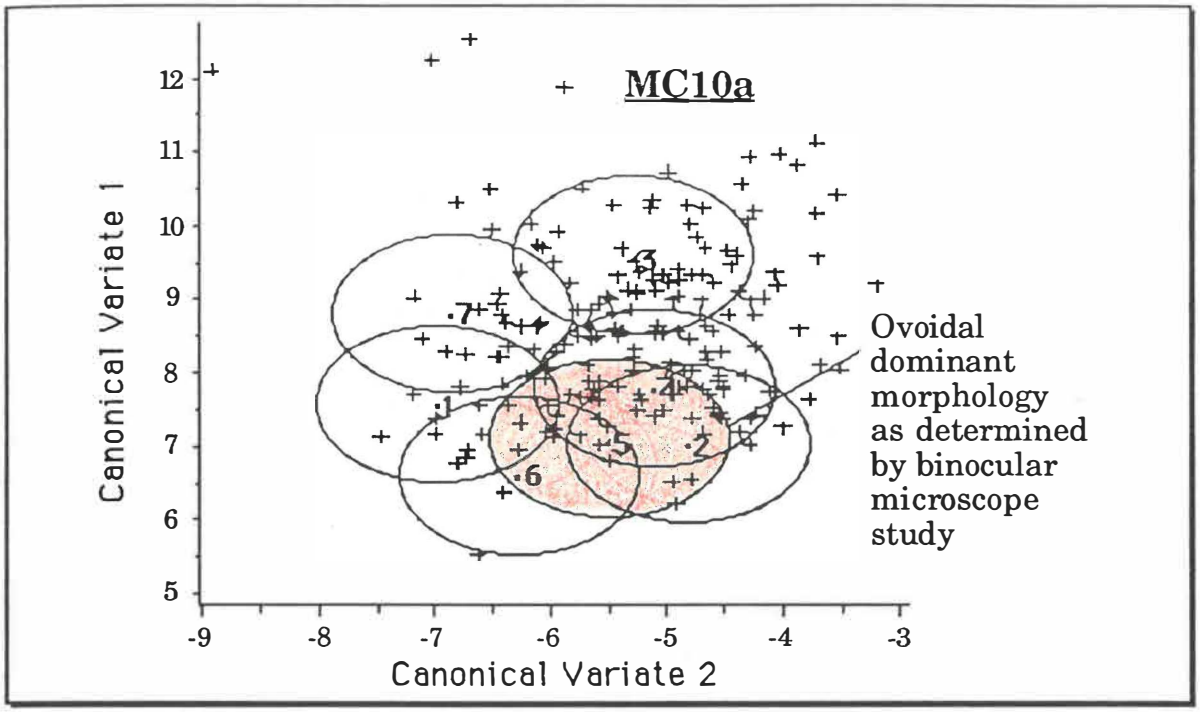

Fig. 5-10a

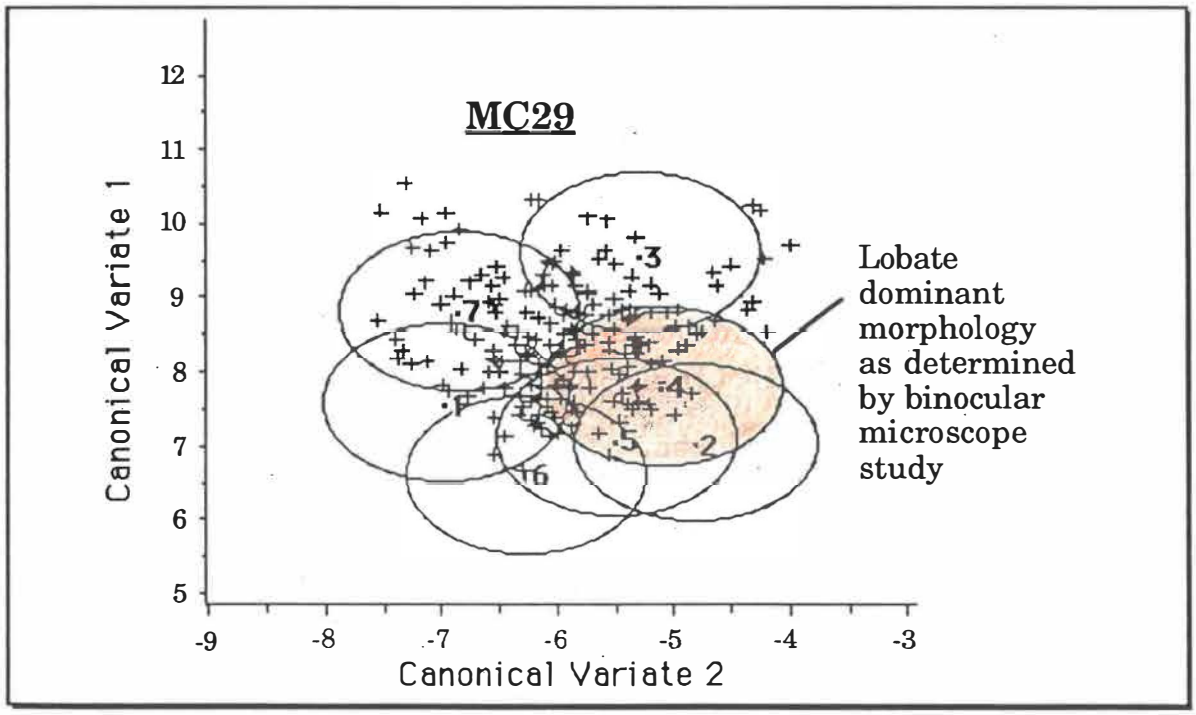

Fig. 5-10b

(caption next page)

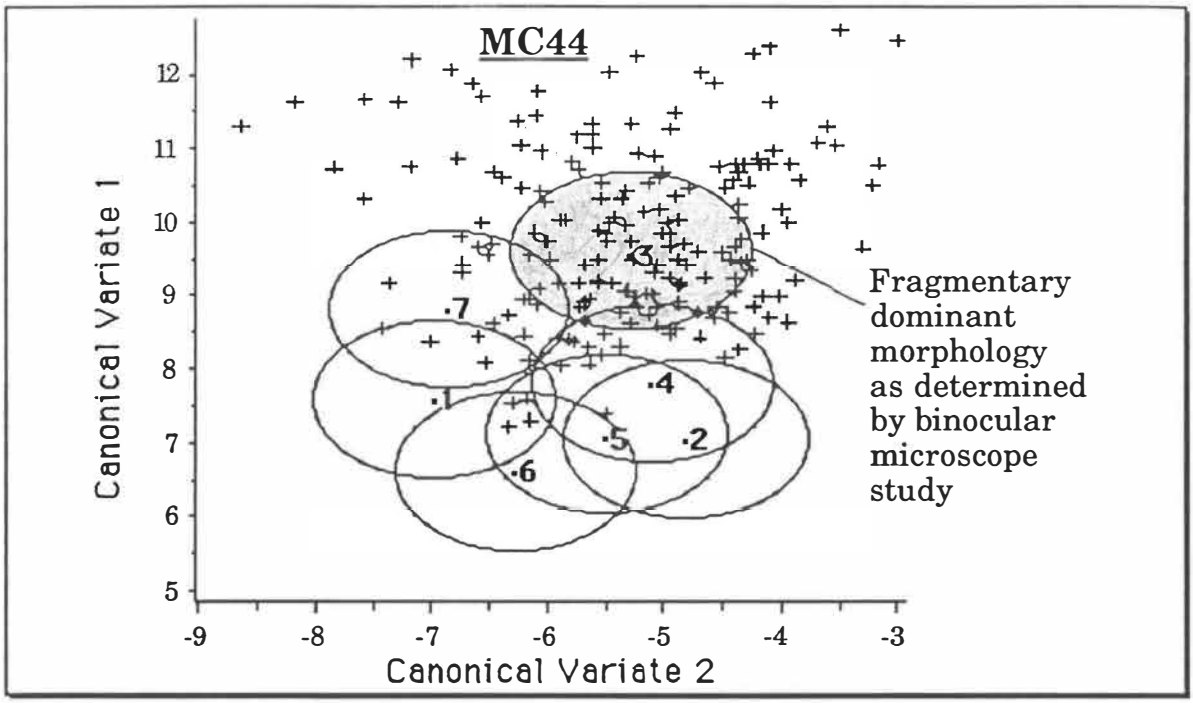

Fig. 5-10c

KEY TO FIELD NUMBERS	
1 - Capsule	**5** - Ovoidal
2 - Cauliflower	**6** - Tabular
3 - Fragmentary	**7** - Vermicular
4 - Lobate	

Fig 5-10a to Fig. 5-10c Grain shape image analysis data for samples MC10a, MC29 and MC44 transformed by the canonical variate latent vectors CV1 and CV2 of Table 5-3 and plotted over the 80% probability fields of the seven morphological forms investigated. The dominant morphological form as determined by the binocular microscope investigation is shaded in each diagram.

5-1-2D Improvements to the image analysis model

Retrospect is one of the most powerful tools in scientific investigation. Subsequent to the completion and analysis of this section of work two factors emerged as being highly significant in the collection of the primary data base. These were:

(1) Magnification of images on assimilation must be maintained constant to prevent resolution problems.

(2) A large data base is not required for the development of morphological type probability fields. A small but well defined primary data base from which canonical latent vectors are calculated is more useful in classifying subsequent data.

In summary, two variables: magnification, and time required for collection of the data base, must be considered together if the image analysis technique is to be a viable alternative to the binocular microscope morphological classification technique. This study showed that the time required for collection of the database favours use of an image analyser over the binocular microscope if low magnifications are used. However, resolution becomes a problem at low magnifications in image analysis work. Personal experience would suggest 30 mm^2 is the maximum image analysis field area useful for morphological classification investigations unless a high resolution video camera is available. Another advantage of the image analysis technique is that genetic associations within the data and also the completeness to which a morphological form has evolved within a sample can be made.

(5-2) DIFFERENTIAL THERMAL ANALYSIS (DTA)

The DTA characteristics of six samples (MC6, MC20, MC27a, MC31b, MC36a, MC44) with varying percent expandables was undertaken as part of this study. The data collected is presented in Section D5 of the data booklet. Three of the DTA traces (MC6, MC31b, and MC44) are shown in Fig. 5-11. Fig 5-11 shows that the DTA traces of the three samples are similar in form except for: **(1)** the amplitude of the first endothermic peak in the 50°-150°C region; and (2) the location and amplitude of the third endothermic peak in the 700°-800°C region.

The amplitude of the first endothermic peak (50°-150°C) relates to the percent expandables (refer to Section 2-4-2). With an increasing percentage of expandable layers the amplitude of the first peak increases. This feature is shown by the three samples in Fig. 5-11.

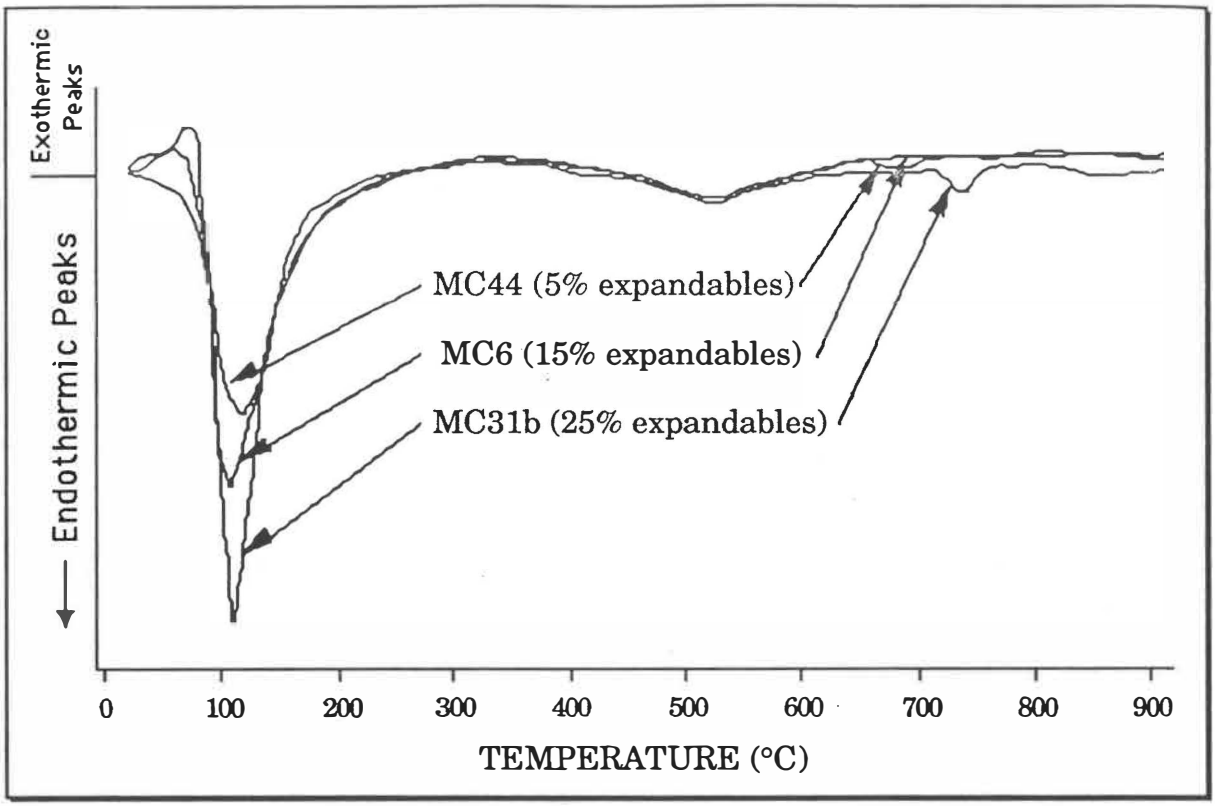

Fig. 5-11 DTA traces of MC44, MC6 and MC31b glauconite concentrates showing the variability in peak heights and shape due to variations in the expandable layer percentage.

The amplitude of the third endothermic peak in the 700°-800°C region has been previously related to the iron content of glauconite (McConchie & Lewis 1978). This was not shown by this DTA investigation. MC44 (25.48 wt% Fe_2O_3) has the highest iron content of the three samples in Fig. 5-11, MC31b (24.15 wt% Fe_2O_3) has the lowest iron content. Yet MC31b has the largest endothermic peak in the 700°-800°C region. The use of the amplitude of the 700°-800°C endothermic peak as diagnostic of the iron content does not seem applicable to the Te Kuiti Group samples studied.

(5-3) X-RAY DIFFRACTION (XRD)

5-3-1 XRD classification of Te Kuiti Group glauconite

XRD traces were obtained from all glauconite concentrates, unless the glauconite sample was too small to permit an XRD mount being prepared. Overall the quality of XRD traces obtained from the Te Kuiti glauconite samples was poor, a feature previously noted by Nelson (1973). This probably reflects the low degree of crystallinity of the glauconite samples (Nelson 1973).

Presenting all the data obtainable from an XRD trace would be superfluous, therefore a synthesis of the relevant classification information is presented in Section D6a and Section D6b of the data booklet.

The XRD data combined with the calculated percent expandable data (see Section A1-6) and disorder coefficient information were used to classify the glauconite samples. Three classification schemes (Table 2-2) were used to classify the glauconite concentrates: **(a)** that of Hower (1961) based on percent expandables; **(b)** Bentor & Kastner (1965), based on the d(001) 10Å peak location and also the presence of the 3.63Å and 3.09Å peaks; and **(c)** McConchie & Lewis (1980), based on expandable content and disorder coefficient values. The results of the above classifications for Te Kuiti Group glauconite are shown in Table 5-4.

Table 5-4 Classification of glauconite samples collected based on their XRD characteristics, expandable content (derived from chemical data), and disorder coefficient value.

Sample	Formation	%Exp	D.C.	H	B&K	McC&L
MC02a	P	11-15		2	2	2
MC06	E	11-15	0.66	2	2	2
MC07	E	21-25	1.70	3	3	2
MC09b	E	11-15	0.70	2	2	2
MC11a	E	0-5	0.52	1	1	2
MC11b	E	0-5	0.44	1	n.d.	2
MC14	E	11-15		2	2	2
MC10a	Wh	21-25	0.68	3	3	2
MC25a	Wh	36-40		3	2	2
MC25b	Wh	31-35	0.57	3	2	2
MC31a	Wh	16-20		2	3	2
MC31b	Wh	21-25		3	2	2
MC31c	Wh	21-25		3	2	2
MC31d	Wh	31-35		3	2	2
MC38a	Wh	26-30	0.92	3	2	2
MC38b	Wh	31-35		3	3	2
MC05b	Ao	16-20		2	1	2
MC13	Ao	16-20		2	2	2
MC18	Ao	6-10		1	1	1
MC19b	Ao	11-15	0.61	2	3	2
MC20	Ao	6-10	0.64	1	1	2
MC21	Ao	11-15	0.65	2	3	2
MC24	Ao	11-15		2	1	2
MC26	Ao	16-20	0.28	2	3	2
MC27a	Ao	11-15		2	n.d.	2
MC28	Ao	11-15	0.45	2	3	2
MC36b	Ao	0-5	0.59	1	2	2
MC44	Ao	6-10	0.77	1	3	2
MC45	Ao	11-15	0.38	2	2	2

(continued next page)

MC19a	Or	16-20	0.60	2	2	2
MC27c	Or	11-15	1.12	2	2	2
MC29	Or	26-30	1.36	3	3	2
MC30	Or	16-20		2	3	2
MC32	Or	31-35		3	n.d.	2
MC37	Or	26-30		3	n.d.	2
MC40	Or	26-30	0.55	3	2	2

%Exp = percent expandables.

D.C. = disorder coeffiecent calculated at 400°C.

H = classification using Hower's (1961) scale:

1 = ≤ 10% expandable layers

2 = 10-20% expandable layers

3 = >20% expandable layers.

B&K = classification using Bentor & Kastner's (1965) scale:

1 = Class 1 (a) peaks at 10.1, 4.53, 3.63, 3.33, and 3.09 Å

2 = Class 1 (b) peaks 3.63 and 3.09 Å absent

3 = Class 2 d(001) >10.1 Å.

McC&L = classification using McConchie & Lewis's (1980) scale:

1 = Class 1 ≤10% expandables and D.C ≤0.25

2 = Class 2 ≤40% expandables and D.C>0.25

3 = Class 3 >40% expandables.

None of the classification schemes is entirely satisfactory in classifying the glauconite concentrates in this study, because:

(a) Hower's classification scheme is easily corrupted by spurious calculations of expandables (described in Section 2-2-2). A classification based solely on percent expandables would seem inadequate.

(b) Bentor & Kastner's limitations on the location of the d(001) (10.1Å) peak are unrealistic. Small errors in 2θ value observations make for large differences in the d(001) peak position. When one considers that sample MC18 (classified as type 1 glauconite by all three classification schemes) has two similar height d(001) peaks at 8.6° (10.282Å) and 8.8° (10.048Å) the problem of division around a 10.1Å peak location is obvious. Bentor & Kastner's classification scheme also uses the combined presence or absence of the 3.09Å and 3.63Å peaks. Random powder mounts in this study often showed the 3.63Å peak to be poorly developed even if the 3.09Å peak was well developed, making classification difficult. A computer-generated XRD pattern for ASTM file 9-439 glauconite showed the 3.63Å peak has a very low reflectance intensity for type mineral glauconite (see Section A3-3). This and the observed random powder traces leads to the conclusion that the use of the 3.63Å peak is not valid in the classification of glauconite samples.

(c) McConchie & Lewis's disorder coefficient is also problematic; often the expandable content of the glauconite differs markedly from the calculated disorder coefficient. For example, MC26 has a disorder coefficient of 0.28 (lowest of all samples investigated) and yet MC26 has a high expandable content of 16%-20%. MC44 with only 6%-10% expandables has a much higher disorder coefficient of 0.77. Whether there is a need to redefine the disorder coefficient classification boundaries used by McConchie & Lewis (1980) or an alteration to the temperature of firing for the calculation of the disorder coefficient (see Section 2-2-2) is an area of possible further research. Until such questions are answered the classification scheme suggested by McConchie & Lewis (1980) cannot be reliably used for the Te Kuiti Group glauconites.

All of the XRD classification schemes used showed Te Kuiti Group glauconite is dominated by the poorly-crystalline phase glauconite; only a few of the collected samples exhibited the more crystalline mica-like phase glauconite.

The average percent expandable content of the sampled formations was plotted (Fig. 5-12). Bentor & Kastner (1965) noted that glauconites formed in argillaceous marls have a higher proportion of expandable layers than glauconite of equivalent age formed in cleaner (less-terrigenous influenced) sandstones. This feature is apparent in Fig. 5-12; the glauconite from Aotea Sandstone has a lower percentage of expandable layers (10% average) than glauconite from the Whaingaroa Siltstone (26% average). The Elgood Limestone samples were all from very pure calcitic limestone with a low terrigenous content; this is reflected by the low percent expandables observed for these samples (10% average). The Orahiri Limestone samples by comparison have a much higher percent expandable content (22% average). This reflects one or more of:

(a) A semi-enclosed, more terrigenous influenced regime in the south of the study area compared with the north depocentres.

(b) The progenitor material of glauconite in many Orahiri Limestones has been shown by morphological studies to be micaceous, as evidenced by the presence of vermicular grains. The difference in expandable content may represent a progenitor influence (i.e., micaceous silicate versus calcitic material) rather than an environmental influence.

(c) Burial and cessation of glauconitisation occurred earlier in the Orahiri Limestone compared with other Te Kuiti Group formations.

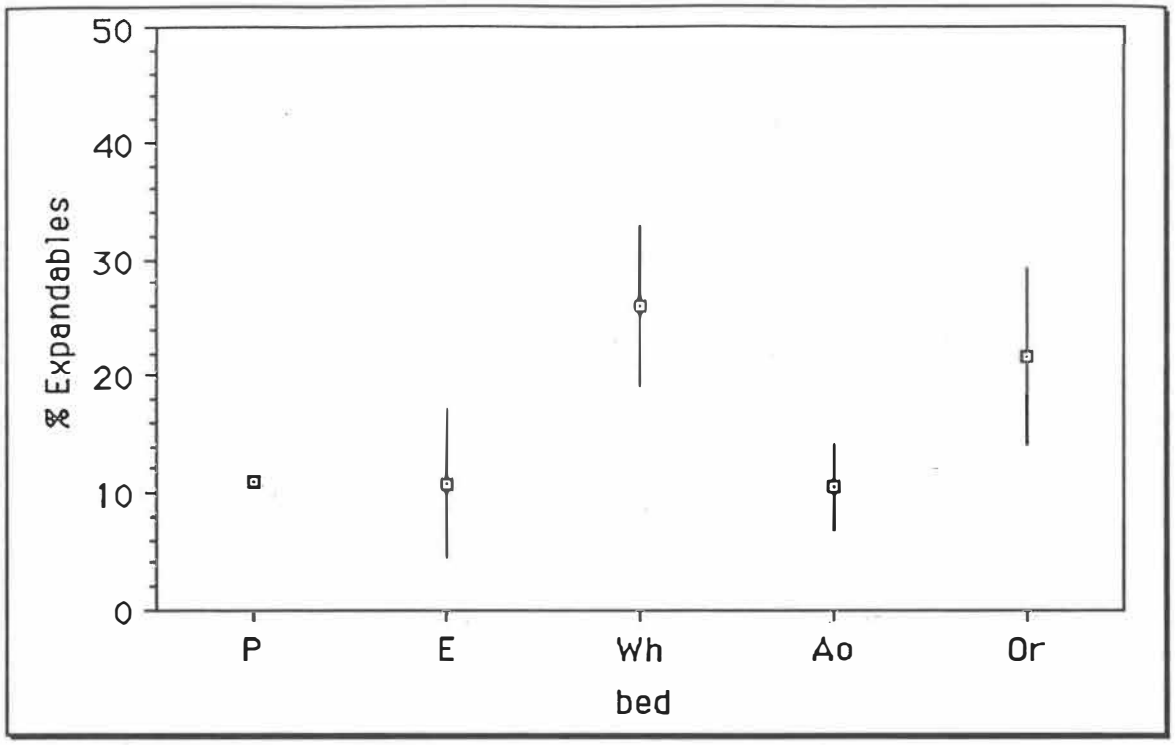

Fig 5-12 Average percent expandable content calculated from K_2O content (see Section A1-6) and population one standard deviation for four glauconite bearing formations within the Te Kuiti Group. No standard deviation is given for Pukemiro Sandstone as only one XRD percent expandable calculation was made for this bed.

5-3-2 Theoretical XRD classification scheme

Owing to the inability of the classification schemes to consistently classify the glauconite samples collected an alternative classification scheme with less dependence on physical XRD techniques was sought. Toward this end two computer programmes were used to: **(a)** determine the structural composition of the glauconite from chemical data (Shelx and Clayform programs); and **(b)** theoretically calculate the XRD trace expected from a given structural composition (Lazy Pulverix program).

By assigning 1000 to the d(001) peak intensity and then calculating all other peak heights and locations relative to d(001) it should be possible to see shifts in peak height and location caused by changes in expandable layer content and crystal occupancy. Because of time constraints only three samples were used to create the theoretical XRD traces of varying expandable content (Fig. 5-13). Electron microprobe data for $\%K_2O + \%Na_2O$ was used in combination with fig.1 of Velde & Odin (1975) to determine the basal lattice c-spacing.

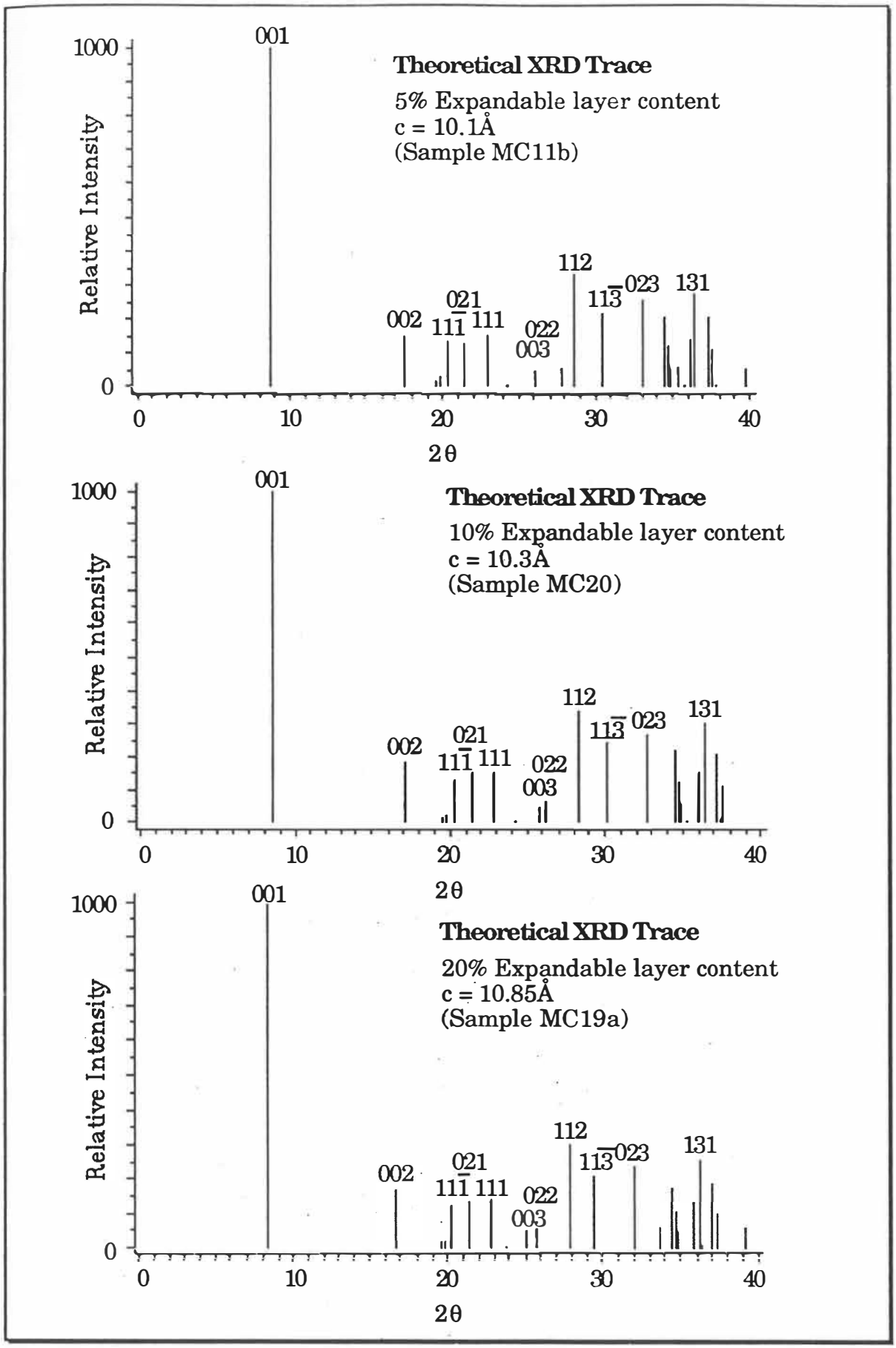

(caption next page)

Fig 5-13 Theoretically calculated XRD traces. Derived from chemical data collected for glauconite from selected Te Kuiti Group samples.

The resultant theoretical XRD traces do not show significant differences in form. This can be predominantly attributed to the basal lattice spacings being similar and differences in lattice-point occupancy between the samples being small. These results suggest that a **theoretical** XRD trace based classification of glauconite is not able to be made using the computer techniques of this study. However, the computer generated XRD data from the chemistry of ASTM 9-439 glauconite is very similar to the physical XRD data recorded for ASTM 9-439 glauconite. Therefore, the techniques developed in this study may be applicable for the generation of theoretical XRD Miller indices for glauconite (thereby negating the necessity to set up tedious precession camera mounts).

Chemical data using XRF and EMP can be obtained for glauconite quickly and with relative ease. There are well established literature correlations between chemistry (particularly $\%K_2O$ content) and the mineralogical form of glauconite present in the deposit. As chemical investigations generally generate more reproducible results than XRD techniques, it would seem logical to move away from an XRD based classification and toward a chemically based classification for glauconites.

(5-4) INFRARED ANALYSIS (IR)

Two lines representing shifts in the 9-11μm peak position versus the measured expandable content were calculated from the data of Manghnani & Hower (1964) and McConchie (1978). Overlain on this plot were the data for infrared peak position versus the % expandable content calculated from chemical data in this study (Fig. 5-14). The infrared data and the degraded illite content of the samples are listed in Section D7 of the data booklet. Most of the data on Fig. 5-14 do not plot near the interpolation lines **1** and **2** of Fig. 5-14. McConchie (1978) observed that almost all the spurious points he detected in his study (i.e., those lying away from the trend of Manghnani & Howers (1964) data, line **1** on Fig. 5-14) contained a significant proportion of degraded illite. This feature was tested for in several samples. Only 4 of the 13 samples tested had statistically significant degraded illite, of these, only 2 plotted away from the correlation lines 1 and 2 on Fig. 5-14. Fitting of a second degree polynomial to the data showed a low correlation (R=0.48) exists

between 9-11μm IR peak position and %expandables. The most significant feature of the relationship is that the trend of the polynomial is reversed above 980μm from the calculated lines of Manghnani & Hower (1964) and McConchie (1978). Nakamoto (1978) assigns peaks in silicates in the 9-11μm region to υSi-O vibrations. Whether the expandable IR peak relationship could be related to the fact that interlayer cation content increases with increasing expandables and hence the strongly polar K^+ and Na^+ affect the stretching υSi-O bond could not be determined. Another possibility is that the point of inflexion of the second degree polynomial curve could represent the most stable bonding energy for the Si-O bond (interestingly the molecular SiO_4 absorption band is approximately 975μm).

McConchie (1978) suggested that shifts in the 9-11μm peak position are caused either by an increase in the number of montmorillonitic layers or a change in the layer charge. Correlations between the tetrahedral, octahedral and interlayer charge versus the 9-11μm peak position were calculated. R values ranged from 0.37 for tetrahedral charge versus infrared peak position to 0.12 for octahedral charge versus infrared peak position. A general increase in tetrahedral layer charge was observed with increasing 9-11μm infrared peak wavelength. As the Si-O bond is in the tetrahedral layer of glauconite it would seem logical to expect that changes in the 9-11μm peak position will correspond most closely to changes in the tetrahedral layer charge rather than the octahedral or interlayer charge.

Overall, the infrared information was of poor quality. The data show a wide degree of scatter and any conclusions can only be considered tentative.

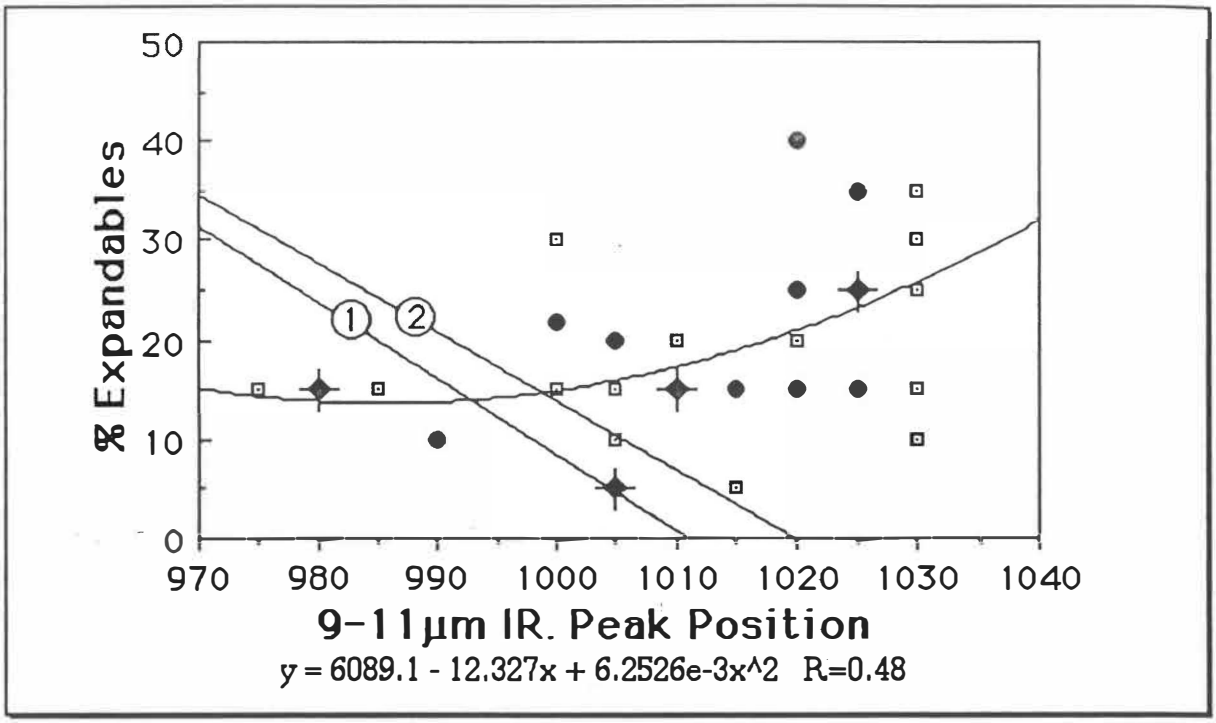

KEY

⊡ Sample

● Sample for which degraded illite content was calculated

✦ Sample whose degraded illite content was statistically significant (i.e., greater than 10% degraded illite)

1 Best line of fit through Manghnani & Hower's (1964) data

2 Best line of fit through McConchie's (1978) data

Fig. 5-14 Scatter plot of glauconite expandable content calculated from $\%K_2O$ chemical data versus the position of the the 9-11µm infrared peak position. The data for expandability and 9-11µm peak position in this study do not fit the correlation lines of McConchie or Manghnani & Hower. The formula and correlation of the second degree polynomial fitted to the data in this study is shown below the x-axis label.

(5-5) X-RAY FLUORESCENCE ANALYSIS (XRF)

McConchie (1978) undertook a comprehensive XRF study of glauconites in the South Island of New Zealand. Much of the following section represents a comparison of the results obtained from that study with the results obtained in this study of Te Kuiti Group glauconites. The correlation matrix for the elements analysed using the Phillips PW1404 automatic sequential X-ray spectrometer at Victoria University, Wellington is shown in Table 5-5. The chemical data obtained using XRF are listed in Section D8 of the data booklet.

5-5-1 Major element analysis

As described in Section 2-5-7 several isomorphous substitutions in the glauconite lattice are possible and these cause mineralogical variability in glauconite. McConchie (1978) hypothesized that owing to the type of substitutions a negative correlation should exist between Fe and Si and also between Fe and Al. However, for the data in this study the correlation of Fe with Si is statistically insignificant (R=0.021) and the correlation of Fe with Al is also low (R=-0.698). The correlations do not agree with the electron microprobe (EMP) correlation data from glauconite grain centres (discussed in Section 5-6). The divergence between XRF and EMP correlations for Fe, Si, and Al is possibly due to surface contamination by trace amounts of Fe oxide and some quartz grain contamination of the sample. Some contamination is inevitable in a bulk glauconite sample irrespective of how carefully the sample is cleaned and prepared.

A moderate negative correlation is observed between Mg and Al (R=-0.828) (Fig. 5-15a). McConchie (1978) suggested that high Fe or Al contents would restrict the entry of Mg into octahedral positions in glauconite but that the charge effects would be balanced by the ability of tetrahedral Al to retain interlayer Mg. For the Te Kuiti Group samples there appears to be an artificially good relationship between Al and Mg caused by two distinct glauconite compositional series. For the Mg/Al relationship in the Te Kuiti Group the regression line is forced through two point populations defining the interpolation line and hence the relationship is highly correlated (Fig. 5-15a). The data form two distinct groupings, that of a low-Mg/high-Al major group and a separate high-Mg/low-Al group. The high-Mg/low-Al group consists of: MC19a (OrB5), MC19b (Ao4), MC21 (Ao4), MC26 (Ao4), MC27a (Ao4), MC27c (OrA2), and MC28 (Ao4).

Table 5-5 XRF chemical data correlation matrix for all sample analysis data listed in Section D8 of the data booklet.

	SiO_2	TiO_2	Al_2O_3	Fe_2O_3	MnO	MgO	CaO	Na_2O	K_2O	P_2O_5	LOI	Ga	Pb	Rb	Sr
TiO_2	-0.226	.	.	.	.	.	.	.	.	.	.	.	.	.	.
Al_2O_3	-0.182	0.588	.	.	.	.	.	.	.	.	.	.	.	.	.
Fe_2O_3	0.021	-0.651	-0.698	.	.	.	.	.	.	.	.	.	.	.	.
MnO	-0.316	0.254	0.313	0.201	.	.	.	.	.	.	.	.	.	.	.
MgO	0.493	-0.368	-0.828	0.460	-0.346	.	.	.	.	.	.	.	.	.	.
CaO	-0.635	0.538	0.452	-0.699	-0.078	-0.567	.	.	.	.	.	.	.	.	.
Na_2O	-0.128	0.541	0.359	-0.496	0.080	-0.283	0.526	.	.	.	.	.	.	.	.
K_2O	0.367	-0.676	-0.531	0.840	0.061	0.410	-0.831	-0.544	.	.	.	.	.	.	.
P_2O_5	-0.332	0.594	0.462	-0.741	-0.267	-0.448	0.817	0.475	-0.643	.	.	.	.	.	.
LOI	-0.494	0.544	0.431	-0.766	-0.117	-0.395	0.832	0.365	-0.944	0.619	.	.	.	.	.
Ga	0.020	0.575	0.709	-0.533	0.272	-0.456	0.191	0.255	-0.430	0.204	0.340	.	.	.	.
Pb	-0.246	0.113	0.239	0.175	0.417	-0.239	-0.088	0.024	0.111	-0.148	-0.125	0.192	.	.	.
Rb	0.185	-0.331	-0.250	0.645	0.334	0.145	-0.591	-0.340	0.739	-0.493	-0.758	-0.204	0.383	.	.
Sr	-0.327	0.541	0.380	-0.763	-0.377	-0.373	0.869	0.555	-0.810	0.796	0.768	0.220	-0.279	-0.693	.
Th	-0.381	0.497	0.609	-0.736	-0.149	-0.654	0.804	0.474	-0.633	0.784	0.642	0.393	-0.153	-0.504	0.807
U	-0.224	0.309	0.311	-0.104	0.020	-0.423	0.237	0.186	-0.000	0.420	-0.041	0.098	0.468	0.156	0.145
Y	-0.257	0.583	0.554	-0.619	-0.181	-0.447	0.589	0.343	-0.467	0.817	0.437	0.256	0.290	-0.182	0.586
As	-0.521	-0.213	0.034	0.522	0.603	-0.227	-0.164	-0.300	0.358	-0.379	-0.253	-0.082	0.543	0.371	-0.455
Sc	0.141	0.214	0.612	-0.659	-0.183	-0.357	0.279	0.233	-0.533	0.312	0.457	0.483	-0.225	-0.544	0.472
V	-0.358	-0.204	0.240	0.315	0.576	-0.421	-0.092	-0.219	0.258	-0.250	-0.191	0.095	0.241	0.203	-0.316
Cr	0.138	0.173	0.083	0.221	0.437	0.034	-0.409	-0.406	0.413	-0.223	-0.380	0.191	0.242	0.501	-0.514

	SiO_2	TiO_2	Al_2O_3	Fe_2O_3	MnO	MgO	CaO	Na_2O	K_2O	P_2O_5	LOI	Ga	Pb	Rb	Sr
Ba	-0.343	0.553	0.495	-0.351	0.290	-0.496	0.495	0.627	-0.359	0.466	0.221	0.328	0.369	-0.001	0.344
La	-0.211	0.548	0.608	-0.568	-0.170	-0.441	0.408	0.218	-0.426	0.606	0.435	0.401	0.366	-0.258	0.467
Ce	-0.300	0.449	0.640	-0.594	-0.255	-0.599	0.564	0.368	-0.481	0.644	0.465	0.396	0.052	-0.368	0.687
Ni	-0.349	0.200	0.386	-0.215	0.262	-0.471	0.388	0.247	-0.136	0.475	0.137	0.116	0.154	-0.000	0.155
Cu	0.048	0.230	-0.023	0.189	0.210	0.174	-0.359	-0.176	0.113	-0.279	-0.074	0.142	0.576	0.226	-0.342
Zn	0.134	-0.034	-0.199	0.030	-0.081	0.212	-0.053	-0.137	0.151	0.170	-0.105	-0.050	-0.153	-0.022	-0.160

	Th	U	Y	As	Sc	V	Cr	Ba	La	Ce	Ni	Cu
U	0.282	.	.	.	.	.	.	.	.	.	.	.
Y	0.615	0.518	.	.	.	.	.	.	.	.	.	.
As	-0.229	0.157	-0.178	.	.	.	.	.	.	.	.	.
Sc	0.391	-0.202	0.279	-0.351	.	.	.	.	.	.	.	.
V	0.022	0.087	-0.218	0.691	-0.023	.	.	.	.	.	.	.
Cr	-0.202	0.074	0.002	0.289	-0.352	0.289	.	.	.	.	.	.
Ba	0.449	0.555	0.480	0.077	0.017	0.028	-0.091	.	.	.	.	.
La	0.529	0.442	0.875	-0.106	0.391	-0.162	0.073	0.269	.	.	.	.
Ce	0.755	0.390	0.705	-0.126	0.558	-0.049	-0.233	0.380	0.786	.	.	.
Ni	0.376	0.344	0.438	0.126	0.082	0.379	0.091	0.590	0.195	0.161	.	.
Cu	-0.407	0.128	0.105	0.221	-0.154	-0.001	0.378	-0.076	0.329	-0.092	-0.166	.
Zn	-0.094	0.037	0.018	-0.176	-0.214	0.029	0.275	0.040	-0.162	-0.378	0.572	-0.041

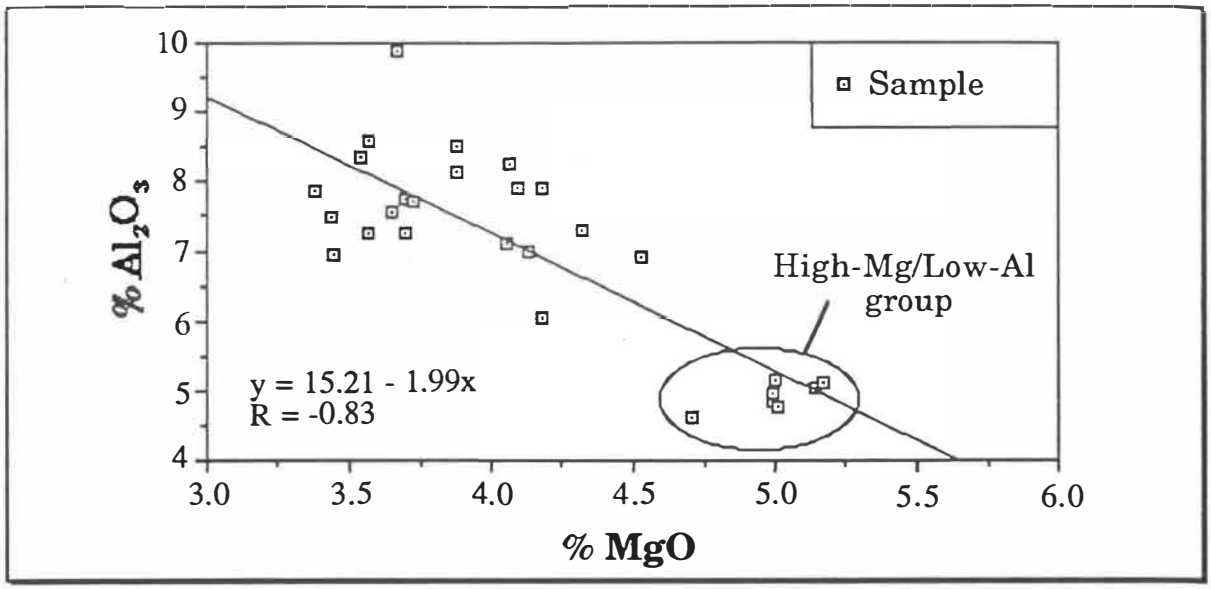

Fig. 5-15a

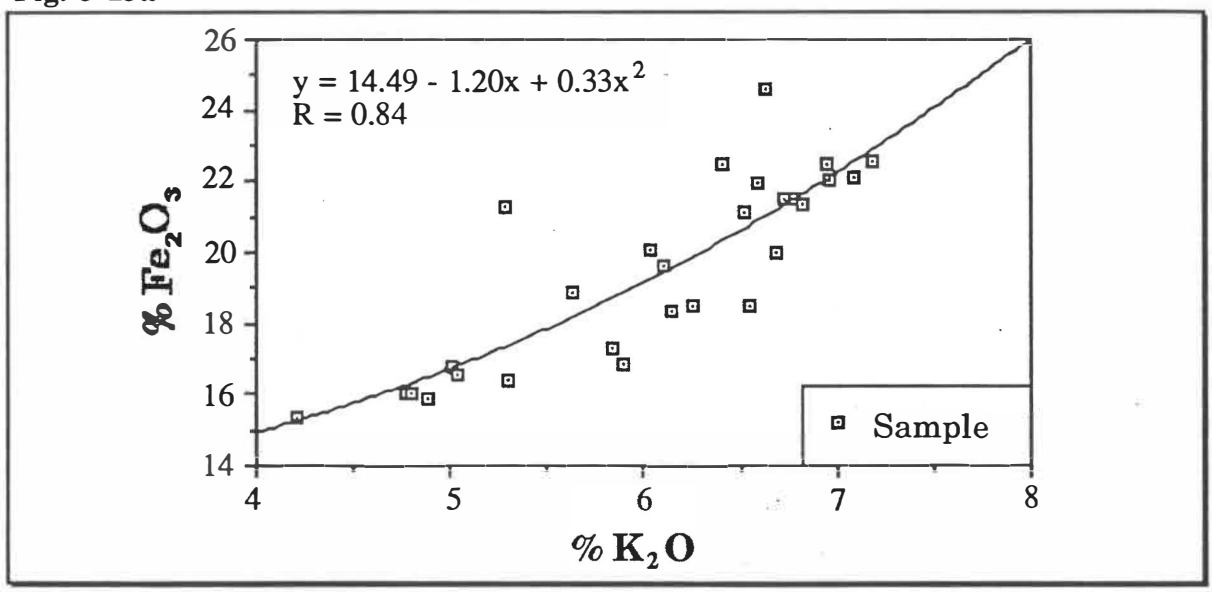

Fig. 5-15b

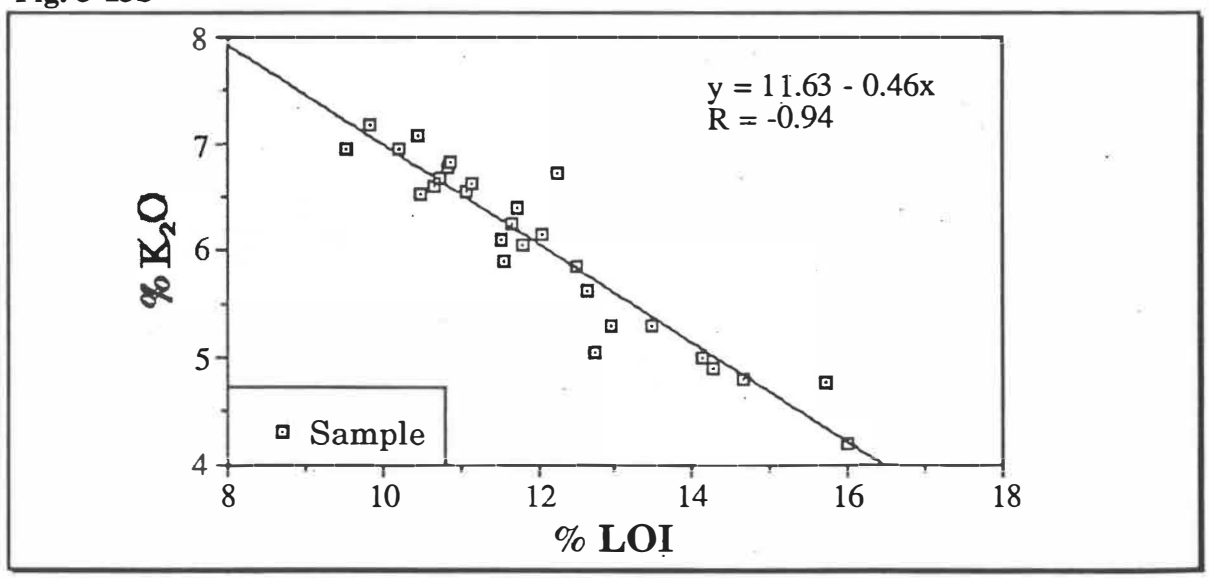

Fig. 5-15c

(caption next page)

Fig 5-15 (a) Relationship between Al_2O_3 content and MgO content of XRF analysed samples. Two groups appear to be divisible based on their Al/Mg ratio. The high-Mg/low-Al group glauconites from the Otorohanga - Waitomo - Te Kuiti area are circled.

(b) Relationship between K_2O and Fe_2O_3 content. With increasing glauconitisation the Fe_2O_3 content increases and the K_2O content also rises.

(c) Relationship between water content (LOI) and K_2O content (a surrogate for expandable layer content). LOI = loss on ignition (XRF).

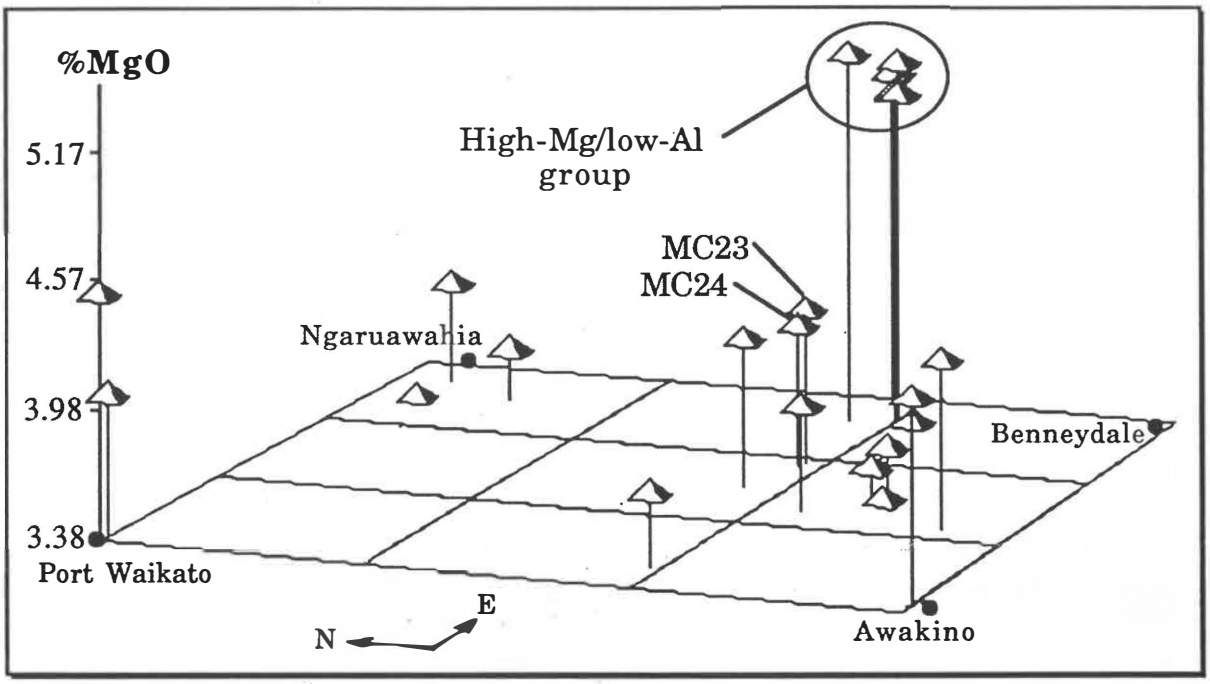

Fig. 5-16 Three dimensional scatter plot showing the relationship between MgO content of the XRF analysed samples and their geographic location. The high-Mg/low-Al group is circled for easy identification.

Previous stratigraphic work by Nelson (1978a) evidenced a small semi-enclosed embayment, bordered to the east, west and south, extended through the Otorohanga - Waitomo - Te Kuiti area during deposition of the Aotea Sandstone (see Map 2 for centre locations). This embayment persisted in the local Te Kuiti area during deposition of the Orahiri Limestone. The locations of all the samples in the high-Mg/low-Al group are from within this

embayment; indeed samples MC23 (Ao4) and MC24 (Ao4) collected only 10km west of the hypothesized embayment have a significantly lower Mg content compared to those from within the embayment (Fig. 5-16). This suggests the embayment was semi-isolated from terrigenous input from the major depocentre further west. High-Mg contents of the glauconite suggest more clay-rich suspensions flowed into the semi-enclosed embayment area. A possible reason for the strong distinction in Mg content is that sea currents may have been partially restricted within the embayment compared with the depocentre further west.

There is a strong correlation between K and Fe (R=0.840) (Fig.5-15b). This correlation is expected, as K is adsorbed into interlayer lattice positions during development of the glauconite grain. Another of the primary processes in the development of glauconite is the adsorption and subsequent incorporation of iron into the silicate lattice (Hower 1961). There has been some debate as to whether Fe content controls the uptake of K into the glauconite lattice or whether the processes of uptake of the two elements is separate (e.g., Hower 1961 versus Bentor & Kastner 1965). With increasing glauconitisation it would be expected that there would be an increase in both Fe and K content but the relationship may not be linear. The trend of the data in Fig. 5-15b is not linear and suggests the uptake of the two elements is indeed separate.

The Fe to Al correlation is low for the XRF data (R=-0.698). The negative correlation suggests the glauconite lattice has a high initial Al/Fe ratio which decreases with the evolution of the glauconite grain. The decrease in Al/Fe is caused by: **(1)** the adsorption of iron from pore waters into the lattice; and **(2)** Fe^{3+} and Fe^{2+} replacing octahedral Al^{3+}.

The correlation of K content and water content is very strong (Fig. 5-15c). This confirms the previous observations of Manghnani & Hower (1964), McRae & Lambert (1968), and McConchie (1978) that water content decreases with decreasing expandable layer content.

5-5-2 Trace element analysis

McConchie (1978) has suggested four groupings of trace elements based on their statistical analysis (the definition of his statistical parameter is not given but from his text it appears to be the correlation of one element versus another). The groupings given by McConchie (1978) are:

(1) Mn, Ti, V, Zr, Y.

(2) P, S.

(3) Rb, Sr.

(4) Cu, Ga, Ni, Pb, Zn.

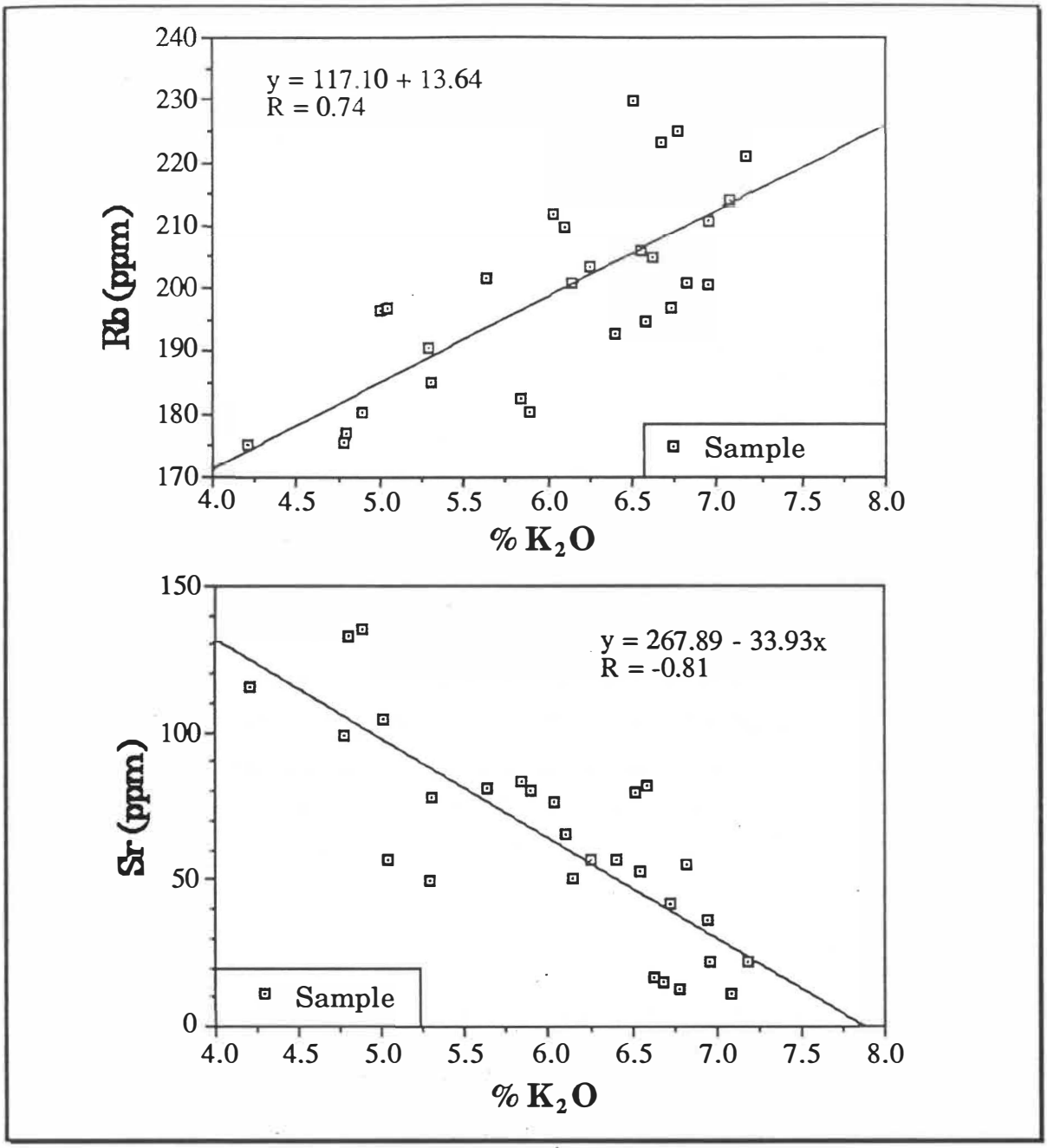

Fig. 5-17 Scatter plots of Rb and Sr versus K_2O content for XRF samples analysed in this study.

The correlations between the first group of elements in this study was very low (Table 5-5). McConchie (1978) suggests the elements of this group occupy octahedral sites in the glauconite lattice replacing Fe^{3+}, Fe^{2+}, and Mg^{2+}. Comparing the ionic radius and charge of Mn^{4+}, Ti^{4+}, and Zr^{4+} with those of Fe^{3+}, Fe^{2+}, and Mg^{2+} it is possible for such replacements to occur. However, the inclusion of V, a 5+ valency ion and Y^{3+}, with an ionic radius of 0.92 in the first group of elements does not seem justifiable on ionic radius and ionic charge grounds.

Determining the validity of the second grouping of McConchie (1978) was not possible in this study as data for S were not available.

The relationships between the third group of elements (Sr and Rb) is well documented in the literature (e.g., Hower 1961; McConchie 1978). Fig. 5-17 shows scatter diagrams of Sr vs K_2O and Rb vs K_2O. Because of the correlation between Rb, Sr and the %expandables in glauconite Hower (1961) assigned both elements to interlayer positions. There is a strong relationship between Rb, Sr, LOI, and K_20 which supports the conclusion that Rb and Sr are interlayer cations. A strong relationship exists between Sr and Ca (R=0.869) and Ca and LOI (water content or expandability) (R=0.832). This combined with the similar ionic potentials (Sr^{2+}=1.8 and Ca^{2+}=2.0) suggests Ca is also present as an exchangeable interlayer cation. Possibly, Ca should be included as a member of this third group of elements.

Elements of the fourth group of McConchie (1978) have low correlations with all other elements, except for Ga. Ga which correlates with Al, and in many cases behaves similarly to Al in the lattice, should be eliminated from the fourth group of elements. The fourth group elements are generally of low solubility and their concentration in the glauconite lattice appears to be related to initial concentration in solution rather than the degree of glauconitisation (Degens et al. 1957; Potter et al. 1963; Shimp et al. 1963 in McConchie 1978). This group of elements could be termed a low-mobility index group.

Recent work on greywackes indicates possible additions of other trace elements to this low-mobility index group could include: La, Ce, Nd, Th, Zr, Hf, Nb, and Sc (Bhatia & Crook 1986). Balashov & Kazakov (1968, p.609) observed "glauconite inherits the rare earth composition of marine suspensions". McConchie (1978) noted Cu, Zn, and Pb may be useful elements for paleoenvironmental reconstruction, because: **(1)** the relative immobility and low residence time of these elements in sea water (Holand 1978); and **(2)** the ability of glauconite to adsorb these elements from solution independent from the glauconitisation process (Krauskopf 1956). Of McConchie's (1978) fourth group of elements it was determined that Pb and Ni would be the most satisfactory indicators of provenance for glauconite samples in this study.

Fig. 5-18a shows a three dimensional representation of the concentration of Pb as a function of geographic location of the sample. The samples are all similar in their Pb concentrations except for MC44 (AoA), MC38a (WhA), and MC36b (Ao3) which are significantly enriched in Pb compared to other samples. Fig. 5-18b shows the correspondence of Ni content and geographic location. In the Ni example 5 samples have much higher than average Ni concentration, the samples are: MC6 (E), MC5b (Te.Ak.), MC11b (E), MC35

(AoA), and MC36b (Ao3). For both the Ni and Pb concentration data there does not appear to be a relationship between stratigraphic bed and element concentration.

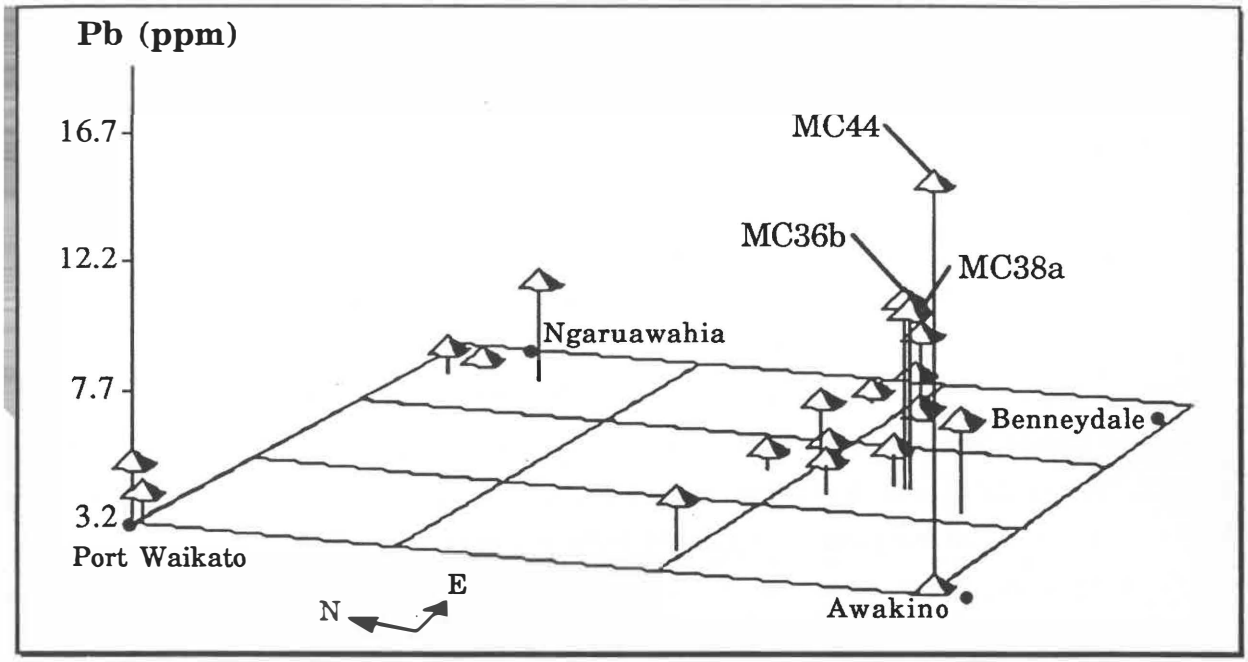

Fig. 5-18a

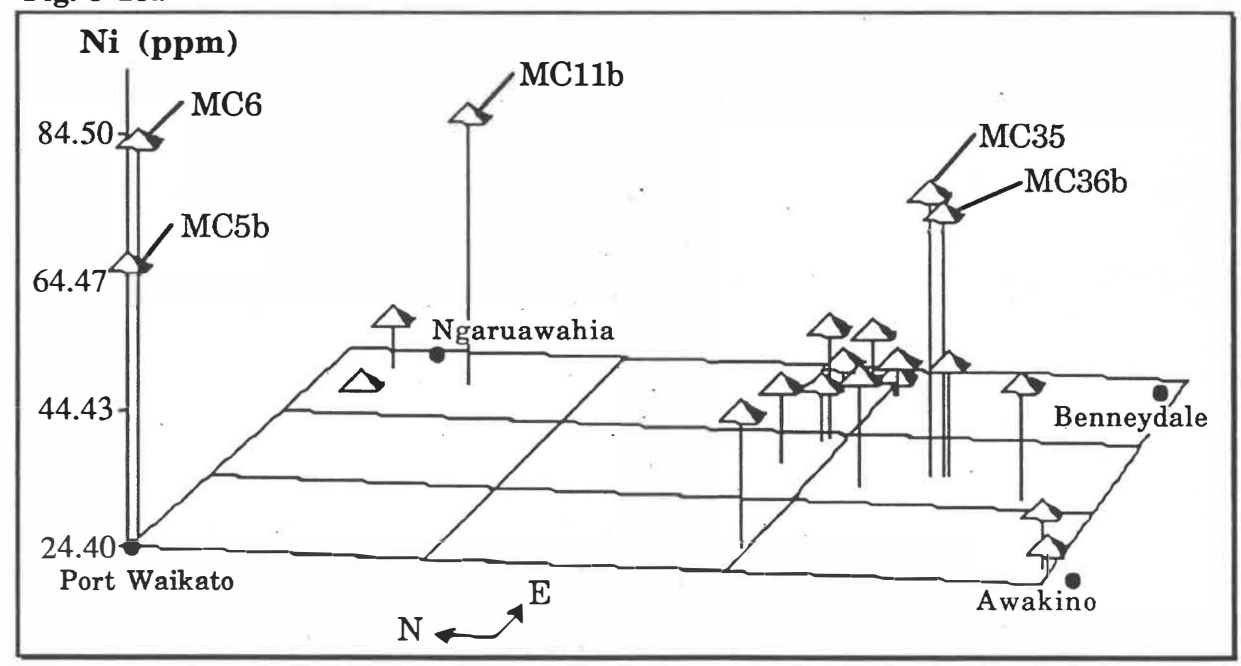

Fig. 5-18b

Fig. 5-18 **(a)** Pb concentration (ppm) with respect to geographic location of the sample (data from XRF analysis).

(b) Ni concentration (ppm) with respect to geographic location of the sample (data from XRF analysis).

The environment of formation is difficult to interpret based on the scatter plots although Fig. 5-18a and 5-18b do suggest glauconite formation in the Mairoa area was near a landmass (high Ni and Pb) and those in the Waitomo area were in mid-outer shelf positions (low Ni and Pb); these results conflict with the Mg data of Section 5-5-1 (the reason for this is discussed in Section 5-6).

Data from the north of the study area have a high Ni and low Pb content. Whether this indicates a different source material (i.e., possible chemical changes between Oparau facies greywackes west of the Waipa Fault and Morrinsville facies greywackes east of the Waipa Fault) and thus drainage basin influence on the glauconite chemical composition could not be determined. The ratio of Ni to Pb is very high for the samples MC5b (Te.Ak.), MC6 (E), MC25a (Wh), MC31b (Wh), and MC35 (Ao) when compared to the other data. Possibly, this can be related to the ionic potential of the two elements and the nearness of shoreline or terrigenous influences. At present this conclusion is hypothetical, much more intensive sampling of a specific stratigraphic horizon is required before a comprehensive picture of the depositional setting of the Te Kuiti Group formations can be established using the above trace element techniques.

If retention of the trace element chemical signature of the progenitor material is proposed for glauconite, then the chemistry of the source rock should exert an influence on the chemistry of the glauconite formed. Few trace element studies of sedimentary rocks have been made (e.g., Bhatia & Taylor 1981; Peterman et al. 1981; Bhatia & Crook 1986). Bhatia & Crook (1986) have shown the relationships between La and Th, La and Sc, and Ti and Zr are useful in discriminating between greywackes from various tectonic settings. A scatter plot of Ti/Zr versus La/Sc for Te Kuiti Group glauconites shows most samples fall in the continental island arc field of the above authors (Fig. 5-19). It must be stressed this does not imply that the glauconite developed in this type of tectonic environment. Rather, that the progenitor substrate material from which the glauconite has formed has influenced the trace element composition of the glauconite. McConchie's (1978) Ti/Zr data are almost all greater than 30 (unfortunately La and Sc were not analysed). This suggests South Island glauconites developed from a significantly different progenitor substrate compared to Te Kuiti Group glauconites.

Chemical data for Te Kuiti Group glauconite suggests that the glauconite progenitor was of similar composition in the north and south (except for MC44 which appears incongruous with the other data). Whether specific trace element concentrations in glauconite could determine if the glauconite progenitor was from a westerly or easterly direction (i.e., the Waipa or Morrinsville Terrains) was not established.

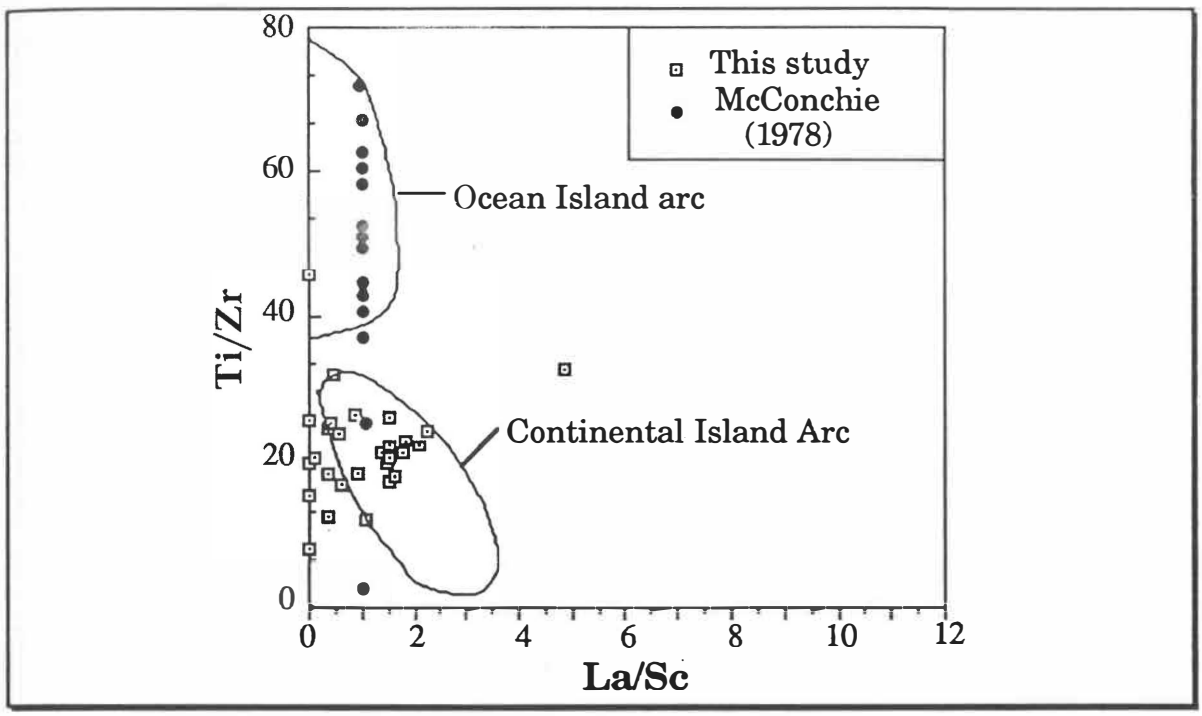

Fig. 5-19 Scatter plot of the ratio of Ti/Zr versus La/Sc for samples of Te Kuiti Group glauconite from this study and Cretaceous to lower Tertiary glauconite from the South Island of New Zealand. The overlain oceanic island arc and continental island arc fields are those of Bhatia & Crook (1986) for greywackes. McConchie's (1978) data for South Island glauconites have been arbitrarily assigned a La/Sc ratio of **one** as no data was available for this axis of the plot. There is a sharp distinction evident in the Ti/Zr ratio for Te Kuiti Group glauconites and the data of McConchie for South Island glauconites.

Balashov & Kazakov (1968) suggest that Ce/ La ratios in glauconite are useful in determining the climate in which the marine depocentre was formed. Ce/La ratios below one indicate arid climates and Ce/La ratios above one indicate humid climates. Nelson (1978b) noted that a gradual increase in sea temperatures occurred through the time period of deposition of the Te Kuiti Group. Samples were investigated from the Te Kuiti Group for their Ce/La ratio to see if there was a change in Ce/La ratio paralleling the increase in sea-water temperature. The sparse data (Fig. 5-20) show an increase in the Ce to La ratio compatible with the hypothesized increase in sea temperature during the period of deposition of the Te Kuiti Group.

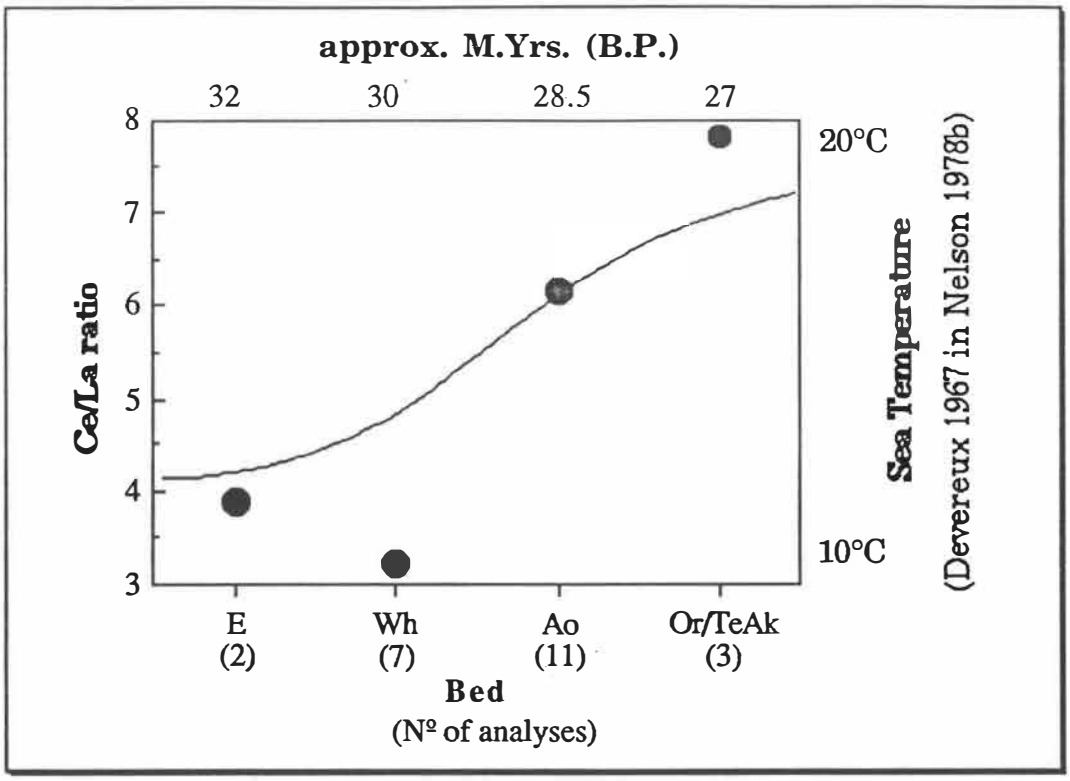

Fig. 5-20 Average Ce/La ratio of glauconites from selected formations within the Te Kuiti Group (filled circles). Paleotemperature curve (solid line) for the late Eocene - Oligocene sea temperature in New Zealand (redrawn from Nelson 1978b). E=Elgood Limestone, Wh=Whaingaroa Siltstone, Ao=Aotea Sandstone, Or/TeAk=Orahiri Limestone or Te Akatea Siltstone (lateral time equivalents).

The Elgood Limestone Ce/La data was restricted to samples from the northern portion of the study area. Possibly latitude differences in average sea temperature can be invoked to account for the slightly elevated Ce/La ratio in Elgood Limestones compared with Whaingaroa Siltstone. The conclusion of Balshov & Kazakov (1968) that the Ce/La ratio is a humidity or aridity measure would seem irrelevant in a marine setting. The evidence presented suggests that an equilibrium coefficient (which will be temperature dependent) controls Ce/La ratios in glauconite. This feature of glauconites is an interesting finding in that the Ce/La ratio of glauconites may be a useful paleoenvironmental temperature indicator.

(5-6) ELECTRON MICROPROBE ANALYSIS (EMP)

The EMP data for each sample was first normalized using the method discussed in Section 2-3-3 thereby giving all analyses a return of 91.68%. From these analyses the average concentration of an element within a sample was calculated from the 3 to 7 point analyses made on selected grains from that sample. The raw data, normalized data, and sample average probe analysis data are given in Section D9a to D9c of the data booklet.

EMP analyses were made on the central portion of grains, XRF analyses were made on crushed bulk glauconite samples. XRF studies suggested the existence of a region of high-Mg content glauconite in the Otorohanga - Waitomo - Te Kuiti area. A three-dimensional scatter plot of the Mg content of grain centres as determined by EMP analysis (Fig. 5-21) showed that this feature was a factor of the bulk glauconite sample composition rather than the grain glauconite composition.

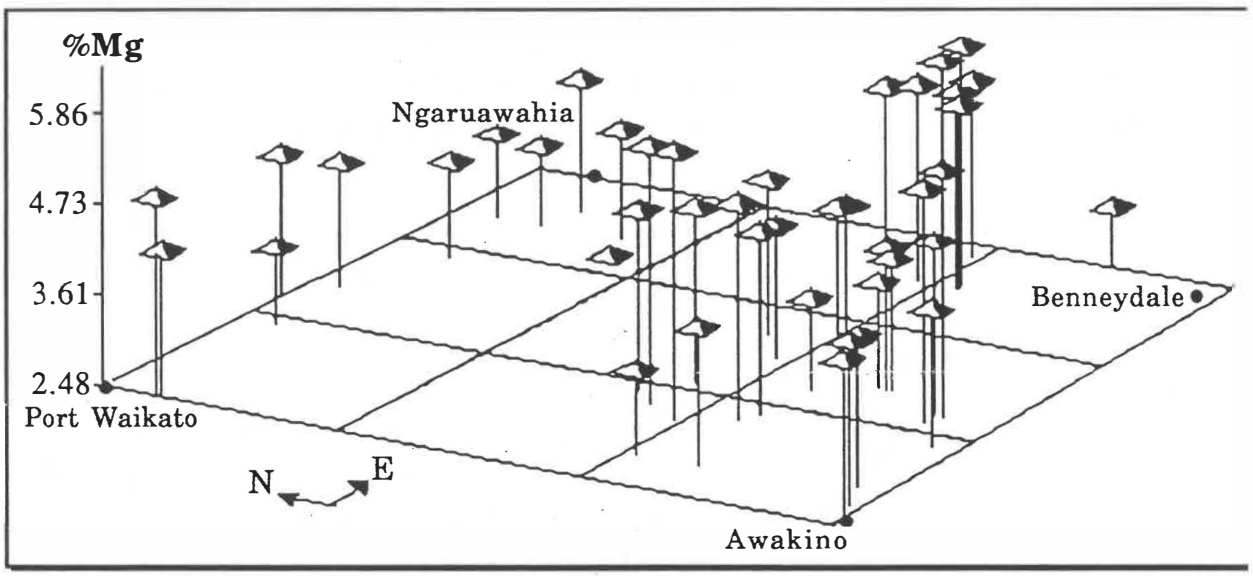

Fig. 5-21 Three dimensional scatter plot of the average glauconite Mg content as determined by EMP analysis.

From this evidence it would seem that the degree of glauconitisation is the controlling factor on the apparent Mg anomaly. The Mg anomaly will be apparent in XRF rather than EMP data because XRF gives a bulk average chemical composition while EMP analysis is from grain centres of the most glauconitised grains within a sample. This factor explains the apparently anomalous Ni and Pb concentrations with respect to geographic location found for the XRF data. McConchie (1978, p.43) states, "clays including

glauconite, have a tendency to concentrate.....Cu, Zn, and Pb". If glauconitisation ceases because of unfavorable formational conditions the assimilation of Cu, Zn and Pb will also cease. Glauconitisation ceased earlier the Otorohanga - Waitomo - Te Kuiti area because of high terrigenous input. This causes anomalously **low** Pb and Ni contents in the glauconites from this area.

These conclusions indicate that bulk glauconite composition is more useful in paleoenvironmental reconstruction compared with composition of the grain centre. This is because grain centres have evolved toward an end member composition. Because of the bulk sample requirement for XRF analyses the technique is prone to contamination problems. Therefore, the point specific EMP analysis is probably more useful in studying the glauconitisation process.

The correlation between elemental analyses from EMP and also the calculated layer lattice charges from Clayform for the glauconite samples are shown in Table 5-6. From this information several important relationships between element pairs were found.

Fig. 5-22a to 5-22d shows the scatter plot of several important element pairs in the sampled glauconites. There is a strong negative correlation between Si and Fe (R=0.75) and Fe and Al (R=0.65), which is expected given the nature of the possible substitutions within the glauconite lattice. The correlation between Fe and K is low (R=0.55). This supports the argument of Bentor & Kastner (1965) that Fe and K uptakes are independent of the glauconitisation process and do not depend on a charge balancing process as suggested by Hower (1961). The correlation between Al and K (R=0.64) is interesting in that a possible explanation for this correlation is the ability of Fe to replace Al in the tetrahedral layer during glauconitisation. Al content in the tetrahedral layer and the ability of Fe to replace this Al may be a controlling factor on the glauconitisation process (this of course assumes that K content is a reliable measure of the degree of glauconitisation).

Table 5-6 Average electron microprobe data correlation matrix.

	tet	oct	int	Si	Al	Ti	Fe	Mn	Mg	Ca	Na	K	Ni	Cr
oct	-0.779	.	.	.	.	.	.	.	.	.	.	.	.	.
int	-0.055	-0.583	.	.	.	.	.	.	.	.	.	.	.	.
Si	0.955	-0.668	-0.174	.	.	.	.	.	.	.	.	.	.	.
Al	-0.334	0.578	-0.487	-0.117	.	.	.	.	.	.	.	.	.	.
Ti	-0.099	0.253	-0.274	0.013	0.512	.	.	.	.	.	.	.	.	.
Fe	-0.58	0.322	0.238	-0.747	-0.499	-0.345	.	.	.	.	.	.	.	.
Mn	0.059	0.024	-0.116	0.061	0.113	0.326	-0.12	.	.	.	.	.	.	.
Mg	-0.158	0.072	0.09	-0.229	-0.379	-0.156	0.304	-0.112	.	.	.	.	.	.
Ca	-0.16	0	0.208	-0.032	0.234	0.203	-0.203	-0.101	0.117	.	.	.	.	.
Na	-0.048	-0.309	0.555	-0.085	-0.041	-0.046	-0.055	-0.081	0.05	-0.064	.	.	.	.
K	0.185	-0.49	0.54	-0.008	-0.664	-0.412	0.354	0.016	-0.067	-0.486	-0.048	.	.	.
Ni	-0.073	0.013	0.075	-0.083	0.111	0.15	-0.023	0.157	-0.104	0.205	-0.067	-0.02	.	.
Cr	-0.295	0.126	0.18	-0.334	-0.048	-0.121	0.194	-0.103	0.485	0.041	0.292	-0.074	0.006	.
Cl	-0.101	0.121	-0.062	-0.106	-0.075	0.153	0.141	0.036	0.222	0.007	0.087	-0.161	-0.103	0.258

tet = tetrahedral layer charge
oct = octahedral layer charge
int = interlayer charge
Si = SiO_2
Al = Al_2O_3
Ti = TiO_2
Fe = Fe_2O_3
Mn = MnO
Mg = MgO
Ca = CaO
Na = Na_2O
K = K_2O
Ni = NiO
Cr = Cr_2O_3
Cl = Cl^-

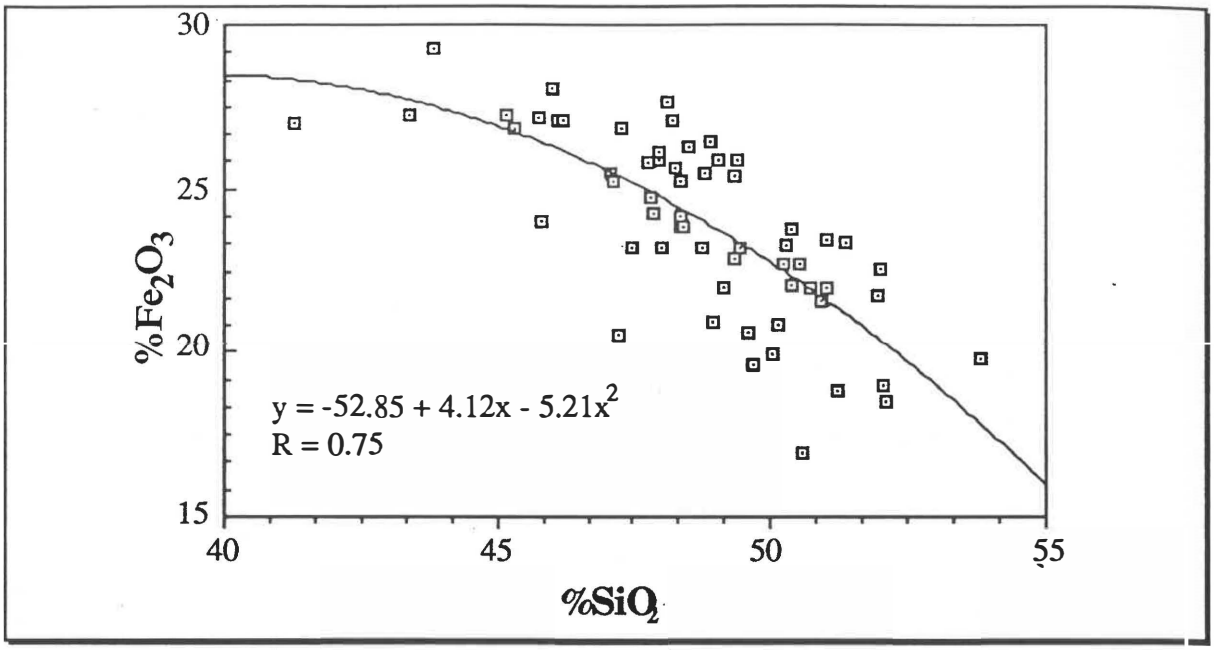

Fig. 5-22a

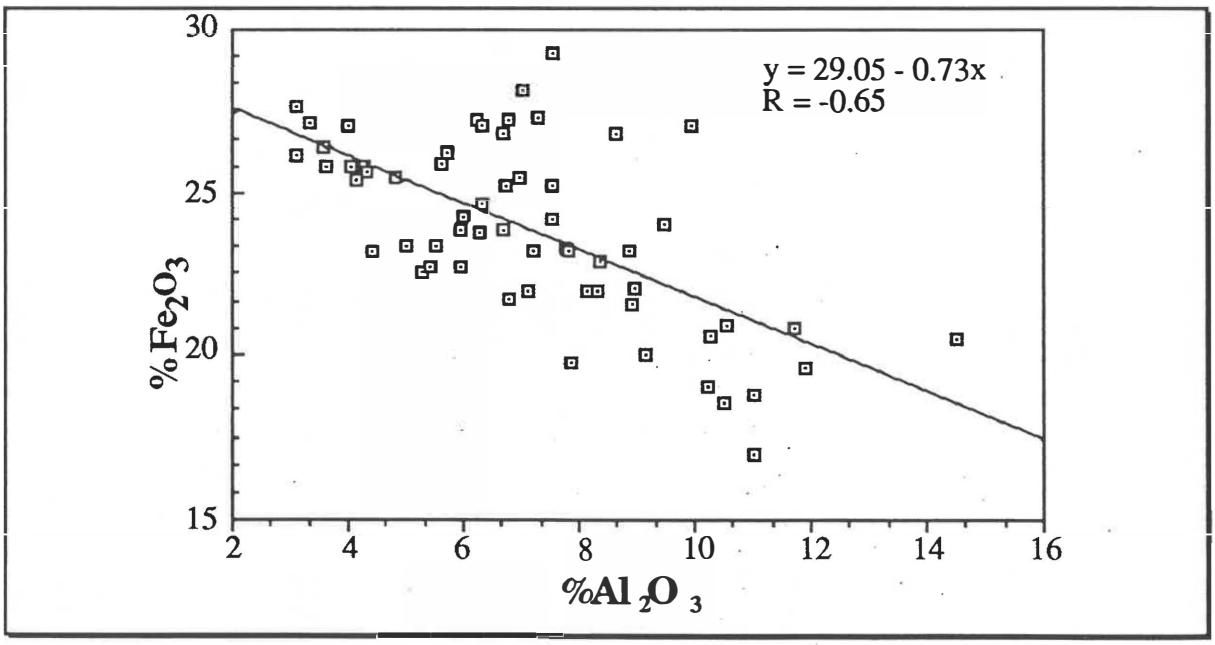

Fig. 5-22b

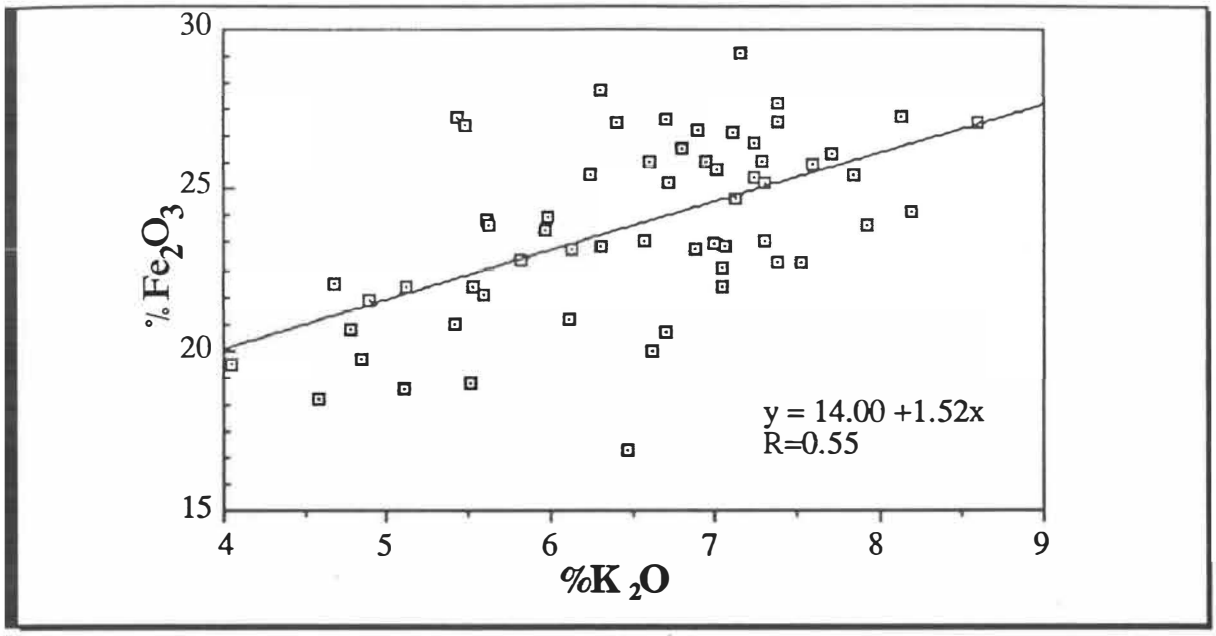

Fig. 5-22c

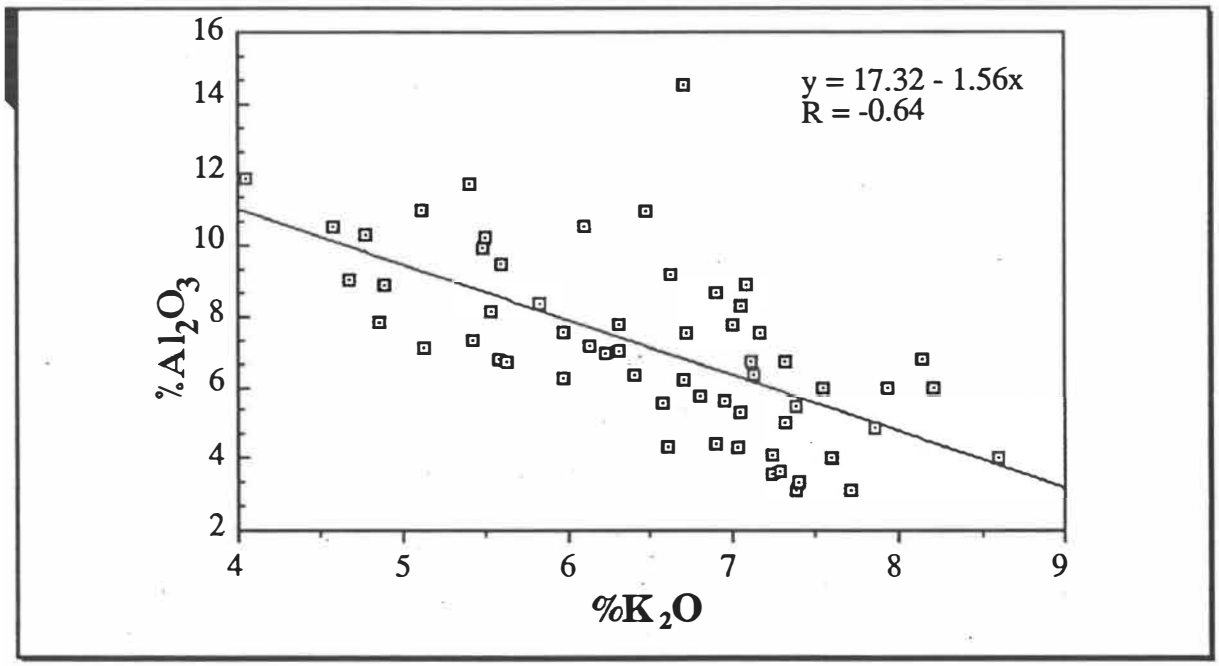

Fig. 5-22d

Fig. 5-22 **(a)** Scatter plot $\%SiO_2$ versus $\%Fe_2O_3$ average sample EMP analyses.

(b) Scatter plot $\%Fe_2O_3$ versus $\%Al_2O_3$ average sample EMP analyses.

(c) Scatter plot $\%Fe_2O_3$ versus $\%K_2O$ average sample EMP analyses.

(d) Scatter plot $\%Al_2O_3$ versus $\%K_2O$ average sample EMP analyses.

EMP data may be found in Section D9 of the data booklet.

As unmodified EMP chemical data were unable to discriminate between the formations of the Te Kuiti Group it was necessary to employ multivariate statistical techniques to distinguish the formations. The data base used in this portion of the study was the normalized data base before the average for the sample was calculated. Use of the unaveraged data meant a higher sample number was available; this enabled more within bed variance to be accounted for.

Canonical variate analysis was applied to the data to distinguish the following seven stratigraphic horizons: Pukemiro Sandstone, Mangakotuku Siltstone, Elgood Limestone, Whaingaroan Siltstone, Aotea Sandstone, Orahiri Limestone, and Waitomo Sandstone. A reasonable separation of the formations was possible using the 12 listed variates (i.e., the major elements analysed using the EMP) (Table 5-7). It was expected that the semi-confined highly evolved central portions of the glauconite grains analysed using the EMP should have trended toward a common end member. However, the results suggest a significant difference in chemical composition exists between the glauconite in the constituent formations of the Te Kuiti Group. The canonical variate loadings (Table 5-7) show TiO_2, and MnO are the two most important chemical discriminating variables (Cr_2O_3, NiO and Cl^- have high loadings but are of very low concentrations in the glauconite). The result is significant in that it should be possible to correlate drill core samples to a stratigraphic horizon in the Te Kuiti Group with a reasonable degree of certainty based on their glauconite EMP chemical analysis.

The percentage variation accounted for by each canonical variate could be improved upon by the addition of trace element data and morphological data into the canonical model. Unfortunately, there was insufficient time to incorporate these factors into the present model. Also a problem arises when there is insufficient sample available to obtain XRF trace element data or morphological data. Currently, I am unaware of any canonical variate model that can account for missing values within a data set. Finally, some of the horizons sampled in this study have few chemical analyses, in particular Mangakotuku Siltstone (15 analyses from 3 samples) and Waitomo Sandstone (15 analyses from 3 samples). More sample analyses should be obtained before the canonical latent vector loadings should be considered diagnostic of these horizons. Fig. 5-23 shows a graphical representation of the horizon group centroids (calculated from the average formation composition) and the 80% probability of correct classification ellipsoids.

Table 5-7 Canonical variate analysis results.

Formation	Variable Mean Data (wt%)											
↓	SiO_2	Al_2O_3	TiO_2	Fe_2O_3	MnO	MgO	CaO	Na_2O	K_2O	NiO	Cr_2O_3	Cl
P	47.77	8.61	0.05	24.49	0.02	3.56	0.33	0.03	6.78	0.02	0.02	0.02
M	49.21	7.83	0.04	23.49	0.02	3.67	0.67	0.02	6.34	0.01	0.02	0.00
E	44.25	7.57	0.05	28.10	0.02	3.86	0.89	0.24	6.78	0.02	0.03	0.01
Wh	50.20	8.41	0.12	21.51	0.02	4.07	2.02	0.09	5.19	0.02	0.04	0.01
Ao	48.31	5.72	0.06	24.17	0.02	4.49	1.66	0.21	7.00	0.02	0.03	0.01
Or	45.69	8.33	0.16	25.11	0.05	4.93	1.09	0.26	5.96	0.02	0.05	0.03
Wt	49.08	5.96	0.18	23.88	0.02	5.40	0.84	0.10	6.12	0.01	0.04	0.04

P=Pukemiro Sandstone
M=Mangakotuku Siltstone
E=Elgood Limestone
Wh=Whaingaroa Siltstone
Ao=Aotea Sandstone
Or=Orahiri Limestone
Wt=Waitomo Sandstone

Canonical Variate Loadings

Variate	CV1	CV2	CV3
SiO_2	-1.310	3.414	-3.919
Al_2O_3	-1.586	3.722	-3.953
TiO_2	2.957	5.317	-4.173
Fe_2O_3	-1.515	3.569	-3.994
MnO	5.527	16.906	-5.190
MgO	-0.097	4.827	-3.270
CaO	-0.900	3.767	-4.231
Na_2O	-1.231	3.809	-3.412
K_2O	-1.646	4.419	-3.287
NiO	6.699	6.161	-4.451
Cr_2O_3	5.427	1.341	-28.994
Cl^-	-0.192	10.043	-5.313

(CV = canonical variate)

Percentage of variation explained by each canonical variate

	CV1	CV2	CV3
%	40.61	30.04	13.03
Total%	40.61	70.65	83.68

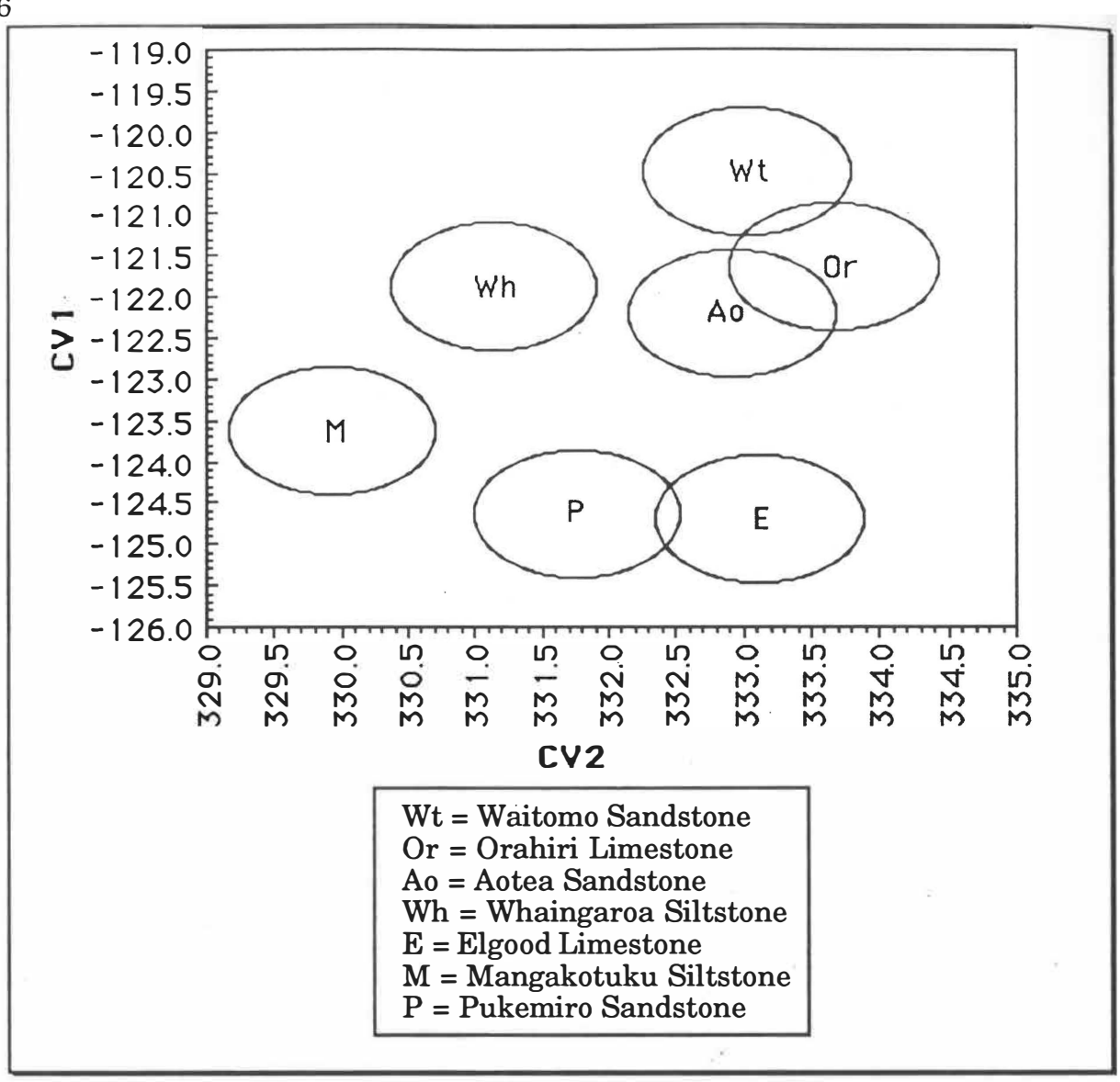

Fig. 5-23 Representation of the 80% probability ellipsoids of correct classification based on the two canonical variate vectors CV1 and CV2 for the seven formations listed in the key. The values of CV1 and CV2 can be found in Table 5-7.

The average chemical compositional data for the formations in Table 5-7 was input into the "Clayform" program to calculate the average glauconite mineralogical composition for the seven formations and also the average Te Kuiti Group glauconite composition. The results are shown in full in Section D10 of the data booklet. A summary of the calculated structural formulae are presented below:

Pukemiro Sandstone

$(Si_{3.57}\ Al_{0.42})\ (Al_{0.34}\ Fe^{3+}_{1.16}\ Fe^{2+}_{0.22}\ Mg_{0.40})\ (Ca_{0.02}\ K_{0.65})\ O_{10}(OH_2)$

Mangakotuku Siltstone

$(Si_{3.67}\ Al_{0.33})\ (Al_{0.35}\ Fe^{3+}_{1.11}\ Fe^{2+}_{0.21}\ Mg_{0.41})\ (Ca_{0.05}\ K_{0.60})\ O_{10}(OH_2)$

Elgood Limestone

$(Si_{3.40}\ Al_{0.60})\ (Al_{0.08}\ Fe^{3+}_{1.36}\ Fe^{2+}_{0.26}\ Mg_{0.44})\ (Ca_{0.07}\ Na_{0.04}\ K_{0.66})\ O_{10}(OH_2)$

Whaingaroa Siltstone

$(Si_{3.68}\ Al_{0.32})\ (Al_{0.41}\ Fe^{3+}_{1.00}\ Fe^{2+}_{0.19}\ Mg_{0.44})\ (Ca_{0.16}\ Na_{0.01}\ K_{0.49})\ O_{10}(OH_2)$

Aotea Sandstone

$(Si_{3.64}\ Al_{0.35})\ (Al_{0.16}\ Fe^{3+}_{1.15}\ Fe^{2+}_{0.22}\ Mg_{0.51})\ (Ca_{0.13}\ Na_{0.03}\ K_{0.67})\ O_{10}(OH_2)$

Orahiri Limestone

$(Si_{3.45}\ Al_{0.55})\ (Al_{0.20}\ Fe^{3+}_{1.20}\ Fe^{2+}_{0.23}\ Mg_{0.56})\ (Ca_{0.09}\ Na_{0.04}\ K_{0.57})\ O_{10}(OH_2)$

Waitomo Sandstone

$(Si_{3.67}\ Al_{0.33})\ (Al_{0.19}\ Fe^{3+}_{1.13}\ Fe^{2+}_{0.21}\ Mg_{0.60})\ (Ca_{0.07}\ Na_{0.01}\ K_{0.58})\ O_{10}(OH_2)$

Interestingly the octahedral magnesium content of the glauconite for the seven formations increases up the stratigraphic succession. A possible explanation for this lies in the adsorption of Mg from pore waters during formation of the glauconite. It has been suggested that initial deposition of calcite in the Te Kuiti Group was as high-Mg calcite and some aragonite (Nelson 1978b; Nelson & Hume 1987). During initial diagenesis near the seafloor Mg is lost from the high-Mg calcite. It has been suggested that the released Mg is absorbed into smectitic clay lattices (Russell 1970 in Nelson 1978b). For the Te Kuiti Group "the content of calcium carbonate increases up through the group" (Nelson & Hume 1987, p.346), therefore the amount of Mg released by diagenesis of the high-Mg calcite should increase stratigraphically upward. As the calculated glauconite compositions show an increase in Mg content of the glauconite stratigraphically upward it is highly likely that some of the Mg released from the high-Mg calcite during diagenesis was incorporated into the glauconite lattice.

The formation glauconite compositions were combined to calculate a range formula for **Te Kuiti Group glauconite**:

$(Si_{3.40\text{-}3.68}\ Al_{0.32\text{-}0.60})\ (Al_{0.08\text{-}0.41}\ Fe^{3+}_{1.00\text{-}1.36}\ Fe^{2+}_{0.19\text{-}0.26}\ Mg_{0.40\text{-}0.60})\ (Ca_{0.02\text{-}0.16}\ Na_{0.00\text{-}0.04}\ K_{0.49\text{-}0.67})\ O_{10}(OH_2)$

When compared with the average compositional formula for 15 **New Zealand glauconites** calculated by Nelson (1973):

$(Si_{3.66}\ Al_{0.34})\ (Al_{0.43}\ Fe^{3+}_{1.04}\ Fe^{2+}_{0.17}\ Mg_{0.41})\ (Ca_{0.05}\ Na_{0.08}\ K_{0.61})\ O_{10}(OH_2)$

it can be seen that the average New Zealand glauconite is almost entirely encompassed within the range formula for Te Kuiti Group glauconite. The exceptions are the octahedral Al content and interlayer Na content which are slightly lower for Te Kuiti Group glauconites. The Fe and Mg contents of Te Kuiti Group glauconite appear in general to be higher than the average New Zealand glauconite analysis. While the differences are real it must be remembered Nelson's data base was from wet chemical analyses and structural formulae were calculated manually (I do not doubt the validity of the results but computer rounding is generally to many more significant

places than manual calculations and hence may cause small changes in the calculated occupancies).

Readers may now be wondering why the high-Mg glauconite from the Otorohanga - Waitomo - Te Kuiti area cannot be attributed to adsorbtion of Mg released from high-Mg calcite. Indeed, many of the samples from the Otorohanga - Waitomo - Te Kuiti area are from highly calcitic horizons. However, if highly calcitic horizons from other areas are investigated (e.g., OrB2 samples MC29, MC30, MC41, MC42, MC43) it is observed that there are no significant enrichments in Mg in these samples. This suggests that an anomaly due to high-Mg calcite releasing Mg causes a change in group average composition, while terrigenous influences cause a specific sample to have a high-Mg content.

5-6-1 Chemical variation across a vermicular grain of glauconite

The EMP analyses above were made on the central portion of the glauconite grain. Several authors have noted the existence of a fine white crystalline material in the peripheral cracks of glauconitic grains (e.g., Triplehorn 1966; Nelson 1973; Velde & Odin 1975; McConchie 1980; Odin & Matter 1981). Point analyses were made using the EMP across such a white crystalline infilling in an attempt to determine what the material present was (Fig. 5-24). Unfortunately, the fine grained infilling did not polish well and this meant returns from this material were low, ranging from 82% to 47% total return. While, it could be argued that the white crystalline material was hydrous and this explained the low percentage returns, defocused beam analyses did not show major changes in return percentages for the white crystalline material. Therefore, this explanation does not seem likely. The raw EMP chemical data were used to generate transect plots of the concentration of several constituent elements of the glauconite lattice (Fig. 5-25). The transect plots show a gradual decrease in SiO_2 content as the EMP analysis point moved into the white crystalline material suggesting a chemical gradient of some form is present in the grain. The three other transect graphs (Fe_2O_3, K_2O, Al_2O_3) seem to have peaks of anomalously high concentration around analysis points 2 to 4.

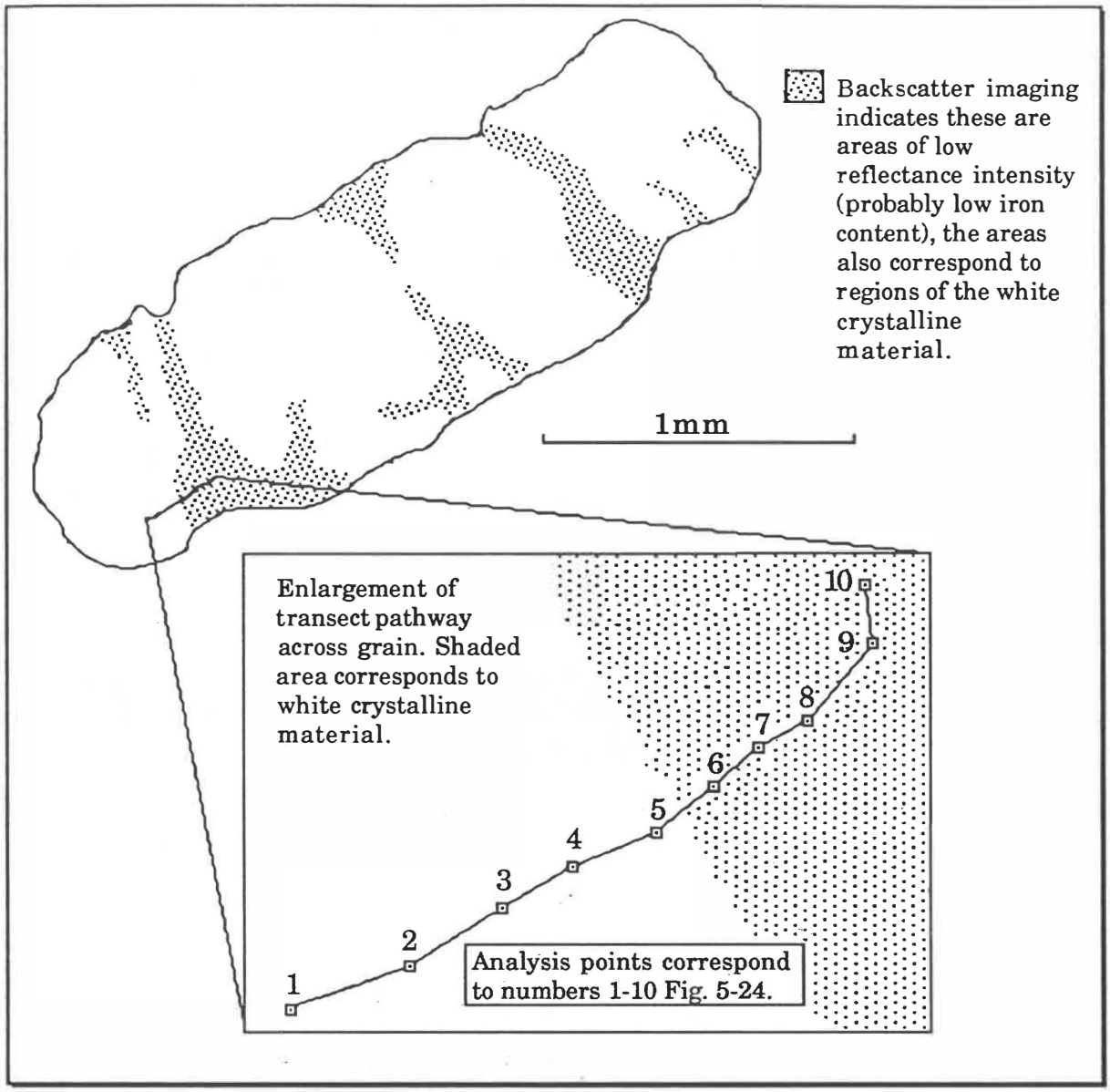

Fig. 5-24 Schematic diagram showing the location of EMP analysis points relative to the back scatter image of the investigated glauconite grain.

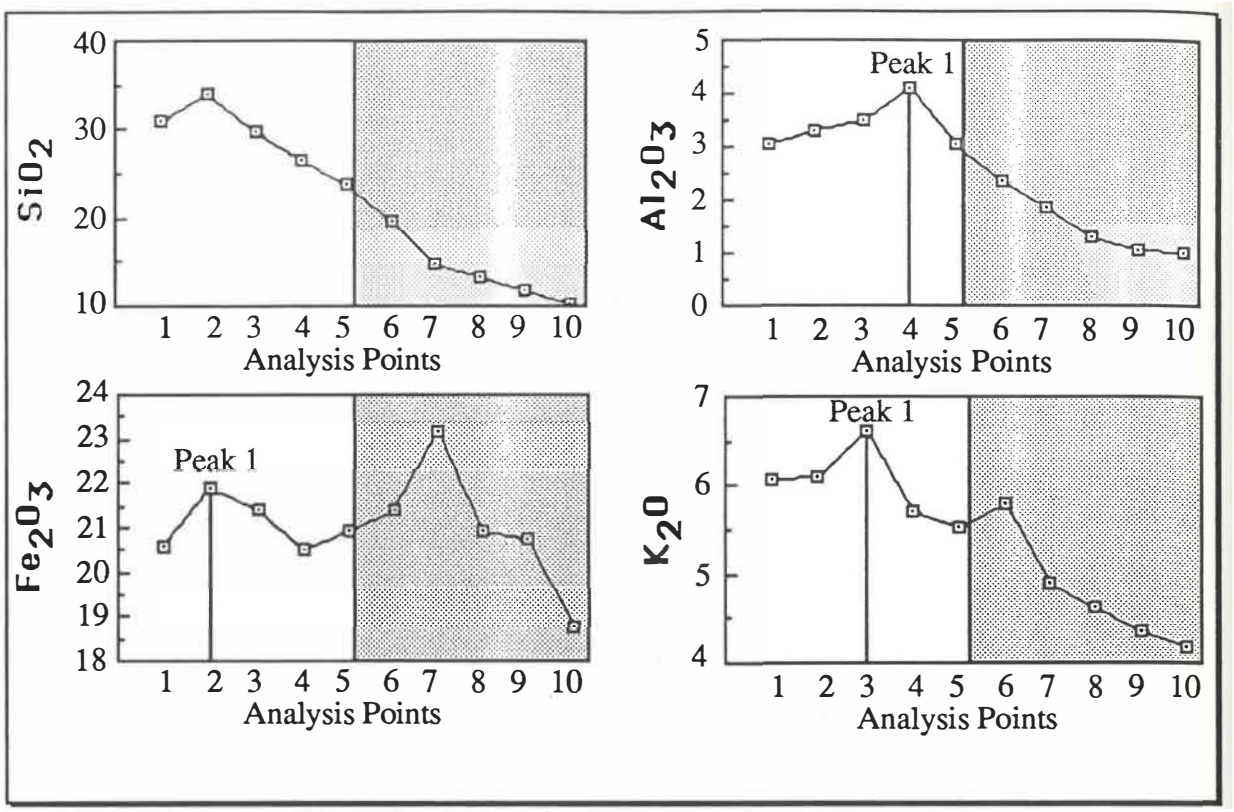

Fig. 5-25 The chemical variability of the sample points 1 to 10 as shown in Fig. 5-24 (data collected using the EMP). Shaded area of graphs represents the white crystalline material in the non-glauconite portion of the vermicular grain. The elemental concentrations are all in wt% in the above graphs.

The first peak of anomalous concentration (peak 1) encountered in the transect is Fe_2O_3, then K_2O, then Al_2O_3 . This suggests a zonation of elements exists in glauconite. The peak ordering above is also shown by Velde & Odin (1975, fig 7) on the left hand side of their microprobe scan across a glauconite pellet. However, only the Al peak was recognized by these authors. All elements decrease in concentration as the analysis point passes into the white crystalline material. The chemical zonation of the glauconite offers a chemical gradient mechanism for the adsorption of elements required for the glauconitisation process. Furthermore, the order of the chemical peaks may offer an insight into the chemical evolution of glauconite as the data would seem to indicate that Fe is preferentially adsorbed before K and Al. The second peaks on the Fe_2O_3 and K_2O transect graphs are more difficult to interpret; they may be a secondary episode of glauconitisation.

CHAPTER (6)

SYNTHESIS

(6) SYNTHESIS

Much of the physical and chemical data obtained in this study have served to reinforce characteristics established in previous studies on glauconite. The aim of this chapter is not to restate these similarities, unless they are pertinent to the Te Kuiti Group, but rather to emphasize some of the new information, techniques, and problems encountered during this study in comparison with the published literature. A summary of the characteristics of glauconite in the Te Kuiti Group sediments is given in Table 6-1.

Table 6-1 Summary characteristics of Te Kuiti Group glauconite as determined in this study.

Technique	Te Kuiti Group Sample Findings
Morphological Analysis	- Exterior morphology is dominated by ovoidal form glauconite. - Order of abundance of morphological forms in Te Kuiti Group is ovoidal » fragmentary » lobate > casts; only trace quantities of tabular, capsule and vermicular grains are present. - Ovoidal grain content decreases and lobate grain content increases up the stratigraphic succession Elgood Limestone, Whaingaroa Siltstone, Aotea Sandstone, Orahiri Limestone. - Fragmentary grain content in all horizons is >25%. - The high fragmentary and ovoidal contents, and the low lobate content suggests Te Kuiti Group glauconite has a significant allogenic component. - The highly fragile, cast-formed glauconite and lobate glauconite grains are probably authigenic glauconite. - Internal fabric is dominated by random microcrystalline glauconite.

Image Analysis Study

- Image analysis is a viable alternative to binocular morphological investigation of glauconite morphology. However, the techniques developed in this study require refinement before they can be applied generally.
- Image analysis results show genetic relationships and probable morphological evolutionary pathways in the glauconitisation process.

X-Ray Diffraction Analysis

- XRD data shows a predominance of poorly crystalline glauconite in Te Kuiti Group lithologies.
- Theoretical XRD trace generation is useful in determining peak location but because literature classifications are based on peak shape the method is of limited use in classifying glauconite.
- Criticisms of literature XRD classification schemes leads to the conclusion that classification of glauconite should move from physical XRD schemes toward chemical classification of glauconite.
- Chemically calculated expandable content shows a relationship between host sediment lithology and expandable clay content of glauconites (e.g., Whaingaroa Siltstone average percent expandables = 26%, Elgood Limestone average percent expandables = 10%).

X-ray Fluorescence Analysis

- A high-Mg anomaly in glauconites from the Otorohanga
- Waitomo - Te Kuiti area supports stratigraphic evidence presented by Nelson (1978a) that a semi-enclosed embayment existed during deposition of the Te Kuiti Group in this area.
- Ni and Pb trace element data suggests sedimentation rates due to terrigenous input were higher in the Otorohanga - Waitomo - Te Kuiti area than in adjacent depocentres.
- A correlation between sea temperature changes and average La/Ce ratio of glauconite is suggested in Te Kuiti Group glauconites.

Electron Microprobe Analysis

- Major element analyses are capable of distinguishing stratigraphic horizons in the Te Kuiti Group. The small sample size required for EMP analysis means the technique may be a viable method for classifying drill core samples of glauconite.
- Average glauconite mineral formulae show a definite increase in Mg content stratigraphically upward in the Te Kuiti Group. Previously, Mg released from metastable high-Mg calcite during diagenesis had been thought to be incorporated into smectitic clays. The average compositional formulae from this study suggest that some of the Mg is absorbed into the glauconite lattice. The stratigraphic increase in Mg content upward can be accounted for by the corresponding increase in calcite content of the Te Kuiti Group upward.
- A transect across white crystalline material bordering a vermicular grain showed a gradual decrease in Si content and zones of enrichment moving successively outward of Fe, K, and Al. This suggests that a chemical potential driving mechanism for the development of glauconite should be investigated.

External morphological studies confirm the finding of Nelson (1973) that ovoidal glauconite dominates Te Kuiti Group glauconites. The order of abundances other than the ovoidal class differs from that given by Nelson & Hume (1987). Overall the order of abundances found was: ovoidal » fragmentary » lobate > casts; only trace quantities of tabular, capsule, and vermicular form glauconite were found. In particular the much higher proportion of fragmentary glauconite reported in this study is notable. The high fragmentary component (>25% in all beds), low abundance of lobate grains, and relative abundance of ovoidal grains can be used to infer that significant reworking of glauconite has occurred during formation of the Te Kuiti Group glauconite deposits. This evidence suggests the Te Kuiti Group has a significant allogenic glauconite component.

Morphological studies show the main internal fabric in Te Kuiti Group glauconite is random microcrystalline. Only when vermicular grains occur does an oriented microcrystalline fabric become significant.

A new technique for the study of the non-calcareous portion of limestone rock slides (termed 3D slides) was developed. The technique involved the

acidification of 0.3mm thick limestone slides containing glauconite. The 3D slides showed that the cast component of limestone glauconite is highly fragile and often pseudomorphs the internal cavities of calcareous skeletons. Because it is highly unlikely that these cavities could be consistently infilled with a degraded clay progenitor, the discarded theories of direct chemical precipitation of glauconite should be reinvestigated. The highly fragile nature of the encapsulating body in this form of glauconite leads to the conclusion that this is predominantly authigenic glauconite.

Morphological studies in the past have been based on type morphological specimens and visual division of samples into classes using the binocular microscope. As division based on visual appraisal of the similarity of literature type specimens and sample specimens is somewhat subjective personal interpretation may arise. This is probably best exemplified by the rather arbitrary distinction between ovoidal and lobate grains. The necessity to move away from an empirical classification and change to experimentally measurable variables is vital for reproducibility of a classification. Physical measurement of single grains is tedious and time consuming, but the advent of the image analyser offers a potential solution. This study has shown it is possible to rapidly measure several physical features of each glauconite grain using the image analyser. Canonical variate analysis can then be used to create classification ellipsoids for individual grain types centred on group centroids. Type specimens (in effect end members) are used in establishing the location of the group centroids, and as one moves away from the centroid the probability of a correct classification decreases. This means the image analysis technique is more reliable than the binocular microscope technique as there is no requirement to fit grains arbitrarily into one morphological group or another. Even though the model presented here has certain pitfalls, many of which have been alluded to in the text, new information with respect to genetic association of grain types in the Te Kuiti Group has become evident. For example, there appears to be an association between ovoidal, lobate and cauliflower glauconite grains in the Te Kuiti Group not previously recognised. On a wider scope the image analyser has exciting prospects in grain morphology studies with respect to provenance and reworking of materials other than glauconite (e.g., quartz).

Physical XRD studies of glauconite show that Te Kuiti Group lithologies are dominated by poorly crystalline glauconite with very few samples approaching the more ordered micaceous-structure glauconite. The difficulties of calculating the expandable clay content of glauconite are discussed and the problems of existing literature classification schemes investigated. The results lead to the conclusion that no current physical XRD classification technique is adequate for the classification of glauconite.

The use of a theoretical XRD-generating program shows the ability of computers to produce XRD traces for glauconite. The theoretical traces are in some respects superior to physical traces, particularly because noise is eliminated. However, the theoretical traces do not show peak assymmetry and "sharpness" of peaks. Since previous XRD classification schemes for glauconite have been based on these features the use of theoretical XRD traces for classifying glauconite is not possible using current XRD-generating programmes. Again, I raise the question of the validity of using a visual,empirical term such as "sharp" in a classification scheme. It would seem more practical to move away from the XRD classification of glauconite towards a chemical classification based on K_2O content. K_2O content has a known relationship to the type of glauconite and can be determined relatively easily using EMP.

Average expandable clay data for beds in the Te Kuiti Group exemplify the relationship known to exist between host sediment lithology and glauconite type present in the sediment. Glauconite from mudstones has a higher proportion of expandable layers compared with glauconite from sandstones and limestones (Burst 1958a,b; Bentor & Kastner 1965). In the Te Kuiti Group the Whaingaroa Siltstone has an average percent expandable content of 26% whereas Elgood Limestone has an average percent expandable content of 10%.

Manghanani & Hower (1964) and McConchie (1978) have observed a relationship between expandable layer content and infrared peak position in the 9-11μm region. Data from this study did not show this trend. McConchie (1978) showed that almost without exception the glauconite which did not fit the model had significant degraded illite content. Again, this was not found to be the case in this study. The only conclusion drawn from this failed experiment is that the Te Kuiti Group glauconite expandable species is probably predominantly montmorillonitic in form, with only minor degraded illite.

XRF analysis delimits a region of high-Mg low-Al glauconite in the Waitomo area. Nelson (1978a) suggested a semi-enclosed embayment in this region during formation of the Te Kuiti Group. The high Mg content may reflect a higher than normal (for the Te Kuiti Group overall) terrigenous input. This would lead to an increase in smectitic clays (Mg-rich) during development of the glauconite. Areas more remote from a direct terrigenous input have more Fe-rich glauconites due to the relative abundance of this element over Mg in most sedimentary settings.

Ni and Pb contents of glauconites from the Otorohanga - Waitomo - Te Kuiti area are lower than the average for Te Kuit Group glauconites. This may be evidence for a higher sedimentation rate, which would cause the

glauconitisation process to be terminated more quickly and thereby limit the period over which Ni and Pb can be absorbed into the glauconite lattice. This inference is supported by the immature nature of glauconite from this area. This can be seen particularly well in Fig. 5-12 where the Orahiri Limestone glauconite has a higher percent expandables compared with Elgood Limestone glauconite; both formations are dominated by clean, coarse grained, highly calcareous limestones. It has been previously established that the proportion of expandable layers in glauconite decreases as the grain evolves. As many of the Orahiri Limestone samples in this study were from the Waitomo area they unduly bias the average percent expandable calculation toward higher values for the Orahiri Limestone (this also explains the large standard deviation for Orahiri Limestone glauconite samples). Collectively the information suggests that the Waitomo area was a major topographical drainage point for the surrounding landmass in the Oligocene. A possible modern environmental analogy is the Firth of Thames - Hauraki Gulf area, but with lower sediment discharge rates to allow glauconite development to proceed.

Trace element data correlations were rather poor in this study which generally negated the distinction of the 4 chemical affinity groups outlined by McConchie (1978). Some revision of the elements comprising these groups based on theoretical geochemistry would seem to be required. The substitution of Mn^{3+}, Ti^{4+} and Zr^{4+} for the octahedral cations Fe^{3+}, Fe^{2+}, and Mg^{2+} in glauconite is feasible on an ionic radius and charge basis. The inclusion of V, a 5+ valency ion, and Y^{3+}, with an ionic radius of 0.92, does not seem feasible. Therefore, V^{5+} and Y^{3+}should be excluded from the first group of chemically related elements proposed by McConchie (1978).

A more important group of trace elements is that for which no correlation would be expected with glauconite. The included elements are probably the most useful in the reconstruction of paleoenvironmental conditions during the formation of glauconite because the concentration of the species in solution essentially controls their concentration in the glauconite lattice. McConchie (1978) suggested that Cu, Ga, Ni, Pb, and Zn where reasonable paleoenvironmental discriminators. Recent work on greywackes has shown La, Ce, Nd, Th, Zr, Hf, Nb, and Sc are also useful paleoenvironmental discriminators. Many of the above elements are routinely analysed for by XRF. Therefore, the only limitation on applying paleoenvironmental reconstruction to glauconite would seem to be the ability to obtain enough sample for the XRF technique.

Average Ce/La ratios for glauconites from four horizons within the Te Kuiti Group progressively increased with upward stratigraphic position. It is also known that during the deposition of the Te Kuiti Group there was an

overall increase in seawater temperatures. This raises the possibility that the equilibrium partition coefficient between Ce and La in glauconite is controlled by temperature. This has exciting potential and may mean that glauconite can be used as a paleotemperature indicator. However, much more data are required before the suggested relationship between Ce/La in glauconite and paleotemperatures is accepted.

While XRF analysis of bulk glauconite samples showed significant changes in the chemical composition between samples the EMP of the central portion of glauconites, from the same samples, showed only subtle differences. This leads to the conclusion that bulk XRF sample analysis is probably a more sensitive technique for paleoenvironmental reconstruction compared to EMP analysis. This is not to say that EMP analysis cannot distinguish between formations in the Te Kuiti Group, but rather that environmental differences in the same formation are not easily distinguished.

A moderately large data base of EMP major element information was collected in this study. Canonical variate models show that the glauconite from each of the investigated formations has significantly different chemistries which enables the formations to be statistically differentiated based on chemical composition. The calculated canonical vectors suggest that EMP major element chemistry of a small glauconite sample from a drill core or a hand specimen can be stratigraphically correlated with a reasonable degree of certainty. The data base is good for the upper Te Kuiti Group south of Pirongia, but much smaller for the lower Te Kuiti Group north of Pirongia. Possible modification of the canonical vectors calculated in this study may eventuate with the addition of data from other studies.

The Te Kuiti Group is dominated by calcitic beds. Much of the original calcite is thought to have been in the form of high-Mg calcite. Because of near-surface diagenesis following deposition, much of the Mg has been lost from the original material; this explains the present widespread occurrence of low-Mg calcite in the Te Kuiti Group (Nelson 1978b). Calculated mineral formulae for glauconite from beds within the Te Kuiti Group show a stratigraphic increase in Mg content of glauconite upward through the Group. Since the calcite content increases stratigraphically upward through the Group it is concluded that Mg released from high-Mg calcite in particular was the source of the increasing amounts of Mg absorbed into the glauconite lattice.

An EMP transect across the border between a white crystalline unidentified phase and otherwise obviously glauconitic material showed a chemical zonation of the glauconite grain. While only one transect was made similar chemical results were found in previous literature EMP transects

(e.g., Velde & Odin 1975). The chemical zonation is interesting in that it may offer a chemical potential mechanism for the glauconitisation process.

One of the aims of this study was to increase the understanding of glauconite *per se*. The results of this study have shown certain deficiencies in previous literature studies on glauconite. An aspect not fully addressed in the previous chapter is that of the genesis of glauconite. The results presented in this thesis have not fully endorsed any model previously presented in the literature. Cast formed glauconite suggests the possibility of direct chemical precipitation of glauconite. Glauconitised echinoderm spines show definite zonation, which supports Odin & Matter's (1981) model of glauconitisation. EMP chemical evidence partly supports Bentor & Kastner's (1965) assertion that Fe and K are uptaken independently during the glauconitisation process, but the data do show a general trend of increasing K with increasing Fe which supports Burst's (1958a,b) layer lattice model. The multiple process model of Bornhold & Giresse (1985) would appear to be closest to reality as the authors accept that a combination of models is really required to adequately describe the glauconitisation process. Amouric & Parron (1985) showed destabilization of an "x-phase" into a non-crystalline product from which glauconite mica forms. Whether this x-phase is an Fe-, K-rich glauconitic smectite, degraded layer silicate, or calcitic progenitor seems irrelevant in the glauconitisation process. Rather, it would appear that given suitable Eh, pH, and elemental abundances of Fe and K, glauconitisation can and does proceed on a variety of substrates. Glauconitisation should be considered a polygenetic formational process.

REFERENCES

REFERENCES

Ahmad, N.; Jones, R.L.; Beavers, A.H. 1968: Genesis, mineralogy, and related properties of West Indian soils. (1) Montserrat Series derived from glauconitic sandstone, Central Trinidad. *Journal of Soil Science*. 19 : 1 - 8.

Alexiades, C.A.; Jackson, M.L. 1966: Quantitative clay mineralogical analysis of soils and sediments. *Clays and Clay Minerals.* 14 : 35 - 52.

Amouric, M.; Parron, C. 1985: Structure and growth mechanism of glauconite as seen by high resolution transmission electron microscopy. *Clays and Clay Minerals.* 33 : 473 - 482.

Austin, G.S.; Leininger, R.K. 1976: The effect of heat treating sedimented mixed-layer illite-smectite as related to quantitative clay mineral determinations. *Journal of Sedimentary Petrology.* 46 : 206 - 215.

Bailey, S.W. (chairman) 1980a: Comment - Summary of recommendations of the AIPEA nomenclature committee. *Clays and Clay Minerals.* 28 : 73 - 78.

Bailey, S.W. 1980b: *Structures of layer silicates.* In: Brindley, G.W.; Brown,G. (eds.) *Crystal Structures of Clay Minerals and their X-Ray identification.* Mineralogical Society Monograph Number 5. Mineralogical Society, London.

Ballance, P.F. 1964: Streaked-out mud ripples below Miocene turbidites, Puriri formation, New Zealand. *Journal of Sedimentary Petrology.* 34 : 91 - 101.

Balashov, Yu.A.; Kazakov, G.A. 1968: Fractionation of the rare earths in glauconites. *Geochemistry International.* 5 : 607 - 612.

Barshad, I. 1950: The effect of the interlayer cations on the expansion of the mica type of crystal lattice. *American Mineralogist.* 35 : 225 - 238.

Basset, W.A. 1960: Role of hydroxyl orientation in mica alteration. *Bulletin of the Geological Society of America.* 71 : 449 - 455.

Bayliss, P.; Syvitski, J.P.M. 1982: Clay diagenesis in recent marine fecal pellets. *Geo-Marine Letters.* 2 : 83 - 88.

Bell, D.L.; Goodell, H.G. 1967: A comparative study of glauconite and the associated clay fractions in modern marine sediments. *Sedimentology* 9 : 169 - 202.

Bentor, Y.K.; Kastner, M. 1965: Notes on the mineralogy and origin of glauconite. *Journal of Sedimentary Petrology.* 35 : 155 - 166.

Berg-Madsen, V. 1983: High-Alumina glaucony from the middle Cambrian of Öland and Bornholm, Southern Boltoscandia. *Journal of Sedimentary Petrology.* 53 : 875 - 893.

Bhatia, M.R.; Crook, K.A.W. 1986: Trace element characteristics of graywackes and tectonic setting discrimination of sedimentary basins. *Contributions to Mineralogy and Petrology.* 92 : 181 - 193.

Bhatia, M.R.; Taylor, S.R. 1981: Trace element grochemistry and sedimentary provinces: a study from the Tasman Geosyncline, Australia. *Chemical Geology.* 33 : 115 - 126.

Bhattacharyya, D.P. 1983: Origin of Bertherine in Ironstones. *Clays and Clay Minerals.* 31 : 173 - 182.

Birch, G.F.; Willis, J.P.; Richard, R.S. 1976: An electron microprobe study of glauconites from the continental margin off the West Coast of South Africa. *Marine Geology.* 22: 271 - 284.

Bjerkli, K.; Östomo-Saeter, J.S. 1973: Formation of glauconite in foraminiferal shells on the continental shelf off Norway. *Marine Geology.* 14 : 169 - 178.

Bodine, M.W. (Jnr.) 1987: Clayform: A Fortran 77 computer program apportioning the constituents in the chemical analysis of a clay or other silicate mineral into a structural formula. *Computers and Geosciences.* 13 : 77 - 88.

Bornhold, B.D.; Giresse, P. 1985: Glauconitic sediments on the continental shelf off Vancouver Island, British Columbia, Canada. *Journal of Sedimentary Petrology.* 55 : 653 - 664.

Brindley, G.W. 1980: *Order-disorder in Clay Mineral Structures.* In. G.W. Brindley; G. Brown (eds.) *Crystal Structures of Clay Minerals and their X-ray Identification. Mineralogical Society Monograph Nº 5.* Mineralogical Society, London. : 125 - 197.

Brongiart, A. 1823: *Mémoire sur les Terrains de Sédiments Supérieurs Calcaréo-Trappéens du Vicentin.* Levrault, Paris. 85 p.

Brown, R.W. 1954: *Composition of Scientific Words.* Geo. W. King Printing Co., Baltimore, Md. 882 p.

Buck, E.C. 1919: Bibliography on the extraction of potash from complex mineral silicates. *Metallurgy and Chemistry in England.* 18: 33 - 95.

Buckley, H.A.; Bevan, J.C.; Brown, K.M.; Johnson, L.M.; Farmer, V.C. 1978: Glauconite and celadonite: Two seperate mineral species. *Mineralogical Magazine.* 42 : 373 - 382.

Burst, J.F. 1958a: "Glauconite" Pellets: Their mineral nature and applications to stratigraphic interpretations. *Bulletin of the American Association of Petroleum Geologists.* 42 : 310 - 327.

Burst, J.F. 1958b: Mineral heterogeneity in "glauconite" pellets. *The American Mineralogist.* 43 : 481 - 497.

Carozzi, A.V. 1958: Micro-mechanisms of sedimentation in the epicontinental environment. *Journal of Sedimentary Petrology* 28 : 133 - 150.

Carozzi, A.V. 1960: *Microscopic Sedimentary Petrology.* Wiley, New York. 485p.

Charlton, H.W. 1918: Recovery of potash from greensand. *American Journal of Science.* 45 : 142.

Cimbalnikova, A. 1971: Chemical variability and structural heterogeneity of glauconites. *American Mineralogist.* 56 : 1385 - 1398.

Clarke, F.W. 1903: Composition of glauconite and greenalite. *Monographs of the United States Geological Survey.* 43 : 243 - 247.

Clarke, F.W. 1908: The Data of Geochemistry. *United States Geological Bulletin.* 330 : 439 - 442.

Cloos, P.; Fripiat, J.J.; Vielvoye, L. 1961: Mineralogical and chemical characteristics of a glauconitic soil of the Hageland region (Belgium). *Soil Science.* 91 : 55 - 65.

Cloud, P.E. (Jnr.) 1955: Physical limits of Glauconite formation. *Bulletin of the American Association of Petroleum Geologists.* 39 : 484 - 492.

Collet, L.W. 1908: *Les Dépots Marins.* Doin, Paris. 320 p.

Cornes, J.J.S. 1940: Notes on water softening properties and potash content of some New Zealand greensands. *New Zealand Journal of Science and Technology.* B22(1) : 35 - 37.

Correns, C.W. 1937: *Scientific results of the German Atlantic Expedition on the exploration and survey ship METEOR 1925 -1927. Part III. "The sediments of the Equatorial Atlantic ocean".* S. Defant. : 278 - 298.

Dana, J.D. 1882: *Descriptive mineralogy 5th ed.* John Wiley & Sons, New York. 1827 p.

De Bruyn, C.M.A.; Van der Marel, H.W. 1954: Mineralogical analysis of soil clays. Part II: Examples of mineral analysis by x-ray diffraction and differential thermal analysis. *Geol. Mijnbouw.* 16 : 407 - 428.

Degens, E.T.; Williams, E.G.; Keith, M.L. 1957: Environmental studies on Carboniferous sediments Part 1. Geochemical criteria for differentiating marine and fresh-water shales. *Bulletin of the American Association of Petroleum Geologists.* 41 : 2427 - 2455.

Devereux, I. 1967: Oxygen isotope paleotemperature measurements on New Zealand Tertiary fossils. *New Zealand Journal of Science.* 10 : 988 - 1011.

Digby, P.G.N.; Kempton, R.A. 1987: *Multivariate analysis of ecological communities.* Chapman and Hall, London. 206 p.

Draper, L. 1967: Wave activity at the seabed around northwestern Europe. *Marine Geology.* 5 : 155 - 159.

Ehlmann, A.J.; Hulings, N.C.; Glover, E.D. 1963: Stages of glauconite formation in modern foraminiferal sediments. *Journal of Sedimentary Petrology.* 33 : 87 - 96.

Eirish, M.V.; Tret'yakova, L.I. 1970: The role of sorptive layers in the formation and change of the crystal structure of montmorillonite. *Clay Minerals.* 8 : 255 - 266.

Fergusson,, D.A. 1986: *Geology of inland Kawhia: Emphasis on Te Kuiti Group stratigraphy and sedimentology.* Unpublished MSc. Thesis, University of Waikato, Hamilton, New Zealand.

Foster, M.D. 1951: The importance of exchangeable magnesium and cation-exchange capacity in the study of montmorillonitic clays. *American Mineralogist.* 36 : 717 - 730.

Foster, M.D. 1969: Studies of celadonite and glauconite. *United States Geological Survey Proffessional Paper* 614F : 17 p.

Galliher, E.W. 1935a: Geology of glauconite. *Bulletin of the American Association of Petroleum Geologists.* 19 : 1569 - 1601.

Galliher, E.W. 1935b: Glauconite genesis. *Bulletin of the Geological Society of America.* 46 : 1351 - 1365.

Galliher, E.W. 1936: Regional petrology of glauconite. *Proceedings of the Geological Society of America.* : 345.

Galliher, E.W. 1939: *Biotite-glauconite transformations and associated minerals.* In: P.D. Trask (ed.). *Recent Marine Sediments.* American Association of Petroleum Geologists. Tulsa, Oklahoma. : 513 - 515.

Giese, R.F. 1971: Hydroxyl orientation in muscovite as indicated by electrostatic energy calculations. *Science.* 172 : 263 - 264.

Giese, R.F. 1973: Hydroxyl orientations - dioctahedral micas. *22nd Annual Clay Mineral Conference.* Alberta, Canada.

Gold, C.M.; Cavell, P.A.; Smith, D.G.W. 1983: Clay minerals in mixtures: Sample preperation, analysis, and statistical interpretation. *Clays and Clay Minerals.* 31 : 191 - 199.

Griffin, G.M. 1971: *Interpretation of x-ray diffraction data.* In: R.E. Carver (ed.) *Proceedures in sedimentary petrology.* Wiley and Sons. : 541 - 569.

Grim, R.E. 1968: *Clay mineralogy.* McGraw - Hill, New York. 596 p.

Grim; R.E.; Rowland, R.A. 1942: Differential thermal analysis of clay minerals and other hydrous minerals. *American Mineralogist.* 27 : 746 - 761.

Grim, R.E.; Bradley, W.F.; Brown, G. 1951: *The mica clay minerals.* In. G.W. Brindley (ed.) *X-Ray Identification and Crystal Structure of Clay Minerals.* Mineralogical Society, London. : 138 - 172.

Gruner, J.W. 1935: The structural relationships of glauconite and mica. *American Mineralogist.* 20 : 699 - 714.

Hallimond, A.F. 1922: On glauconite from the greensand near Lewes, Sussex; the constitution of glauconite. *Mineralogical Magazine.* 19 : 330 - 333.

Harder, H. 1980: Synthesis of glauconite at surface temperatures. *Clays and Clay Minerals.* 28 : 217 - 222.

Hay, R.F. 1967: Sheet 7 Taranaki. Geological Map of New Zealand 1 : 250,000. New Zealand Department of Scientific and Industrial Research, Wellington.

Hein, J.R.; Allwardt, A.O.; Griggs, G.B. 1974: The occurence of glauconite in Monterey Bay, California: diversity, origins, and sedimentary environment significance. *Journal of Sedimentary Petrology.* 44: 562 - 571.

Henderson, J.; Grange, L.I. 1926: The geology of the Huntly - Kawhia Subdivision. *New Zealand Geological Survey Bulletin Nº 28* : 112p.

Hendricks, S.B.; Ross, C.S. 1941: Chemical composition and genesis of glauconite and celadonite. *American Mineralogist.* 26 : 683 - 708.

Hoebeke, F.; Dekeyser, W. 1954a: Evolution thermique de la glauconite. *C.R. Acad. Science.* 238 : 1143 - 1144.

Hoebeke, F.; Dekeyser, W. 1954b: L'oxydation de la glauconite à basse température. *C.R. Acad. Science.* 238 : 2171 - 2173.

Holmes, A. 1919: Non-German sources of potash. *Geological Magazine.* 56 : 251 - 254 and 340 - 350.

Hopkins, J.C. 1966: *The Te Kuiti Group in the west Piopio area.* Unpublished MSc. Thesis, University of Auckland, Auckland, New Zealand.

Hopkins, J.C. 1970: Stratigraphy, petrography, and origin of the Te Kuiti Group in the west Piopio area. *Transactions of the Royal Society of New Zealand.* 8: 1 - 26.

Hoskins, A.P. 1895: On glauconite from Woodburn, Carrickfergus, County Antrim. *Geology Magazine.* 32: 317 - 321.

Hough, J.L. 1940: Sediments of Buzzards Bay, Massachusetts. *Journal of Sedimentary Petrology.* 10 : 19 - 32.

Hower, J. 1961: Some factors concerning the nature and origin of glauconite. *American Mineralogist.* 46 : 313 - 334.

Hughes, A.D.; Whitehead, D. 1987: Glauconitization of detrital silica substrates in the Barton Formation (Upper Eocene) of the Hampshire Basin, southern England. *Sedimentology.* 34 : 825 - 835.

Hutton, C.O. & Seelye 1941: Composition and properties of some New Zealand glauconites. *American Mineralogist.* 26 : 595 - 604.

Imbrie, J.; Poldervaart, A. 1959: Mineral compositions calculated from chemical analyses of sedimentary rocks. *Journal of Sedimentary Petrology.* 29 : 588 - 595.

Ireland, B.J.; Curtis, C.D.; Whiteman, J.A. 1983: Compositional variation within some glauconites and illites and implications for their stability and origins. *Sedimentology*. 30 : 769 - 786.

James, H.L. 1966: Chemistry of iron-rich sedimentary rocks. *United States Geological Survey Proffessional Paper*. 440W : 61 p.

Jamieson, G.A. 1968: *Geology of the Aria district.* Unpublished MSc. Thesis, University of Auckland, Auckland, New Zealand.

Jonas, E.C.; Thomas, G.L. 1960: Hydration properties of K-deficent clay micas. *Clays and Clay Minerals*. 8 : 183 - 192.

Kamp, P.J.J. 1986: The mid-Cenozoic Challenger Rift System of western New Zealand and it's implications for the age of the Alpine Fault inception. *Geological Society of America Bulletin*. 97 : 255 - 281.

Kear, D. 1971: Basement rock facies - northern North Island. *New Zealand Journal of Geology and Geophysics*. 14 : 275 - 283.

Kear, D.; Schofield, J.C. 1959: Te Kuiti Group. *New Zealand Journal of Geology and Geophysics*. 2: 685 - 717.

Kear, D.; Schofield, J.C. 1978: Geology of the Ngaruawahia Subdivision. *New Zealand Geological Survey Bulletin*. Nº 88. 168p.

Keferstein, C. 1828: *Deutschland, geognostischgelogisch dargestellt.* Weimar, 5 : 510 - 511.

King, P.R. 1978: *Sedimentology of the Waikato Coal Measures, South Auckland, New Zealand.* Unpublished thesis, University of Waikato, Hamilton, New Zealand.

Konta, J. 1967: Remarks to some terms in the paper "Morphology, internal structure, and origin of glauconite pellets". *Sedimentology* 8 : 169 - 170.

Koster, 1982: International Clay Conference 1981. In:Van Olphen, H.; Veniale, F. (eds.). *The crystal structure of 2:1 layer silicates.* Developments in Sedimentology 35. Elsevier, Amsterdam. 827p.

Krauskopf, K.B. 1956: Factors controlling the concentrations of thirteen rare metals in sea water. *Geochemica Cosmochimica Acta.* 9 : 1 - 32.

Logvinenko, N.V. 1982: Origin of glauconite in the recent bottom sediments of the ocean. *Sedimentary Geology.* 31 : 43 - 48.

Logvinenko, V.A.; Nikolaeva, I.V.; Kameneva, M.Yu. 1985: Study of dehydration processes ın glauconite-group minerals by thermogravimetry under quasiequilibrium conditions. *Transactions of the Institute Of Geology and Geophysics., Akaud. Nauk. SSSR., Sib. Otd.* 610 : 143 - 150.

Lowe, D.J.; Nelson, C.S. 1983: *Guide to the nature and methods of analysis of the clay fraction of tephras from the South Auckland Region, New Zealand.* Occasional Report Nº 11, University of Waikato, Department of Earth Sciences.

MacEwan, D.M.C.; Wilson, M.J. 1980: *Interlayer and intercalation complexes of Clay Minerals.* In: G.W. Brindley; G. Brown (eds.) *Crystal Structures of Clay Minerals and their X-ray Identification. Mineralogical Society MOnograph Nº 5.* Mineralogical Society, London.

Manghnani, M.H.; Hower J. 1964: Glauconites: Cation exchange capacities and infrared spectra. Part I. The cation exchange capacity of glauconite. *American Mineralogist.* 49 : 586 - 598.

Mansfield, G.R. 1922: Potash in the greensands of New Jersey. *Bulletin of the United States Geological Survey Nº* 727 : 146p.

Marwick, J. 1946: The Geology of the Te Kuiti Subdivision. *New Zealand Geological Survey Bulletin Nº* 41: 99p.

McConchie, D.M. 1978: *Cretaceous and Lower Tertiary glauconite in the South Island of New Zealand.* Unpublished Thesis, University of Canterbury, New Zealand.

McConchie, D.M.; Lewis, D.W. 1978: Authigenic, perigenic, and allogenic glauconites from the Castle Hill Basin, North Canterbury, New Zealand. *New Zealand Journal of Geology and Geophysics.* 21 : 199 - 214.

McConchie, D.M.; Lewis, D.W. 1980: Varieties of glauconite in late Cretaceous and early Tertiary rocks of the South Island of New Zealand, and new proposals for classification. *New Zealand Journal of Geology and Geophysics.* 23 : 413 - 437.

McConchie, D.M.; Ward, J.B.; Cann, V.H.; Lewis, D.W. 1979: A Mössbauer investigation of glauconite and its geological significance. *Clays and Clay Minerals.* 27 : 339 - 348.

McRae, S.G. 1972: Glauconite. *Earth Science Reviews.* 8 : 397 - 440.

McRae, S.G.; Lambert, J.L.M. 1968: A study of some glauconites from Cretaceous and Tertiary formations in southeast England. *Clay Minerals.* 7 : 431 - 440.

Miesch, A.T. 1962: Computing mineral compositions of sedimentary rocks from chemical analyses. *Journal of Sedimentary Petrology.* 32 : 217 - 225.

Millot, G. 1964: *Géologie des Argiles.* Masson, Paris. 339 p.

Murray, J.W.; Mackintosh, E.E. 1968: Occurence of interstratified glauconite-montmorillonoid pellets, Queen Charlotte Sound, British Columbia. *Canadian Journal of Earth Sciences.* 5 : 243 - 247.

Murray, J. ; Renard, A.F. 1891: *Report on Deep-Sea deposits based on the specimens collected during the voyage of H.M.S. "Challenger" in the years 1872 to 1876.* H.M.S.O., London. 525 p.

Nakamoto, K. 1978: *Infrared and Raman spectra of inorganic and coordination compounds.* Wiley, New York. 448 p.

Nelson, C.S. 1973: *Stratigraphy and sedimentology of the Te Kuiti Group, Waitomo County.* Unpublished PhD Thesis, University of Auckland, Auckland, New Zealand.

Nelson, C.S. 1978a: Stratigraphy and paleontology of the Oligocene Te Kuiti Group, Waitomo County, South Auckland, New Zealand. *New Zealand Journal of Geology and Geophysics.* 21 : 553 - 594.

Nelson, C.S. 1978b: Temperate shelf carbonate sediments in the Cenozoic of New Zealand. *Sedimentology.* 25 : 737 - 771.

Nelson, C.S.; Hume, T.M. 1977: Relative intensity of tectonic events revealed by the Tertiary sedimentary record in the North Wanganui Basin and adjacent areas, New Zealand. *New Zealand Journal of Geology and Geophysics.* 20 : 369 - 392.

Nelson, C.S.; Hume, T.M. 1987: Paleoenvironmental controls on mineral assemblages in a shelf sequence, Te Kuiti Group, South Auckland. 30 : 343 - 362.

Nelson, C.S.; Burns, D.A.; Rodgers, K.A. 1983: The taxonomic status and isotopic evidence for paleoenvironments of giant oysters from the Oligocene Te Kuiti Group. *New Zealand Journal of Geology and Geophysics.* 26: 289 - 299.

Nicholls, G.D. 1962: A scheme scheme for recalculating the chemical analyses of argillaceous rocks for comparative purposes. *American Mineralogist.* 47 : 34 - 46.

Nutting, P.G. 1943: Some standard thermal dehydration curves of minerals. *United States Geological Survey Professional Paper 197E.* : 197 - 217.

Oakley, K.P. 1943: Glauconite sand of Brackelsham Beds, London Basin. *Wartime Pamphlet Geological Survey of England and Wales.* 33 : 1 - 27.

Odin, G.S. 1972: Observations nouvelles sur la structure de la glauconie en accordéon; description du processus de genèse par néoformation. *Sedimentology.* 19 : 285 - 294.

Odin, G.S.; Letolle, R. 1980: Glauconitization and phosphatization environments: A tentative comparison. *Society of Economic Paleontologists and Mineralogists Special Publication.* Nº 29 : 227 - 237.

Odin, G.S.; Matter, A. 1981: De Glauconiarum origine. *Sedimentology.* 28 : 611 - 641.

Odom, I.E. 1976: Microstructure, mineralogy and chemistry of Cambrian glauconite pellets and glauconite, Central U.S.A. *Clays and Clay Minerals* 24: 232 - 238.

Owens, J.P.; Sohl, N.F. 1973: Glauconites from the New Jersey - Maryland coastal plain; their K/Ar ages and application in stratigraphic studies. *Geological Society of America Bulletin.* 84 : 2811 - 2838.

Pearson, M.J. 1978: Quantitative clay mineralogical analyses from the bulk chemistry of sedimentary rocks. *Clays and Clay Minerals.* 26 : 423 - 433.

Peterman, Z.E.; Coleman, R.C.; Bunker, C.M. 1981: Provenance of Eocene greywackes of the Fluornoy Formation near Aness, Oregon - a geochemical approach. *Geology.* 9 : 81 - 86.

Player, R.A. 1958: *The Geology of North Kawhia.* Unpublished thesis, University of Auckland, Auckland, New Zealand.

Porrenga, D.H. 1967: Glauconite and chamosite as depth indicators in the marine environment. *Marine Geology.* 5 : 495 - 501.

Potter, D.H.; Shimp, N.F.; Whitters, J. 1963: Trace elements in marine and fresh water argillaceous sediments. *Geochemica et Cosmochemica Acta.* 27 : 669 - 694.

Prather, J.K. 1905: Glauconite. *Journal of Geology.* 13 : 509 - 513.

Pryor, W.A. 1975: Biogenic sedimentation and alteration of argillaceous sediments in shallow marine environments. *Bulletin of the American Association of Petroleum Geologists.* 86 : 1244 - 1254.

Reynolds, R.C. 1980: *Interstratified Clay Minerals.* In: G.W. Brindley; G. Brown (eds.) *Crystal Structures of Clay Minerals and their X-ray identification. Mineralogical Society Monograph Nº 5.* Mineralogical Society, London.

Reynolds, R.C.; Hower, J. 1970: The nature of interlayering in mixed-layer illite-montmorillonites. *Clays and Clay Minerals* 18 : 25 - 36.

Ross, C.S. 1926: The optical properties and chemical composition of glauconite. *Proceedings of the United States National Museum.* 69 : 1 - 15.

Rolf, R.M.; Kimball,C.W.; Odom, I.E. 1977: Mössbauer characteristics of Cambrian glauconite, Central U.S.A. *Clays and Clay Minerals.* 25 : 131 - 137.

Russ, 1985: *Practical stereology.* DApple systems, 355 West Olive Avenue, Suit 100, Sunnyvale, California.

Russell, K.L. 1970: Geochemistry and halmyrolysis of clay minerals, Rio Ameca, Mexico. *Geochemica et Cosmochemica Acta.* 34 : 893 - 907.

Sabatier, M. 1949: Recherches sur la glauconie. *Bulletin Soc. Fr. Minéral. Cristallogr.* 72: 474 - 542.

Schneider, H. 1927: A study of glauconite. *Journal of Geology.* 35 : 289 - 310.

Schnepfe, M.M.; May, I.; Naeser, C.R. 1964: Cesium and strontium sorption studies on glauconite. *United States Geological Survey Proffessional Paper.* 501B : 95 - 99.

Schultz, L.G. 1971: Lithium and potassium absorbtion, dehydroxylation temperature and structural water content of aluminous smectites. *Clays and Clay Minerals.* 17 : 115 - 150.

Seed, D.P. 1965: The formation of vermicular pellets in New Zealand glauconites. *American Mineralogist.* 50 : 1097 - 1106.

Shreve, R.N. 1921: Action of lime on greensand. *Journal of Industry Engineering and Chemistry.* 13 : 693.

Simpson, E.S. 1934: Glauconite; its distribution and uses. *Chemistry Engineering and Mineralogy Reviews.* 26 : 391 - 394.

Smulikowski, K. 1954: The problem of glauconite. *Archeaology and Mineralogy.* 18: 21 - 120.

Stoffers, P.; Pluger, W.; Walter, P. 1984: Geochemistry and mineralogy of continental sediments from Westland, New Zealand. *New Zealand Journal of Geology and Geophysics.* 27 : 351 - 365.

Swift, D.J.P. 1970: Quarternary shelves and the return to grade. *Marine Geology.* 8 : 5 - 30.

Takahashi, J. 1939: Synopsis on glauconitisation. In P.D. Trask (ed.): Recent Marine Sediments. *American Association of Petroleum Geologists Special Publication.* 4 : 503 - 512.

Takahashi, J.; Yagi, T. 1929: Peculiar mud grains and their relation to the origin of glauconite. *Economic Geology.* 24 : 838 - 854.

Tapper, M.; Fanning, D.S. 1968: Glauconite pellets: X-ray patterns from individual pellets of lobate and vermiform morphology. *Clays and Clay Minerals* 16: 275 - 283.

Thompson, G.R.; Hower, J. 1975: The mineralogy of glauconite. *Clays and Clay Minerals.* 23 : 289 - 300.

Triplehorn, D.M. 1966: Morphology, internal structure and origin of glauconite pellets. *Sedimentology* 6 : 247 - 266.

Twenhofel, W.H. 1936: The greensands of Wisconsin. *Economic Geology.* 31 : 472 - 487.

Valeton, I; Abdul-Rassak, A.; Klussmann, D. 1982: Mineralogy and geochemistry of glauconite pellets from Cretaceous sediments in northwest Germany. *Geol. Jahrb. D52.* : 5 - 93.

Van Andel, T.H.; Psotma, H. 1954: *Recent sediments of the Gulf of Paria. Orinoco Shelf Expedition.* V.1. Verh. K. Ned. Akad. Natuurkd. reeks 1, B. XX, 5: 245p.

Van Houten, F.B.; Purucker, M.E. 1984: Glauconite peloids and chamositic ooids - favourable factors, constraints and problems. *Earth Science Reviews.* 20 : 211 - 243.

Van Wie, W.A. 1971: The petrology of the Floyds Knob glauconite (abstract). *Geological Society of America Abstracts.* 3 : 284 - 285.

Velde, B. 1976: The chemical evolution of glauconite pellets as seen by microprobe determinations. *Mineralogical magazine.* 40 : 753 - 760.

Velde, B.; Odin, G.S. 1975: Further information related to the origin of glauconite. *Clays and Clay Minerals.* 23 : 376 - 381.

Vella, P. 1967: Eocene and Oligocene sedimentary cycles in New Zealand. *New Zealand Journal of Geology and Geophysics.* 10 : 119 - 145.

Von Gumbel, C.W. 1886: Uber die Natur and Bildungsweise des Glaukonits. *Sber. Bayer. Akad. Wiss.* 16 : 417 - 449.

Von Humboldt, A. 1823: *See Schneider, H. 1927.*

Warshaw, C.M. 1957: *The Mineralogy of Glauconite.* Unpublished Thesis Pennsillvania State University, University Park, Pennsillvania.

Weaver, C.E.; Pollard,L.D. 1973: *The Chemistry of Clay Minerals.* Elsevier Scientific Publishing Company, Amsterdam.

Wermund, E.G. 1961: Glauconite in early Tertiary sediments of Gulf Coast Province. *American Association of Petroleum Geologists Bulletin* 45. : 1667 - 1696.

Xingzhen, H. 1983: Features and sedimentary environment of recent glauconite in China and comparison between recent and fossil glauconites. *Scientia Sincia (Series B).* 26: 755 - 773.

Zumpe, H.H. 1971: Microstructures in Cenomanian glauconite from the Isle of Wight, England. *Mineralogical Magazine.* 38 : 215 - 224.

Zvyagin, B.B. 1957: Determination of the structure of celadonite by electron diffraction. *Soviet Physical Crystallography.* 2: 388 - 394.

APPENDICES

APPENDIX I

METHODOLOGY: CONDITIONS, NEW TECHNIQUES, AND AMMENDMENTS TO LITERATURE TECHNIQUES FOR THE STUDY OF GLAUCONITE

(A1-1) CONTAMINANT REMOVAL BY ACIDIFICATION

A problem found in this study of Te Kuiti Group glauconite was the highly calcitic nature of the sediment enclosing glauconite grains for many samples. McConchie (1978) avoided what he termed "indurated" samples in favour of "friable and loose samples", which could be disaggregated by hand crushing in warm water. Nelson (1973) crushed the whole rock then frantz separated the glauconitic component. Following this primary concentration impurities were hand picked from the sample. Nelson (1973) noted that this extraction process does not completely remove glauconite grains with inclusion contaminants; chemical analyses made on glauconite extracted using this technique are often contaminated, particularly with Ca.

Hutton & Seelye (1941) questioned the validity of using glauconite which has interacted with acid solutions for extended periods because acid solutions leach ions from the glauconite lattice. Experiments were undertaken to test the validity of this assertion. Sample MC44 (Ao-4) was selected for the tests to determine the effects of dilute hydrochloric acid on glauconite, because:

(a) MC44 is from an essentially disaggregated, friable, sandstone bed. This means extraction of glauconite can be made using the frantz magnetic separator techniques described in Section A1-3.

(b) MC44 is essentially disaggregated but contains a minor calcitic component. This means that either hand-picking removal of the contaminant or HCl dissolution of the contaminant is possible.

(c) MC44 is easily accessible, recognizable, and of significant glauconite concentration at the sample site.

(d) MC44 contains a significant proportion of fragmentary glauconite. Acid attack should be more vigorous in a fragmentary-dominated deposit than an ovoidally-dominated deposit, owing to the increased surface area of fragmented grains.

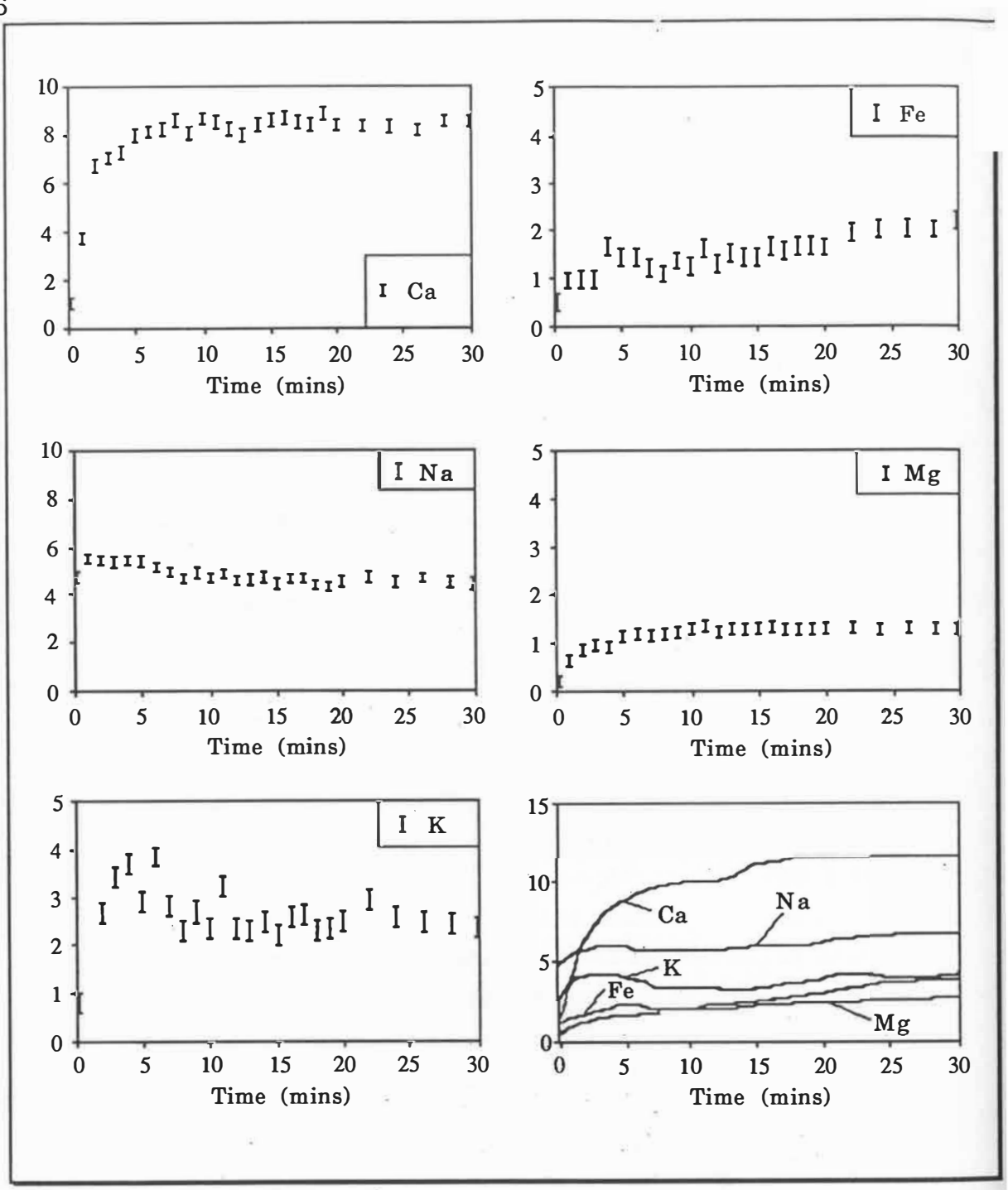

Fig. A1-1 Preliminary acid interaction test: dissolution data plots. Spline interpolation curves for all elements are shown in lower right graph (37th degree interpolation using SAS on VAX/VMS system version 4.7).

A1-1-1 Acid dissolution test

To test if dilute HCl significantly removed ions from the glauconite lattice in a short time interval, the following experiment was devised.

20 g of glauconite concentrate was placed in 2 litres of 1 M HCl and stirred. Precise aliquots (20ml) of solution were removed at 1 min intervals for 20 minutes, and then at 2 min intervals for a further 10 min. The removed aliquots were stored in glass vials and analyzed using a Pye Unicam SP9 atomic absorption spectrophotometer linked to a P2000C Philips portable computer. The elements analyzed were: Ca, Mg, Na, K, and Fe (see data booklet Section D1 for results). As solution volume and hence concentration is changing with the removal of samples for subsequent analysis the concentration measured directly from atomic absorption must be corrected for the dilutive removal effect. The mathematical justification for the dilutive effect is shown in Section A1-1-1a.

True concentration data were plotted against time of removal (Fig. A1-1). The data show a rapid increase in Ca content for approximately 5 min. This is interpreted as the dissolution of carbonate contaminant in the sample. Mg, Na, and Fe show only small increases in concentration over the 5-30 min time-period. For the first 5 min period rapid increases in Mg, Na, and Fe are attributed to dissolution of the carbonate fraction and surface reactions with exposed glauconite surfaces. K content increases rapidly, then decreases after 7 min; the cause of this is unknown. The author notes that McConchie & Lewis (1980) observed diagenetic leaching removed potassium and thereby formed degraded illitic layers within glauconitic material. Possibly, K released from the contaminants in MC44 is being re-adsorbed onto surface exposed degraded illite layers (at present this is purely hypothetical, but it does explain why only two samples in this study (MC27c and MC31b) show more than 10% degraded illite content). The minimum detectable limit of degraded illite using the methodology of McConchie (1978) is 10%.

A1-1-1a Correction justification for acid dissolution test

Assume an initial volume V_o of pure acid and nothing released into it.

After time t_1 suppose m_1 moles of an element Z has been leached from the glauconite into solution.

Then concentration: **(1)** $C_1 = \frac{m_1}{V_o}$

If a small volume of solution is removed V_* then the number of moles remaining is: **(2)** $C_1V_o - C_1V_* = C_1(V_o - V_*)$

N.B. - The concentration is still C_1 in the remaining solution, but the number of moles has changed.

After time t_2 a further m_2 moles of Z has been leached.

If nothing had been removed the concentration would be:

(3) $C_2 = \frac{(m_1+m_2)}{V_o} = \frac{m_2}{V_o} + \frac{m_1}{V_o}$

$C_2 = C_1 + \frac{m_2}{V_o}$

The actual concentration is $C'_2 = \frac{[C_1(V_o-V_*)+m_2]}{(V_o-V_*)}$

(4) $C'_2 = C_1 + \frac{m_2}{(V_o-V_*)}$

From (3), $m_2 = (C_2-C_1)V_o$ and from (4), $m_2 = \frac{(C'_2-C_1)}{(V_o-V_*)}$ moles have been removed into solution.

From which, (5) $C'_2 = C_1 + (C_2-C_1)\left(\frac{V_o}{(V_o-V_*)}\right)$

or, (6) $C_2 = (C'_2-C_1)\left(\frac{(V_o-V_*)}{V_o}\right) + C_1$ can be derived.

If another V_* is removed, the number of moles that remains is:

(7) $C'_2(V_o-V_*)-C'_2V_* = C'_2(V_o-2V_*)$

After time t_3 a further m_3 moles has been produced.

If nothing had been removed:

(8) $C_3 = \left(\frac{(m_1+m_2+m_3)}{V_o}\right)$

The actual concentration is:

(9) $C'_3 = \frac{[C'_2(V_o-2V_*) + m_3]}{(V_o-2V_*)}$

$= C'_2 + \frac{m_3}{(V_o-2V_*)}$

Using (8) and (3) we can derive : $m_3 = (C_3-C_2)V_o$

Thus (9): $C'_3 = C'_2 + \left[\frac{(C_3-C_2)}{(V_o-2V_*)}\right]V_o$

Rearrangement leads to: $C_3 = C_2 + (C'_3-C'_2)\frac{(V_o-2V_*)}{V_o}$

From this we can derive an iterative formulae for all situations of $n \geq 2$.

$$\textbf{For } n \geq 2 \qquad C_n = C_{n-1} + [C'_n - C'_{(n-1)}]\left(\frac{V_o-(n-1)V_*}{V_o}\right)$$

Where C_n is the concentration at the nth reading, C'_n is the apparent concentration (i.e., that actually measured in the sample). C_{n-1} and C'_{n-1} are

the corresponding previous sample readings. n is the number of aliquots removed.

When n=1, $C_1 = C'_1$ and $C_o = C'_o = 0$.

In all cases V_o is the initial volume of the acid and V_* is the volume withdrawn.

N.B. - There is no requirement for $t_1=t_2=t_n$ but V_* must be the same in all removals.

Obviously, the calculation of C_n is impractical on a calculator, particularly if the number of samplings is large. To assist in the calculation of true concentration data a Fortran-77 program was written on the University of Waikato VAX/VMS (system version 4.7). The following is the program listing:

```
c  Programme variables
   character*1 ans
   integer i,j,k,reply,valid
   real time,Cm,Ct,Cmp,Ctp,init_vol,aliquot
   real in(1000,3)
c  Output file definition
   open(unit=2,file='outdata.data',status='new')
c  Define variable initial values
   i=0
   valid=1
   k=1
c  Data input
   write(6,800)
   accept *,init_vol
   write(6,810)
   accept *,aliquot
   write(6,820)
   accept *,time
   do 300 while ((time.ne.1111).and.(i.lt.1000))
      i=i+1
      write(6,830) time
      accept *,Cm
c  Data test loop
      write(6,840) time,Cm
      accept 850,ans
      if ((ans.EQ.'N').or.(ans.EQ.'n')) then
         valid = 0
```

```
          else
          valid = 1
        end if
c  Data input into array if input defined correct by user
        if (valid.EQ.1) then
          in(i,1) = time
          in(i,2) = Cm
          else
          i=i-1
        end if
      write(6,820)
      accept *,time
300   continue
c  Assignment of first array value Ct to Cm
      time = in(k,1)
      Ctp = in(k,2)
      Cmp = in(k,2)
      in(k,3) = Ctp
      write(6,*)'  Time(mins)      Concentration Measured
     *    Concentration True'
      write(6,*)'  Time(mins)      Concentration Measured
      *   Concentration True'
      write(6,860) time,Cmp,Ctp
      write(2,860) time,Cmp,Ctp
c  Data manipulation and calculation of true concentration section
        do 600 k=2,i
          j = k-1
          Ctp = in(j,3)
          Cm = in(k,2)
          Cmp = in(j,2)
            Ct = (init_vol-(j*aliquot))
            Ct = Ct/init_vol
            Ct = Ctp+((Cm-Cmp)*Ct)
          in(k,3) = Ct
          time = in(k,1)
c  Output
        write(6,860) time,Cm,Ct
        write(2,860) time,Cm,Ct
600     continue
      write(6,*) '*'
```

```
      write(6,*) '**********data output end**********'
      write(6,*) ' An output file called "outdata.data" has been
     * created'
      write(6,*) '************************************************'
      STOP
800   Format('+Enter the initial volume of acid (mls) ==> ',$)
810   Format('+Enter the aliquot size removed (mls) ==> ',$)
820   Format('+Enter the time reading in minutes <1111 to exit> ==> '
     * ,$)
830   Format('+Enter the measured concentration for ',f6.1,' mins==> '
     * ,$)
840   Format('+Are the inputs time (mins)= ',f6.1,'concentration= ',
     * f10.5,' O.K ? [<return> or <n>] ==> ',$)
850   Format (1A)
860   Format(1x,1F5.1,16x,1F10.5,16x,1F10.5)
      END
```

A1-1-2 XRD test

To test if acidification significantly altered XRD traces, a sample of crushed MC44 was split into two subsamples: subsample **(A)** was acidified in 1M HCl for 5 min then washed in distiled water, subsample **(B)** was not acidified. Four oriented slides of each subsample were made and scanned (see Section A1-6 for machine settings and preparation technique).

The XRD scans show small differences in the d(001) peak shape. There is a broadening of the base of the d(001) peak and reduction in the height of the d(001) peak by 5% to 15%. There is little change in the height or shape of the d(003) peak. Fig. A1-2 shows traces for the two subsamples which show the maximum variation in the d(001) peak height.

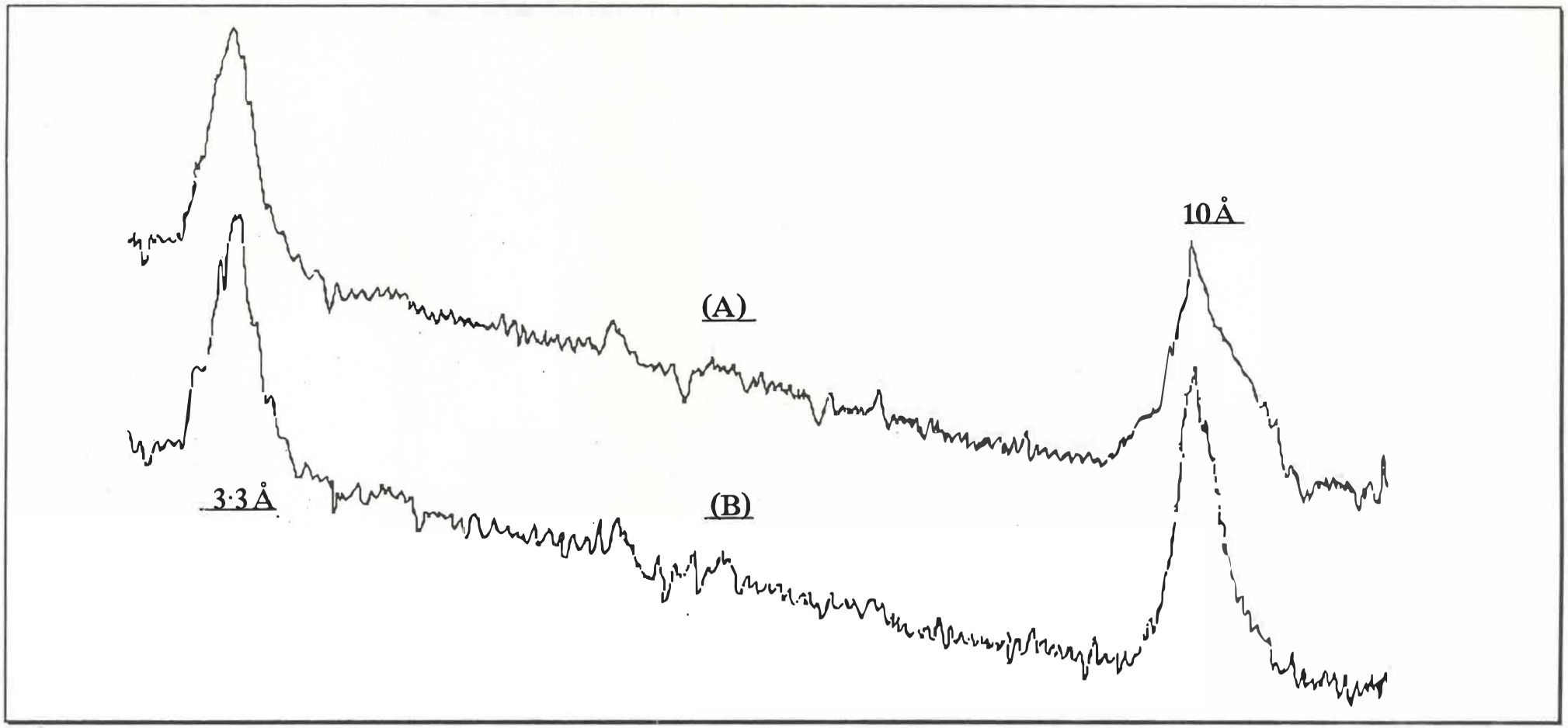

Fig. A1-2 Physical XRD traces for two samples of MC44: trace sample **(A)** was acidified in 1M HCl for 5min; trace sample **(B)** was not acidified.

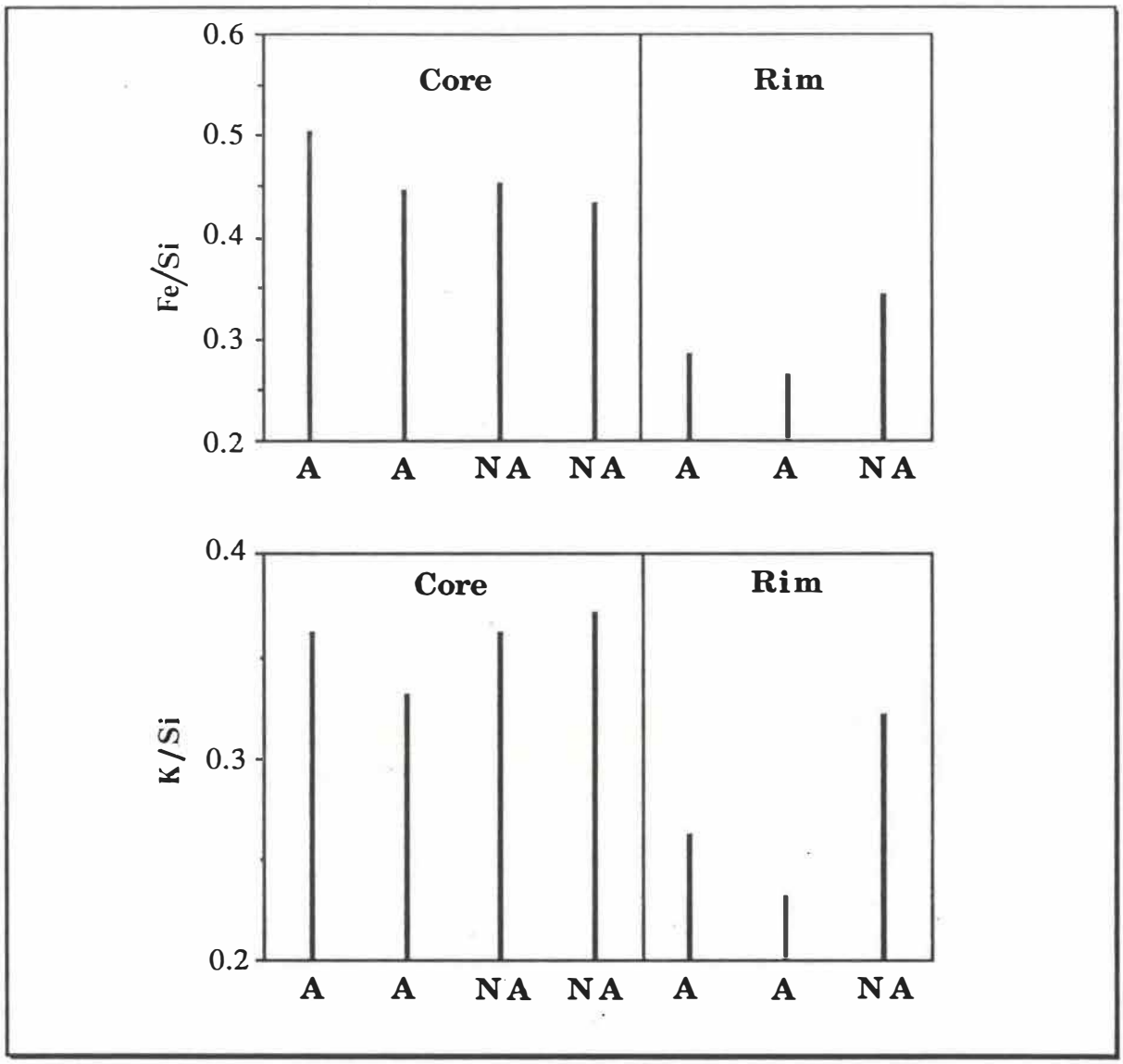

Fig. A1-3 Peak intensity of major lattice ions (Fe and K) relative to the silica peak intensity for core and rim sites on selected acidified **(A)** and non-acidified **(NA)** MC44 sample grains. Scanning electron microscope energy dispersive analysis data source.

A1-1-3 EMP test

A sample of average glauconite grains from MC44 was handpicked and divided into two subsamples: **(A)** was acidified for 5 min in 1M HCl; **(B)** was not acidified. The subsamples were then mounted in epoxy resin stubs (see Section A1-10) and analyzed for major elements using the University of Waikato scanning electron microscope (energy dispersive technique). These results, while only qualitative, show that the rim of the glauconite grains is

depleted in Fe and to a lesser degree K (relative to the silica peak) compared to the core of the grains (Fig. A1-3). This elemental distribution is similar to that found by Velde & Odin (1975) for pelletal glauconite. The samples which have been acidified show increased depletion of K and Fe near the rim of the grain but the depletion does not extend into the centre of the grains.

A1-1-4 Contaminant removal by acidification conclusions

(1) Acidification in low concentration HCl removes carbonate cements faster than leaching of significant quantities of glauconite lattice ions.

(2) Variation in XRD traces was observed after acid solution interaction. However, in most cases the variation was smaller than the experimental error in calculating expandable contents, degraded illite contents, or disorder coefficients. Some of the variation can be attributed to the visual fitting of a baseline to the XRD trace.

(3) There is a zone of low K, low Fe content at the edge of MC44 samples which becomes increasingly depleted with acid solution interaction. Probe analyses were restricted to central portions of acidified glauconitic grains to negate this effect.

Overall, acidification in dilute HCl would appear to be a valid technique for the removal of calcitic cements provided: **(a)** the acid strength is low (1M HCl is recommended); and **(b)** the acid is not left in contact with the glauconite grains for extended periods (5 min is the experimentally suggested maximum for 1M HCl). Agitation of the sample during acid solution interaction and washing is recommended, as this enhances the decalcification process.

(A1-2) DRYING OF SAMPLES

The temperature glauconite samples are dried at must not be near 100°C as elevated temperatures affect the ability of smectitic clays to expand when exposed to an ethylene glycol atmosphere (Grim 1968, in McConchie 1978). The recommended maximum temperature of 40°C for 24 hours used by McConchie (1978) was used in this study for the drying of sediments containing glauconite.

(A1-3) FRANTZ MAGNETIC SEPARATION OF GLAUCONITE

As glauconite is paramagnetic, separation of the mineral from the supporting matrix is usually made with the aid of a Frantz magnetic separator (e.g., Bell & Goodell 1967; Hein et al. 1974; McConchie 1978; Stoffers et al. 1984; Bornhold & Giresse 1985; Hughes & Whitehead 1987). Bentor & Kastner (1965) have shown that the magnetic susceptibility of glauconitic material is a function of the Fe content of the glauconite. As the Fe content of glauconite is variable, magnetic field strength is not an optimizable parameter for mineral separation.

The problem with set magnetic extraction currents (e.g., the 0.35A setting of McConchie (1978)) is, a bias in glauconite type may be introduced; more evolved glauconitic grains have a higher Fe content than less evolved glauconitic grains. Because Te Kuiti Group glauconite has a large proportion of nascent glauconite, this fraction would be under-represented in the glauconite concentrate if high currents (e.g., 0.5A) with the inclined plane machine setting were used.

To obviate the problem, a variation on established frantz glauconite extraction techniques was developed. The Frantz was set in near vertical mode and a washed,disaggregated,sieved sample was passed through an inclined plane to the magnetic field (Fig. A1-4). The sample was captured in two traps at the base of the Frantz, the outer container catching non-magnetic to weakly paramagnetic material, the inner container the variably paramagnetic glauconitic material. There was no set current used for the extraction and "purity" was assessed under a binocular microscope (several samples were also tested using XRD techniques). Generally, currents of around 0.5A gave the best separation. If the sample had a low glauconite concentration or a high proportion of nascent glauconite then higher currents were required to deflect the glauconite out of the stream of non-magnetic material. The primary concentrate was re-run through the frantz to purify the sample. The use of this method resulted in glauconitic concentrates of 98% purity. The concentrates also had a range of evolutionary development because a range of deflections and hence iron contents could be captured in the inner trap. Subsequent contaminant removal was made by hand-picking under a binocular microscope.

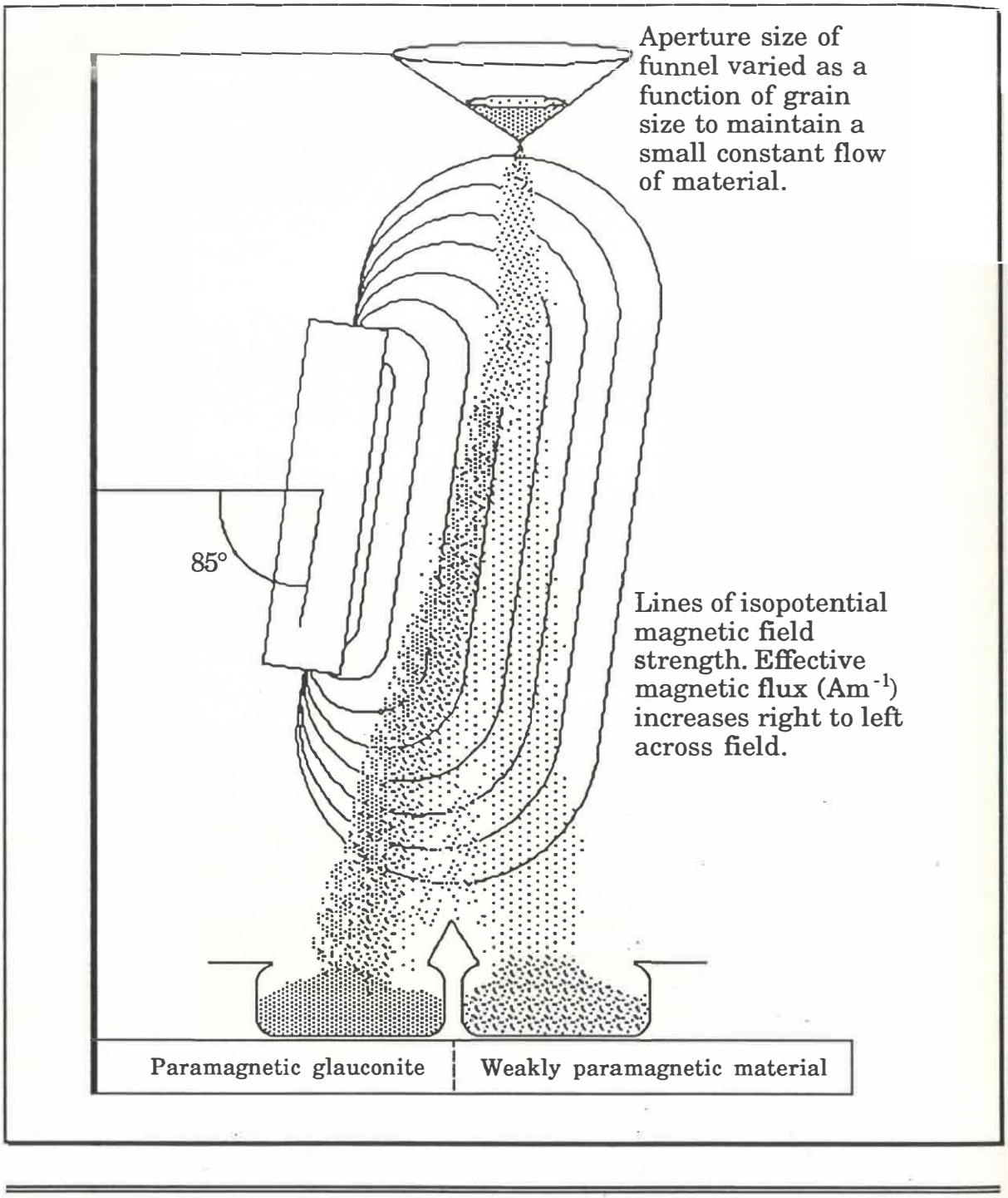

Fig A1-4 Skematic diagram of the Frantz magnetic seperator conditions used to extract glauconite from crushed Te Kuiti Group sediments.

(A1-4) IMAGE ANALYSIS

McConchie (1978) noted that visual discriminant techniques are inherently subjective. While McConchie was referring to XRD trace interpretations, a direct analogy can be drawn with visual classification of grain morphologies. In this study both binocular morphology classification, and image analysis

morphological classifications were made on selected samples. The latter of these techniques is less operator biased as the variables leading to classification are numerical rather than abstract (e.g., formfactor versus rough). It is hoped that this method of grain classification will be adopted by future researchers on glauconite grain morphology. The image analysis technique also has implications for other mineral grain type provenance studies based on rounding indices (e.g., quartz provenance studies).

A1-4-1 Basic image analysis theory

Image analysis uses video assimilation of an image, then binary division of that image into areas of preset light intensity range. The contrast cutoff divisions (i.e., the specific pixel combinations the computer considers to be within the user's specified intensity range) are defined by the user. This may appear confusing to the inexperienced user so the image analysis theory is explained via the following example:

(a) A single lobate pellet was mounted on a brass stub and photographed using the University of Waikato's SEM. The resulting photograph was then scanned using the image analyser. Fig. A1-5 shows the grey scale display of the video image. The image shown is the computer interpretation and division of a black and white photograph into 64 grey-levels; the range of the levels is controlled by the contrast and allowable light intensity; set by the user.

(b) The grey-scale image was then digitised into pixels of specific grey-levels (i.e., each pixel is assigned a value 1 to 64) and stored.

(c) The image can now be converted into a binary image. This involves tabulating the grey-levels as a histogram then telling the computer to essentially "switch on" any pixel block with a value within a defined portion of the grey-level histogram.

(d) The video image is now re-created with only the blocks within the required grey-levels illuminated (Fig. A1-6).

The use of a photographic source for information acquisition is significant, in that it allows previous photographic information in journals, books, etc. to be incorporated in new studies. Unfortunately, literature photographs are often of low contrast and are difficult to assimilate on a video source. To alleviate this problem I found that applying a Fourier edge-finding algorithm of Sobel type, then recombining this edited grey-image with the original grey-image, greatly enhanced edge features of photographs. More information on these edge-enhancement features of the image analyser can be found in the Imageplus Technical Manual, appendix 5.

Fig. A1-5 Grey-scale image of a single large lobate grain photographed using the scanning electron microscope

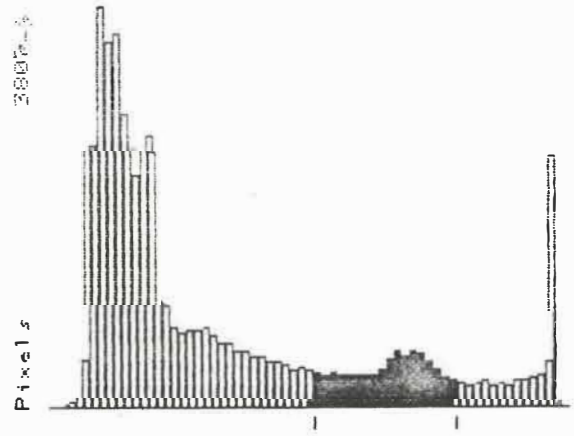

Total image brightness = 21.44 +- 17.85
Mask region brightness = 41.96 +- 4.86
Total image area = 48768 Pixels
Mask region area = 13.33 %

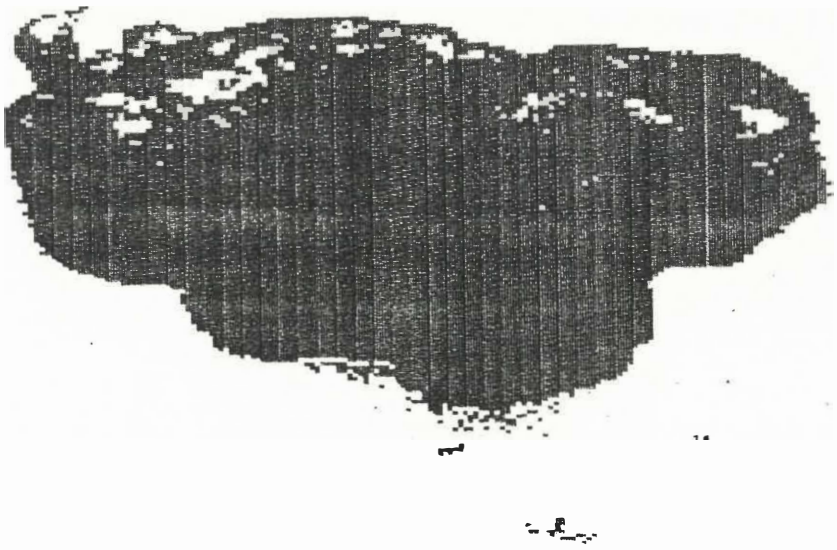

Fig. A1-6 Grey-scale histogram of the grey-scale image Fig.A1-5 and binary representation of the selected region within the grey-scale histogram.

As it would be time consuming and costly to take innumerable photographs of grains for image analysis, use was made of slides prepared for standard binocular morphological study. The slides consisted of a standard thin section glass slide with a piece of double sided sellotape attached to one side. The glauconite sample was sprinkled onto the sellotape and excess material removed by inverting the slide. The slides were then mounted on a diffuse-light backlit stage. Suitable contrast levels were then set to maximize the silhouette effect. This technique is advantageous in that:

(1) Slides are easily and rapidly prepared from glauconite concentrates.

(2) Silhouette images have well defined edges and therefore do not require mathematical transformation to enhance the edge.

(3) The technique requires minimal physical interaction with the grains, hence fracturing is not a problem.

After production of the binary image seven variables were calculated:

(A) Length = the longest projected, or Feret's dimension of the feature. The Feret axes are determined in 8 directions.

(B) Area = the number of contiguous pixels in the binary image are summed and converted to the user defined measurement scale.

(C) Formfactor = $\frac{4\pi \times \text{Area}}{\text{Perimeter}^2}$. The maximum value is 1.0, values less than this indicate increased irregularity. Perimeter is defined as the sum of the pythagorean distance between the end points of each line of pixels converted to the user defined measurement scale.

(D) Aspect = $1 + \frac{4}{\pi} \times \left(\frac{\text{Length}}{\text{Width}} - 1\right)$, where Width = $\frac{4 \times \text{Area}}{\pi \times \text{Length}}$

(E) Convexicity = $\frac{\text{Convex Perimeter}}{\text{Perimeter}}$. The convex perimeter is analogous to the perimeter measured by wrapping a string tightly around the object. Convexicity values decrease from 1.0 with increasing surface irregularity.

(F) Fractal = The degree of roughness of the outline of the feature. Smooth features have a value of 1.0 while outlines that are locally rough have a higher value.

(G) Fibre = $(0.3181 \times P) + \sqrt{(0.033012 \times P^2) - (0.41483 \times \text{Area})}$, which is an estimate of the length of long slender objects that are curved and lie in the plane of the image.

More information on these parameters and the running of the image analyser can be found in: Imageplus Operators Manual © 1982-1986 Scientific MicroPrograms 213 Merwin Road, Raleigh, NC 27606 and Practical Stereology (Russ 1985).

A data base was established containing grains representative of several morphological forms. Fossil casts and internal molds are excluded as this morphological type can have a highly varied form and are more easily distinguished by standard visual techniques. Table A1-1 lists the morphological form and number of grains for which the seven variables were calculated.

Table A1-1 Morphological groups and numbers of grains used to develop a morphology class discrimination function from image analysis data. Multiply the number of grains by seven to calculate the number of variables used in development of a discriminant function for each morphology class. The number of grains used to test the model are also shown below the morphological groups.

Morphology Class	Number of Grains
Ovoidal or Spheroidal	100
Tabular or Discoidal	50
Lobate	70
Vermicular	70
Capsule Shaped Pellets	80
Fragmentary	100
Spongy, Cauliflower, Serrulate	60

Sample Number	Number of Grains
MC10a	200
MC29	200
MC44	200

Grains are from binocular morphological slides and the following literature photo sources: Ehlmann et al. (1963); Seed (1965); Triplehorn (1966); Bell & Goodell (1967); Tapper & Fanning (1968); McRae 1972; Nelson (1973); McConchie (1978); McConchie & Lewis 1978,1980; Odin & Matter (1981); Bayliss & Syvitski (1982); Berg-Madsen (1983); Stoffers et al. (1984); Bornhold & Giresse (1985).

The variables were tabulated and investigated using canonical variate and principal component analysis techniques in the Genstat 5 Release 1.2 (VAX/VMS system version 4) statistical package. The output led to

discriminant functions and group centroids being established. These can be used to classify grains into different morphological groups. Three samples of known morphological group bias (from binocular microscope investigations) were used to test the model.

(A1-5) DIFFERENTIAL THERMAL ANALYSIS (DTA)

Use was made of a STONE DTA apparatus present in Earth Sciences, University of Waikato. Machine settings and the techniques of sample preparation are described in Lowe & Nelson (1983, p.37-43). The resultant traces were digitized into 10°C increment tables and are presented in Section D5 of the data booklet.

(A1-6) X-RAY DIFFRACTION ANALYSIS (XRD)

Samples were mounted on ground glass slides using the dropper on glass slide (DOGS) and random powder methods of preparation. A review of preparation techniques is given in McConchie (1978). Samples in the DOGS preparation category were dried in a dust-free fume cupboard using an infra-red lamp. Sample drying times were restricted to less than 20 minutes to prevent particle size segregation (Grim 1968; Austin & Leininger (1976) in McConchie 1978).

The XRD scan conditions used were:

kV	40
mA	20
chart speed	10 mm/°2θ
chart drive	10 mm/s
time constant	1.0 s
slit	0.2 mm
range	5^3 c/s.

Several literature classification schemes (e.g., Table 2-2) were used to distinguish the various types of glauconite suggested by other authors.

The possibility of a theoretical classification scheme for glauconite was investigated using a computer XRD trace generating program in Chemlib VAX/VMS4 called "Lazy Pulverix" and also structural layer charges from the "Clayform" program. To determine the mineral lattice parameters for glauconite, chemical data from ASTM file 9-439 for type mineral glauconite was used. The data was run through the "Clayform" computer program to determine the minerals lattice composition. The primary element positions within the glauconite lattice were approximated using Zviagin's (1957)

celadonite data. The site occupancy of a structural position was calculated using the Chemlib VAX/VMS 4 "Shelx" program. This information combined with the mineral lattice composition calculated from the "Clayform" program was used to calculate the true site occupancy for a mineral formula derived from chemical data. The ASTM file 13-259 for montmorillonite was used as the expandable component. Use of montmorillonite as the expandable component was based on Nelson's (1973) Te Kuiti Group XRD observations. An example calculation for type mineral glauconite and some of the generated computer data is shown in Appendix 3.

Because of difficulties calculating % expandables using literature techniques the expandable content of the glauconite was determined from chemical data based on the correlation between expandable content and potassium content. Data on % expandable content and $\%K_2O$ content was tabulated from the following literature sources: McRae & Lambert (1968); Cimbalnikova (1971); Thompson & Hower (1975); and McConchie (1978). The regression equation of a fitted line and the correlation between the two variables was calculated, the relationship found was:

$\%\text{Expandables} = -7.79 \times \%K_2O + 68.7$ **(R= -0.82)**.

(A1-7) INFRARED (IR.)

Infrared disks were prepared using the KBr preparation technique of Lowe & Nelson (1983,p.33-34). KBr disks that appeared cloudy were rejected and fresh disks made. The samples were not scanned for the full infrared spectral wavelength of 2.5 to 50μm (frequency range 4000 to 200 cm^{-1}); only the 1200 to 850 cm^{-1} Si – O vibration region was scanned. Peak position within this range was used to predict the percent expandables based on correlations made by Manghnani & Hower (1964) and McConchie (1978).

(A1-8) X-RAY FLUORESCENCE (XRF)

Crushed samples of 20g size were collected in glass vials and sent to Victoria University, Wellington for investigation using the Philips PW1404 Automatic Sequential X-Ray Spectrometer Facility. Full major and trace element analyses were made. The samples were then tested using the "clayform" mineral structure program (Bodine 1986) to establish the class of mineral glauconite dominant in the sample and to detect spurious samples (i.e., those with a high level of contamination not detected under the binocular microscope).

(A1-9) ELECTRON MICROPROBE ANALYSIS (EMP)

Samples for EMP analysis were hand picked from glauconite concentrates under the binocular microscope. The glauconite grains were mounted in epoxy resin stubs and polished using diamond pastes; the final polish was made using 2μm aluminium powder. The sample stub was wrapped in "glad-wrap" to minimise surface oxidation and stored in an empty camera-film cannister.

Analysis for the major oxides in the glauconite grains was made at Victoria University, Wellington using the Jeol JXA-733 Electron Probe X-ray Microanalyser. Probe current was set at 120×10^{-8}A with an accelerating voltage of 15kV. Samples were tested with a focused and defocused beam to see if volatisation was problematic. A slightly defocused beam was used in all the listed EMP analyses to minimise K and Na volatisation.

APPENDIX II

STRATIGRAPHIC SECTIONS AND SAMPLE LOCALITY INFORMATION

Using field data simplified stratigraphic sections were constructed, these are shown in the following pages . Grid references are given using the grid coordinate system of NZMS1 and NZMS260 series topography maps.

Some samples in this study were obtained from stored specimens at Waikato and Auckland Universities. The sample number, grid reference of collection, formation collected in the Te Kuiti Group, location of literature stratigraphic information for the sample, and the lodgement number in the relevant rock collection are listed in Table A2-1.

Some samples were obtained from the New Zealand Geological Survey (N.Z.G.S.) rock-core store at Huntly. The sample number, grid reference, drill hole number (listed on the Coal Resources Survey drillhole log forms N.Z.G.S., Ruakura Research Station, Hamilton), depth over which sample was taken, and the formation from which the sample was taken are listed in Table A2-2.

For construction of the panel diagram (map pocket) several type sections were extrapolated onto the north - south projection line. The location of these type localities on NZMS1 and NZMS260 topographical maps are listed below:

Type Section Nº	NZMS1 grid ref.	NZMS260 grid ref	Literature Source
G	N52/562082	S12/920335	Kear & Schofield (1959)
W		R13/653176	Nelson (1988) pers.com
H	N56/568664 & N56/597647-603643	S14/914953 & S14/940937-946933	Kear & Schofield (1959)
F	N55/394540-465551	R14/752844-817852	Kear & Schofield (1959)
J	N73/495083 & N73/446085-445088	R15/832424 R15/788427-787430	Kear & Schofield (1959)
K	N74/659967	S16/979313	Kear & Schofield (1959)
C58	N82/401801	R16/739168	Nelson (1977)
C191	N91/276458	R17/616858	Nelson (1977)

Abbreviation and symbol key for stratigraphic columns

Description Abbreviations

a./abund. = abundant
approx. = approximately
av./aver. = average
bioturb. = bioturbation
bndry. = boundary
calc. = calcitic
conglom. = conglomerate
cont. = content
det. = detect
devel. = development
diam. = diameter
diff. = difficult
disting. = distinguish
Elg.Lst. = Elgood Limestone
evid. = evidence
foss. = fossils
fossilif. = fossiliferous
frag./frags. = fragment/s
gen. = general
glauc. = glauconite
horiz. = horizontal
impt. = important
inc. = increases
incip. = incipient
lithol. = lithological
lst. = limestone
med. = medium
mod. = moderate
occas. = occasional
Or.Lst. = Orahiri Limestone
oyst.= oyster
pebb. = pebble
poss. = possibly
predom. = predominantly
qtz. = quartz
r. = rare
s. = some
sed./seds. = sediments
sst. = sandstone
stratig.= stratigraphy
subang. = subangular
Te.Ak. Zst. = Te Akatea Siltstone
topo. = topographic
unident. = unidentified
v. = very
veg. = vegetation
zst. = siltstone

Graphical Symbols

C - oyster shell macrofossil
F - unidentified macrofossil
ff - fragmented macrofossils
G - glauconite

- sandstone
- calcareous sandstone
- sandy siltstone
- siltstone
- limestone
- limestone incipient bedding
- undulose flaggy limestone
- conglomerate
- pebbles
- bioturbation
- iron staining

Column Number : MC3

Grid Reference : (NZMS260) R13/720204 (NZMS1)

Slope : eroded hilltop remnants Aspect : northwest

Vegetation : pasture

Relevant literature : Purser (1961)

Accessory notes : Approx. 10m below known adjacent hillside Dunphail Siltstone contact.

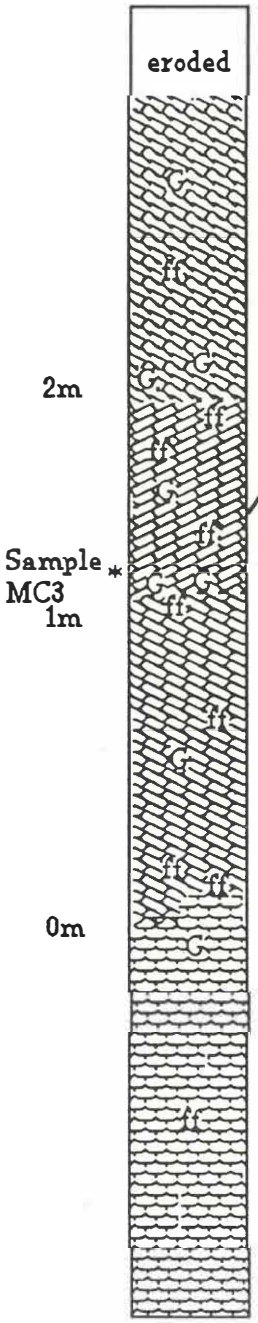

Contact - Dunphail Siltstone contact not seen in section

Elg.Lst. - Tan coloured lst., well developed undulose flags at the top of the section (5cm average width) grading downward into incipient flag development, numerous cross bedded members, highly calcitic, fine grained, average grain size fSU, composed of fragmented shell hash (average material size<0.5cm) some quartz and rare opaques present in hand specimen, moderate glauconite content appeared to increase near boundaries of cross bedded units, low porosity means this horizon often forms aquitard below Dunphail siltstone in region.

Contact - Basal contact not seen in section

Column Number : MC5

Grid Reference : (NZMS260) R13/653175 (NZMS1)

Slope : cliff face Aspect : north

Vegetation :

Relevant literature : Nelson 1988 unpublished column

Accessory notes : Region consists of bluffs of Glenn Massey Limestone overlain by AoA lst. and capped with Te.Ak. Zst.

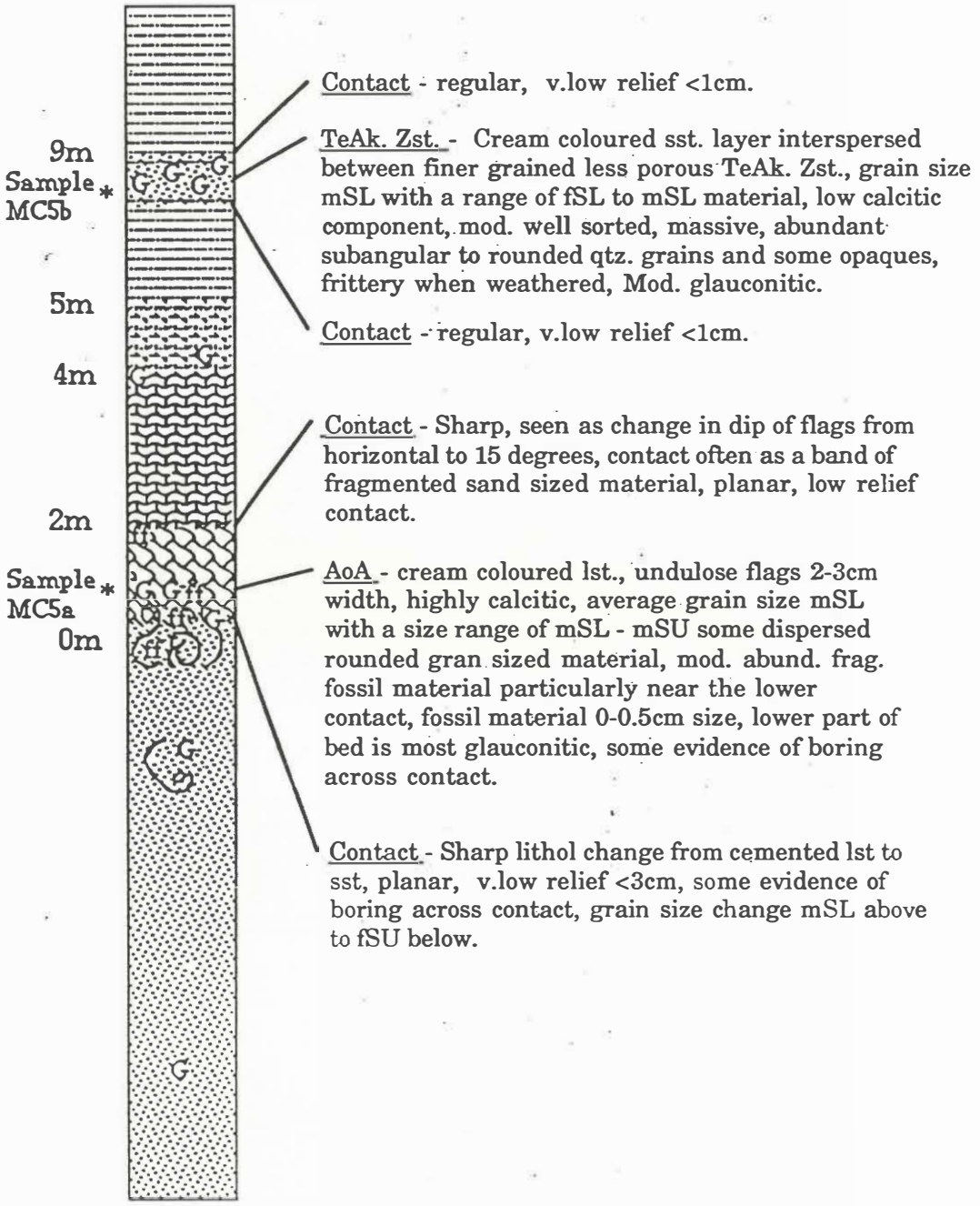

Column Number : MC6

Grid Reference : (NZMS260) R13/645177 (NZMS1)

Slope : 30° Aspect : north

Vegetation : Pasture, nearby totara forest remnant

Relevant literature :

Accessory notes : The sample is from the greensand contact betwee Elg. Lst. and Glen Massey Sst.

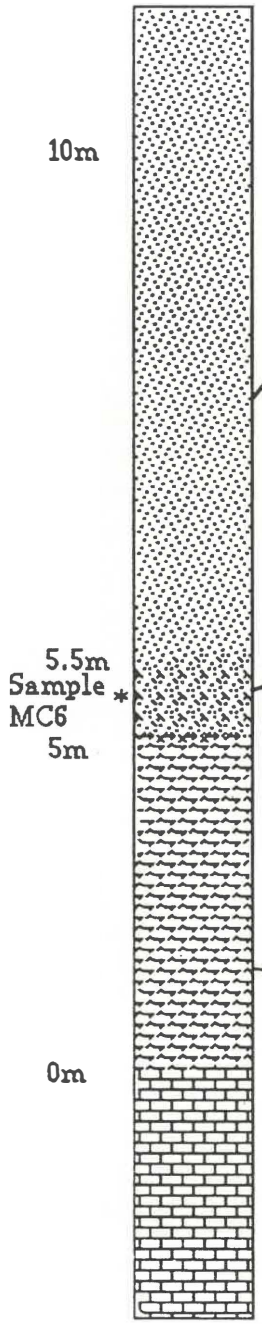

Glen Massey Sst. - cream to grey coloured sst., frittery in outcrop, massive, occas. shell frags 1cm diam. some calcitic material, abund. qtz., forms distinctive, overhanging bluffs in surrounding area, grain size fSU.

Contact - green grey sst., graditional, undulose 7cm relief contact , well sorted, med. porosity, grain size mSL average with a range of fSU to mSU, mod. - highly calcitic, highly glauconitic, massive.

Elg. Lst. - Creamy colured lst., blocky form, incip bedding near contact becomes more defined further down section, flaggy at base, abundant highly fragmented shell hash 0-0.5cm diam. material, highly calcitic with some quartz. Mod. - low glauc. cont.

Column Number : MC7

Grid Reference : (NZMS260) R13/650148 (NZMS1)

Slope : cliff section Aspect : north

Vegetation : isolated patches of adventive weeds.

Relevant Literature : Purser (1961)

Accesory notes : Elg.Lst. is highly cemented so sample was removed from near conglom. layer.

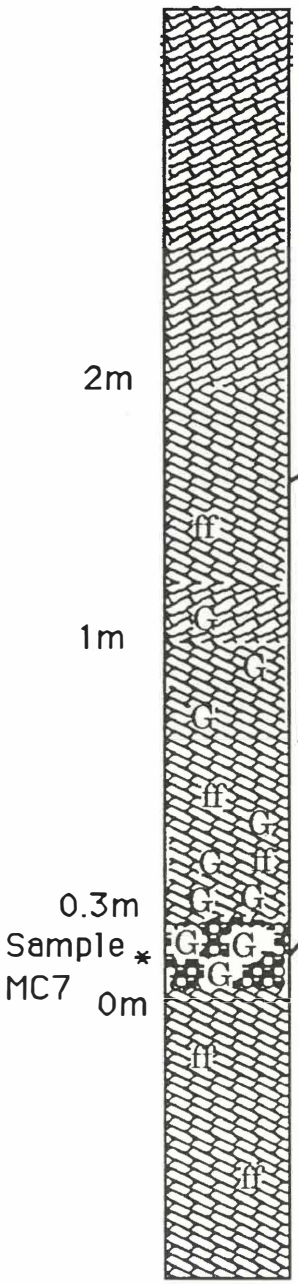

Contact - Upper contact of Elg.Lst. not seen in section.

Elg.Lst. - Creamy white coloured lst., well devel. flags 2cm width, flags become more undulose and less well devel. upward from sample, flags are often cross bedded in units approx. 1m thick, highly calcitic, average grain size mSU with a range from mSL - crsSL, predom. frag. shell material with mod. qtz. and some opaques, glauconite content inc. down column and in interflag reions, frag. shell mat. is disartic av. length 1cm, mod - low glauc cont.

Conglom. - This conglom. appears to be locally formed but is traceable in surrounding outcrop for >50m laterally, greeny tan in colour, poorly sorted, grain size average mSU with a range of fSU - crsSU, larger material is subang. to rounded in form, larg sPbl greywake material, highly calcitic, massive unsorted, highly glauc.

Contact - Basal contact of Elg.Lst. not seen in section.

Column Number : MC11

Grid Reference : (NZMS260) S14/942937 (NZMS1)

Slope : 30° Aspect : South

Vegetation : Pasture

Relevant literature : Kear & Schofield (1978)

Accessory notes : Dunphail Bluffs section

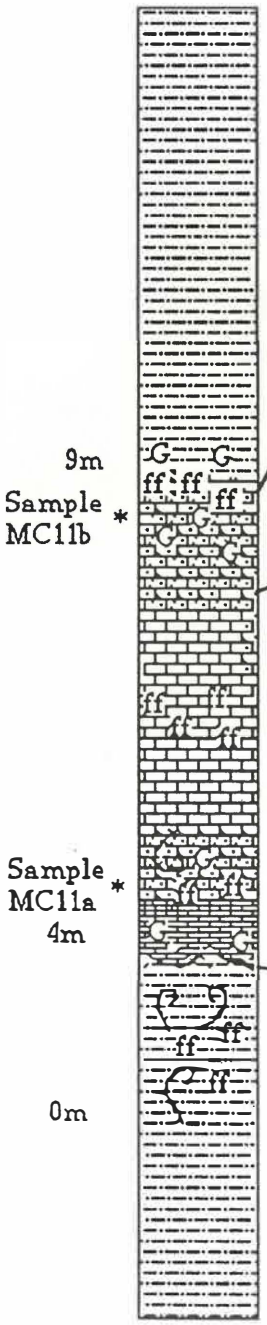

Contact - graditional contact change from fSU to mSU material, undulose regular bndry., relief 1-5cm, abund calcitic and qtz. grains some opaques., poorly exposed.

Elg.Lst. - Tan to creamy green lst., undulose flags which decrease in size from 10cm to 5cm in the central part of the bed and also at the base of the bed, highly calcitic, mean grain size mSU, low porosity, angular to subangular qtz. grains, fragmented shell hash at top of bed material becomes much more finely fragmented toward centre of bed, more non-calcitic qtz material near base and top of bed (excluding hash at very top), high glauconite content near upper and lower contacts, forms prominant weathering bluff in region.

Contact - Gradational mSU above to fSL below, irregular relief 5-7cm poorly exposed due to debri fall from overlying Dunphail Siltstone. Mod calcitic with some opaques and abund. qtz. In some areas difficult to determine if sandier contact was weathered Elg.Lst.

Column Number : MC12

Grid Reference : (NZMS260) S14/930909 (NZMS1)

Slope : 60° Aspect :

Vegetation : adventive grasses

Relevant literature : Kear & Schofield (1978)

Accessory notes : Sample taken 15cm into face to negate weathering effects.

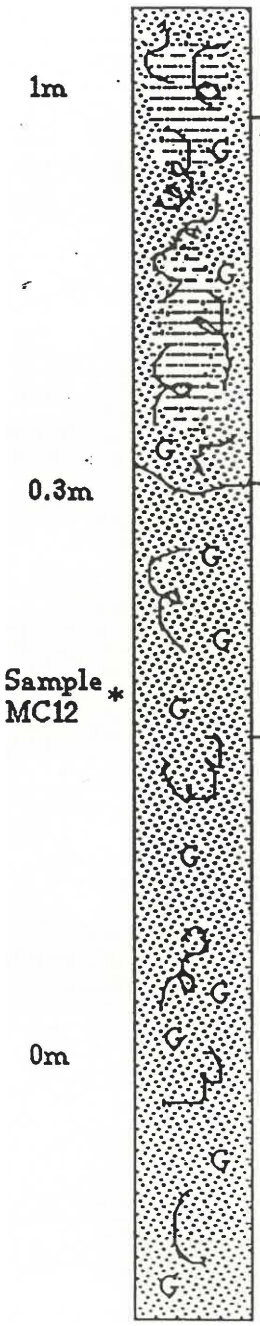

Contact - Upper contact not seen in section

Mangakotuku Siltstone - Grey coloured zst. at top of column grading to a fawn coloured zst. nearer basal contact, massive with inliers of laminated zst., fSU average grain size material, inliers of silty material, extensively bioturbated, mod. glauc. cont.

Contact - Distinct, irregular >30cm relief contact, evidenced as a rapid increase in glauc. cont.

Pukemiro Sandstone - Green grey sst., massive, fSU average grain size, less bioturb. evidence compared to overlying strata, high glauc. cont.

Contact - Lower contact not seen in section.

Column Number : MC14

Grid Reference : (NZMS260) S15/919646 (NZMS1) N65/583329

Slope : Quarry face Aspect : South

Vegetation None

Relevant literature Kear & Schofield (1978)

Accessory notes : Elgood Lst. quarry face >30m height.

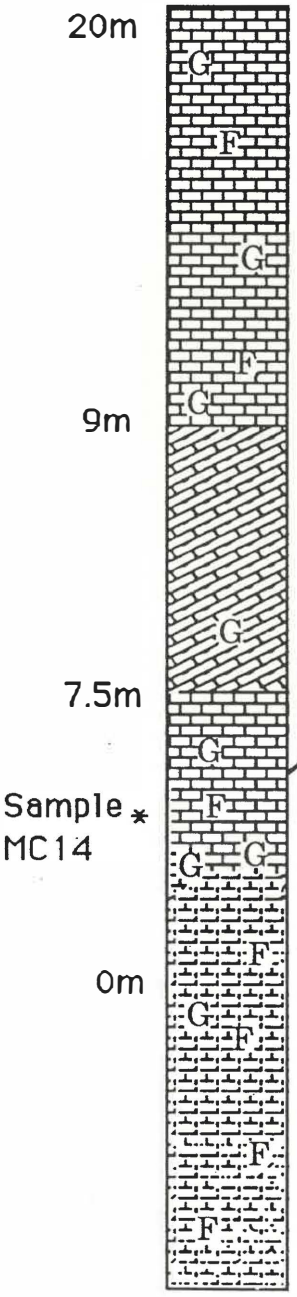

Upper Contact with Waitemata Group sed. not seen as hilltop was eroded.

Elgood Lst. - Green grey lst., incip flags at base grading upward to well devel. (5-7cm width) flags nearer cross bedded bed, cross bedded bed appears to be same lithol. as rest of column (aprox 1.5m width), mod. calcitic, mean grain size mSL (range fSU - mSU), abund. angular to subangular qtz. grains, some fragmented (2-4cm diam.) shell cast replacements probably reprecip. calc., no trace fossils evid., mod. glauc. cont.

Lower contact not seen. Noted was a decrease in flagginess towards base and a slight coarsening of sediments in some areas along quarry face.

Column Number : MC17

Grid Reference : (NZMS260)R15/744437 (NZMS1) N73/389095

Slope : 30-45° Aspect : West

Vegetation : Pasture

Relevant Literature : Nelson (1977) Ferguson (1986)

Accessory notes : Below outcrop is flaggy OrB1 cliffs (4m height)

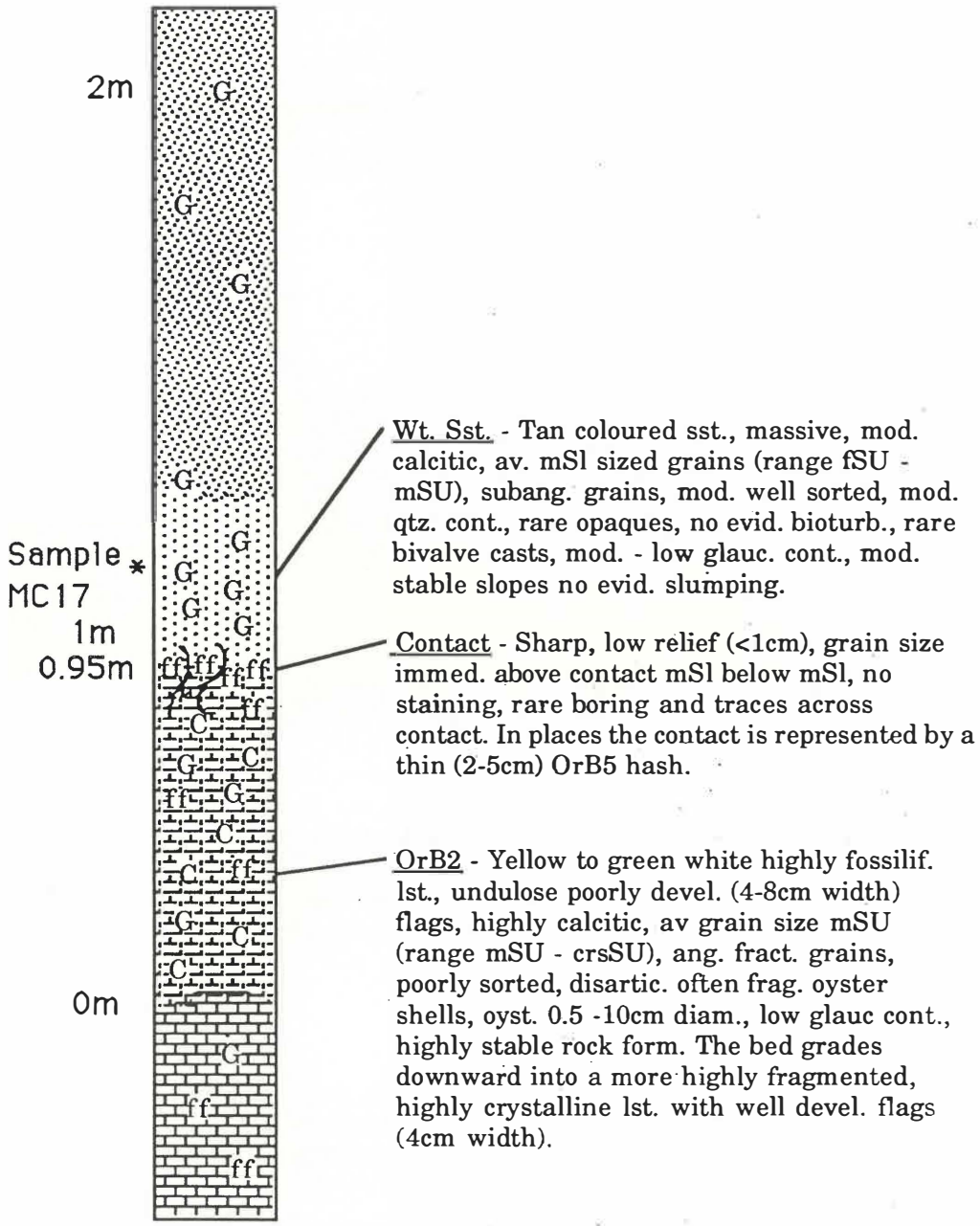

Column Number : MC.19

Grid Reference : (NZMS260) S16/974373 (NZMS1) N74/651032

Slope : 60° Aspect : northwest

Vegetation : hillslope pasture

Relevant literature : Nelson (1977) esp. C25

Accessory notes : Orahiri Lst. forms prominant bluff, base is undercut into Aotea Sst.

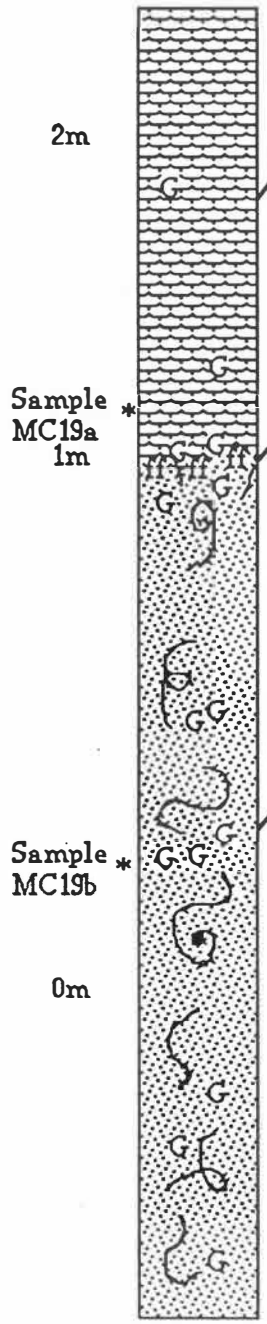

OrB1 - Grey to creamy white lst., incip. flags 5-7cm width, highly calcitic, predom. v.small fragmented calcitic material but some angular qtz. grains mSU in size, well sorted, low glauconite cont.

Contact - Mod.-sharp to graditional boundary, often undulose 5cm relief, often as afossil hash of mSU sized material, mod. well sorted materials, qtz. grains are angular, abundant unident. opaques, highly calcitic, some evidence of bioturb. across boindary, mod.- high glauc. cont., poss. eroded OrB5 bed.

Ao4 - Grey green sst., massive, mod. calcitic, very well sorted fSU sized material, abund. qtz., mod. abund. opaques, extensive bioturb. traces, mod. glauc. cont. which increases in isolated inliers within the deposit.

Column Number : MC20

Grid Reference : (NZMS260) R16/822368 (NZMS1) N73/485022

Slope : cliff face Aspect : northwest

Vegetation :

Relevant literature : Nelson (1977)

Accessory notes : Base of column is a grassed slope which is 20-30m above greywacke exposure.

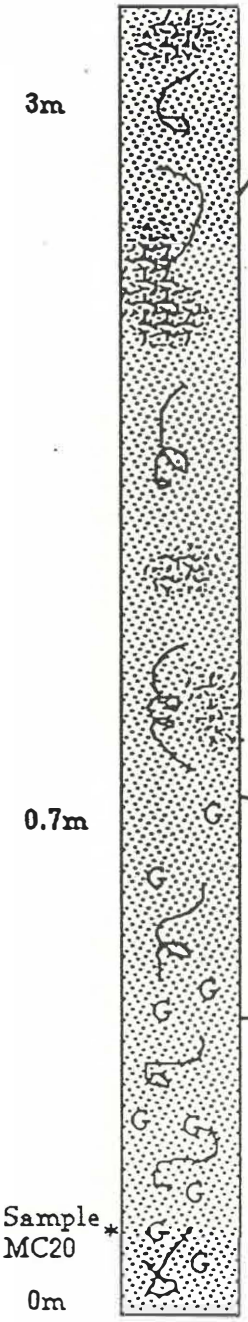

Ao3 - Green grey sst., massive sst. with some isolated regions that appear blocky when weathered, mod. calcitic, average mSU grain size, size range fSU - mSU, well sorted, predom. rounded qtz., some biotub. traces, mod.-low glauc. cont.

Contact - Gradational, diffuse contact, glauc. cont. inc. rapidly below contact.

Ao4 - Grey green sst., massive, mod. calcitic, average grain size fSU, well sorted, evid. of biotub., mod.-high glauc. cont., sheet weathers.

Contact - Lower contact not seen in section.

Column Number : MC21

Grid Reference : (NZMS260) S16/002342 (NZMS1) N74/683999

Slope : Roadcut Aspect : Northerly

Vegetation : Adventive grasses

Relevant literature : Nelson (1977, 1978a)

Accessory notes : Composite lateral column (0.5km length).

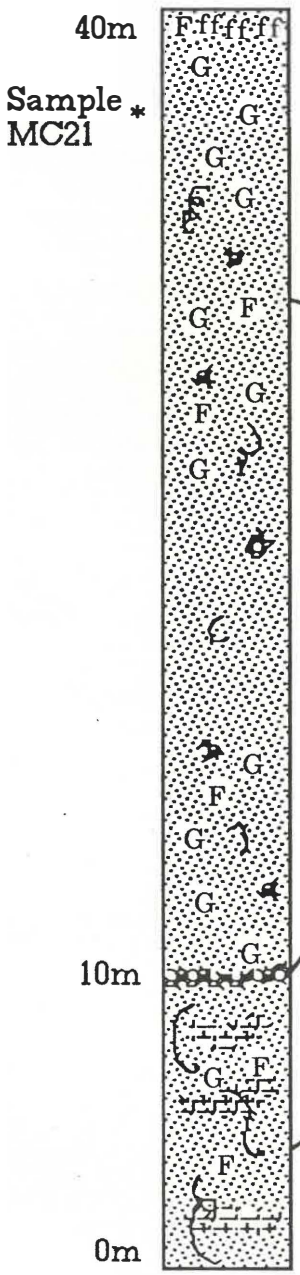

Ao4 - Grey green highly glauconitic sandstone, massive, low calcite content, average grain size mSL (range fSU - crsSL), mod. abund. qtz. subang. to rounded, occas. pebbles (0.5 - 2cm diam.), inc. in % of pebbles downward, pebbles rounded greywacke, occas. shell frags. (0.5 - 1cm diam.), occas. smal (5cm length) bioturb. traces, mod. stable outcrop face which sheet weathers, fossil hash at 40m may indicate a change in lithol int sandier less glauc. rich seds.

Contact - Inc in glauc. cont. near contact (0-10cm), low relief (1-3cm), mod. well defined as a lag gravel, probably erosion rather than storm event boundary, very little grain size change above to below contact mSl average grain size, notable absence of pebbles belo contact.

Ao3 - Grey coloured sst., incip. flag devel. (30cm width), low glauc. cont., rare fossil casts, rare bioturb. traces, average grain size mSL.

Column Number : MC23

Grid Reference : (NZMS260) R16/869335 (NZMS1) N73/538987

Slope : 80° Aspect : south

Vegetation : very little as recent slip face

Relevant literature : Nelson (1977)

Accessory notes : Farmer said coal corp had been drilling the coal seam which outcrops in valley floor approx. 10m below glauc. sample.

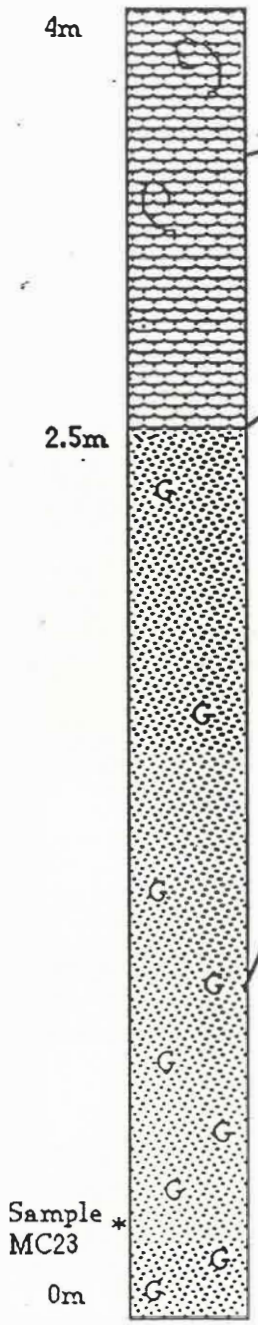

Ao3 - Creamy white calcareous sst., incip. bedding, often appears blocky, highly calcitic, fine grained fSU matrix, some inliers of fragmented shell material, some evidence of bioturb.

Contact - Sharp, regular low relief <2cm relief, decrease in calcitic content and change to massive sst. are most impt. features disting. contact, grain size increases fSU to mSU across contact.

Ao4 - Grey green sst., massive, mod. calcitic, mSU average grain size, abundant qtz., mod. abund. opaques, sheet weathers, glauc. cont. inc. downwards, abund. glauc. at base of column, mod. porous bed.

Contact - Lower contact not seen in section, however 50m to west and approx. 10m downward Waikato coal measures outcrop these are overlain by very narrow Whaigaroa Slst. (1m thickness).

Column Number : MC24

Grid Reference : (NZMS260) R16/868337 (NZMS1) N73/537989

Slope : recent slip face Aspect : southeast

Vegetation : adventive weeds

Relevant literature : Nelson (1977)

Accessory notes :

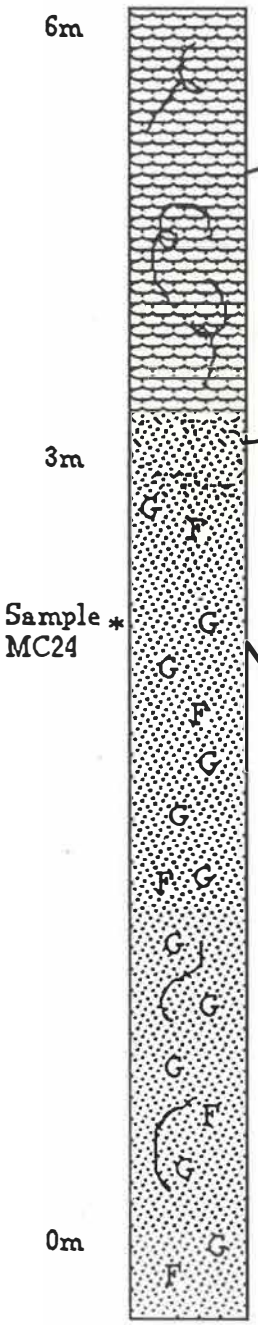

Ao3 - creamy white calcareous sst., incip. flagginess, several trace fossil markings found, fSU average grain size, difficult to access in section due to steep slopes.

Contact - Gradational diffuse contact, regular with small relief, contact visible as change from low glauc cont. above to high glauc. cont. below, grain size increases across the contact from fSU to mSU, some inliers of unidentified fine pinky coloured material.

Ao4 - Green grey sst., mod.-highly calcitic, well cemented sst., massive, mSU average grain size, size range mSU - crsSL, numerous fossil bivalve shell casts casts appear disarticulate but predom. not frag., highly glauc., sheet weathers.

Column Number : MC25

Grid Reference : (NZMS260) R16/686319 (NZMS1) N73/338964

Slope : 70° Aspect : East

Vegetation :

Relevant literature : Nelson (1977)

Accessory notes : Contact between WhA and Wh2 contact form is unusual due to high sand content

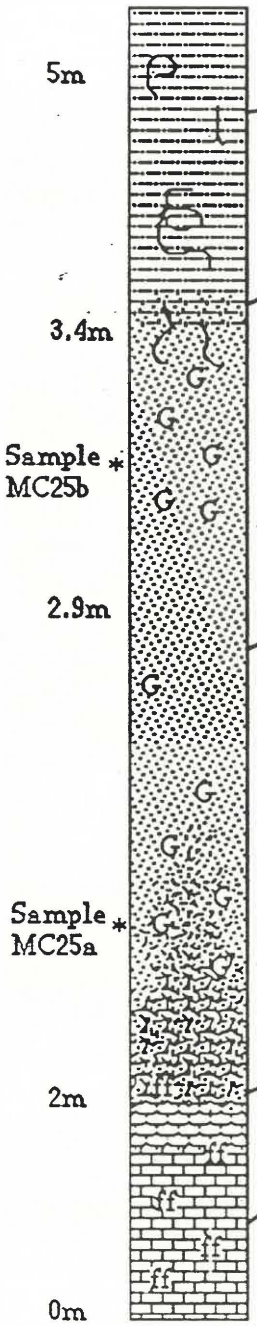

Wh2 - Grey frittery zst., massive, some evid. of bioturb., low glauc. cont.

Contact - Gradational bndry, seen in outcrop as change from frittery to massive deposit, grain size increases across bndry mSL below too small to det. above., some biotub. across bndry.

Wh2 - Grey green sandy zst., massive in gen. some areas of incip. bedding poorly defined, grain size average mSL, mod. sorted, mod. calcitic, mod.- low glauc. cont., gradational change downward to fawn coloured sandy zst., sparse fragmented calcitic material, graditional change from massive to hummocky stratification downward, mod. sorted., mod. glauc cont.

Contact - gradational, change from lst. to sandy zst., bedding becomes more defined

WhA - creamy white lst., highly crystalline, highly calcitic, large crsSL shell frags. domin. deposit, low glauc. cont., often fluted where weathered

Contact - Lower contact not seen

Column Number : MC26

Grid Reference : (NZMS260) S16/962296 (NZMS1) N74/641947

Slope : 50° Aspect : southwest

Vegetation : moss and lichen covered, surrounding hill pasture

Relevant literature : Nelson (1977) esp. C32

Accessory notes : Small stream in valley floor sumps around 50m east of sample locality.

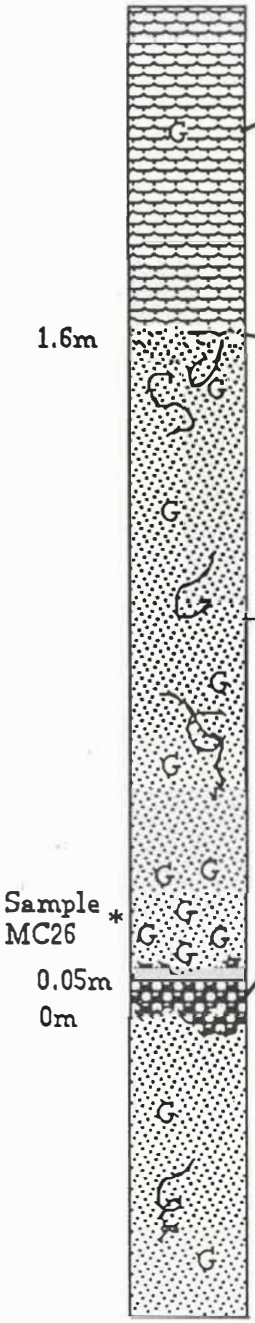

OrB1 - creamy white lst. with occas. dark green glauc. grains, incip. bedding, orange colouration when weathered, highly calcitic, low glauc. cont.

Contact - Gradational, appears irregular but diff. to disting. often veg. covered, occas. as fossil hash which is mod. cemented with mod. abund. gran sized pebbles, often iron stained, low glauc. cont.

Ao4 - Grey green sst., massive, mod. calcitic, grain size average mSL, predom. subang. qtz. grains, some opaques, weathers as sheets, well sorted., occas. trace fossils gen. increase in intensity of bioturb up bed, top of bed has a low glauc content which increases downward.

Conglom. - this bed does not appear to be a basal contact as the bed above and below is identical in description. Massive deposit, undulose, predom. gran sized material, some fossil hash preserved near base of deposit, matrix grain size mSL, rounded pebbles crsSU - sPbl, shell frags sPbl - sCbl. Glauc. content could not be det. as iron oxidation of pebbles appeared in ferrous state.

Contact - Lower contact not observed.

Column Number : MC28

Grid Reference : (NZMS260) S16/959292 (NZMS1) N74/637943

Slope : Undercut bluff Aspect : south

Vegetation

Relevant literature : Nelson (1977) esp. C32

Accessory notes : Concentrated greensand band above Aotea Sst which is undercut below Orahiri Lst.

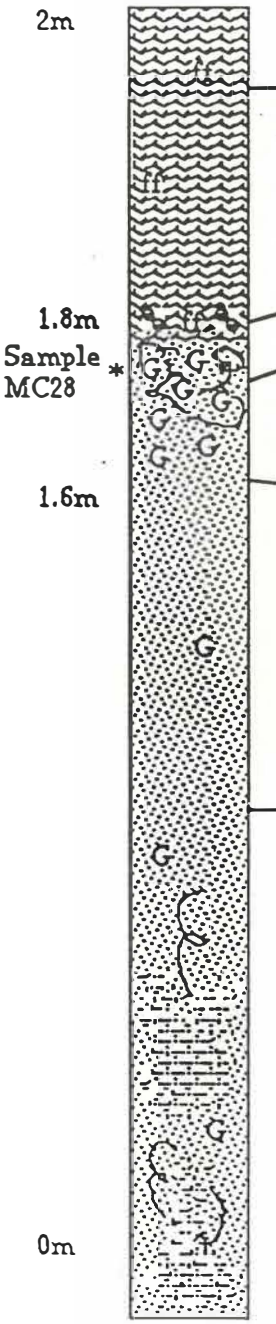

Contact - Upper contact not seen in section

OrB1 - Greeny grey to creamy grey lst., mod. - incip. flag devel., fSU - mSU size range material, occas. pebbles near base, occas. frag. shell material, low glauc. cont.

Contact - Distinct, slighty undulose 5-10cm relief.

Ao4 - Dark green sst., massive, mod. well sorted, inliers of cemented pinkish clasts, extensive biotub. at top of bed, low calcite cont., highly glauc.

Contact - Gradational contact over 15cm, regular low relief.

Ao2 - Creamy white sst. at top grading into a grey sst. nearer base, massive, mod. sorted, average grain size fSU, mod. calcitic, occas. bioturb. traces becoming more common at base of bed, mod. glauc. cont., bed becomes finer grained at base.

Contact - Lower contact not seen in section

Column Number : MC29

Grid Reference : (NZMS260) R16/735262 (NZMS1) N73/393903

Slope : roadcut Aspect :

Vegetation : surrounded by pasture

Relevant literature : Nelson (1977)

Accessory notes :

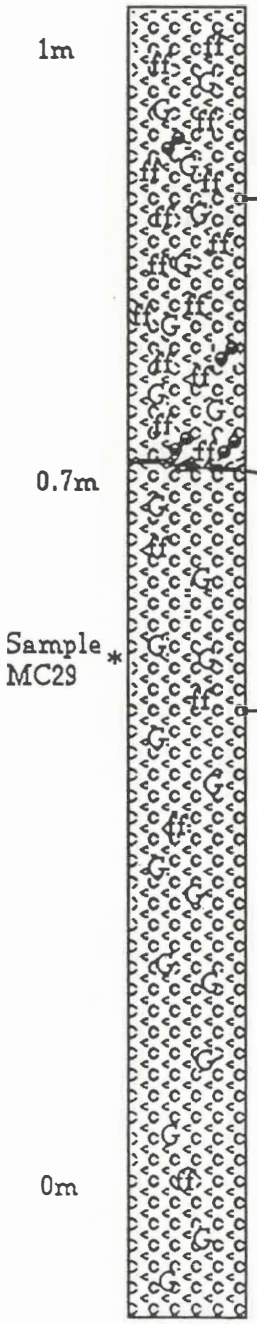

Contact - Upper contact not seen in section

OrB2 - Grey green lst., highly fragmented fossil hash, occass. gran sized rounded greywacke pebbles near basal contact, highly calcitic, high glauc. cont.

Contact - Distict, irregular undulose >10cm relief on boundary

OrB2 - Grey green lst, green grey matrix of fragmented material with large 10cm isolated cream white oyster shells, unbedded although oyster shells are predom. concave upward giving pseudo-bedding, highly calcitic, fSU matrix, high glauc. cont.

Contact - Lower contact not seen in section

Column Number : MC30

Grid Reference : (NZMS260) R16/763249 (NZMS1) N82/424890

Slope : roadcut Aspect : west

Vegetation : pasture

Relevant literature : Nelson (1977)

Accessory notes : Sample MC30 is a composite of two drill samples. Both samples were combined as they were from same stratig. horiz.

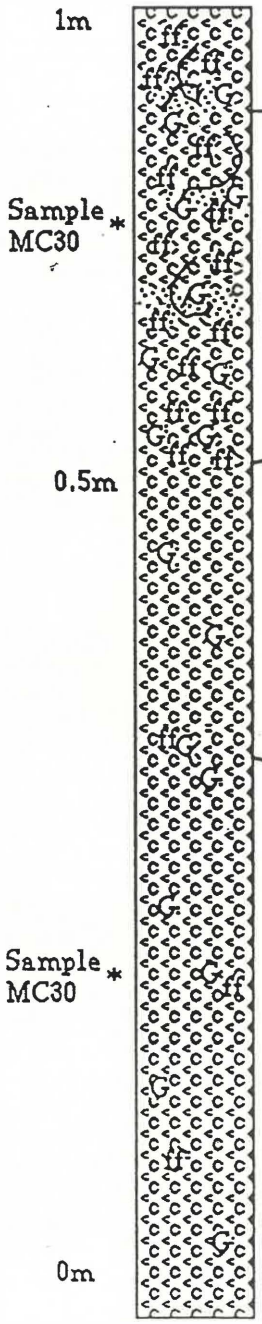

Contact - Upper contact not seen in section

OrB2 - Green grey lst., highly frag. fossilif. hash., non-bedded, inliers of sandier less calc. material, fSU rounded qtz. grains, frag. hash material 0.1 - 0.5 cm length, some evid. of biotub., mod.- high glauc. cont.

Contact - Sharp distinct contact, distinctive change from highly frag. fossil hash above to whole intact shell tests below.

OrB2 - Green grey lst., dominated by indiv. oyster shells up to 12cm long and 2cm thick, oyster shells are disartic., no bedding evident but oyster shells appear predom. concave upward which gives deposit a pseudo-bedded appearance, poorly sorted matrix comprised of frag. shell remains and subangular qtz. grains., mod.- low glauc. cont.

Contact - Lower contact not seen in section

Column Number : MC31

Grid Reference : (NZMS260) R16/787234 (NZMS1) N82/451874

Slope : roadcut Aspect : west

Vegetation :

Relevant literature : Nelson (1977)

Accessory notes : This roadcut outcrop was very fresh probably only 1-2 days old exposure.

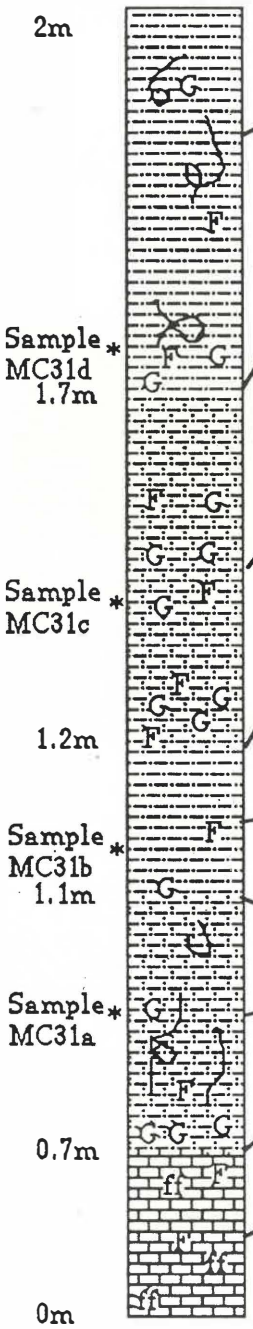

Contact - Upper contact not seen in section

1 Wh2 - Blue grey zst., fine grained, massive, mod. calcitic, occ. bioturb. traces, glauc cont. increases towards base, glauc. cont. low overall, frittery when weathered.

2 Contact - Intraformational change from v.fine grained material above to fSU average grain size material below, sharp distinct contact, low relief <2cm.

3 Wh2 - Tan sandy zst., fSU average grain size, often appears blocky, mod. calcitic, mod.- low glauc. cont. increases near base.

Contact - Intraformational colour change of deposit from tan above to blue grey below, also appears to be a decrease in average grain size below, often contact as iron stained layer, mod. relief 2-3cm bndry, distinct.

Wh2 - same description as blue grey zst. Nº 1 at top of column but no evidence of bioturb., glauc. cont. low throughout.

Contact - Same description as contact Nº 2

Wh2 - same description as Nº 3, except some evid. of biotub.

Contact - Distinct, irregular, mod. relief 0 - 5cm, rapid increase in calcite cont. of seds.

WhA - cream white lst., highly crystalline, well devel flags 1cm width near contact becoming incip. near base of column, low glauc. cont.

Column Number : MC32

Grid Reference : (NZMS260) R16/862224 (NZMS1) N82/534865

Slope : vertical roadcut Aspect : east

Vegetation : Nearby farm pasture and adventive roadside species.

Relevant literature : Nelson (1977, 1978a)

Accessory notes : The local area is dominated by OrB1 outcrops.

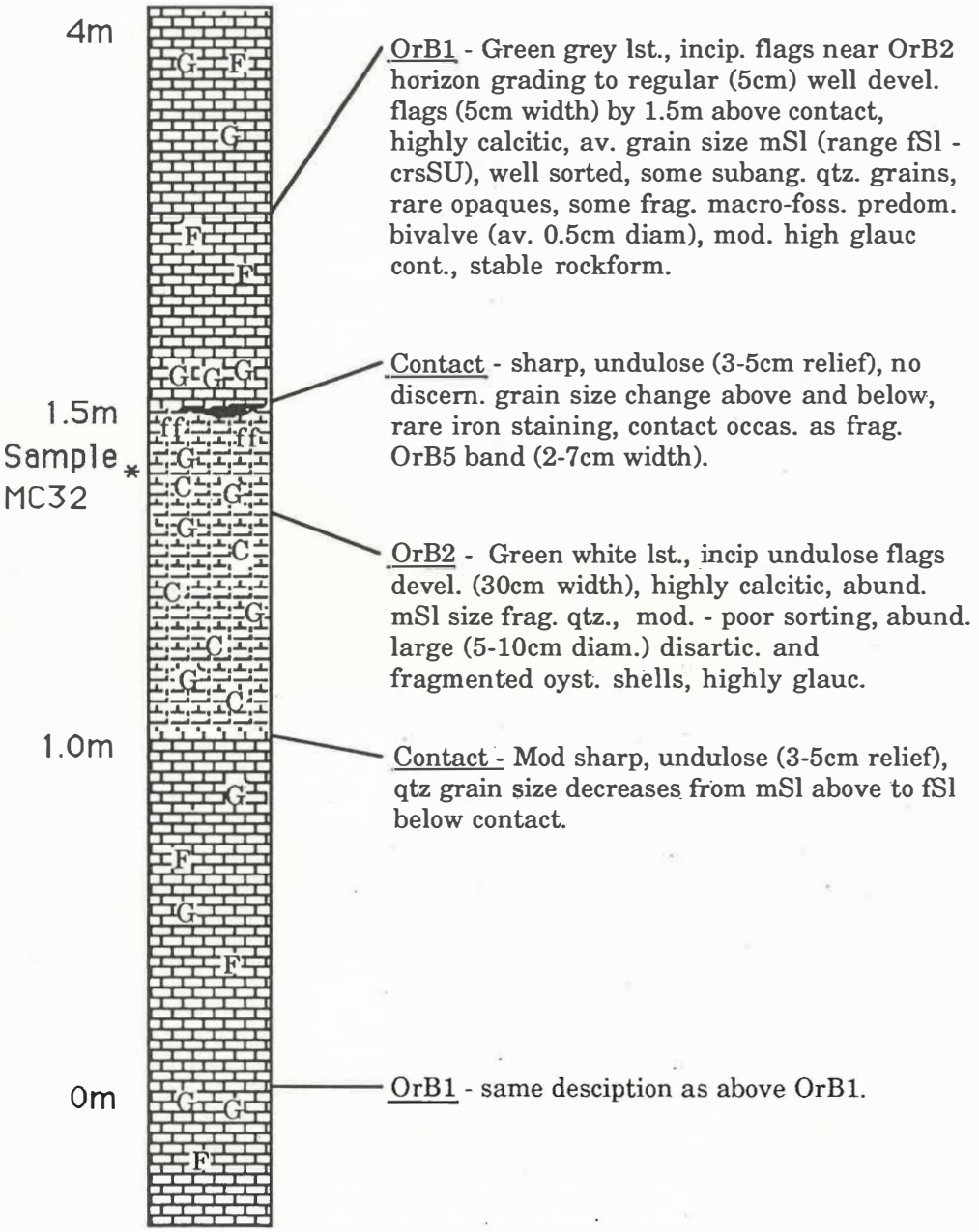

Column Number : MC35

Grid Reference : (NZMS260) R16/817140 (NZMS1) N82/487772

Slope : Aspect :

Vegetation : Adventive grasses.

Relevant literature : Nelson (1977) esp. C69.

Accessory notes : Exposed bank of material on wall of tomo.

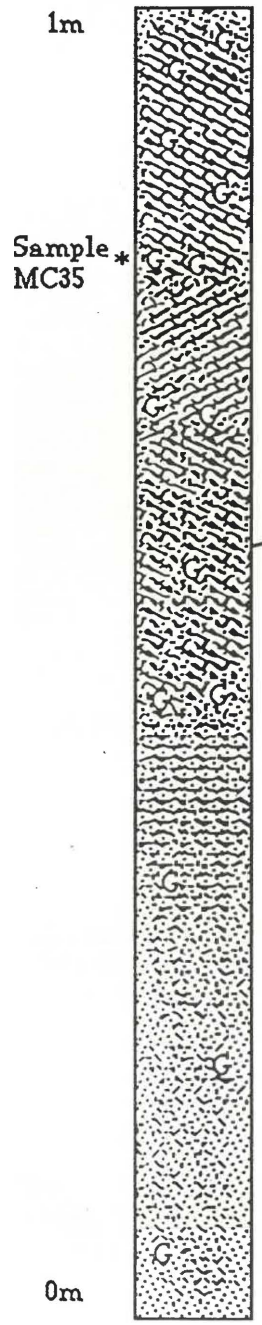

Contact - Upper contact not seen in section

AoA - Tan grey calcareous sst., incip. flag devel., flag surfaces are unduluse and often cross bedded in variable thickness 5-20cm units, flagginess more developed toward top of section, coarse grained mSL average grain size material, mod. glauc.

Contact - Lower contact not seen in section

Column Number : MC36

Grid Reference : (NZMS260) R16/806126 (NZMS1) N82/475757

Slope : Undercut bank Aspect : northwest

Vegetation :

Relevant literature : Nelson (1977) esp. C99

Accessory notes : Numerous phreatic tubes are present in this horizon.

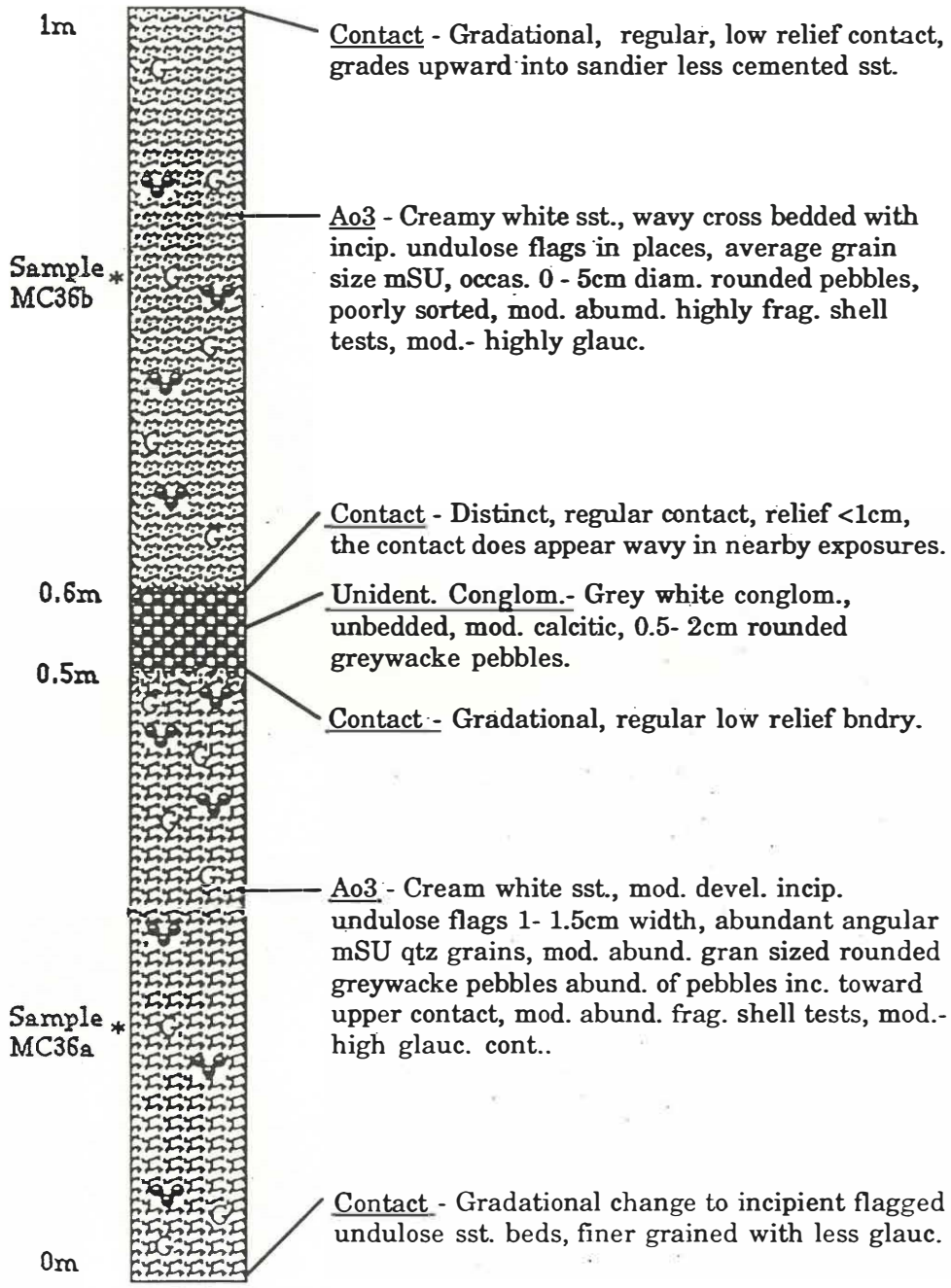

Column Number : MC38

Grid Reference : (NZMS260) R16/802122 (NZMS1) N82/471752

Slope : stream bank Aspect :

Vegetation : surrounded by pasture

Relevant literature : Nelson (1977)

Accessory notes :

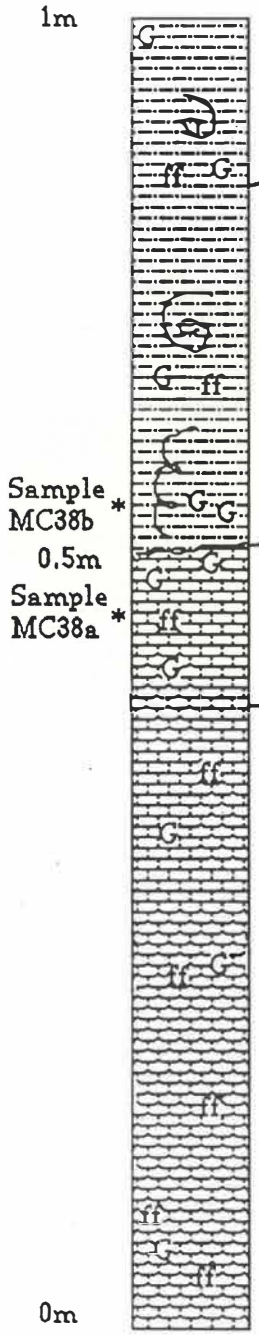

Wh2 - Blue grey zst., mod. calcitic, massive, mod.- poorly sorted, highly variable grain size fSU - gran range, abund. frag. shell material, some evid. of bioturb., matrix material is very small, larger grains are predom. subang. qtz., abund. unident. opaques, mod. glauc. cont., frittery when weathered.

Contact - Distinct, undulose 2-3cm relief bndry, often as an oxidised weathering front.

WhA - Blue grey lst., bedding v. poorly devel., highly calcitic, abund. frag. shell material, lst. material is better sorted than overlying zst., inc. in glauc content upward, mod. - low glauc. cont.

Contact - Basal contact not seen in section

180 Column Number : MC40

Grid Reference : (NZMS260) R17/762961 (NZMS1) N91/432575

Slope : roadcut Aspect : east

Vegetation : scrub ferns, adventive grasses

Relevant literature : Nelson (1977) esp. C166

Accessory notes : Below section is Ao. sst. (not seen), section grades into highly calcitic very well devel. flagginess OrA lst.

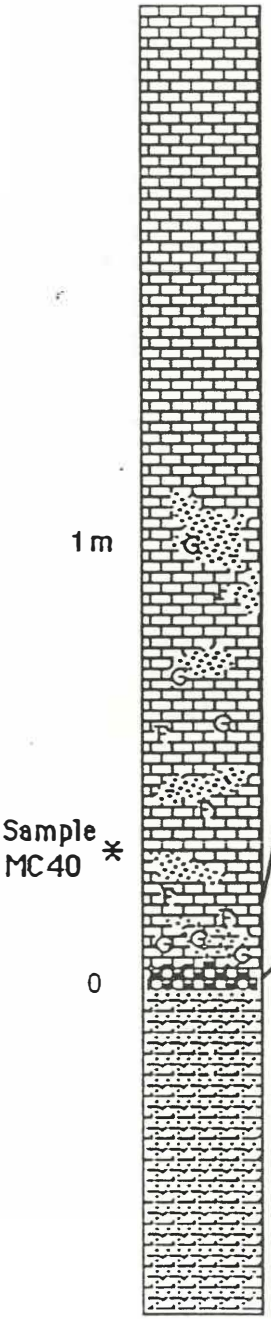

Contact - Not seen at outcrop but a graditional increase in calcite content and an increase in flagginess of surrounding outcrops of Or.Lst. suggests OrA dominates local stratig. to eroded hilltops.

OrA2 - Grey green Lst., incip. to mod. bedding becoming increasingly flaggy upward in column, mod. calcitic, average grain size mSU with a wide range from mSL to crsSL, often larger gran sized glauconitic pebbles scattered in substrate., sand sized grains subangular qtz., inliers of sandier material, fine fossil hash scattered near base of column 1cm av. length frags., highly glauconitic particularly nearer contact at base

Contact - Sharp, low relief 1-3cm, contact as a lag conglomerate of rounded greywacke material gran to mPbl size, contact material is calcitic probably secondary solution infilling, abundant quartz grains.

Column Number : MC41

Grid Reference : (NZMS260) R17/748936 (NZMS1) N91/418547

Slope : 5° Aspect : valley floor

Vegetation : farmland

Relevant literature : Nelson (1977) esp. C166

Accessory notes : Isolated exposure in valley floor OrB2 enables stratig. positioning.

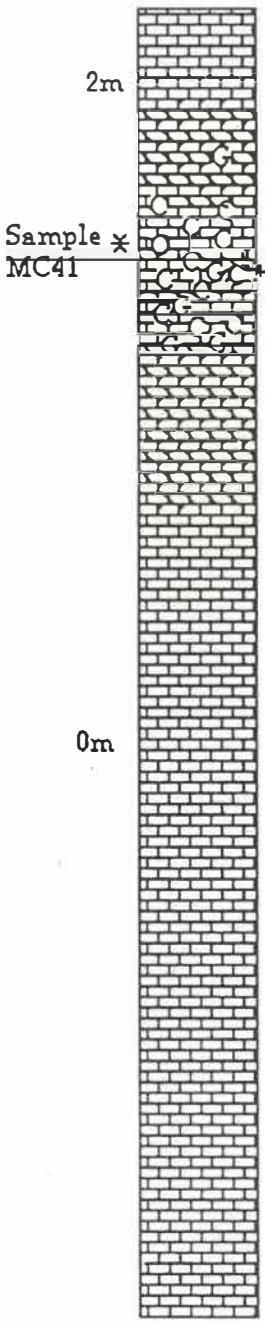

Contact - not seen in outcrop

OrB2 - Grey green matrix with cream white oyster shell fossil remains, Lst., mod. well devel. flags 3-5cm becomes more flaggy nearer column base., undulose flags, highly calcitic, grain size of matrix mSl aver. with a range of fSL - crsSL, poorly sorted, predom. ang. frags. of calcitic material with some qtz. and rare opaques, numerous fossil oyster shells as large average 5cm range 2-10cm macro fossil component, often oyster shells are intact and some appear to orientate along the flag surfaces, exposed surfaces are often fluted, mod. glauc. cont., forms a stable cemented exposure in nearby regions this site chosen for sampling as it appeared to be the most glauconitic in region.

Contact - Not seen in outcrop.

Column Number : MC43

Grid Reference : (NZMS260) R17/759911 (NZMS1) N91/431520

Slope : 40° Aspect : West

Vegetation : Farmland, willow covered riverbank and gorse.

Relevant literature : Nelson (1977) esp. C182

Accessory notes : In cliffs on east of Mokau River 0.5km upstream from bridge.

Contact - Unseen in column.

OrB2 - Creamy coloured limestone, incip. undulose flags approx 4cm width, flagginess becomes more prominant near base of column, highly calcitic, average grain size fSU, range of grain size fSU - mSU, moderately well sorted, med. porosity, abundant angular fractured calcitic grains and angular quartz grains common, often fluted in exposed outcrop, abundant disarticulate oyster shells often fragmented, average oyster frag. 7cm length with a large range of 1-15cm, low glauconite content overall but quite concentrated in the matrix surrounding the fragmented oyster material, forms stable cemented bluffs bordering Mokau River.

Contact - sharp change from oyster rich horizon into highly fragmented calcitic material, relief of 5cm on lithol. boundary change, flagginess is predomin. incipient untill the second oyster horizon is passed and then flagginess becomes better developed.

Column Number : MC45

Grid Reference : (NZMS260) R17/525817 (NZMS1) N91/178410

Slope : vertical outcrop face Aspect : north

Vegetation : adventive grasses

Relevant literature : Nelson (1977)

Accessory notes : Bexley tunnel section eastern cliff face

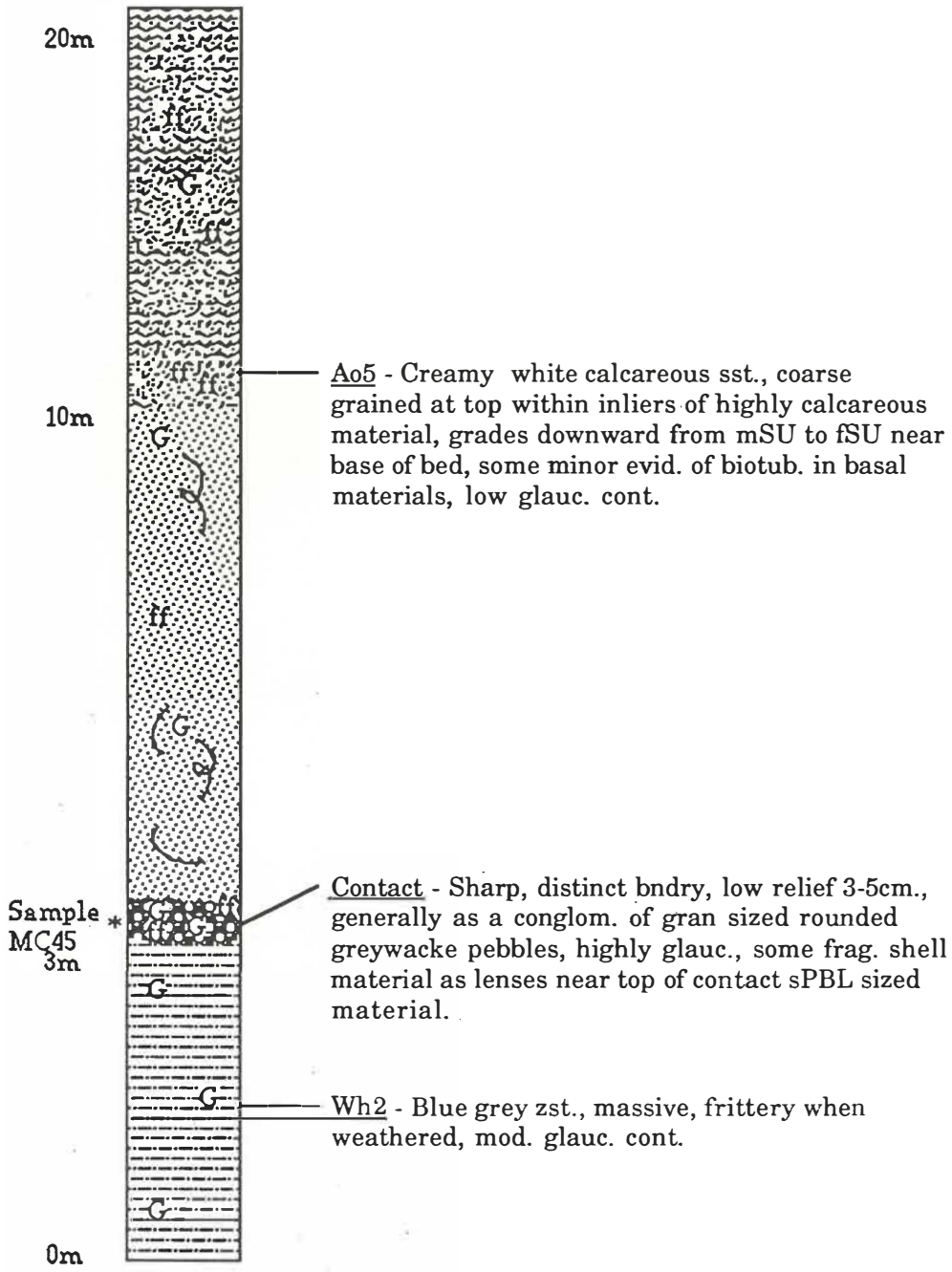

Table A2-1 Hand specimens of glauconitic Te Kuiti Group sediments collected by other authors and used in this study.

Sample	NZMS1	NZMS260	Formation †	Source	Rock Store Nº *
MC10c		S13/975087	Pukemiro Sst.	Harris (1986)	WT25137 & WT25138
MC13	N55/383605	R14/744904	Waitetuna Lst. (AoA)	Harris (1986)	WT25239
MC15		R16/763397	Waitetuna Lst. (AoA)	Fergusson (1986)	WU23962
MC16		R15/815453	Aotea Sst. (Ao4)	Fergusson (1986)	WU23975 & WU23977
MC18		R15/787425	Aotea Sst. (Ao5)	Fergusson (1986)	WU24104
MC22		R16/755379	Orahiri Lst. (OrB1)	Fergusson (1986)	WU24068 &WU24069
MC27a	N74/642943	S16/963292	Waitetuna Lst. (AoA)	Nelson (1973,1977)	AK16056
MC27b	N74/642943	S16/963292	Aotea Sst. (Ao4)	Nelson (1973,1977)	AK16060
MC27c		S16/962292-961294	Orahiri Lst. (OrA2)	Harris (1986)	WT25173
MC27d		S16/962292-961294	Waitomo Sst.(Wt)	Harris (1986)	WT25176
MC27e	N74/642943-640945	S16/963292-961294	Waitomo Sst. (Wt)	Nelson (1973,1977)	AK16076
MC33	N82/333825-339838	R16/678192-684204	Whaingaroa Zst. (Wh2)	Nelson (1973,1977)	AK16243
MC37	N83/718768	S16/028130	Orahiri Lst. (OrA2)	Nelson (1973,1977)	AK16812
MC42	N91/363528	R17/698920	Orahiri Lst. (OrB2)	Nelson (1973,1977)	AK16888

† - Abbreviated formation, member, and bed information follows convention of Nelson (1977)

* - WT & WU prefix samples held in Earth Sciences Rock Store, University of Waikato
AK prefix samples held in Petrology Collection, Department of Geology, University of Auckland.

Table A2-2 Drill hole samples as drill washings or core samples. Drill hole numbers are those of the Waikato Coal Resource Survey; forms lodged at the N.Z. Geological Survey, Ruakura, Hamilton.

Sample	NZMS1	NZMS260	Drill Hole Nº	Sampled Depth (m)†	Sampled Unit
MC1a	N51/460017	R13/825278	8374	452.69 - 466.43	Pukemiro Sst.
MC1b	N51/460017	R13/825278	8374	346.00 - 354.30	Elgood Lst.
MC1c	N51/460017	R13/825278	8374	5.25 - 10.25	Te Akatea Zst.
MC1d	N51/460017	R13/825278	8374	10.25 - 13.80	Aotea Sst.
MC2a	N51/452949	R13/816216	8383	378.20 - 392.84	Pukemiro Sst.
MC2b	N51/452949	R13/816216	8383	292.08 - 378.20	Mangakotuku Zst.
MC2c	N51/452949	R13/816216	8383	255.44 - 273.76	Elgood Lst.
MC2d	N51/452949	R13/816216	8383	31.60 - 85.98	Whaingaroa Zst.
MC4a	N52/588950	S13/940214	8111	744 - 748	Pukemiro Sst.
MC4b	N52/588950	S13/940214	8111	577.00 - 623.5	Elgood Lst.
MC8a	N51/525868	R13/880140	8395	363.15 - 372.33	Pukemiro Sst.
MC8b	N51/525868	R13/880140	8395	257.57 - 280.53	Mangakotuku Zst.
MC8c	N51/525868	R13/880140	8395	252.98 - 257.57	Elgood Lst.
MC9a	N52/602827	S13/949101	8239	357.81 - 363.90	Mangakotuku Zst.
MC9b	N52/602827	S13/949101	8239	266.46 - 303.0	Elgood Lst.
MC10a*		S13/975087	7153	1.58 - 61.77	Whaingaroa Zst.
MC10b*		S13/975087	7153	162.28 - 167.16	Pukemiro Sst.

† - Represents the depth below drill hole collar in metres.

* - Solid core samples (all other samples are as drill-washings)

APPENDIX III

DERIVATION OF A THEORETICAL XRD TRACE FOR ASTM 9-439 FILE LISTING OF A TYPE MINERAL GLAUCONITE.

(A3-1) CALCULATION OF SITE LOCATION AND OCCUPANCY

Fractional crystal coordinates for celadonite were input into the Chemlib VAX/VMS4 "Shellx" program.

IN DATA-

Title Glauconite

Cell 0.7107 5.234 9.066 10.16 90.0 100.5 90.0

Symmetry -X Y -Z (This indicates a monoclinic C2/m symmetry group)

1 O1 1 -0.340 0.212 0.337

↓

20 O7 1 0.375 0.330 0.121

QUT DATA-

	Atom	X/A	X/B	X/C	S.O.F. (Site occupancy factor)
1	O1	-0.340	0.212	0.337	1.00
2	O2	-0.125	0.170	0.121	1.00
3	Si1	-0.067	0.167	0.291	1.00
4	HO1	-0.121	0.500	0.123	0.50
5	K1	0.000	0.500	0.500	0.25
6	Fe1	0.000	0.328	0.000	0.50
7	O3	0.000	0.000	0.337	0.50
8	Mg1	0.000	0.000	0.000	0.25

Atom positions 9 to 20 can be generated from these data points by symmetry transformations.

Using the above results the type mineral for glauconite is:

$K_{0.25}Mg_{0.25}Fe_{0.5}Si_1O_{2.5}OH_{0.5}$ or as the standard mica representation $KMgFe_2Si_4O_{10}(OH)_2$

(A3-2) USE OF SITE OCCUPANCY AND MINERAL FORMULA TO DETERMINE LATTICE FORM.

Chemical composition data for ASTM 9-439 mineral glauconite and the relevant lattice parameters were input into the VAX/VMS4 "Clayform" program

OUT DATA-

ASTM 9-439 glauconite type mineral glauconite

CLAY-MINERAL STRUCTURAL FORMULA
CHEMICAL ANALYSIS 2:1 layer clay (mica type)

Oxygen equivalents per formula unit = 11

	weight %	mole %		Site Occupancies	
			Tetrahedral	Si	3.86624
SiO_2	53.5900	69.4831		Al	0.13376
TiO_2	0.1500	0.1463		Total	4.00000
Al_2O_3	8.9000	6.8000			
Fe_2O_3	15.1200	7.3761	Octahedral	Al	0.62299
FeO	3.2000	3.4698		Fe^{3+}	0.82085
MgO	3.3700	6.5138		Fe^{2+}	0.19307
CaO	0.0600	0.0833		Mg	0.36245
Na_2O	0.2100	0.2640		Total	1.99936
K_2O	7.0900	5.8637			
			Interlayer	Ca	0.00464
Total	91.6900	100.0000		Na	0.02937
				K	0.65254
				Total	0.68656

Tetrahedral layer charge = -0.13376
Octahedral layer charge = -0.55744
Interlayer cation charge = 0.69119

---

1. Components deleted from strucutral formula: TiO_2
2. Number of tetrahedral sites per formula set at 4.
3. Cation site assignments: Standard clay-mineral default.

The calculated occupancy mineral formula is of the form $O_{10}(OH)_2$. To convert to the format used in the theoretical XRD programme VAX/VMS "Lazy Pulverix" divide the site occupancies by 4.

Note - Substitutions in the same lattice position are allowed provided the total site occupancy does not exceed the site occupancy calculated in A3-1.

The above mineral formula can be written as an occupancy formula of the form:

$$(Na_{0.01}K_{0.16}) (Mg_{0.09}) (Al_{0.16}Fe^{3+}_{0.21}Fe^{2+}_{0.05}) (Si_{0.97}Al_{0.03}) O_{2.5} (OH)_{0.5}$$

(A3-3) INPUT OF THE CALCULATED MINERAL LATTICE POSITIONS AND OCCUPANCY INTO CHEMLIB VAX/VMS "LAZY PULVERIX".

IN DATA-

TITLE ASTM 9-439 GLAUCONITE
CELL a=5.234 b=9.066 c=10.16 100.5
SPCGRP C2/M

	Element	X/A	Y/B	Z/C	S.O.F.
ATOM	O	-0.340	0.212	0.337	1.0
ATOM	O	-0.125	0.17	0.121	1.0
ATOM	SI	-0.067	0.167	0.291	0.97
ATOM	AL	-0.067	0.167	0.291	0.03
ATOM	HO	-0.121	0.5	0.123	0.5
ATOM	K	0.0	0.5	0.5	0.16
ATOM	FE	0.0	0.328	0.0	0.26
ATOM	AL	0.0	0.328	0.0	0.16
ATOM	O	0.0	0.0	0.337	0.5
ATOM	MG	0.0	0.0	0.0	0.09

OUT DATA-

INTENSITY CALCULATION FOR ASTM 9-439 GLAUCONITE

MONOCLINIC STRUCTURE
A= 5.23400
B= 9.06600
C= 10.16000
BETA=100.50000
WL= 1.54180

CALCULATION BETWEEN TL = 1.0 AND TH = 25.0 DEGREES THETA

EQUIVALENT POINT POSITIONS

X , Y , Z -X , -Y , -Z +(0 0 0 , $\frac{1}{2}\frac{1}{2}$ 0)
-X , Y ,-Z X , -Y , Z +(0 0 0 , $\frac{1}{2}\frac{1}{2}$ 0)

THERE IS A SYMMETRY CENTRE AT THE ORIGIN

C -CENTRED BRAVAIS LATTICE

CONDITIONS LIMITING POSSIBLE REFLECTIONS

HKL WITH H+K=2N ONLY

NUMBER OF ATOMS IN UNIT CELL

ELEMENT		NUMBER*		OCCUP=		NTOTAL
O	1	8.0	*	1.000	=	8.000
O	2	8.0	*	1.000	=	8.000
O	7	4.0	*	0.500	=	2.000
SI	3	8.0	*	0.970	=	7.760
AL	3	8.0	*	0.030	=	0.240
AL	6	4.0	*	0.160	=	0.640
HO	4	4.0	*	0.500	=	2.000
K	5	2.0	*	0.160	=	0.320
FE	6	4.0	*	0.260	=	1.040
MG	8	2.0	*	0.090	=	0.180

THE COLUMNS CONTAIN

BRAGG ANGLE (THETA)
ANGLE (2THETA)
D-VALUE AND $1/D^2$
SQUARE OF SINE (THETA) MULTIPLIED BY 1000 ($1000\ SIN^2\theta$)
MILLER INDICES (HKL)
INTENSITY OF A POWDER LINE, SCALED TO 1000.

THETA	2THETA	D VALUE	$1/D^2$	$1000\ SIN^2\theta$	H	K	L	INTENSITY
4.43	8.85	9.9899	0.0100	5.95	0	0	1	1000.0
8.88	17.76	4.9949	0.0401	23.82	0	0	2	203.3
9.79	19.58	4.5330	0.0487	28.92	0	2	0	19.9
9.92	19.84	4.4755	0.0499	29.67	1	1	0	23.0
10.21	20.42	4.3497	0.0529	31.41	1	1	-1	149.2
10.76	21.53	4.1279	0.0587	34.88	0	2	1	165.7
11.51	23.03	3.8624	0.0670	39.84	1	1	1	169.7
12.26	24.51	3.6315	0.0758	45.06	1	1	-2	3.5
13.28	26.55	3.3568	0.0887	52.74	0	2	2	64.7
13.39	26.77	3.3300	0.0902	53.59	0	0	3	42.7
14.41	28.82	3.0981	0.1042	61.91	1	1	2	357.0
15.41	30.82	2.9008	0.1188	70.62	1	1	-3	245.9

(etc.)

The output data was graphed using the VAX/VMS4 "SAS" graphical program. The 1°-25° theta (0°-50° 2θ) xrd reflections of the above example are shown in Fig. A3-1.

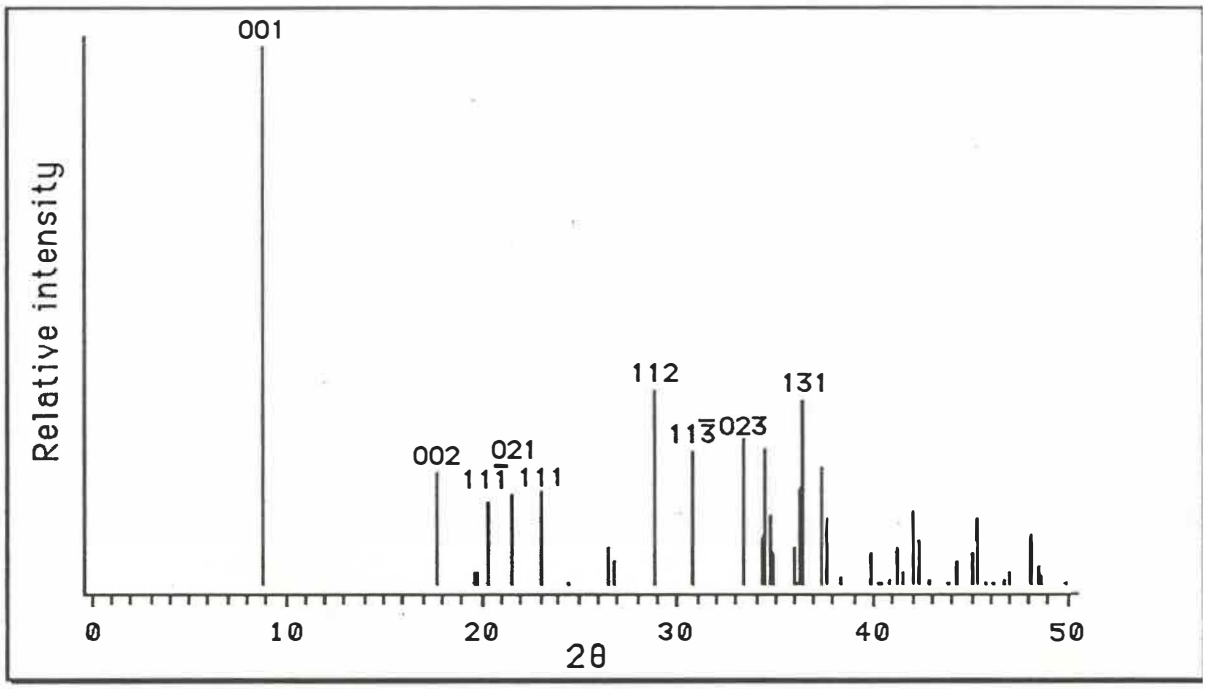

Fig. A3-1 Miller indice and relative intensity of ASTM 9-439 type mineral glauconite peaks calculated theoretically.

APPENDIX IV

CORRELATION OF FIELD NUMBERS, THESIS NUMBERS AND UNIVERSITY OF WAIKATO ROCK STORE NUMBERS.

University of Waikato Rock Store Nº	Field Nº	Thesis Nº	Visor Record Nº	Bed
26183	S29	MC17	472	Wt.Sst.
26186	C32Wt.Sst.	MC27e	475	Wt.Sst.
26179	S35	MC40	468	OrA2
26155	DFS11b	MC22	444	OrB1
26152	ST	MC29	441	OrB2
26171	S14/13	MC30	460	OrB2
26180	S30	MC32	469	OrB2
26187	S36	MC41	476	OrB2
26188	S37	MC43	477	OrB2
26195	S3b	MC19a	484	OrB5
26192	S39b	MC5b	481	TeAk.Zst.
26167	S6	MC20	456	Ao2
26191	S34b	MC39b	480	Ao2
26157	S23	MC36a	446	Ao3
26158	S24	MC36b	447	Ao3
26153	DFS4	MC16	442	Ao4
26164	S5	MC24	453	Ao4
26169	S4b	MC23	458	Ao4
26170	S2	MC26	459	Ao4
26175	SA	MC28	464	Ao4
26184	S3c	MC19b	473	Ao4
26194	S32	MC21	483	Ao4
26154	DFS12	MC18	443	Ao5
26161	Bex.Tunn.	MC45	450	Ao5
26197	A.T.	MC44	486	Ao5
26156	S26	MC35	445	AoA
26162	DFS3	MC15	451	AoA
26178	S39a	MC5a	467	AoA
26181	S34a	MC39a	470	AoA

University of Waikato Rock Store №	Field №	Thesis №	Visor Record №	Bed
26196	CN2	MC27a	485	AoA
26185	7153Wh	MC10a	474	Wh1
26159	S22	MC38b	448	Wh2
26163	S15	MC31a	452	Wh2
26165	S16	MC31b	454	Wh2
26166	S18	MC31d	455	Wh2
26168	S9	MC25b	457	Wh2
26172	S17	MC31c	461	Wh2
26173	S8	MC25a	462	Wh2
26160	S21	MC38a	449	WhA
26176	S40	MC6	465	Elg.Lst.
26177	S38b	MC11a	466	Elg.Lst.
26182	S31	MC14	471	Elg.Lst.
26189	S42	MC3	478	Elg.Lst.
26190	S41	MC7	479	Elg.Lst.
26193	S38c	MC11b	482	Elg.Lst.
26198	8239M	MC9a	487	Mang.Zst.
26151	S27	MC12	440	Pk.Sst.
26174	7153P	MC10b	463	Pk.Sst.